



**HAL**  
open science

# Shape Optimization of Planar Objects and Antennas Using a Gradient-Based Method. Application to Antenna Arrays or to Multi-Receiver Antennas in MIMO Systems

Massimo Zoppi

► **To cite this version:**

Massimo Zoppi. Shape Optimization of Planar Objects and Antennas Using a Gradient-Based Method. Application to Antenna Arrays or to Multi-Receiver Antennas in MIMO Systems. Electromagnetism. Université de Nice Sophia-Antipolis; Florence University, 2012. English. NNT: . tel-03216164

**HAL Id: tel-03216164**

**<https://hal.science/tel-03216164>**

Submitted on 4 May 2021

**HAL** is a multi-disciplinary open access archive for the deposit and dissemination of scientific research documents, whether they are published or not. The documents may come from teaching and research institutions in France or abroad, or from public or private research centers.

L'archive ouverte pluridisciplinaire **HAL**, est destinée au dépôt et à la diffusion de documents scientifiques de niveau recherche, publiés ou non, émanant des établissements d'enseignement et de recherche français ou étrangers, des laboratoires publics ou privés.



UNIVERSITÉ  
**FRANCO  
ITALIENNE**

UNIVERSITÀ  
**I T A L O  
FRANCESE**



**UNIVERSITÉ NICE - SOPHIA ANTIPOLIS**

**Laboratoire d'Electronique, Antennes et  
Télécommunications (LEAT)**

**Ecole Doctorale STIC, Information and Communication Sciences  
& Technologies**

**FLORENCE UNIVERSITY**

**Department of Electronics and  
Telecommunications (DET)**

**Faculty of Engineering and Computer Science**

**Massimo ZOPPI**

**Shape Optimization of Planar Objects and Antennas  
Using a Gradient-Based Method.  
Application to Antenna Arrays or to Multi-Receiver  
Antennas in MIMO Systems.**

Thèse Soutenue le 17 Décembre 2012

*Supervisor LEAT:*            *Dr. Christian PICHOT*  
*Supervisor DET:*           *Prof. Dr. Giuseppe PELOSI*

*External Reviewer:*       *Dr. Bernard Duchêne*  
*External Reviewer:*       *Prof. Dr. Andrea Massa*

# **TABLE OF CONTENTS**

## **CHAPTER 1**

<b>INTRODUCTION</b> .....	p.1
1.1 Inverse Problem Overview .....	p.2
1.2 Development Overview .....	p.4

## **CHAPTER 2**

<b>ELECTROMAGNETIC THEORY</b> .....	p.6
2.1 Short Overview .....	p.7
2.2 General Definition .....	p.7
2.3 EFIE and MFIE Equation Definition .....	p.11
2.4 Reaction Concept .....	p.13
2.5 Variational Equation .....	p.14
2.6 Reduction of Rumsey's Reaction Equations .....	p.14
2.7 Subdomains Variational Equation Definition .....	p.16

## **CHAPTER 3**

<b>SR3D STRUCTURE</b> .....	p.17
3.1 Old SR3D Structure .....	p.18
3.2 New SR3D Structure: General Description .....	p.20
3.3 New SR3D Structure: Reaction Matrix .....	p.21
3.4 New SR3D Structure: Source Vector .....	p.25
3.4.1. Source Vector Dipole .....	p.25
3.5 New SR3D Structure: Reaction Matrix Discretization .....	p.27
3.6 New SR3D Structure: Sources Vector Discretization .....	p.29
3.6.1.Source Vector Dipole Implementation .....	p.29

**CHAPTER 4**

<b>SR3D IMPLEMENTATION</b>	p.31
4.1 Full-Numerical Technique	p.33
4.1.1. Reaction Matrix	p.34
4.1.2. Dipole Source Vector	p.35
4.2 Semi-Numerical Technique	p.36
4.2.1. Reaction Matrix	p.37
4.2.2. Dipoe Source Vector	p.39

**CHAPTER 5**

<b>SR3D DERIVATIVE WITH RESPECT TO THE MESH</b>	p.40
5.1 SR3D Mesh Derivative: General Description	p.41
5.2 SR3D Derivative of the Reaction Matrix with Respect to the Mesh	p.42
5.3 SR3D Derivative of the Source Vector with Respect to the Mesh	p.46
5.3.1. Derivative of Dipole Source	p.46
5.4 SR3D Derivative of the Discretized Reaction Matrix with Respect to the Mesh ..	p.49
5.5 SR3D Derivative of the Discretized Source Vector with Respect to the Mesh .....	p.50
5.5.1. Implementation of the Derivative of the Dipole Source Vector	p.50

**CHAPTER 6**

<b>SR3D MESH DERIVATIVE IMPLEMENTATION</b>	p.52
6.1 Full-Numerical Technique	p.54
6.1.1. Reaction Matrix Derivative	p.54
6.1.2. Source Vector Derivative	p.57
6.2 Semi-Numerical Technique	p.59
6.2.1. Reaction Matrix Derivative	p.59

**CHAPTER 7**

<b>OPTIMIZATION</b>	p.63
7.1 Optimization Terms Calculation	p.65
7.1.1. Direct Problem	p.65
7.1.2. Inverse Problem and Cost Functional	p.66
7.2 Optimization Routine	p.67

**CHAPTER 8**

<b>CODE VALIDATION</b> .....	p.68
8.1 Validation of the Derivative of the Linear System Elements .....	p.69
8.2 Cost Functional Gradient Derivative Validation .....	p.71
8.3 First Example: Optimization Pattern Over the Criterion Map .....	p.74
8.4 Second Example: Scattered Field Evolution .....	p.76
8.5 Conclusion and Further Steps .....	p.78

**CHAPTER 9**

<b>NUMERICAL EXPERIMENTS</b> .....	p.79
9.1 Planar Array I .....	p.81
9.2 Planar Array II .....	p.87
9.3 Linear Array I .....	p.93
9.4 Parasitic Elements I .....	p.99
9.5 Parasitic Elements II .....	p.105
9.6 Parasitic Elements III .....	p.111
9.7 Passive Antennas I .....	p.117
9.8 Passive Antennas II .....	p.123

<b>GENERAL CONCLUSION</b> .....	p.129
---------------------------------	-------

<b>ANNEXES</b> .....	p.132
Annex 1: Numerical Discretization Method .....	p.132
Annex 2: Basis Functions .....	p.140
Annex 3: Semi-Numerical Technique .....	p.142
Annex 4: Derivative Calculations .....	p.149
Annex 5: Scattered Field Derivative with Respect to the Mesh .....	p.166
Annex 6: SR3D Frequency Derivatives .....	p.168

<b>BIBLIOGRAPHY</b> .....	p.172
---------------------------	-------

**CHAPTER 1:**  
**INTRODUCTION**

# Chapter 1 - Introduction

The inverse scattering problem of finding the optimal location multi-antennas systems has received a growing interest in the fast few years as MIMO systems have demonstrated the potentiality to significantly increase the channel capacity but many other applications using multiple objects or multi-antenna systems such as radar applications, inverse scattering including microwave imaging could be of interest concerning this study.

In this thesis, we describe the development of a method based on an integral formulation of the EM problem (SR3D code) for finding the solution of an inverse scattering problem, which is the optimal location of 3D or 2D multiple metallic objects or multiantenna systems illuminated by dipoles or planar waves from imposed constraints (e.g. radiation patterns).

Many inverse scattering algorithms based on gradient methods are using forward and adjoint problems for calculating the cost functional derivative. Here, in order to avoid finding a solution for every adjoint problem and to develop a more general method, we are calculating directly the derivative of the cost functional. In this way, we have directly access to the sensitivity of the cost functional versus parameters we are interested in.

We want to emphasize that the main core of this work is the development of an inverse scattering method based on an integral formulation of the EM problem, by calculating directly the derivative of the cost functional. In this way, we obtain a high sensitivity as well as also the coupling effect between structure elements is taken into account. First results have been achieved using a gradient-based algorithm using the optimization procedure. But, the code SR3D being modular it is possible to change the optimization algorithm without modifying the main electromagnetic structure of the SR3D code.

## C1.1 Inverse Problem Overview

We can divide optimization algorithms into two main classes: deterministic methods which, in general terms, behaves predictably and stochastic methods that generate and use random variables. There are many methods for solving the inverse problem (i.e. geometry array synthesis), using optimization algorithms as Genetic Algorithm (GA), Particle Swarm Optimization (PSO) or Conjugate Gradient Method. Of course, every optimization method has some advantages and weak points. Usually, a genetic algorithm needs a considerable number of computations and iterations before finding the convergence towards the optimum; on the other hand, it is a global optimization method, meaning that it is able to find the global optimum of the problem. Of course, the conjugate gradient method needs less iterations and computations but they can have local convergence, meaning that they can be trapped in a local minimum. This is why the construction of the cost functional is of great importance.

In the literature, we can find many publications about array geometry synthesis, (a similar problem with respect to the MIMO antennas optimal location). For instance, a PSO method has been used in order to synthesize of a linear array in [20], where no coupling between elements is taken into account.

In computer science, PSO is a computational method that optimizes a problem by iteratively trying to improve a candidate solution with regard to a given measure of quality. PSO optimizes a problem by having a population of candidate solutions, for instance particles, and moving these particles around in the search-space according to simple mathematical formulae over the particle's position and velocity. Each particle's movement is influenced by its best known local position and guided towards the best known positions in the search-space. This is expected to move the swarm towards the best solutions. PSO is a metaheuristic method as it makes few or no assumptions about the problem being optimized and can search over very large spaces of

candidate solutions. However, metaheuristics such as PSO do not guarantee that an optimal solution is ever found. As a matter of fact, PSO does not use the gradient of the problem being optimized, which means PSO does not require that the optimization problem be differentiable as is required by classic optimization methods such as gradient descent and quasi-newton methods.

A similar problem regarding the array antenna position synthesis is reported in [25], where a Genetic Algorithm has been used; once again no coupling effect between elements is taken into account.

In the computer science field of artificial intelligence, a genetic algorithm (GA) is a heuristic search that mimics the process of natural evolution. This heuristic is routinely used to generate useful solutions for optimization and search problems. Genetic algorithms belong to the larger class of evolutionary algorithms (EA), which generate solutions to optimization problems using techniques inspired by natural evolution, such as inheritance, mutation, selection, and crossover. In a genetic algorithm, a population of strings (called chromosomes or the genotype of the genome), which encode candidate solutions (called individuals, creatures, or phenotypes) to an optimization problem, is evolved towards better solutions. Traditionally, solutions are represented as binary strings of 0s and 1s, but other encodings are also possible. The evolution usually starts from a population of randomly generated individuals and happens in generations. In each generation, the fitness of every individual in the population is evaluated, multiple individuals are stochastically selected from the current population (based on their fitness), and modified (recombined and possibly randomly mutated) to form a new population. The new population is then used in the next iteration of the algorithm. Commonly, the algorithm terminates when either a maximum number of generations has been produced, or a satisfactory fitness level has been reached for the population. If the algorithm has terminated due to a maximum number of generations, a satisfactory solution may or may not have been reached.

Another array antenna position synthesis methods are proposed in [37] and [38], where an optimization conjugate method is used, the derivative of the cost functional calculating directly. The optimization is based on the noise-corrupted scattered field data, but, the analysis still does not involve the element coupling effect.

In numerical analysis, the conjugate gradient method is an algorithm generally used for the numerical solution of particular systems of linear equations, for symmetric and positive-definite matrices. The conjugate gradient method is an iterative method, so it can be applied to sparse systems that are too large to be handled by direct methods such as the LU decomposition. Such systems often arise when numerically solving partial differential equations. The conjugate gradient method can also be used to solve unconstrained optimization problems such as energy minimization. This method has a faster convergence than the stochastic ones but, on the other hand, the gradient method requires the optimization problem to be differentiable.

In this work, we have chosen to use a deterministic algorithm to define the optimization framework. Usually, complex electromagnetic problems, using a high element mesh number, require a considerable burden of computational time. Normally, this is not adequate for using a genetic algorithm due to an huge number of iterations needed. So, even if this class of algorithm may converge to the global minimum, we have the drawback of computation time for the forward modeling. Deterministic algorithms have faster convergence towards the minimum but, on the other hand, the global convergence is not guaranteed. Fortunately, there are some techniques able to improve the convergence performance of deterministic algorithms. Adding a priori or extra information or fixing some constraints, using equalization for example, to the optimization procedure or by modifying the cost functional using regularization for example,

for an easier global convergence. In terms of constraints, we can, for instance, to fix the location of some antennas or prohibited the superimposition of two objects. We can also add extra information to the deterministic algorithm using a frequency hopping technique, where the optimization aim is performed with respect to several frequencies and defining the final cost functional combining the results derived from each frequency of interest. These techniques are able to modify the smoothness of the cost functional in order to ease the global minimum investigation. Improving the efficiency in global convergence for deterministic algorithm, leads to handle complex electromagnetic optimization problems, with a good degree of accuracy, and spatial resolution, related to the global convergence.

The works reported in [20], [25], [30] and [38], consider only non-full-wave optimization. Therefore, no electromagnetic coupling between the antenna elements has been taken into account, reducing the accuracy of the optimization results. In many applications, it is essential to consider the coupling between objects, such as MIMO applications, because the spatial diversity between the antennas [2] is a critical parameter of the system itself. But many problems require a full-wave method optimization solver, to retrieve the optimal location of objects or antennas. For instance, Andújar A. [3], involves the design of two ground plane boosters for wireless handheld devices. The boosters need to be correctly located along the edges of the ground plane of the device, to achieve the desired effect. As the coupling between boosters and ground plane is considered, a full-wave method is needed to apply an optimization procedure able to retrieve the optimal position of the boosters.

The main idea of this work is to define a full-wave optimization procedure able to retrieve the optimal location of multiple objects or multi-antenna systems. We combine the benefits of a full-wave optimization method and the accuracy of the analytical calculation of the gradient of the cost functional. Therefore, we are able to solve antenna location optimization problems as [38] and obtain a good accuracy with respect to the cost functional gradient. We have chosen to use the SR3D software [13], [14], [23], that utilizes a MoM method with an integral formulation of the electromagnetic problem; SR3D is a proprietary software of France Telecom developed since 80s by Orange Labs La Turbie.

## C1.2 Developments Overview

In figure C1.1, we report a generic structure with three patch antennas over a ground plane.

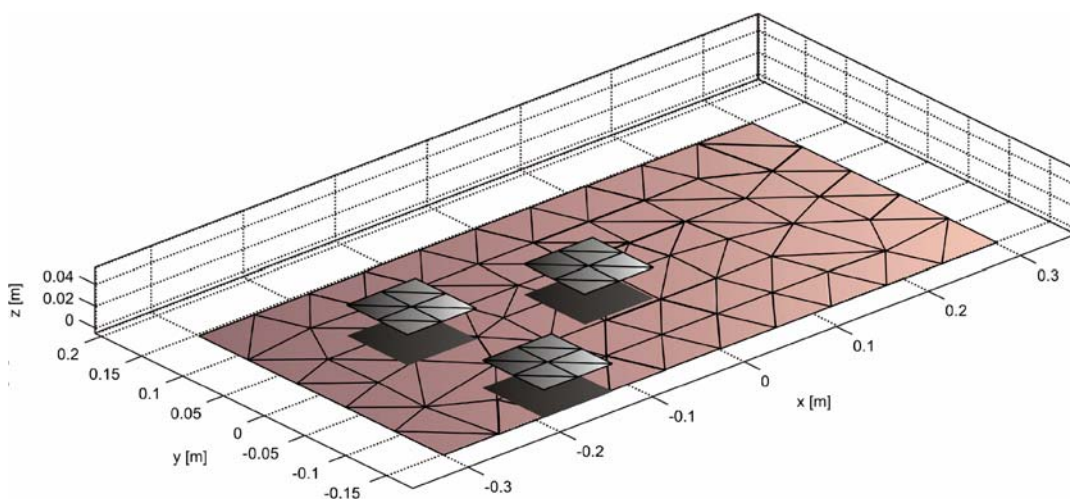


Figure C1.1: Three patch antennas over ground plane

Our optimization method is suitable to retrieve the position of the patch antennas with respect to a desired electromagnetic parameter.

The strong point of this work is represented by the direct calculation of the surface currents gradient with respect to the geometry, for every object in the environment.

This allows us to use any optimization method we, since every electromagnetic parameter depends on the surface currents and its derivative. For instance, if we want to obtain a desired scattered field with respect to the location of the three antennas in figure C1.1 we can define the scattered field gradient with respect to the geometry (using the derivative of the currents) in order to compute the cost functional gradient and then to apply the optimization algorithm.

We can also use this method for optimizing the antennas impedance or minimizing the coupling effect between the antennas, by changing the value of the cost functional and its gradient without modifying the main structure of the SR3D code.

In the following, we will show how to implement the current derivative modules within the SR3D software along with different of optimization test-cases.

**CHAPTER 2:**  
**ELECTROMAGNETIC THEORY**

## Chapter 2 - Electromagnetic Theory

### C2.1 Short Overview

In the next paragraphs, the theory of the EM problem will be shown, starting from Maxwell equations. The goal is to describe the reaction concept using a variational equation, and to use it in a numerical form inside the SR3D software using the MoM method. A definition of direct and inverse problem is given subsequently:

1. Direct Problem: when the applied sources, object shapes and their electromagnetic properties are known, the result of their interaction has to be determined;
2. Inverse Problem: when the interaction of the electromagnetic field is known in a certain domain and some information are kept from it in order to describe the environment and the objects defined inside of the analysis domain.

### C2.2 General Definition

SR3D is based on the MoM (Method of Moments) to solve direct EM problems. In this short summary, the basic theory of SR3D software is described. So the beginning is the introduction of the symmetric Maxwell equations.

Consider a homogeneous, isotropic domain  $\Omega$  of volume  $V$  and boundary  $\Gamma$ . The electromagnetic wave is described by  $\underline{E}$ ,  $\underline{H}$ , electric and magnetic fields, respectively, that verify Maxwell equations with a time-dependance  $e^{-j\omega t}$ :

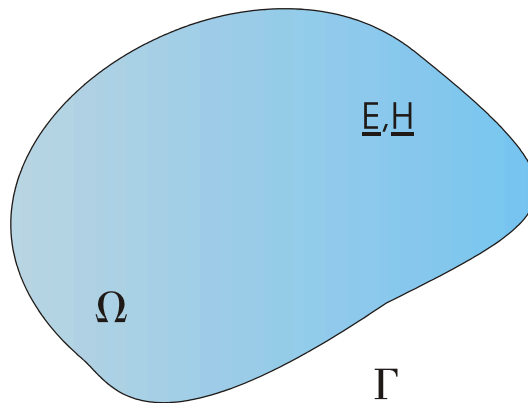


Figure C2.1 Domain  $\Omega$

$$\begin{aligned}
 \nabla \times \underline{E} &= j\omega \underline{B} - \underline{M} \\
 \nabla \times \underline{H} &= -j\omega \underline{D} + \underline{J} \\
 \nabla \cdot \underline{D} &= \rho_e \\
 \nabla \cdot \underline{B} &= \rho_m
 \end{aligned}
 \tag{C2.1}$$

with:

$\omega$ angular frequency	$\underline{B}$ magnetic induction
$\underline{D}$ electric induction	$\underline{M}$ magnetic current density
$\underline{J}$ electric current density	$\rho_e$ electric charge density
$\rho_e$ electric charge density	$\rho_m$ magnetic charge density

The magnetic and electric charge densities are defined as:

$$\begin{aligned}\underline{\nabla} \cdot \underline{J} - j\omega\rho_e &= 0 \\ \underline{\nabla} \cdot \underline{M} - j\omega\rho_m &= 0\end{aligned}\quad (\text{C2.2})$$

At last the definition of constitutive equations where  $\epsilon$  is the permittivity,  $\epsilon_r$  the relative permittivity and  $\epsilon_0$  the permittivity of free space ( $8.854 \times 10^{-12} \text{ F/m}$ ) and  $\mu$  is the permeability,  $\mu_r$  the relative permeability and  $\mu_0$  the permeability of free space ( $4\pi \times 10^{-7} \text{ (H/m)}$ ):

$$\begin{aligned}\underline{D} &= \epsilon \underline{E} \\ \underline{B} &= \mu \underline{H} \\ \underline{J} &= \sigma \underline{E} \\ \underline{M} &= \sigma_m \underline{H}\end{aligned}\quad (\text{C2.3})$$

with:  $\boxed{\epsilon = \epsilon_0 \epsilon_r, \quad \mu = \mu_0 \mu_r}$

Also the boundary conditions are needed in order to obtain the uniqueness of Maxwell equations solution, so we have:

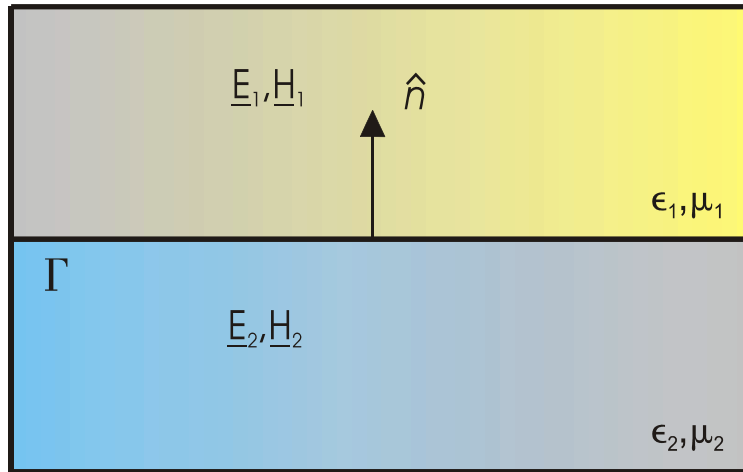


Figure C2.2: Boundary between medium 1 and medium 2

$$\begin{aligned}\hat{n} \times (\underline{H}_2 - \underline{H}_1) &= \underline{J}_s \\ \hat{n} \times (\underline{E}_2 - \underline{E}_1) &= -\underline{M}_s \\ \hat{n} \cdot (\underline{D}_2 - \underline{D}_1) &= \rho_{es} \\ \hat{n} \cdot (\underline{B}_2 - \underline{B}_1) &= \rho_{ms}\end{aligned}\quad (\text{C2.4})$$

In the case of a PEC boundary, we can write C2.4 as:

$$\begin{aligned}
 \hat{n} \times \underline{H}_2 &= \underline{J}_s \\
 \hat{n} \times \underline{E}_2 &= 0 \\
 \hat{n} \cdot \underline{E}_2 &= \frac{\rho_{es}}{\epsilon_2} \\
 \hat{n} \cdot \underline{H}_2 &= 0
 \end{aligned} \tag{C2.5}$$

Let's apply now the operator  $\Delta(\cdot) = \nabla \nabla \cdot (\cdot) - \nabla \times \nabla \times (\cdot)$  on the two first equations C2.1 obtaining:

$$\begin{aligned}
 \Delta \underline{E} + \Delta k^2 \underline{E} &= -\frac{\underline{J}}{\omega \epsilon} (\nabla \nabla \cdot \underline{J} + k^2 \underline{J}) + \nabla \times \underline{M} \\
 \Delta \underline{H} + k^2 \underline{H} &= -\frac{\underline{J}}{\omega \mu} (\nabla \nabla \cdot \underline{M} + k^2 \underline{M}) - \nabla \times \underline{J}
 \end{aligned} \tag{C2.6}$$

$$\text{with: } \boxed{k^2 = \omega^2 \mu \epsilon}$$

The electromagnetic field must satisfy the next two conditions, so-called radiation conditions (C2.7) and finite energy conditions (inside  $\Omega$ ) (C2.8), respectively:

$$\begin{aligned}
 \lim_{r \rightarrow \infty} (\hat{n} \times \nabla \times \underline{E} - jk \underline{E}) &= o\left(\frac{1}{r}\right) \\
 \lim_{r \rightarrow \infty} (\hat{n} \times \nabla \times \underline{H} - jk \underline{H}) &= o\left(\frac{1}{r}\right)
 \end{aligned} \tag{C2.7}$$

$$\begin{aligned}
 \int_{\Omega} \|\underline{E}\|^2 d\Omega &< \infty \\
 \int_{\Omega} \|\underline{H}\|^2 d\Omega &< \infty
 \end{aligned} \tag{C2.8}$$

Let's now consider the Green's function or system impulse response  $G(r, r')$  solution of  $(\Delta + k^2)G(r, r') = -\delta(r, r')$ . Then the general solution is:

$$G(R) = \frac{e^{jkR}}{(4\pi R)} \tag{C2.9}$$

$$\text{with: } \boxed{
 \begin{aligned}
 R &= \|r - r'\| \in \mathfrak{R}^3 \\
 r &\equiv \text{measurement point coordinates} \\
 r' &\equiv \text{observation point coordinates}
 \end{aligned}
 }$$

If the convolution product is applied on (C2.6) the impulse response of electromagnetic field in  $R$  is obtained:

$$\begin{aligned}\underline{E}(r) &= \frac{j}{\omega\epsilon}(\underline{\nabla}\underline{\nabla}\cdot + k^2)(\underline{J}(r') \times G(r, r')) - \underline{\nabla} \times (\underline{M}(r') \times G(r, r')) \\ \underline{H}(r) &= \frac{j}{\omega\mu}(\underline{\nabla}\underline{\nabla}\cdot + k^2)(\underline{M}(r') \cdot G(r, r')) + \underline{\nabla} \times \underline{J}(r') \times G(r, r')\end{aligned}\quad (\text{C2.10})$$

Let's now focus on the Huygens' equivalence principle. This principle says that is possible to replace the real sources defined in the application domain  $\Omega$  with superficial sources on a closed surface, leaving the electromagnetic field unchanged.

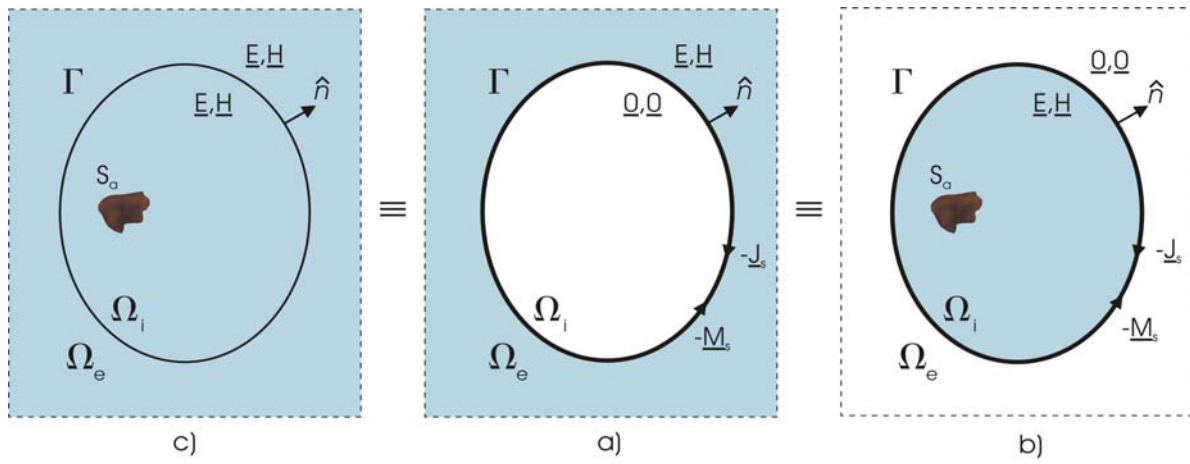


Figure C2.3: Huygens' principle applied on problem c)

Based on Huygens' principle is possible to replace the case c) with a) or b). In these two last cases closed interfaces are introduced and superficial currents are defined over them in order to satisfy the Maxwell equations, defined for the original problem c). These superficial currents are defined as follows:

$$\begin{aligned}\underline{J}_s &= \hat{n} \times \underline{H}_s \\ \underline{M}_s &= -\hat{n} \times \underline{E}_s \\ \rho_{es} &= \epsilon \hat{n} \cdot \underline{E}_s \\ \rho_{ms} &= \mu \hat{n} \cdot \underline{H}_s\end{aligned}\quad (\text{C2.11})$$

Finally, we can replace the problem c) with problem a) or b) using the superficial currents while maintaining the uniqueness of the solution. The theory showed with the Huygens' principle allows us to substitute the general inhomogeneous volumic problem with an ensemble of homogeneous and superficial problems.

### C2.3 EFIE and MFIE Equations Definition

Let us define a general electromagnetic problem within inhomogeneous structure placed inside the domain  $\Omega_2$  :

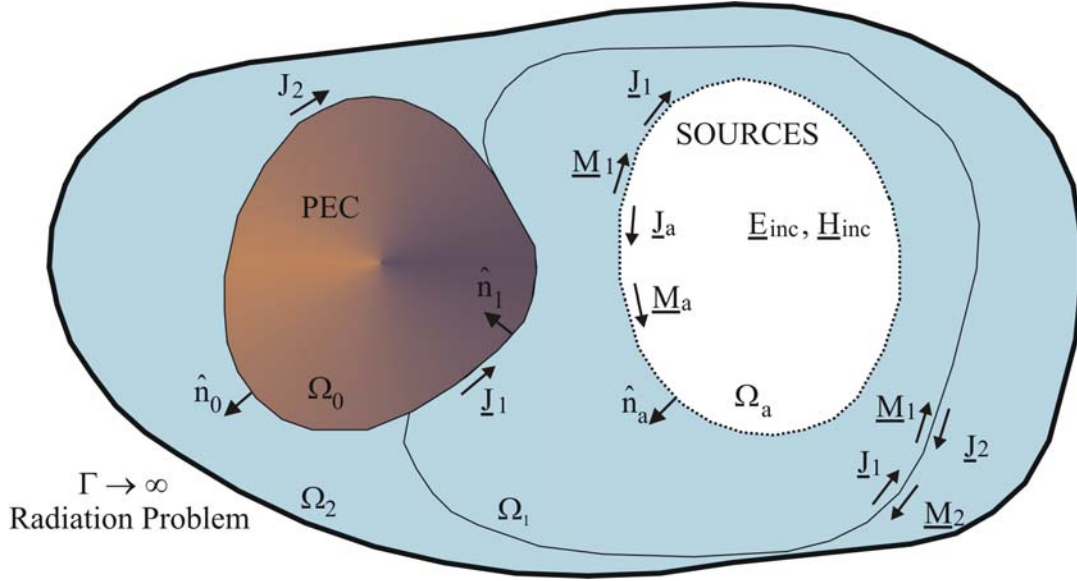


Figure C2.4: General inhomogeneous volumic problem

If we apply Huygens' principle of the problem shown in Figure C2.4, we can describe this inhomogeneous problem as an ensemble of diffraction problems with electromagnetic field generated by equivalent surface sources, radiating from discontinuity surfaces. These surfaces can be decomposed into homogeneous subdomains and described using the Green's theorem.

The Green's theorem allows us to obtain an integral representation of the diffracted field (EFIE/MFIE) using the superficial current distributions  $\underline{J}_s$  and  $\underline{M}_s$  defined by Huygens' principle. Using EFIE and MFIE, we are able to describe, the dependance between superficial currents and the incident field (SOURCES see Fig.4).

The numerical solution of these equations is based on the Rumsey reaction concept. From on Figure C2.4 and applying the Huygens' principle, the total field can be written as follows:

$$\begin{aligned} \underline{E}(r) &= \underline{E}^{inc}(r) + \underline{E}^{dif}(r) \\ \underline{H}(r) &= \underline{H}^{inc}(r) + \underline{H}^{dif}(r) \end{aligned} \quad (C2.12)$$

$$\text{with: } \boxed{\underline{E}, \underline{H} = f(\underline{J}^{inc}, \underline{M}^{inc})}$$

The sources in Figure C2.4 are replaced by surface currents as follows:

$$\begin{aligned} \underline{J}^{inc} &= \underline{J}_a \\ \underline{M}^{inc} &= \underline{M}_a \end{aligned} \quad (C2.13)$$

In that way, subdomains are coupled through the density currents defined on the discontinuity interface. Moreover, the boundary conditions between  $\Omega_1$  and  $\Omega_2$  are given by the equation (C2.14) and the boundary conditions between  $\Omega_0$  and  $\Omega_2$  are given by the equation (C2.15):

$$\begin{aligned}\hat{n}_1 \times \underline{H}_1 + \hat{n}_2 \times \underline{H}_2 &= \underline{J}_1 + \underline{J}_2 = \underline{0} \\ \hat{n}_1 \times \underline{E}_1 + \hat{n}_2 \times \underline{E}_2 &= -(\underline{M}_1 + \underline{M}_2) = \underline{0}\end{aligned}\quad (\text{C2.14})$$

$$\begin{aligned}\hat{n}_0 \times \underline{H}_1 &= (\underline{J}_1 + \underline{J}_2) = \underline{J}_0 \\ \hat{n}_0 \times \underline{E}_1 &= -(\underline{M}_1 + \underline{M}_2) = \underline{0}\end{aligned}\quad (\text{C2.15})$$

That also means we have surface currents on physical defined interfaces (es. PEC interface). We will integrate now the impulse response (C2.10) in the whole domain (volumic). Since we have equivalent surface currents we can integrate over a closed surface domain  $\Gamma$ . In (C2.16) we have given the total electromagnetic field:

$$\begin{aligned}\underline{E}(r) &= \underline{E}^{inc}(r) + j\omega\mu \oint_{\Gamma} G(r, r') \underline{J}(r') d\Gamma + \\ &\quad \frac{j}{\omega\varepsilon} \oint_{\Gamma} \underline{\nabla}_{r'} G(r, r') \underline{\nabla}_{\Gamma} \cdot \underline{J}(r') d\Gamma - \underline{\nabla} \times \oint_{\Gamma} G(r, r') \underline{M}(r') d\Gamma\end{aligned}\quad (\text{C2.16})$$

$$\begin{aligned}\underline{H}(r) &= \underline{H}^{inc}(r) + j\omega\varepsilon \oint_{\Gamma} G(r, r') \underline{M}(r') d\Gamma + \\ &\quad \frac{j}{\omega\mu} \oint_{\Gamma} \underline{\nabla}_{r'} G(r, r') \underline{\nabla}_{\Gamma} \cdot \underline{M}(r') d\Gamma - \underline{\nabla} \times \oint_{\Gamma} G(r, r') \underline{J}(r') d\Gamma\end{aligned}$$

And the same is done for incident part of electromagnetic field in (C2.17):

$$\begin{aligned}\underline{E}^{inc}(r) &= j\omega\mu \oint_{\Gamma} G(r, r') \underline{J}_a(r') d\Gamma + \\ &\quad \frac{j}{\omega\varepsilon} \oint_{\Gamma} \underline{\nabla}_{r'} G(r, r') \underline{\nabla}_{\Gamma} \cdot \underline{J}_a(r') d\Gamma - \underline{\nabla} \times \oint_{\Gamma} G(r, r') \underline{M}_a(r') d\Gamma\end{aligned}\quad (\text{C2.17})$$

$$\begin{aligned}\underline{H}^{inc}(r) &= j\omega\varepsilon \oint_{\Gamma} G(r, r') \underline{M}_a(r') d\Gamma + \\ &\quad \frac{j}{\omega\mu} \oint_{\Gamma} \underline{\nabla}_{r'} G(r, r') \underline{\nabla}_{\Gamma} \cdot \underline{M}_a(r') d\Gamma + \underline{\nabla} \times \oint_{\Gamma} G(r, r') \underline{J}_a(r') d\Gamma\end{aligned}$$

If we finally consider the equation (C2.18):

$$\nabla \times \oint_{\Gamma} \phi(\underline{v}, \underline{v}') \underline{\Psi}(\underline{v}') dS = \oint_{\Gamma} \underline{\Psi}(\underline{v}') \times \underline{\nabla}_{\underline{r}'} \phi(\underline{v}, \underline{v}') dS + \frac{1}{2} \hat{n} \times \underline{\Psi}(\underline{v}') \quad (\text{C2.18})$$

Applying equation (C2.18) on equations (C2.16) we obtain:

$$\begin{aligned} \hat{n} \times \underline{E}^{inc}(\underline{r}) &= -\hat{n} \times \left\{ j\omega\mu \oint_{\Gamma} G(\underline{r}, \underline{r}') \underline{J}(\underline{r}') d\Gamma + \right. \\ &\quad \left. \frac{j}{\omega\varepsilon} \oint_{\Gamma} \underline{\nabla}_{\underline{r}'} G(\underline{r}, \underline{r}') \underline{\nabla}_{\Gamma} \cdot \underline{J}(\underline{r}') d\Gamma - \oint_{\Gamma} \underline{M}(\underline{r}') \underline{\nabla}_{\underline{r}'} G(\underline{r}, \underline{r}') d\Gamma - \frac{1}{2} \hat{n} \times \underline{M}(\underline{r}') \right\} \\ \hat{n} \times \underline{H}^{inc}(\underline{r}) &= -\hat{n} \times \left\{ j\omega\varepsilon \oint_{\Gamma} G(\underline{r}, \underline{r}') \underline{M}(\underline{r}') d\Gamma + \right. \\ &\quad \left. \frac{j}{\omega\mu} \oint_{\Gamma} \underline{\nabla}_{\underline{r}'} G(\underline{r}, \underline{r}') \underline{\nabla}_{\Gamma} \cdot \underline{M}(\underline{r}') d\Gamma + \oint_{\Gamma} \underline{J}(\underline{r}') \times \underline{\nabla}_{\underline{r}'} G(\underline{r}, \underline{r}') d\Gamma + \frac{1}{2} \hat{n} \times \underline{J}(\underline{r}') \right\} \end{aligned} \quad (\text{C2.19})$$

The equations (C2.19) are designed respectively as the Electric Field Integral Equation (EFIE) and the Magnetic Field Integral Equation (MFIE). For EFIE, we consider a Perfect Electric Conductor (PEC) boundary, instead for MFIE a Perfect Magnetic Conductor (PMC) one.

#### C2.4 Reaction Concept

We can now define the variational formulation using the Rumsey reaction concept. Given  $\Omega$ , an homogeneous domain with boundary surface  $\Gamma$ , sources  $(\underline{J}, \underline{M})$  and test sources  $(\underline{J}^{test}, \underline{M}^{test})$  defined tangent with respect to  $\Gamma$  and with boundary condition defined as (C2.11), then the reaction of the sources on the test sources in  $\Omega$  is defined in a bilinear form as follows:

$$R_{\Omega}(\{\underline{J}, \underline{M}\}, \{\underline{J}^{test}, \underline{M}^{test}\}) = \oint_{\Gamma} (\underline{E} \cdot \underline{J}^{test} - (\underline{M}^{test} \cdot \underline{H})) d\Gamma^{test} \quad (\text{C2.20})$$

where the electromagnetic field  $(\underline{E}, \underline{H})$  is generated by surface currents  $(\underline{J}, \underline{M})$  defined inside  $\Omega$ . This concept is also true for the incident electromagnetic field  $(\underline{E}^{inc}, \underline{H}^{inc})$  generated by the surface currents  $(\underline{J}_a, \underline{M}_a)$  inside  $\Omega$ :

$$R_{\Omega}(\{\underline{J}_a, \underline{M}_a\}, \{\underline{J}^{test}, \underline{M}^{test}\}) = \oint_{\Gamma} (\underline{E}^{inc} \cdot \underline{J}^{test} - (\underline{M}^{test} \cdot \underline{H}^{inc})) d\Gamma^{test} \quad (\text{C2.21})$$

The bilinear forms (C2.20) and (C2.21) have symmetric property. So we can write due to the reciprocity principle:

$$R_{\Omega}(\{\underline{J}, \underline{M}\}, \{\underline{J}^{test}, \underline{M}^{test}\}) = R_{\Omega}(\{\underline{J}_a, \underline{M}_a\}, \{\underline{J}^{test}, \underline{M}^{test}\}) \quad (\text{C2.22})$$

### C2.5 Variational Equation

If we use the equations (C2.16) and equations shown in (C2.20) and (C2.21) and apply the boundary conditions we obtain:

$$R_{\Omega}(\{\underline{J}, \underline{M}\}, \{\underline{J}^{test}, \underline{M}^{test}\}) - R_{\Omega}(\{\underline{J}_a, \underline{M}_a\}, \{\underline{J}^{test}, \underline{M}^{test}\}) = 0 \quad (C2.23)$$

If we define  $\underline{E} = j\omega\mu_0\underline{e}$ ,  $\underline{M} = j\omega\mu_0\underline{p}$  and  $\underline{J} = \underline{j}$  and develop equation (C2.20). After some mathematical transformations, we obtain:

$$\begin{aligned} -S(\underline{E}^{inc}, \underline{H}^{inc}, \underline{j}^{test}, \underline{p}^{test}) &= \mu R_1(\underline{j}, \underline{j}^{test}) + \frac{k^2}{\mu_r} R_1(\underline{p}, \underline{p}^{test}) + \\ &R_2(\underline{j}, \underline{p}^{test}) + R_2(\underline{p}, \underline{j}^{test}) \end{aligned} \quad (C2.24)$$

The terms  $R_1$ ,  $R_2$  and  $S$  are defined as follows, (for sake of simplicity we will omit the arguments of the functions):

$$\begin{aligned} R_1(\underline{\alpha}, \underline{\alpha}^{test}) &= \oint_{\Gamma^{test}\Gamma} \oint_{\Gamma} (G)(\underline{\alpha} \cdot \underline{\alpha}^{test}) d\Gamma d\Gamma^{test} - \frac{1}{k^2} \oint_{\Gamma^{test}\Gamma} \oint_{\Gamma} (G)(\underline{\nabla} \cdot \underline{\alpha} \underline{\nabla} \cdot \underline{\alpha}^{test}) d\Gamma d\Gamma^{test} \\ R_2(\underline{\alpha}, \underline{b}^{test}) &= \oint_{\Gamma^{test}\Gamma} \oint_{\Gamma} ((\underline{\nabla}_{r'} G \times \underline{\alpha}) \cdot \underline{\beta}^{test}) d\Gamma d\Gamma^{test} \\ S(\underline{E}^{inc}, \underline{H}^{inc}, \underline{j}^{test}, \underline{p}^{test}) &= \oint_{\Gamma} (\underline{E}^{inc} \cdot \underline{j}^{test} - \underline{p}^{test} \cdot \underline{H}^{inc}) d\Gamma \end{aligned} \quad (C2.25)$$

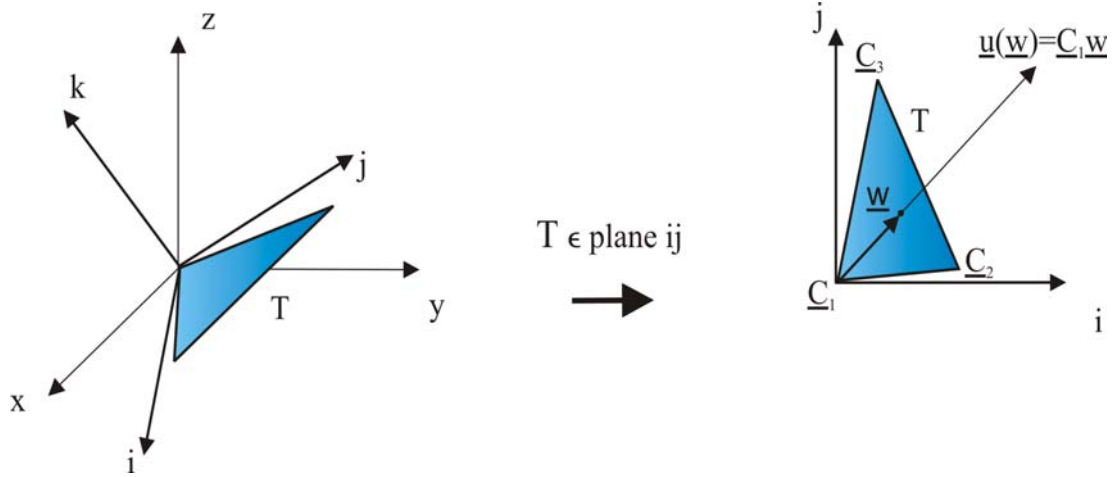
where:

if $\underline{\alpha} = \underline{j}$ then $\underline{\beta} = \underline{p}$
or if $\underline{\alpha} = \underline{p}$ then $\underline{\beta} = \underline{j}$

Note that, in equation (C2.25), inside  $R_1$ ,  $R_2$  terms, the basis functions  $\underline{j}, \underline{p}$  are defined using an implicit form (i.e. through the generic basis  $\underline{a}, \underline{b}$ ). That is owing to the fact that, as we can see from equation (C2.24), the reaction term  $R_1$  depends on bases of the same kind while the reaction term  $R_2$  depends on bases of different kinds. About the  $S$  term we can simply use the  $\underline{j}, \underline{p}$  representation as we can easily understand from equation (C2.24). See Annex 2 for an detailed definition of the  $\underline{j}, \underline{p}$  basis functions.

### C2.6 Reduction of Rumsey's Reaction Equations

A reduction of the Rumsey reaction equations has been performed. That reduction is important since we need to perform a mesh derivative of equations (C2.25). A more simple representation of these equation means an easier treatment of the relative mesh derivative definition. We reduce the complexity of the  $\underline{\nabla} \cdot \underline{a}$  terms of equation (C2.25); considering the triangles in a two-dimensional reference coordinates rather than a three-dimensional one.

Figure C2.5: Generic orthonormal vector  $\underline{u}$  related to triangle  $T$ 

As vector  $\underline{u}$  is an orthonormal vector basis (see Annex 2), we can write:

$$\underline{u} = (\hat{i} + \hat{j})$$

$$\underline{\nabla} \cdot \underline{u} = \left( \frac{\partial i}{\partial i} + \frac{\partial j}{\partial j} \right) = 2 \quad (\text{C2.26})$$

where:  $\underline{u} = \underline{a}, \underline{b}$

According to equation A2.1:

$$\underline{\nabla} \cdot \underline{\alpha} = H(\underline{\nabla} \cdot \underline{u}) = 2H \quad (\text{C2.27})$$

$$H = \frac{1}{2\Lambda}, \quad \Lambda = \text{structure surface}$$

The equation (C2.25), according to the equation (C2.27), becomes:

$$R_1(\underline{\alpha}, \underline{\alpha}^{test}) = \oint_{\Gamma^{test}} \oint_{\Gamma} (G)(\underline{\alpha} \cdot \underline{\alpha}^{test}) d\Gamma d\Gamma^{test} - \frac{4HH^{test}}{k^2} \oint_{\Gamma^{test}} \oint_{\Gamma} (G) d\Gamma d\Gamma^{test}$$

$$R_2(\underline{\alpha}, \underline{\beta}^{test}) = \oint_{\Gamma^{test}} \oint_{\Gamma} ((\underline{\nabla}_r G \times \underline{\alpha}) \cdot \underline{\beta}^{test}) d\Gamma d\Gamma^{test} \quad (\text{C2.28})$$

$$S(\underline{E}^{inc}, \underline{H}^{inc}, \underline{j}^{test}, \underline{p}^{test}) = \oint_{\Gamma^{test}} (\underline{E}^{inc} \cdot \underline{j}^{test} - \underline{p}^{test} \cdot \underline{H}^{inc}) d\Gamma$$

### C2.7 Subdomains Variational Equation Definition

If we apply the Huygens' principle on the homogeneous domain  $\Omega$ , we can operate a subdivision and obtain  $\Omega_i$  subdomains bounded by  $\Gamma_i$  surfaces. Therefore, the equation (C2.23) becomes:

$$\sum_{i=1}^{N_d} R_{\Omega_i}[(\{\underline{J}_a, \underline{M}_a\} + \{\underline{J}_i, \underline{M}_i\}), (\{\underline{J}_i^{test}, \underline{M}_i^{test}\})] = 0 \quad (C2.29)$$

The equation (C2.24) becomes as well:

$$-\sum_{i=1}^{N_i} S(\underline{E}_i^{inc}, \underline{H}_i^{inc}, \underline{j}_i^{test}, \underline{p}_i^{test}) = \sum_{i=1}^{N_d} \mu R_{1i}(\underline{j}_i, \underline{j}_i^{test}) + \frac{k^2}{\mu_r} R_{1i}(\underline{p}_i, \underline{p}_i^{test}) + R_{2i}(\underline{j}_i, \underline{p}_i^{test}) + R_{2i}(\underline{p}_i, \underline{j}_i^{test}) \quad (C2.30)$$

**CHAPTER 3:**  
**SR3D STRUCTURE**

## Chapter 3 - SR3D Structure

In this chapter, we first define the MoM linear system implemented inside the old version of SR3D. Then, we show the new version of SR3D starting from the Rumsey reaction equation found in Chapter 2. We introduce the main linear system expression and then give a detailed description of every term of the linear system (reaction matrix and source vector).

### C3.1 Old SR3D Structure

The old SR3D structure does not prove to be practical to use for the derivation of the mesh owing to the high complexity of the previous implemented expressions. For sake of the completeness, the old SR3D  $A, D, T, F$  operator expressions are shown in equation (C3.1). We consider only the coupling between triangles  $T_K T_L$  related to the impedance matrix (no changes affect the source vector of the MoM linear system) as reported in Figure (C3.1).

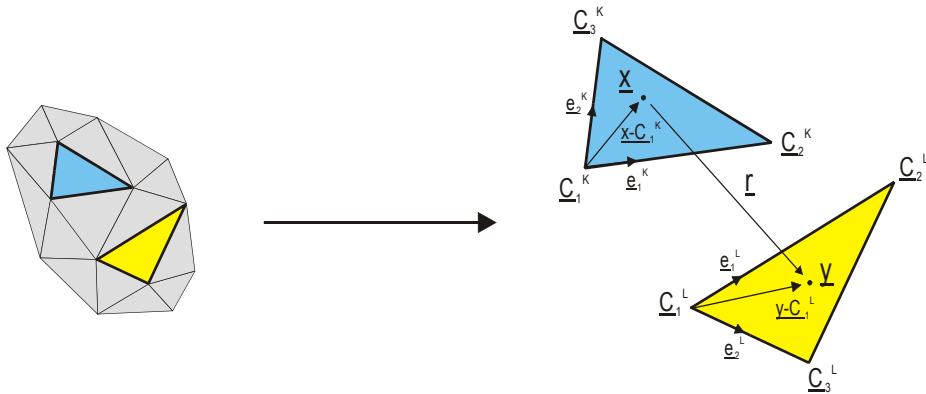


Figure C3.1: Single couple of triangles  $T_K T_L$  from global mesh environment in old SR3D structure

where  $\underline{C}_s^T$  is the summit  $s$  of the generic triangle  $T$ :

$$\underline{C}_s^T = C_{cs}^T = \left[ C_{1s}^T, C_{2s}^T, C_{3s}^T \right] \in \mathfrak{R}^3, \quad c, s = 1, 2, 3$$

and:

$$\underline{r} = (\underline{y} - \underline{x}), \quad r = \|\underline{y} - \underline{x}\|, \quad \underline{x}, \underline{y} \in \mathfrak{R}^3$$

Finally,  $\underline{e}_1^T, \underline{e}_2^T$  together with the vector  $\underline{w} - C_1^T$ , with  $\underline{w} \in \mathfrak{R}^3$  as generic Cartesian point in the tridimensional space, form a vector basis that identifies all the points inside the triangle surface. Then, the old SR3D  $A, D, T, F$  operators are defined in the old basis as follows:

$$\begin{aligned} A_{cs}^{KL}(\phi) &= \oint_{T_K T_L} \oint \phi(\underline{x}, \underline{y}) H_K^t \left[ \tilde{\Theta}^K(\underline{x}) \right]_c \left[ \tilde{\Theta}^L(\underline{y}) \right]_s H_L dy dx \\ D_{cs}^{KL}(\phi) &= H_K \delta_3^c \delta_3^s H_L \oint_{T_K T_L} \oint \phi(\underline{x}, \underline{y}) dy dx \\ T_{cs}^{KL}(\psi) &= \oint_{T_K T_L} \oint \psi(\underline{x}, \underline{y}) H_K^t \Delta_{cs}^{KL}(\underline{x}, \underline{y}) H_L dy dx \\ F_{cs}^{KL}(\phi) &= A_{cs}^{KL}(\phi) - \frac{4}{k^2} D_{cs}^{KL}(\phi) \end{aligned} \quad (C3.1)$$

Let's define all the functions inside the equations C3.1 starting from the Green's function.

$$\phi = \frac{e^{jkr}}{r}, \quad \psi = (jkr - 1) \frac{e^{jkr}}{r^3}$$

where:  $k$  is the wavenumber of the plane wave

Then, we have the terms that depend on the vector basis shown previously and relative to a local coordinate system:

$$\begin{aligned} \tilde{\Theta}^K(\underline{x}) &= \left[ \underline{e}_1^K | \underline{e}_2^K | (\underline{x} - \underline{C}_1^K) \right], & \tilde{\Theta}^L(\underline{y}) &= \left[ \underline{e}_1^L | \underline{e}_2^L | (\underline{y} - \underline{C}_1^L) \right] \\ \tilde{\Delta}_{cs}^{KL}(\underline{x}, \underline{y}) &= \det \left( \text{col}_s(\tilde{\Theta}^L(\underline{y})) \mid \text{col}_c(\tilde{\Theta}^K(\underline{x})) \mid (\underline{y} - \underline{x}) \right) \end{aligned}$$

If we consider the Figure C3.2, we can finally define the matrix  $H^T$ ; considering the generic  $\underline{w} \in \mathfrak{R}^3$  Cartesian point and the generic triangle  $T$ .

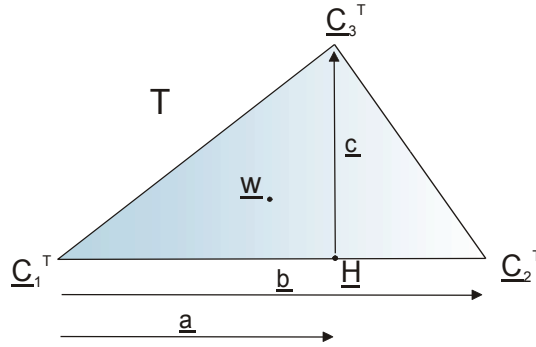


Figure C3.2: triangle  $T$  main geometric variables.

$$\underline{a} = \underline{H} - \underline{C}_1^T, \quad \underline{b} = \underline{C}_2^T - \underline{C}_1^T, \quad \underline{c} = \underline{C}_3^T - \underline{H}$$

$$H_T = \frac{1}{2\Lambda_T} \cdot \begin{pmatrix} -\|\underline{a}\| & 0 & -\|\underline{b}\| \\ -\|\underline{c}\| & 0 & 0 \\ 1 & 1 & 1 \end{pmatrix} \quad \text{and} \quad \Lambda_T = \frac{\|\underline{b}\| \|\underline{c}\|}{2}$$

In order to transform the terms from the local to the global coordinate system, it is necessary to perform the following operations:

$$\begin{aligned} \Theta^K(\underline{x}) &= H_K \tilde{\Theta}^K(\underline{x}), & \Theta^L(\underline{x}) &= \tilde{\Theta}^L(\underline{x}) H_L \\ \Delta_{cs}^{KL}(\underline{x}, \underline{y}) &= H_K \tilde{\Delta}_{cs}^{KL}(\underline{x}, \underline{y}) H_L \end{aligned}$$

The new SR3D version does not consider the local basis transformation to calculate the coupling between triangles coupling. This leads to an easier mathematical expressions of operators  $A, D, T, F$ . See the paragraph C3.2 to compare the differences between the old version and the

new one. We point out that the source vector has not been modified so it is not reported in this paragraph.

### C3.2 New SR3D Structure: General Description

The new SR3D representation is definitely more precise than the old one. Now we start the description from the general expression of the linear system of the MoM, showed as follows:

$$[Z][\Phi] = [S] \quad (C3.2)$$

The reaction matrix  $[Z]$  is related to the mesh elements,  $[\Phi]$  is the vector of the unknown density current fluxes (i.e. the basis function amplitudes, see Annex 2, equation (A2.3)) and  $[S]$  is the vector of the sources. Let's consider the electromagnetic problem shown in Figure (C3.3) where both metallic and dielectric structures are present.

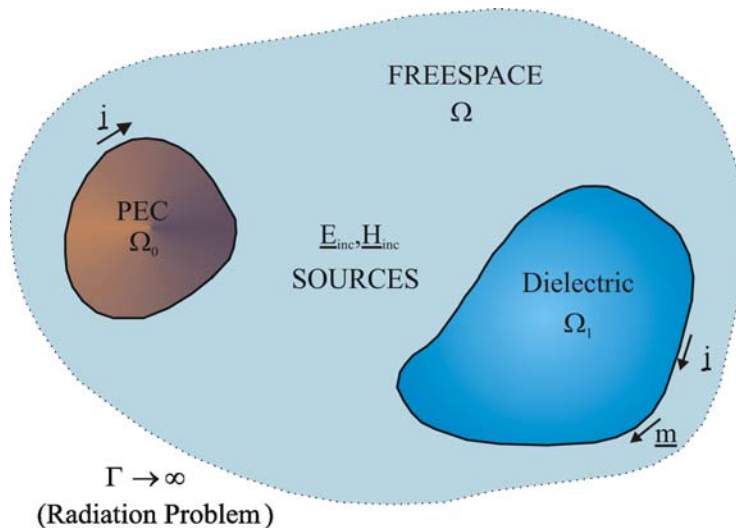


Figure C3.3: Generic electromagnetic problem

In this chapter, we want to focus the attention on one sub-linear system related to a single couple of the mesh basic elements defined in the discretized-domain  $\Omega$ . We consider the same for the reaction of the source over the structure but, only the reaction between the source and one triangle will be taken into account. In the reaction case, these mesh elements are defined as triangles as shown in Figure (C3.4) with the  $T_K$   $T_L$  triangles. This is possible since we can consider the whole reaction as a sum of sub-reactions as reported in equation (C2.24).

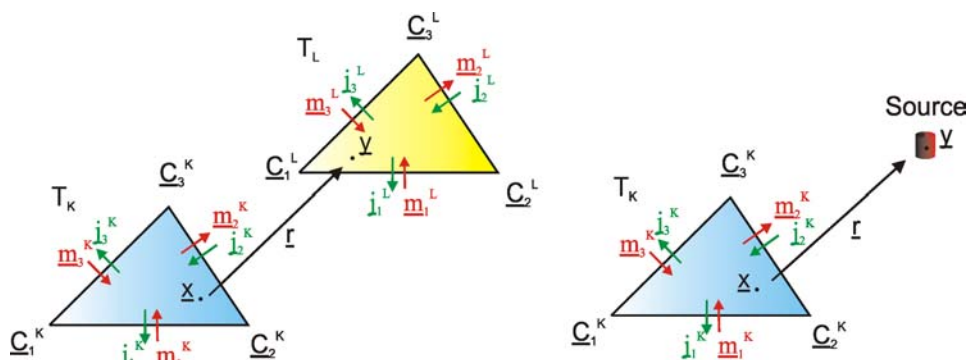


Figure C3.4: Interaction triangle-triangle (right) and triangle-source

Starting from this equation, we can give the Rumsey reaction form related to a single couple of triangles  $T_K T_L$ :

$$-S(\underline{E}^{inc}, \underline{H}^{inc}, \underline{j}^K, \underline{p}^K) = \mu R_1^{KL}(\underline{j}^L, \underline{j}^K) + \frac{k^2}{\mu_r} R_1^{KL}(\underline{p}^L, \underline{p}^K) + R_2^{KL}(\underline{j}^L, \underline{p}^K) + R_2^{KL}(\underline{p}^L, \underline{j}^K) \quad (C3.3)$$

Where the  $R$  and the  $S$  terms are defined in equation (C3.4):

$$\begin{aligned} R_1(\underline{\alpha}^L, \underline{\alpha}^K) &= \oint_{T_K T_L} \oint_{T_K T_L} G(\underline{x}, \underline{y}) (\underline{\alpha}^L(\underline{y}) \cdot \underline{\alpha}^K(\underline{x})) dy dx - \frac{4H_K H_L}{k^2} \oint_{T_K T_L} \oint_{T_K T_L} G(\underline{x}, \underline{y}) dy dx \\ R_2(\underline{\alpha}^L, \underline{\beta}^K) &= \oint_{T_K T_L} \oint_{T_K T_L} ((\nabla_{\underline{y}} G(\underline{x}, \underline{y}) \times \underline{\alpha}^L(\underline{y})) \cdot \underline{\beta}^K(\underline{x})) dy dx \\ S(\underline{E}^{inc}, \underline{H}^{inc}, \underline{j}^K, \underline{p}^K) &= \oint_{T_K} (\underline{E}^{inc} \cdot \underline{j}^K - \underline{p}^K \cdot \underline{H}^{inc}) dx \end{aligned} \quad (C3.4)$$

$$\text{where: } \boxed{H_T = \frac{1}{2\Lambda_T}, \quad \Lambda_T, \text{ triangle T surface}}$$

The equivalent sub-linear system relative to the equation C3.3 for the  $T_K T_L$  triangles is defined as:

$$\begin{bmatrix} Z^{KL} \end{bmatrix} \begin{bmatrix} \Phi^L \end{bmatrix} = \begin{bmatrix} S^K \end{bmatrix} \quad (C3.5)$$

In the following, we describe every term of the equation (C3.5), starting from the reaction matrix  $Z^{KL}$  composed of a part of the  $R$  terms of equation (C3.3); then the source vector will be taken into account.

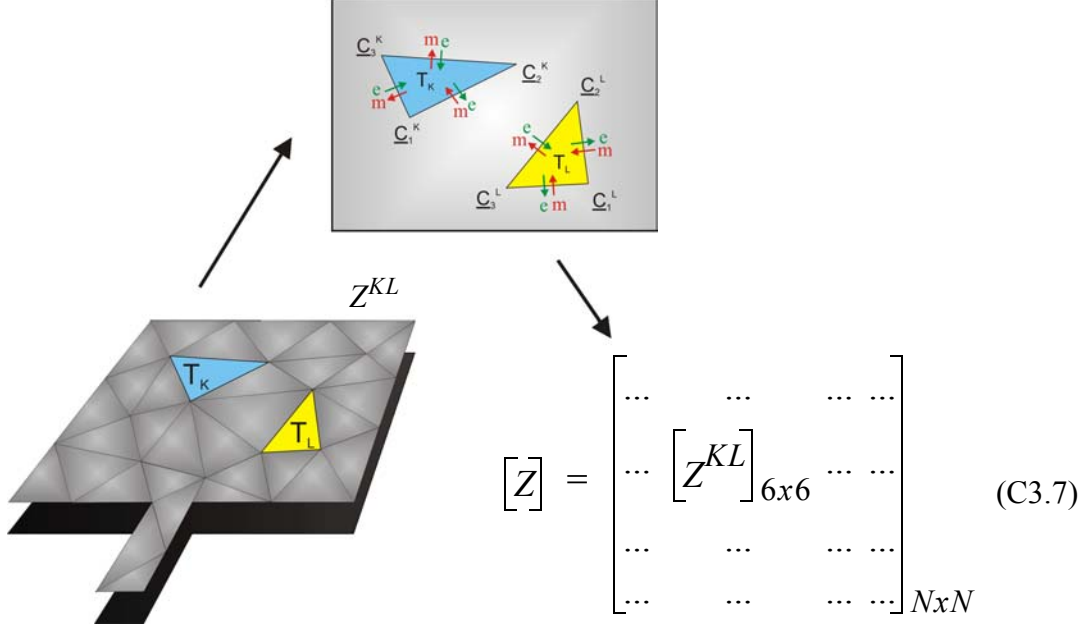
### C3.3 New SR3D Structure: Reaction Matrix

Let us describe the  $Z^{KL}$  matrix of equation (C3.5) representing the coupling effect between a pair of the mesh elements (triangles defined in the discretized-domain  $\Omega$  shown in Figure C3.3). We consider a reaction matrix with two generic triangles (metallic or dielectric, inside  $\Omega$ ), so we obtain a  $6 \times 6$   $Z^{KL}$  matrix as we can see from equation (C3.6).

$$\begin{bmatrix} Z^{KL} \end{bmatrix}_{2C \times 2S} = \begin{bmatrix} \begin{bmatrix} Z_{ee}^{KL} \end{bmatrix}_{C \times S} & \begin{bmatrix} Z_{em}^{KL} \end{bmatrix}_{C \times S} \\ \begin{bmatrix} Z_{me}^{KL} \end{bmatrix}_{C \times S} & \begin{bmatrix} Z_{mm}^{KL} \end{bmatrix}_{C \times S} \end{bmatrix} \quad (C3.6)$$

$$\text{where: } \boxed{\begin{aligned} C, S &= 3 \\ C &= \text{number of cartesian coordinates} \\ S &= \text{number of triangle vertices} \\ e &= \text{electric reaction} \\ m &= \text{magnetic reaction} \end{aligned}}$$

We would like to support equation (C3.6) with the figure below since this is an important theoretical point. We also try to match the pure mathematical treatment to a real electromagnetic problem. So in equation (C3.7), we represent the reaction matrix relative to a couple of triangles  $T_K T_L$  defined on the surface of a patch antenna ( $[Z]$  is the whole reaction matrix given in equation (C3.2)).



The  $Z$  matrix is composed of  $N$  rows and  $N$  columns, where  $N$  is the number of degrees of freedom of the entire structure. As first step, we define the terms of the matrix  $Z^{KL}$  reported in equation (C3.6). Let's consider the triangles  $T_K T_L$ , we define all the geometry variables (see Figure (C3.4)).

$$\begin{aligned} \underline{r} &= (\underline{y} - \underline{x}), \quad r = \|\underline{y} - \underline{x}\|, \quad \underline{x}, \underline{y} \in T_K, T_L \in \mathfrak{R}^3 \\ \underline{x} &= [x_1, x_2, x_3], \quad \underline{y} = [y_1, y_2, y_3] \\ \underline{C}_s^T &= C_{cs}^T = [C_{1s}^T, C_{2s}^T, C_{3s}^T] \in \mathfrak{R}^3, \quad c, s = 1, 2, 3 \end{aligned} \quad (C3.8)$$

where:  $c$  is the Cartesian coordinate index and  $s$  is the vertex index number

Then, the terms of the matrix  $Z^{KL}$  are defined as follows:

$$\begin{aligned} [Z_{ee}^{KL}]_{CxS} &= \mu [R_{ee}^{KL}]_{CxS} I_{se} \\ [Z_{me}^{KL}]_{CxS} &= [R_{me}^{KL}]_{CxS} I_{se} \\ [Z_{me}^{KL}]_{CxS} &= [R_{me}^{KL}]_{CxS} I_{sm} \\ [Z_{mm}^{KL}]_{CxS} &= \frac{k^2}{\mu} [R_{mm}^{KL}]_{CxS} I_{sm} \end{aligned} \quad (C3.9)$$

Where  $\mu$  is the magnetic permeability of the materials,  $k$  the wavenumber of the electromagnetic radiation and the  $I$  terms are the coupling terms (-1 or +1), related to the degrees of freedom, needed to represent the global reaction matrix. Finally we can find the  $R$  reaction terms in equation (C3.3). The first and the last terms in equation (C3.9) are related to  $R_1$  term and the others to  $R_2$  term. In other words, using this reference we, can explicit these terms as follows:

$$\begin{aligned} R_{ee}^{KL}, R_{mm}^{KL} &\leftrightarrow R_{1\alpha\alpha}^{KL} \quad \text{same kind of current in the reaction, ee or mm} \\ R_{em}^{KL}, R_{me}^{KL} &\leftrightarrow R_{2\alpha\beta}^{KL} \quad \text{different kind of current in the reaction, em or me} \end{aligned} \quad (\text{C3.10})$$

The complete expression of these terms are given in equation (C3.4).

Let's now define the new SR3D  $A, D, T$  operators (to compare with the old version in equation (C3.1)) used inside the terms in equation (C3.3). They are defined as follows:

$$\begin{aligned} A^{KL}(G) &= \oint \oint G(\underline{x}, \underline{y}) (\underline{\alpha}^L(\underline{y}) \cdot \underline{\alpha}^K(\underline{x})) dy dx \\ D^{KL}(G) &= \overset{T_K T_L}{H_K H_L} \oint \oint G(\underline{x}, \underline{y}) dy dx \\ T^{KL}(G) &= \overset{T_K T_L}{\oint \oint} ((\underline{\nabla}_{\underline{y}} G(\underline{x}, \underline{y}) \times \underline{\alpha}^L(\underline{y})) \cdot \underline{\beta}^K(\underline{x})) dy dx \end{aligned} \quad (\text{C3.11})$$

$$\text{where: } \boxed{G = \frac{e^{jkr}}{r}, \quad r = \|\underline{y} - \underline{x}\|}$$

We can operate a further modification of these operators. Let's define the extended form of the basis  $\underline{\alpha}$  and  $\underline{\beta}$  for the triangles  $T_K, T_L$  (see Annex 2) and the mixed product defined inside the  $T(\ )$  operator:

$$\begin{aligned} [\Theta^K(\underline{x})] &= \underline{\alpha}^K = \underline{\beta}^K = [H_K(\underline{C}_3x) | H_K(\underline{C}_1x) | H_K(\underline{C}_2x)] \\ [\Theta^L(\underline{y})] &= \underline{\alpha}^L = \underline{\beta}^L = [H_L(\underline{C}_3y) | H_L(\underline{C}_1y) | H_L(\underline{C}_2y)] \\ [\Delta^{KL}(\underline{x}, \underline{y})] &= [\underline{\nabla}_{\underline{y}} G(\underline{x}, \underline{y}) \times \underline{\alpha}^L(\underline{y})] \cdot \underline{\beta}^K(\underline{x}) \end{aligned} \quad (\text{C3.12})$$

$$\text{where: } \boxed{\begin{aligned} H_K &= \frac{1}{2\Lambda_K}, & \Lambda_K &, \text{ surface triangle K} \\ H_L &= \frac{1}{2\Lambda_L}, & \Lambda_L &, \text{ surface triangle L} \end{aligned}}$$

As we can see from equation (C3.12), we can define the  $\Theta^T$  matrix through the product between the  $H$  terms and a new matrix  $B^T$ :

$$\begin{aligned} \left[ \Theta^K(\underline{x}) \right] &= H_K \left[ (\underline{C}_3x) | (\underline{C}_1x) | (\underline{C}_2x) \right] = H_K \left[ B^K(\underline{x}) \right] \\ \left[ \Theta^L(\underline{y}) \right] &= H_L \left[ (\underline{C}_3y) | (\underline{C}_1y) | (\underline{C}_2y) \right] = H_L \left[ B^L(\underline{y}) \right] \end{aligned} \quad (C3.13)$$

$$\text{where: } \boxed{\begin{aligned} B^K(\underline{x}) &= \left[ (\underline{C}_3x) | (\underline{C}_1x) | (\underline{C}_2x) \right] \\ B^L(\underline{y}) &= \left[ (\underline{C}_3y) | (\underline{C}_1y) | (\underline{C}_2y) \right] \end{aligned}}$$

About the  $\Delta^{KL}$  term, we can write, according to equations (C3.8) and (C3.13):

$$\text{with: } \phi(r) = G(r) = \frac{e^{jkr}}{r}, \quad \psi(r) = \frac{\partial \phi(r)}{\partial r} = (jkr - 1) \frac{e^{jkr}}{r^3},$$

$$\underline{\nabla} G(r) = \underline{\nabla} \phi(r) = \psi(r) \cdot r$$

We obtain:

$$\begin{aligned} \left[ \Delta^{KL}(\underline{x}, \underline{y}) \right]_{cs} &= \psi(r) \cdot r \times H_L \left[ B^L(\underline{y}) \right]_s \cdot H_K \left[ B^K(\underline{x}) \right]_c = \\ &= \psi(r) \left\{ H_K \left[ B^K(\underline{x}) \right]_c \times H_L \left[ B^L(\underline{y}) \right]_s \right\} \cdot r = H_K H_L \psi(r) \left[ \Omega^{KL}(\underline{x}, \underline{y}) \right]_{cs} \end{aligned} \quad (C3.14)$$

$$\left[ \Omega^{KL}(\underline{x}, \underline{y}) \right]_{cs} = \det \left( \begin{array}{c|c|c} \text{col}_s \left[ B^L(\underline{y}) \right] & \text{col}_c \left[ B^K(\underline{x}) \right] & \left[ \underline{y} - \underline{x} \right] \end{array} \right)$$

$$\text{where: } \boxed{\left[ B^T(\underline{w}) \right]_i = \text{col}_i \left[ B^T(\underline{w}) \right]}$$

Now we are ready to define a more convenient form for  $A$ ,  $D$ ,  $T$  operators. Their new forms are given in equation (C3.15) ( $c$  and  $s$  are the matrix cell indices):

$$\begin{aligned} \left[ A^{KL}(\phi) \right]_{cs} &= H_K H_L \oint_{T_K T_L} \oint \phi(\underline{x}, \underline{y}) \left[ B^K(\underline{x}) \right]_c^t \left[ B^L(\underline{y}) \right]_s dy dx \\ \left[ D^{KL}(\phi) \right]_{cs} &= H_K H_L \oint_{T_K T_L} \oint \phi(\underline{x}, \underline{y}) dy dx \\ \left[ T^{KL}(\psi) \right]_{cs} &= H_K H_L \oint_{T_K T_L} \oint \psi(\underline{x}, \underline{y}) \left[ \Omega^{KL}(\underline{x}, \underline{y}) \right]_{cs} dy dx \end{aligned} \quad (C3.15)$$

$$\text{where: } \boxed{\begin{aligned} c, s &= 1, 2, 3 \\ c &= \text{Cartesian coordinates index} \\ s &= \text{triangle vertex index} \end{aligned}}$$

This represent a good result because the reaction expressions are defined now in a very clear way. Then it would be easier to find out their derivatives with respect to both mesh and frequency variables. We want to emphasize an aspect about the frequency derivative: as we can notice the frequency dependance concerns only the Green's function kernels (i.e.  $\phi, \psi$ , see equation (C3.14)). That is convenient because in this case we only need to derivate the kernels with respect to the frequency to obtain the derivatives. In order to do that, we need a further passage in equation (C3.9) using the linearity of operators  $A, D, T$ .

$$\begin{aligned}
\left[ Z_{ee}^{KL} \right]_{cs} &= \mu \left\{ \left[ A^{KL}(\phi) \right]_{cs} - \frac{4}{k^2} \left[ D^{KL}(\phi) \right]_{cs} \right\} I_{se_{cs}} = \mu \left\{ \left[ A^{KL}(\phi) \right]_{cs} + \left[ D^{KL}(-4k^{-2}\phi) \right]_{cs} \right\} I_{se_{cs}} \\
\left[ Z_{em}^{KL} \right]_{cs} &= \left[ T^{KL}(\psi) \right]_{cs} I_{se_{cs}} \\
\left[ Z_{me}^{KL} \right]_{cs} &= \left[ T^{KL}(\psi) \right]_{cs} I_{sm_{cs}} \\
\left[ Z_{mm}^{KL} \right]_{cs} &= \frac{k^2}{\mu} \left\{ \left[ A^{KL}(\phi) \right]_{cs} - \frac{4}{k^2} \left[ D^{KL}(\phi) \right]_{cs} \right\} I_{sm_{cs}} = \frac{1}{\mu} \left\{ \left[ A^{KL}(k^2\phi) \right]_{cs} - 4 \left[ D^{KL}(\phi) \right]_{cs} \right\} I_{sm_{cs}}
\end{aligned} \tag{C3.16}$$

We can notice from equation (C3.16) that we obtain a total of four different Green's function kernels without changing anything in the  $A, D, T$  operators definition. These new four kernels are defined, according to the equations (C3.8), as follows:

$$\begin{aligned}
\phi &= \frac{e^{jkr}}{r}, & \psi &= (jkr - 1) \frac{e^{jkr}}{r^3}, \\
\Gamma &= -\frac{4}{k^2} \frac{e^{jkr}}{r}, & \chi &= k^2 \frac{e^{jkr}}{r}
\end{aligned} \tag{C3.17}$$

Finally, we have the following discrete expressions for the  $Z_{xx}^{KL}$  terms:

$$\begin{aligned}
\left[ Z_{ee}^{KL} \right]_{cs} &= \mu \left\{ \left[ A^{KL}(\phi) \right]_{cs} + \left[ D^{KL}(\Gamma) \right]_{cs} \right\} I_{se_{cs}} \\
\left[ Z_{em}^{KL} \right]_{cs} &= \left[ T^{KL}(\psi) \right]_{cs} I_{se_{cs}} \\
\left[ Z_{me}^{KL} \right]_{cs} &= \left[ T^{KL}(\psi) \right]_{cs} I_{sm_{cs}} \\
\left[ Z_{mm}^{KL} \right]_{cs} &= \frac{1}{\mu} \left\{ \left[ A^{KL}(\chi) \right]_{cs} - 4 \left[ D^{KL}(\phi) \right]_{cs} \right\} I_{sm_{cs}}
\end{aligned} \tag{C3.18}$$

### C3.4 New SR3D Structure: Source Vector

The source vector of the linear system takes into account the sources defined inside the analysis domain. We define for the moment the source reaction with one generic triangle (metallic or dielectric). We obtain a  $6 S^K$  vector size as we can see from equation (C3.19). We consider an electric dipole as source for the scattering problems.

*C3.4.1 Source Vector Dipole:* we consider the reaction between a source dipole in freespace and a single triangle of the mesh since this is true for every triangle of the discretized structure. So let's describe the vector  $S^K$  that is the source vector of equation (C3.5) representing the cou-

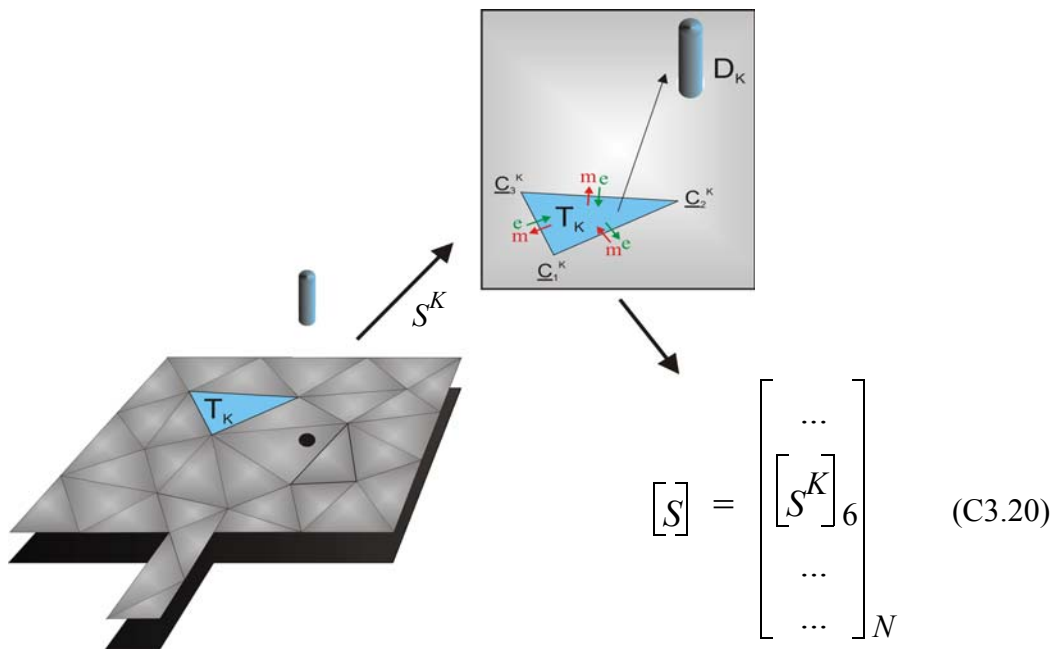
pling effect between a source dipole  $D_K$  and a triangle  $T_K$  of the mesh (triangle defined in the discretized-domain  $\Omega$  shown in Figure C3.3).

$$[S^K]_{2Cx1} = \begin{bmatrix} [S^K]_{Cx1} \\ [S^K]_{Cx1} \end{bmatrix} \quad (C3.19)$$

where:

$C = 3$
$C =$ number of cartesian coordinates
$e =$ electric reaction
$m =$ magnetic reaction

We would support the equation (C3.19) with the figure below since this is an important theoretical point. In equation (C3.20) we represent the source vector reaction over a triangles  $T_K$  defined on the surface of a patch antenna ( $[S]$  is the whole source vector in equation (C3.2)). We assume that the dipole never lies on the triangle surface.



The  $S$  vector is composed of  $N$  columns which is the number of degrees of freedom of the entire structure. So we define the terms of the vector  $S^K$  given in equation (C3.19). Let's consider the triangle  $T_K$  and the dipole  $D_K$ , we define all the geometry variables (see Figure C3.4).

$$\begin{aligned} \underline{r} &= (\underline{x} - \underline{y}^D), \quad r = \|\underline{x} - \underline{y}^D\|, \quad \underline{x} \in T_K \in \mathfrak{R}^3, \quad \underline{y}^D \in D_K \in \mathfrak{R}^3 \\ \underline{x} &= [x_1, x_2, x_3], \quad \underline{y}^D = [y_1^D, y_2^D, y_3^D] \\ \underline{C}_s^K &= C_{cs}^K = [C_{1s}^K, C_{2s}^K, C_{3s}^K] \in \mathfrak{R}^3, \quad c, s = 1, 2, 3 \end{aligned} \quad (C3.21)$$

where:  $c$  is the Cartesian coordinate index and  $s$  is the vertex index number

Then the terms of the vector  $S^K$ , relative to an electric dipole source, in according to the equations (C3.13), (C3.14) and (C3.21), are defined as follows:

$$\begin{aligned} \left[ S_e^K(\underline{m}^D, \underline{y}^D) \right]_c &= -\mu \oint_{T_K} \phi(\underline{x}, \underline{y}^D) \left\{ \left[ \Theta^K(\underline{x}) \right]_c \underline{m}_t^D(\underline{x}, \underline{y}^D) + \right. \\ &\quad \left. + \frac{1}{k \|\underline{x} - \underline{y}^D\|} \left( j - \frac{1}{k \|\underline{x} - \underline{y}^D\|} \right) \left( 2 \left[ \Theta^K(\underline{x}) \right]_c \underline{m}^D - 3 \left[ \Theta^K(\underline{x}) \right]_c \underline{m}_t^D(\underline{x}, \underline{y}^D) \right) \right\} dx \end{aligned} \quad (C3.22)$$

$$\left[ S_m^K(\underline{m}^D, \underline{y}^D) \right]_c = -\mu \oint_{T_K} \psi(\underline{x}, \underline{y}^D) \left[ \varepsilon^K(\underline{x}, \underline{y}^D) \right]_c dx$$

where: $\left[ \varepsilon^K(\underline{x}, \underline{y}^D) \right]_c = \det \left( \text{col}_c \left[ \Theta^L(\underline{y}) \right] \mid \underline{m}^D \mid \underline{r} \right)$ $\underline{m}^D = [m_1^D, m_2^D, m_3^D]$ , dipole D with dipole moment $\underline{m}^D$ $\underline{m}_t^D(\underline{x}, \underline{y}^D) = \underline{m}^D - \left[ \underline{m}^D \cdot \left( \frac{\underline{r}}{r} \right) \right] \cdot \left( \frac{\underline{r}}{r} \right)$ , dipole D trasversal dipolar moment $\underline{m}_t^D$
---

According to equation (C3.13), we can reduce the term  $\varepsilon^K$  in a similar way as already done for the term  $\Delta^{KL}$  in equation (C3.14):

$$\left[ \varepsilon^K(\underline{x}, \underline{y}^D) \right]_c = \det \left( \text{col}_c \left[ \Theta^L(\underline{y}) \right] \mid \underline{m}^D \mid \underline{r} \right) = H_K \left[ \Upsilon^K(\underline{x}, \underline{y}^D) \right]_c \quad (C3.23)$$

with: $\left[ \Upsilon^K(\underline{x}, \underline{y}^D) \right]_c = \det \left( \text{col}_c \left[ B^K(\underline{x}) \right] \mid \underline{m}^D \mid \underline{r} \right)$
--

According to equations (C3.14) and (C3.23), we obtain the reduced form for the source vector terms:

$$\begin{aligned} \left[ S_e^K(\underline{m}^D, \underline{y}^D) \right]_c &= -\mu H_K \oint_{T_K} \phi(\underline{x}, \underline{y}^D) \left\{ \left[ B^K(\underline{x}) \right]_c \underline{m}_t^D(\underline{x}, \underline{y}^D) + \right. \\ &\quad \left. + \frac{1}{k \|\underline{x} - \underline{y}^D\|} \left( j - \frac{1}{k \|\underline{x} - \underline{y}^D\|} \right) \left( 2 \left[ B^K(\underline{x}) \right]_c \underline{m}^D - 3 \left[ B^K(\underline{x}) \right]_c \underline{m}_t^D(\underline{x}, \underline{y}^D) \right) \right\} dx \end{aligned} \quad (C3.24)$$

$$\left[ S_m^K(\underline{m}^D, \underline{y}^D) \right]_c = -\mu H_K \oint_{T_K} \psi(\underline{x}, \underline{y}^D) \left[ \Upsilon^K(\underline{x}, \underline{y}^D) \right]_c dx$$

### C3.5 New SR3D Structure: Reaction Matrix Discretization

Since now we have treated the theoretical issue from an analytical point of view. We want now to show the discretized form for the  $A, D, T$  operators and  $Z_{xx}^{KL}$  terms. The discretization is based on the seven-points Gauss discretization method (see Annex 1).

Remembering that we defined the normalized Gauss method weights  $\gamma_T$  for a generic discretization point defined inside the triangle  $T$ :

$$\gamma_w = \alpha_w \Lambda_T = \frac{\alpha_w}{2H_T} \quad (\text{C3.25})$$

where:  $\alpha_w =$  not-normalized Gauss weight for the  $w$  point

See Annex 2 to find out the  $\Lambda_T$  normalization term definition. Then the discrete form of a generic Green's function kernel  $G(\ )$  is:

$$G(\underline{x}, \underline{y}) = \sum_k \sum_l \gamma_k \gamma_l G(\underline{x}_k, \underline{y}_l) = \frac{1}{4H_K H_L} \sum_k \sum_l \gamma_k \gamma_l G(\underline{x}_k, \underline{y}_l) \quad (\text{C3.26})$$

We can apply this discretization to every kernel reported in equation (C3.17). Then, the discrete form of the triangles  $T_K T_L$  with a seven-point Gauss method representation is shown in Figure C3.5, according to equation (C3.25).

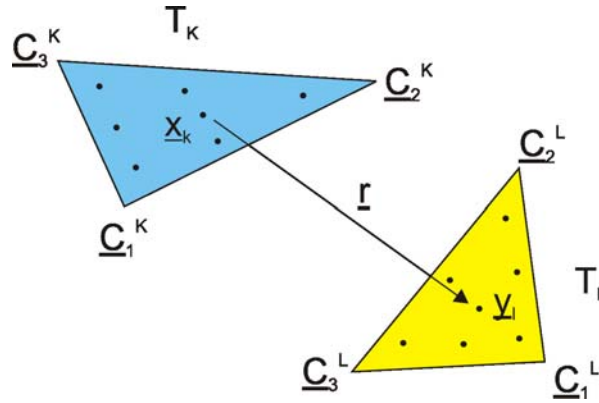


Figure C3.5: Discrete  $T_K T_L$  coupling terms using a 7-point Gauss discretization method

According to the equation (C3.15), and Figure C3.5, the discrete form of the  $A$ ,  $D$ ,  $T$  operators is:

$$\begin{aligned} \left[ A^{KL}(g_1) \right]_{cs} &= H_K H_L \frac{1}{4H_K H_L} \sum_k \sum_l \alpha_k \alpha_l g_1(\underline{x}_k, \underline{y}_l) \left[ B^K(\underline{x}_k) \right]_c^t \left[ B^L(\underline{y}_l) \right]_s \\ \left[ D^{KL}(g_2) \right]_{cs} &= H_K H_L \frac{1}{4H_K H_L} \sum_k \sum_l \alpha_k \alpha_l g_2(\underline{x}_k, \underline{y}_l) \\ \left[ T^{KL}(g_3) \right]_{cs} &= H_K H_L \frac{1}{4H_K H_L} \sum_k \sum_l \alpha_k \alpha_l g_3(\underline{x}_k, \underline{y}_l) \left[ \Omega^{KL}(\underline{x}_k, \underline{y}_l) \right]_{cs} \end{aligned} \quad (\text{C3.27})$$

where:

$$g_1(\underline{x}_k, \underline{y}_l) = \begin{bmatrix} \phi(\underline{x}_k, \underline{y}_l) \\ \chi(\underline{x}_k, \underline{y}_l) \end{bmatrix}, \text{ along with } g_2(\underline{x}_k, \underline{y}_l) = \begin{bmatrix} \Gamma(\underline{x}_k, \underline{y}_l) \\ \phi(\underline{x}_k, \underline{y}_l) \end{bmatrix}$$

$$g_3(\underline{x}_k, \underline{y}_l) = \begin{bmatrix} \psi(\underline{x}_k, \underline{y}_l) \end{bmatrix}$$

As we can see, we can propose a reduced form as follows

$$\begin{aligned}
 \left[ A^{KL}(g_1) \right]_{cs} &= \frac{1}{4} \sum_k \sum_l \alpha_k \alpha_l g_1(x_k, y_l) \left[ B^K(x_k) \right]_c^t \left[ B^L(y_l) \right]_s \\
 \left[ D^{KL}(g_2) \right]_{cs} &= \frac{1}{4} \sum_k \sum_l \alpha_k \alpha_l g_2(x_k, y_l) \\
 \left[ T^{KL}(g_3) \right]_{cs} &= \frac{1}{4} \sum_k \sum_l \alpha_k \alpha_l g_3(x_k, y_l) \left[ \Omega^{KL}(x_k, y_l) \right]_{cs}
 \end{aligned} \tag{C3.28}$$

Finally, we present the discrete form for the  $Z_{xx}^{KL}$  terms:

$$\begin{aligned}
 \left[ Z_{ee}^{KL} \right]_{cs} &= \mu \left\{ \left[ A^{KL}(\phi) \right]_{cs} + \left[ D^{KL}(\Gamma) \right]_{cs} \right\} I_{se_{cs}} \\
 \left[ Z_{em}^{KL} \right]_{cs} &= \left[ T^{KL}(\psi) \right]_{cs} I_{se_{cs}} \\
 \left[ Z_{me}^{KL} \right]_{cs} &= \left[ T^{KL}(\psi) \right]_{cs} I_{sm_{cs}} \\
 \left[ Z_{mm}^{KL} \right]_{cs} &= \frac{1}{\mu} \left\{ \left[ A^{KL}(\chi) \right]_{cs} - 4 \left[ D^{KL}(\phi) \right]_{cs} \right\} I_{sm_{cs}}
 \end{aligned} \tag{C3.29}$$

The presented Rumsey reaction discrete form will be used to calculate the relative derivative expressions with respect to both geometry mesh and frequency. In the following, we will show two different kinds for the numerical implementation of the expressions of equation (C3.29), that will allow to us to treat the singularity issue inside the Green's function kernels and to optimize the computation speed as well.

### C3.6 New SR3D Structure: Sources Vector Discretization

As we did for the reaction matrix, we want now to show the discretized form for the  $S$  vector. The discretization is also based on the seven-points Gauss discretization method (see Annex 1). We consider an electric dipole as source for the scattering problems.

*C3.6.1 Source Vector Dipole Implementation:* we can apply the Gauss discretization method to all the terms reported in equation (C3.24), according to equation (C3.25). Then, the dipole  $D_K$  and the triangle  $T_K$  discrete form with a seven-point Gauss method representation is shown in Figure C3.6.

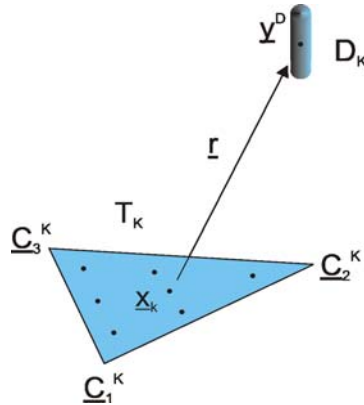


Figure C3.6: Discrete  $T_K D_K$  coupling terms using a 7-point Gauss discretization method

According to equations (C3.14), (C3.21), (C3.23) and Figure C3.6, we obtain the reduced form for the source vector terms:

$$\begin{aligned} \left[ S_e^K(\underline{m}^D, \underline{y}^D) \right]_c &= -\mu H_K \frac{1}{2H_K} \sum_k \alpha_k g_1(\underline{x}_k, \underline{y}^D) \left\{ \left[ B^K(\underline{x}_k) \right]_c^t \underline{m}_t^D(\underline{x}_k, \underline{y}^D) + \right. \\ &\quad \left. + \frac{1}{k \|\underline{x}_k - \underline{y}^D\|} \left( j - \frac{1}{k \|\underline{x} - \underline{y}^D\|} \right) \left( 2 \left[ B^K(\underline{x}_k) \right]_c^t \underline{m}^D - 3 \left[ B^K(\underline{x}_k) \right]_c^t \underline{m}_t^D(\underline{x}_k, \underline{y}^D) \right) \right\} \end{aligned} \quad (C3.30)$$

$$\left[ S_m^K(\underline{m}^D, \underline{y}^D) \right]_c = -\mu H_K \frac{1}{2H_K} \sum_k \alpha_k g_3(\underline{x}_k, \underline{y}^D) \left[ \Upsilon^K(\underline{x}_k, \underline{y}^D) \right]_c$$

$$\text{where: } \begin{cases} g_1(\underline{x}_k, \underline{y}^D) = \phi(\underline{x}_k, \underline{y}^D) \\ g_3(\underline{x}_k, \underline{y}^D) = \psi(\underline{x}_k, \underline{y}^D) \end{cases}$$

And we propose the following reduced form

$$\begin{aligned} \left[ S_e^K(\underline{m}^D, \underline{y}^D) \right]_c &= -\frac{\mu}{2} \sum_k \alpha_k g_1(\underline{x}_k, \underline{y}^D) \left\{ \left[ B^K(\underline{x}_k) \right]_c^t \underline{m}_t^D(\underline{x}_k, \underline{y}^D) + \right. \\ &\quad \left. + \frac{1}{k \|\underline{x}_k - \underline{y}^D\|} \left( j - \frac{1}{k \|\underline{x} - \underline{y}^D\|} \right) \left( 2 \left[ B^K(\underline{x}_k) \right]_c^t \underline{m}^D - 3 \left[ B^K(\underline{x}_k) \right]_c^t \underline{m}_t^D(\underline{x}_k, \underline{y}^D) \right) \right\} \end{aligned} \quad (C3.31)$$

$$\left[ S_m^K(\underline{m}^D, \underline{y}^D) \right]_c = -\frac{\mu}{2} \sum_k \alpha_k g_3(\underline{x}_k, \underline{y}^D) \left[ \Upsilon^K(\underline{x}_k, \underline{y}^D) \right]_c$$

**CHAPTER 4:**  
**SR3D IMPLEMENTATION**

## Chapter 4 - SR3D Implementation

In Chapter 3, we gave the expressions of the MoM linear system, detailing the reaction between a single couple of triangles for the reaction matrix and the reaction between a triangle of the mesh and a source point with respect to the source vector or second member of the linear system (see the equations (C3.7) and (C3.20) for the relative references). In Chapter 4, we show how to numerically implement these discrete equations. The numerical code has been developed entirely in Fortran 77 language.

We have developed two numerical techniques for computing the expressions given in equation (C3.29) and (C3.31). Each technique has some advantages with respect to the relative position of every single couple of triangles  $T_K T_L$  in the 3D space. The first technique is based on the Full-Numerical (FN) technique of the reaction integrals meaning that every mesh integral is calculated using the gaussian quadrature method. The second technique is based on the Semi-Numerical (SN) method where one of the two reaction integrals is calculated analytically and the second one computed using the gaussian quadrature method. In the continuation, a preliminary description of these two techniques, is reported:

*Full Numerical Technique:* this technique is used when the triangles of the couple  $T_K T_L$  are electrically far from each other; is called FAR configuration. The FN technique cannot be applied when the triangles are electrically too close owing to the fact that it will produce a decrease of the computational speed of the integral computation or, in the worse case, when they are superimposed and a singularity inside the Green's function kernels (see equation (C3.17)) appears making even impossible the use of this technique.

The FN implementation is also used for the computation of the source vector, since no singularity appears as the source may be defined on a side of the triangles for a voltage source or never on the structure surface in case of an electrical dipole.

*Semi Numerical Technique:* as already said in the FN technique summary, the SN implementation has been developed in order to be able to treat both electrical CLOSE configurations, increasing the speed of the integral computation, and SINGULAR configurations, when the couple of triangles are superimposed (i.e.  $T_K \equiv T_L$  and  $\mathbf{r} = (\mathbf{x}_l - \mathbf{x}_k) = \mathbf{0}$ , see equation C3.5 for the references). In this development the SN technique can be only applied for coplanar couple of triangles.

The SN technique is convenient as it is faster than the FN implementation for CLOSE configuration; that's because as the distance between two triangles decreases the number of discretization Gauss points increases in order to maintain the same accuracy of results for FN technique. It is clear that when the number of Gauss points starts to be considerable, the computational speed will decrease critically; that's why in that case we prefer to use, the SN implementation.

On the other hand, the SN technique is strictly needed if the triangles are superimposed. In the SUPERIMPOSED case, the SN implementation operates on the Green's function factorization in order to separate the singular part from the regular one. The singular part is treated with a special analytic reduction method whereas the regular part is treated using the Taylor expansion. No SN implementation is used for the computation of the source vector, since no singularity is appearing.

Let's define all the relative positions that may occur for the numerical computation of the reaction matrix in Figure C4.1 and of the source vector in Figure C4.2. We fix a threshold value, called  $D$ , in order to choose which technique to be used between FN and SN. We use this threshold with respect to the barycenters  $\underline{b}$  of the triangles (see figures below).

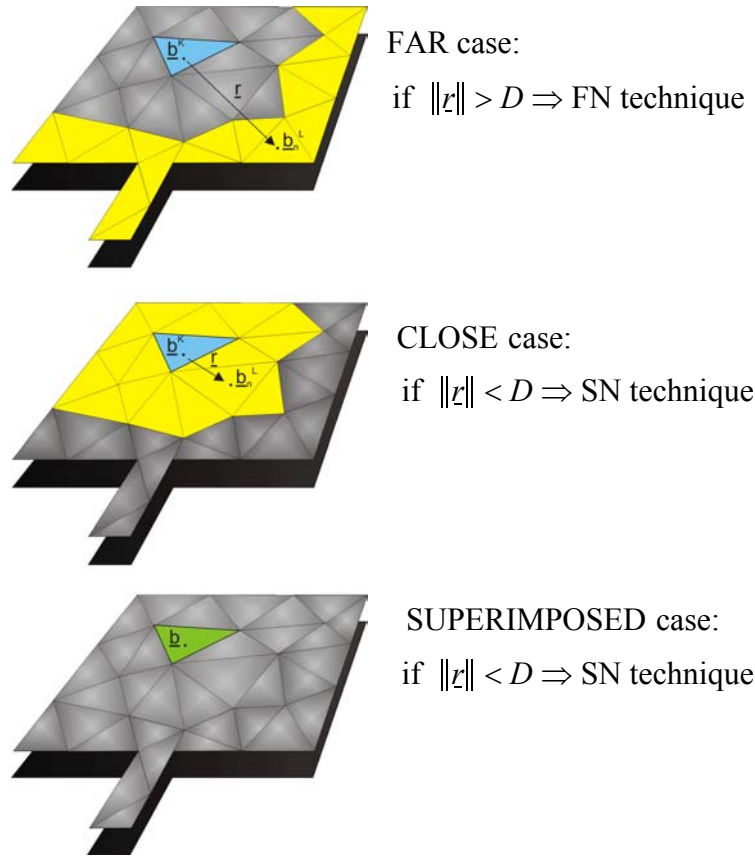


Figure C4.1: Definition of the relative distance for triangles  $T_K T_L$  for the reaction matrix computation

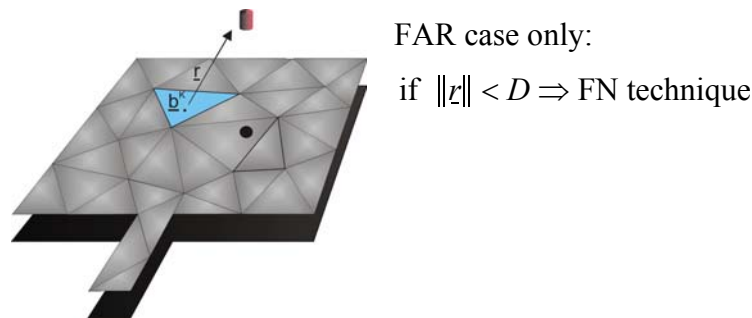


Figure C4.2: Definition of the relative distance for triangle  $T_K$  and a source point for the source vector computation

We must emphasize that only coplanar structures can be studied for the moment owing to the implementation of the SN technique. We will explain and clarify this issue in the following.

### C4.1 Full-Numerical Technique

In Chapter 3, we gave the theoretical expression of both the reaction matrix and source vector. Now we want to describe the numerical implementation of the equations (C3.28), (C3.29) and (C3.31) for the Full-Numerical technique.

*C4.1.1 Reaction Matrix:* the goal is to compute the reaction terms of equation (C3.29) for a single couple of triangles using the Full-Numerical technique. According to Figure (C3.5), equations (C3.8), (C3.15) and equations (C3.27) and (C3.28) (reported in equation (C4.1)), we will describe the terms forming the  $A, D, T$  operators. This technique is easy to apply as all the terms appearing in equation (C4.1) are defined, we only need to perform a double summation for each operator.

$$\begin{aligned} \left[ A^{KL}(g_1) \right]_{cs} &= \frac{1}{4} \sum_k \sum_l \alpha_k \alpha_l g_1(\underline{x}_k, \underline{y}_l) \left[ B^K(\underline{x}_k) \right]_c^t \left[ B^L(\underline{y}_l) \right]_s \\ \left[ D^{KL}(g_2) \right]_{cs} &= \frac{1}{4} \sum_k \sum_l \alpha_k \alpha_l g_2(\underline{x}_k, \underline{y}_l) \\ \left[ T^{KL}(g_3) \right]_{cs} &= \frac{1}{4} \sum_k \sum_l \alpha_k \alpha_l g_3(\underline{x}_k, \underline{y}_l) \left[ \Omega^{KL}(\underline{x}_k, \underline{y}_l) \right]_{cs} \end{aligned} \quad (C4.1)$$

Let's start from the  $\alpha_K$  and  $\alpha_L$  Gauss weights (see Annex 1), they appear inside the integrals as follows (where  $k, l$  are the number of gaussian quadrature points):

$$\begin{aligned} \underline{\alpha}^K(f) &= \Lambda(T_K) \cdot \sum_k \alpha_k \cdot b(\underline{x}_k) \\ \underline{\alpha}^L(f) &= \Lambda(T_L) \cdot \sum_l \alpha_l \cdot b(\underline{y}_l) \end{aligned} \quad (C4.2)$$

with:	$\Lambda(T_K), \Lambda(T_L)$	triangle surfaces
	$b(\ )$	MoM basis function
	$\alpha_k, \alpha_l$	Gauss unweighted coefficients
	$\underline{x}_k, \underline{y}_l$	Gauss points in $T_K, T_L \in \mathfrak{R}^3$

We have the  $g_i$  Green's function kernels in equation (C4.3):

$$\begin{aligned} \phi(\underline{x}_k, \underline{y}_l) &= \frac{e^{jk \|\underline{y}_l - \underline{x}_k\|}}{\|\underline{y}_l - \underline{x}_k\|}, & \psi(\underline{x}_k, \underline{y}_l) &= (jk \|\underline{y}_l - \underline{x}_k\| - 1) \frac{e^{jk \|\underline{y}_l - \underline{x}_k\|}}{\|\underline{y}_l - \underline{x}_k\|^3}, \\ \Gamma(\underline{x}_k, \underline{y}_l) &= -\frac{4}{k^2} \frac{e^{jk \|\underline{y}_l - \underline{x}_k\|}}{\|\underline{y}_l - \underline{x}_k\|}, & \chi(\underline{x}_k, \underline{y}_l) &= k^2 \frac{e^{jk \|\underline{y}_l - \underline{x}_k\|}}{\|\underline{y}_l - \underline{x}_k\|} \end{aligned} \quad (C4.3)$$

The  $B^K$  and  $B^L$  matrices are defined in equation (C4.4) as:

$$\begin{aligned} B^K(\underline{x}_k) &= \left[ \underline{C}_{3x_k}^K \mid \underline{C}_{1x_k}^K \mid \underline{C}_{2x_k}^K \right] \\ B^L(\underline{y}_l) &= \left[ \underline{C}_{3y_l}^L \mid \underline{C}_{1y_l}^L \mid \underline{C}_{2y_l}^L \right] \end{aligned} \quad (C4.4)$$

where:

$C_s w_i = [(w_{1i} - C_{1s}) (w_{2i} - C_{2s}) (w_{3i} - C_{3s})]$
$i$ Gauss point index
$s = 1, 2, 3$ Triangle vertex index

Finally, we have the mixed product defined by the term  $\Omega^{KL}$  reported in equation (C4.5):

$$\left[ \Omega^{KL}(\underline{x}_k, \underline{y}_l) \right]_{cs} = \det \left( \text{col}_s [B^L(\underline{y}_l)] \mid \text{col}_c [B^K(\underline{x}_k)] \mid [\underline{y}_l - \underline{x}_k] \right) \quad (\text{C4.5})$$

$c = 1, 2, 3$ Triangle coordinates index
$s = 1, 2, 3$ Triangle vertex index

Once these terms are calculated, we are able to find the FN reaction terms given in equation (C3.29).

*C4.1.2 Dipole Source Vector:* let's show now how to implement the source vector reported in equation (C3.31) for the Full-Numerical technique. According to Figure C3.6, equations (C3.21), (C3.24) and referring to equations (C3.30) and (C3.31) (reported in equation (C4.6)), we will describe the  $S$  term. This technique is easy to apply as all the terms appearing in equation (C4.6) are defined, we only need to perform a single summation for each operator.

$$\left[ S_{e_c}^K(\underline{m}^D, \underline{y}^D) \right]_c = -\frac{1}{2} \mu \sum_k \alpha_k g_1(\underline{x}_k, \underline{y}^D) \left\{ \left[ B^K(\underline{x}_k) \right]_c^t \underline{m}_t^D(\underline{x}_k, \underline{y}^D) + \right. \\ \left. + \frac{1}{kr_k} \left( j - \frac{1}{kr_k} \right) \left( 2 \left[ B^K(\underline{x}_k) \right]_c^t \underline{m}^D - 3 \left[ B^K(\underline{x}_k) \right]_c^t \underline{m}_t^D(\underline{x}_k, \underline{y}^D) \right) \right\} \quad (\text{C4.6})$$

$$\left[ S_m^K(\underline{m}^D, \underline{y}^D) \right]_c = -\frac{1}{2} \mu \sum_k \alpha_k g_3(\underline{x}_k, \underline{y}^D) \Upsilon_c^K(\underline{x}_k, \underline{y}^D)$$

Let's start from the  $\alpha_K$  Gauss method weights (see Annex 1), they appear inside the integrals as follows (where  $u$  are the generic gaussian quadrature points number):

$$\underline{\omega}^K(f) = \Lambda(T_K) \cdot \sum_k \alpha_k \cdot b(\underline{x}_k) \quad (\text{C4.7})$$

with:	$\Lambda(T_K)$ ,	triangle surfaces
	$b(\ )$	MoM basis function
	$\alpha_k$	Gauss unweighted coefficients
	$\underline{x}_k$	Gauss points in $T_K \mathfrak{R}^3$

Then we have the Green function kernels in equation (C4.8):

$$\phi(\underline{x}_k, \underline{y}^D) = \frac{e^{jk\|\underline{x}_k - \underline{y}^D\|}}{\|\underline{x}_k - \underline{y}^D\|}, \quad \psi_k(\underline{x}_k, \underline{y}^D) = (jk\|\underline{y}^D - \underline{x}_k\| - 1) \frac{e^{jk\|\underline{x}_k - \underline{y}^D\|}}{\|\underline{x}_k - \underline{y}^D\|^3} \quad (\text{C4.8})$$

The  $B^K$  matrices are defined in equation (C4.9) as:

$$B^K(\underline{x}_k) = \left[ \underline{C}_3^K \underline{x}_k \mid \underline{C}_1^K \underline{x}_k \mid \underline{C}_2^K \underline{x}_k \right] \quad (\text{C4.9})$$

where:

$\underline{C}_s w_i = [(w_{1i} - C_{1s})   (w_{2i} - C_{2s})   (w_{3i} - C_{3s})]$
$i$ Gauss point index
$s = 1, 2, 3$ Triangle vertex index

The expressions of the dipole moment  $\underline{m}^D$  and the transversal dipole moment  $\underline{m}_t^D$  are:

$$\underline{m}^D = [m_1^D, m_2^D, m_3^D]$$

$$\underline{m}_t^D(\underline{x}_k, \underline{y}^D) = \underline{m}^D - \left[ \underline{m}^D \cdot (\underline{x}_k - \underline{y}^D) \right] \cdot (\underline{x}_k - \underline{y}^D) \left( \frac{1}{\|\underline{x}_k - \underline{y}^D\|} \right)^2 \quad (\text{C4.10})$$

Finally, we have the mixed product defined by the term  $\Upsilon^K$  reported in equation (C4.11):

$$\left[ \Upsilon^K(\underline{x}_k, \underline{y}^D) \right]_c = \det \left( \text{col}_c [B^K(\underline{x}_k)] \mid \underline{m}^D \mid \underline{x}_k - \underline{y}^D \right) \quad (\text{C4.11})$$

where: $c = 1, 2, 3$ Triangle coordinates index
---

Once these terms are calculated, we are able to find the FN reaction terms given in equation (C3.31).

## C4.2 Semi-Numerical Technique

We want now to describe the numerical implementation of the equations (C3.28), (C3.29) and (C3.31) for the Semi-Numerical technique.

We also assume to study planar structures only, so this reduce, for the moment, the field of application of SR3D but notably simplifies the configuration. Under this hypothesis and according to equation (C2.28), we can say that when we consider the reaction between two planar structures, defined on the  $\gamma$  plane, we have:

$$\Omega^{KL} = (\underline{\nabla}_r \cdot G \times \underline{\alpha}) \cdot \underline{\beta}^{test} \Big|_{\underline{\alpha}, \underline{\beta} \in \gamma} = 0 \quad (\text{C4.12})$$

This leads to obtain a zero value for  $R_2$  term in equation (C2.28) and consequently a zero value for  $T$  operator reported in equation (C3.28). This hypothesis simplifies the model but only planar structures can be treated.

*C4.2.1 Reaction Matrix:* the goal is to compute the reaction terms of equation (C3.29) for a single couple of triangles using the Semi-Numerical technique. According to Figure C3.5, equations (C3.8), (C3.15) and referring to equations (C3.27) and (C3.28) (also reported in equation (C4.13) under the assumption of equation (C4.12)), we describe the terms for the  $A, D$  operators.

$$\begin{aligned} \left[ A^{KL}(g_1) \right]_{cs} &= \frac{1}{4} \sum_k \sum_l \alpha_k \alpha_l g_1(x_k, y_l) \left[ B^K(x_k) \right]_c \left[ B^L(y_l) \right]_s \\ \left[ D^{KL}(g_2) \right]_{cs} &= \frac{1}{4} \sum_k \sum_l \alpha_k \alpha_l g_2(x_k, y_l) \\ \left[ T^{KL}(g_3) \right]_{cs} &= 0 \end{aligned} \quad (C4.13)$$

$$\text{where: } g_1(r) = \begin{bmatrix} \phi(r) \\ \chi(r) \end{bmatrix} = \begin{bmatrix} g(r) \\ k^2 g(r) \end{bmatrix}, \text{ along with: } g_2(r) = \begin{bmatrix} \Gamma(r) \\ \phi(r) \end{bmatrix} = \begin{bmatrix} -\frac{4}{k^2} g(r) \\ g(r) \end{bmatrix}$$

We recall that the main goal of the Semi-Numerical technique is to eliminate the singularity of the Green's function kernels for the superimposed triangle case (see Figure C4.1).

As a result, the equation (C4.13) needs a quite complex mathematical treatment, reported in Annex 3. In this chapter, we only report the main theory with the final expressions for all the terms which are defined inside the reduced  $A, D$  operators.

As said, when triangles  $T_K$  and  $T_L$  are superimposed, a singularity occurs for the Green's function kernels because  $x_k \equiv y_l \rightarrow r = \|x_k - y_l\| = 0$  (see equation (C3.17)). Due to that, we desire to separate the singular part from the regular part inside the  $g$  classical Green's function (see equation (C3.27)). We can use the  $g$  function only, owing to the fact that  $\psi$  does not appear in the SN technique (we do not consider the constant that appears inside the kernels in equation (C4.19)).

$$g(r) = g^0(r) + g^\infty(r) = \frac{e^{jkr}}{r} \quad (C4.14)$$

$$\text{where: } \begin{cases} g^0(r) = \lim_{r \rightarrow 0} g(r) \cong \frac{1}{r} \\ g^\infty(r) = R^\infty(r) = g(r) - g^0(r) \end{cases}$$

The form for the  $g^0$  term is easy to find from equation (C3.17) and the  $g^\infty$  is described in Annex 3. According to equation (C4.14), we can define the generic form of  $A, D$  operators:

$$\begin{aligned} \left[ A^{KL}(g) \right]_{cs} &= \left[ A^{KL}(g^0) \right]_{cs} + \left[ A^{KL}(g^\infty) \right]_{cs} \\ \left[ D^{KL}(g) \right]_{cs} &= \left[ D^{KL}(g^0) \right]_{cs} + \left[ D^{KL}(g^\infty) \right]_{cs} \end{aligned} \quad (C4.15)$$

The final expressions for the equation (C4.15) are reported in the following. More precisely, the equation (C4.16) contains the  $A, D$  operators for the SN technique in case of singularity ( $T_K \equiv T_L, \underline{y}_l = \underline{x}_l$ ) while the equation (C4.17) contains the  $A, D$  operators for the regular SN technique ( $T_K \neq T_L$ ). All the calculations are reported in Annex 3.

$$\begin{aligned} \left[ A^{KL}(\underline{g}^\infty) \right]_{cs} &= \frac{1}{4} \sum_k \sum_l \alpha_k \alpha_l \left\{ t_0^L(\underline{x}_k) \left[ B^K(\underline{x}_k) \right]_c^t \left[ B^L(\underline{x}_l) \right]_s + \right. \\ &\quad \left. + \left[ B^K(\underline{x}_k) \right]_c^t \left[ t_1^L(\underline{x}_k) \middle| t_1^L(\underline{x}_k) \middle| t_1^L(\underline{x}_k) \right]_s \right\} + \\ &\quad + \frac{1}{4} \sum_k \sum_l \alpha_k \alpha_l \left\{ \underline{g}^\infty(\underline{x}_k, \underline{x}_l) \left[ B^K(\underline{x}_k) \right]_c^t \left[ B^L(\underline{x}_l) \right]_s \right\} \Big|_{k \neq l} \end{aligned} \quad (\text{C4.16})$$

$$\left[ D^{KL}(\underline{g}^\infty) \right]_{cs} = \frac{1}{4} \sum_k \sum_l \alpha_k \alpha_l t_0^L(\underline{x}_k) + \frac{1}{4} \sum_k \sum_l \alpha_k \alpha_l \underline{g}^\infty(\underline{x}_k, \underline{x}_l) \Big|_{k \neq l}$$

$$\begin{aligned} \left[ A^{KL}(\underline{g}^\infty) \right]_{cs} &= \frac{1}{4} \sum_k \sum_l \alpha_k \alpha_l \left\{ t_0^L(\underline{x}_k) \left[ B^K(\underline{x}_k) \right]_c^t \left[ B^L(\underline{x}_l) \right]_s + \right. \\ &\quad \left. + \left[ B^K(\underline{x}_k) \right]_c^t \left[ t_1^L(\underline{x}_k) \middle| t_1^L(\underline{x}_k) \middle| t_1^L(\underline{x}_k) \right]_s \right\} + \\ &\quad + \frac{1}{4} \sum_k \sum_l \alpha_k \alpha_l \left\{ \underline{g}^\infty(\underline{x}_k, \underline{y}_l) \left[ B^K(\underline{x}_k) \right]_c^t \left[ B^L(\underline{y}_l) \right]_s \right\} \end{aligned} \quad (\text{C4.17})$$

$$\left[ D^{KL}(\underline{g}^\infty) \right]_{cs} = \frac{1}{4} \sum_k \sum_l \alpha_k \alpha_l t_0^L(\underline{x}_k) + \frac{1}{4} \sum_k \sum_l \alpha_k \alpha_l \underline{g}^\infty(\underline{x}_k, \underline{y}_l)$$

The  $\alpha_K$  and  $\alpha_L$  Gauss method weights (see Annex 1) appear inside the integrals as follows (where  $u, v$  are the numbers of the generic gaussian quadrature points):

$$\begin{aligned} \underline{\mathfrak{S}}^K(f) &= \Lambda(T_K) \cdot \sum_k \alpha_k \cdot b(\underline{x}_k) \\ \underline{\mathfrak{S}}^L(f) &= \Lambda(T_L) \cdot \sum_l \alpha_l \cdot b(\underline{y}_l) \end{aligned} \quad (\text{C4.18})$$

with:	$\Lambda(T_K), \Lambda(T_L)$	triangle surfaces
	$b(\ )$	MoM basis function
	$\alpha_k, \alpha_l$	Gauss unweighted coefficients
	$\underline{x}_k, \underline{y}_l$	Gauss points in $T_K, T_L \in \mathfrak{R}^3$

Then, we have the Green's function kernels in equation (C4.19):

$$\begin{aligned}\phi(\underline{x}_k, \underline{y}_l) &= \frac{e^{jk\|\underline{y}_l - \underline{x}_k\|}}{\|\underline{y}_l - \underline{x}_k\|}, \\ \Gamma(\underline{x}_k, \underline{y}_l) &= -\frac{4}{k^2} \frac{e^{jk\|\underline{y}_l - \underline{x}_k\|}}{\|\underline{y}_l - \underline{x}_k\|}, \quad \chi(\underline{x}_k, \underline{y}_l) = k^2 \frac{e^{jk\|\underline{y}_l - \underline{x}_k\|}}{\|\underline{y}_l - \underline{x}_k\|}\end{aligned}\quad (\text{C4.19})$$

The  $B^K$  and  $B^L$  matrices are defined in equation (C4.20) as:

$$\begin{aligned}B^K(\underline{x}_k) &= \left[ \underline{C}_{3x_k}^K \mid \underline{C}_{1x_k}^K \mid \underline{C}_{2x_k}^K \right] \\ B^L(\underline{x}_l) &= \left[ \underline{C}_{3x_l}^L \mid \underline{C}_{1x_l}^L \mid \underline{C}_{2x_l}^L \right] \\ B^L(\underline{y}_l) &= \left[ \underline{C}_{3y_l}^L \mid \underline{C}_{1y_l}^L \mid \underline{C}_{2y_l}^L \right]\end{aligned}\quad (\text{C4.20})$$

where:

$\underline{C}_s w_i = \left[ (w_{1i} - C_{1s}) \mid (w_{2i} - C_{2s}) \mid (w_{3i} - C_{3s}) \right]$ <p style="text-align: center;"> <math>i</math>                      Gauss point number  <math>s = 1, 2, 3</math>        Triangle vertex number </p>
--

We report the  $t_0^L$  and the  $t_1^L$  functions, defined through the  $v_0^L$  and the  $v_1^L$  functions, using the semi analytical expression in Annex 3. The  $t_0^L$  and the  $t_1^L$  functions are the triangle surface normalized  $v_0^L$  and  $v_1^L$  functions.

$$t_0^L(\underline{x}) = 2H_L v_0^L(\underline{x}); \quad t_1^L(\underline{x}) = 2H_L v_1^L(\underline{x}) \quad (\text{C4.21})$$

Finally,  $v_0^K$  and  $v_1^K$  functions are defined as follows:

$$v_0^L(\underline{x}) = \oint_{T_L} \frac{1}{\|\underline{y} - \underline{x}\|} dy; \quad v_1^L(\underline{x}) = \oint_{T_L} \frac{(y-x)}{\|\underline{y} - \underline{x}\|} dy \quad (\text{C4.22})$$

Once these terms are calculated, we are able to find the SN reaction terms reported in equation (C3.29), with the null term  $T(\psi)$ .

The detailed calculations are reported in Annex 3.

*C4.2.2 Dipole Source Vector:* no Semi-Numerical technique is needed for a dipole source type owing to the fact that the dipole never lies over a mesh triangle. So, the Full-Numerical technique for this kind of source is sufficient.

## **CHAPTER 5:**

# **SR3D DERIVATIVE WITH RESPECT TO THE MESH**

## Chapter 5 - SR3D Derivative with Respect to the Mesh

In this chapter, we show the derivative with respect to the structure mesh of the equations defined in Chapter 3 for the new SR3D version. In particular, we express the derivative of the reaction matrix and the source vector of the MoM linear system terms with respect to the mesh. These derivative terms are used to calculate the currents vector derivative with respect to the mesh.

### C5.1 SR3D Mesh Derivative: General Description

The MoM linear system expression defined in equation C3.2, is reported again hereafter:

$$[\bar{Z}] [\Phi] = [\bar{S}] \quad (\text{C5.1})$$

Given a triangle-discretized generic  $\Omega$  surface, we can identify every vertex of the triangles as the ensemble of  $P_K$  points. We can define the reaction matrix derivative with respect to the  $P_K$  variables, where  $K$  is the number of the points defining the structure.

$$\frac{\partial [\bar{Z}]}{\partial P_{ij}} \Big|_{M \times N} = \begin{bmatrix} \frac{\partial [\bar{Z}]}{\partial P_{ij}} \Big|_{11} & \dots & \frac{\partial [\bar{Z}]}{\partial P_{ij}} \Big|_{1n} \\ \dots & \dots & \dots \\ \frac{\partial [\bar{Z}]}{\partial P_{ij}} \Big|_{m1} & \dots & \frac{\partial [\bar{Z}]}{\partial P_{ij}} \Big|_{mn} \end{bmatrix} \quad (\text{C5.2})$$

where:	$i, j$ = reference derivative point
	$m, n$ = derived element matrix indices
	$M \times N$ = derivative reaction matrix size

We have similiary for the source vector:

$$\frac{\partial [\bar{S}]}{\partial P_{ij}} \Big|_{M \times 1} = \begin{bmatrix} \frac{\partial [\bar{S}]}{\partial P_{ij}} \Big|_1 \\ \dots \\ \frac{\partial [\bar{S}]}{\partial P_{ij}} \Big|_m \end{bmatrix} \quad (\text{C5.3})$$

where:	$i, j$ = reference derivative point
	$m$ = derived element matrix index
	$M$ = derivative source vector size

More precisely, every point has two indices  $i$  and  $j$  referring, respectively, to the cartesian coordinate and to the global vertex number.

We want, for example, to find the mesh derivative gradient of the whole reaction matrix with respect to the  $x$  cartesian direction (i.e  $i = 1$ ) for all the mesh points (i.e  $j = 1, \dots, K$ ). Then, it is needed to calculate  $K$  derivatives with respect to the derivative variables  $P_{11}, P_{12}, \dots, P_{1K}, P_{12}$  and  $P_{13}$ . In order to find the final mesh gradient in the  $x$  direction, we only need to sum all the  $K$  derivative matrix terms for the reaction (using the derivative operator linearity):

$$\frac{\partial [\underline{Z}]}{\partial x} \Big|_{M \times N} = \frac{\partial [\underline{Z}]}{\partial P_{11}} \Big|_{M \times N} + \frac{\partial [\underline{Z}]}{\partial P_{12}} \Big|_{M \times N} + \dots + \frac{\partial [\underline{Z}]}{\partial P_{1K}} \Big|_{M \times N} \quad (\text{C5.4})$$

We can apply that also to the source vector:

$$\frac{\partial [\underline{S}]}{\partial x} \Big|_{M \times 1} = \frac{\partial [\underline{S}]}{\partial P_{11}} \Big|_{M \times 1} + \frac{\partial [\underline{S}]}{\partial P_{12}} \Big|_{M \times 1} + \dots + \frac{\partial [\underline{S}]}{\partial P_{1K}} \Big|_{M \times 1} \quad (\text{C5.5})$$

As seen in Chapter 3, we prefer to analyse the equivalent sub-linear system relative to the equation (C5.1) for the single couple of triangles  $T_K$  and  $T_L$ .

$$[\underline{Z}^{KL}] [\underline{\Phi}^L] = [\underline{S}^K] \quad (\text{C5.6})$$

The derivatives of the reaction matrix and the source vector terms, for equation (C5.6), will be shown in the next section.

### C5.2 SR3D Derivative of the Reaction Matrix with Respect to the Mesh

We can derive the reaction matrix from the sub-linear system reported in equation (C5.6) represented as a  $6 \times 6$  size matrix. As seen in Chapter 3 (in equation (C3.6)), it is defined as follows:

$$[\underline{Z}^{KL}]_{2C \times 2S} = \begin{bmatrix} \begin{bmatrix} Z_{ee}^{KL} \end{bmatrix}_{C \times S} & \begin{bmatrix} Z_{em}^{KL} \end{bmatrix}_{C \times S} \\ \begin{bmatrix} Z_{me}^{KL} \end{bmatrix}_{C \times S} & \begin{bmatrix} Z_{mm}^{KL} \end{bmatrix}_{C \times S} \end{bmatrix} \quad (\text{C5.7})$$

where: $C, S = 3$ $C$ = number of cartesian coordinates $S$ = number of triangle vertices $e$ = electric reaction $m$ = magnetic reaction
---

We assume the triangle  $T_L$  to be the reference triangle for the derivative calculation. Moreover, if the sub-linear system is taken into account, then a new derivative variable is considered instead of  $P_K$ . This new variable is defined as  $C_{uv}^L$ , where the  $L$  represents the dependency on the triangle  $T_L$ . The derivative for equation (C5.7) is still represented by a  $6 \times 6$  matrix.

$$\frac{\partial [Z^{KL}]}{\partial C_{uv}^L} \Bigg|_{2Cx2S} = \begin{bmatrix} \frac{\partial [Z_{ee}^{KL}]}{\partial C_{uv}^L} \Big|_{CxS} & \frac{\partial [Z_{em}^{KL}]}{\partial C_{uv}^L} \Big|_{CxS} \\ \frac{\partial [Z_{me}^{KL}]}{\partial C_{uv}^L} \Big|_{CxS} & \frac{\partial [Z_{mm}^{KL}]}{\partial C_{uv}^L} \Big|_{CxS} \end{bmatrix} \quad (C5.8)$$

where:  $u, v =$  reference derivative point

If we use this new reference variable, we can derive the simple derivatives with respect to one vertex along one cartesian direction. For example, if we want the gradient with respect to  $C_1^L$  vertex along the  $y$  direction for a metallic structure, we only need to compute:

$$\frac{\partial [Z^{KL}]}{\partial C_{21}^L} \Bigg|_{2Cx2S} = \begin{bmatrix} \frac{\partial [Z_{ee}^{KL}]}{\partial C_{21}^L} \Big|_{CxS} & \frac{\partial [Z_{em}^{KL}]}{\partial C_{21}^L} \Big|_{CxS} \\ \frac{\partial [Z_{me}^{KL}]}{\partial C_{21}^L} \Big|_{CxS} & \frac{\partial [Z_{mm}^{KL}]}{\partial C_{21}^L} \Big|_{CxS} \end{bmatrix} \quad (C5.9)$$

Let see Figure (C5.1), for a visual description of the problem:

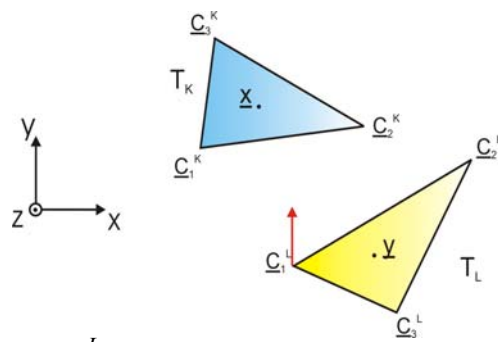


Figure C5.1:  $C_{21}^L$  gradient calculate for the sub-linear system  $Z^{KL}$

Otherwise, when we need the gradient along  $y$  direction, we have to calculate three derivatives and sum the three terms:

$$\frac{\partial [Z^{KL}]}{\partial y} \Bigg|_{2Cx2S} = \frac{\partial [Z^{KL}]}{\partial C_{21}^L} \Bigg|_{2Cx2S} + \frac{\partial [Z^{KL}]}{\partial C_{22}^L} \Bigg|_{2Cx2S} + \frac{\partial [Z^{KL}]}{\partial C_{23}^L} \Bigg|_{2Cx2S} \quad (C5.10)$$

Let see Figure (C5.2) for a visual description of the problem:

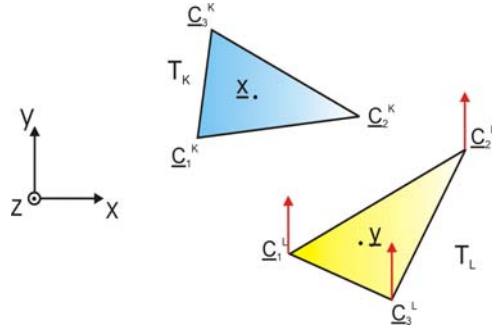


Figure C5.2: Gradient along  $y$  direction for the sub-linear system  $Z^{KL}$

The gradient of the SR3D reaction matrix for a metallic structure is obtained through the reaction matrix derivative with respect to every summit and every direction related to the reference triangle. The gradient is reported in equation (C5.11).

$$\nabla_{C^L} \left\{ \left[ Z^{KL} \right] \right\} \Big|_{3Cx3S} = \begin{bmatrix} \frac{\partial \left[ Z_{ee}^{KL} \right]}{\partial C_{11}^L} \Big|_{CxS} & \frac{\partial \left[ Z_{ee}^{KL} \right]}{\partial C_{21}^L} \Big|_{CxS} & \frac{\partial \left[ Z_{ee}^{KL} \right]}{\partial C_{31}^L} \Big|_{CxS} \\ \frac{\partial \left[ Z_{ee}^{KL} \right]}{\partial C_{12}^L} \Big|_{CxS} & \frac{\partial \left[ Z_{ee}^{KL} \right]}{\partial C_{22}^L} \Big|_{CxS} & \frac{\partial \left[ Z_{ee}^{KL} \right]}{\partial C_{32}^L} \Big|_{CxS} \\ \frac{\partial \left[ Z_{ee}^{KL} \right]}{\partial C_{13}^L} \Big|_{CxS} & \frac{\partial \left[ Z_{ee}^{KL} \right]}{\partial C_{23}^L} \Big|_{CxS} & \frac{\partial \left[ Z_{ee}^{KL} \right]}{\partial C_{33}^L} \Big|_{CxS} \end{bmatrix} \quad (C5.11)$$

Let's now analyse the reaction matrix derivative term by term with respect to a single couple of triangles. We recall the  $R$  terms from the Rumsey reaction in equation (C3.4), so the  $Z^{KL}$  derivative terms are defined as follows:

$$\begin{aligned} \frac{\partial \left[ Z_{ee}^{KL} \right]}{\partial C_{uv}^L} \Big|_{CxS} &= \mu \frac{\partial \left[ R_{ee}^{KL} \right]}{\partial C_{uv}^L} \Big|_{CxS} I_{se_{cs}} \\ \frac{\partial \left[ Z_{em}^{KL} \right]}{\partial C_{uv}^L} \Big|_{CxS} &= \frac{\partial \left[ R_{em}^{KL} \right]}{\partial C_{uv}^L} \Big|_{CxS} I_{se_{cs}} \\ \frac{\partial \left[ Z_{me}^{KL} \right]}{\partial C_{uv}^L} \Big|_{CxS} &= \frac{\partial \left[ R_{me}^{KL} \right]}{\partial C_{uv}^L} \Big|_{CxS} I_{sm_{cs}} \\ \frac{\partial \left[ Z_{mm}^{KL} \right]}{\partial C_{uv}^L} \Big|_{CxS} &= \frac{k^2 \partial \left[ R_{mm}^{KL} \right]}{\mu \partial C_{uv}^L} \Big|_{CxS} I_{sm_{cs}} \end{aligned} \quad (C5.12)$$

In Chapter 3, we have found the  $Z^{KL}$  terms expressions; our task is here to find out the  $Z^{KL}$  derivative form with respect to the geometry of the structure, using the new SR3D  $A, D, T$  operators found in equation (C3.18). So, equation (C5.12) becomes:

$$\begin{aligned}
\left. \frac{\partial [Z_{ee}^{KL}]}{\partial C_{uv}^L} \right|_{CxS} &= \mu \left\{ \left. \frac{\partial [A^{KL}(\phi)]}{\partial C_{uv}^L} \right|_{CxS} + \left. \frac{\partial [D^{KL}(\Gamma)]}{\partial C_{uv}^L} \right|_{CxS} \right\} I_{se_{cs}} \\
\left. \frac{\partial [Z_{em}^{KL}]}{\partial C_{uv}^L} \right|_{CxS} &= \left. \frac{\partial [T^{KL}(\psi)]}{\partial C_{uv}^L} \right|_{CxS} I_{se_{cs}} \\
\left. \frac{\partial [Z_{me}^{KL}]}{\partial C_{uv}^L} \right|_{CxS} &= \left. \frac{\partial [T^{KL}(\psi)]}{\partial C_{uv}^L} \right|_{CxS} I_{sm_{cs}} \\
\left. \frac{\partial [Z_{mm}^{KL}]}{\partial C_{uv}^L} \right|_{CxS} &= \frac{1}{\mu} \left\{ \left. \frac{\partial [A^{KL}(\chi)]}{\partial C_{uv}^L} \right|_{CxS} - 4 \left. \frac{\partial [D^{KL}(\phi)]}{\partial C_{uv}^L} \right|_{CxS} \right\} I_{sm_{cs}}
\end{aligned} \tag{C5.13}$$

The SR3D  $A, D, T$  operator derivatives with respect to the geometry are finally shown in equation (C5.15). In the following, we will change the derivative symbol with respect to the generic triangle  $T$  as follows:

$$\frac{\partial(\_)}{\partial C_{uv}^T} = D_{uv}^T \{ \_ \} \tag{C5.14}$$

We recall that the operator expressions are given in equation (C3.15) and functions  $g_i$  have been defined in (C3.17). Let's now write the derivative of the above-mentioned terms using the new notation ( $c$  and  $s$  are the matrix cell indices):

$$\begin{aligned}
\left[ D_{uv}^L \{ A^{KL}(g_1) \} \right]_{cs} &= H_K H_L \oint_{T_K} \oint_{T_L} \left\{ D_{uv}^L \{ g_1(\underline{x}, D_{uv}^L \{ \underline{y} \}) \} [B^K(\underline{x})]_c^t [B^L(\underline{y})]_s + \right. \\
&\quad \left. g_1(\underline{x}, \underline{y}) [B^K(\underline{x})]_c^t D_{uv}^L \left\{ [B^L(D_{uv}^L \{ \underline{y} \})]_s \right\} \right\} dy dx \\
\left[ D_{uv}^L \{ D^{KL}(g_2) \} \right]_{cs} &= H_K H_L \oint_{T_K} \oint_{T_L} D_{uv}^L \{ g_2(\underline{x}, D_{uv}^L \{ \underline{y} \}) \} dy dx \\
\left[ D_{uv}^L \{ T^{KL}(g_3) \} \right]_{cs} &= H_K H_L \oint_{T_K} \oint_{T_L} \left\{ D_{uv}^L \{ g_3(\underline{x}, D_{uv}^L \{ \underline{y} \}) \} [\Omega^{KL}(\underline{x}, \underline{y})]_{cs} + \right. \\
&\quad \left. g_3(\underline{x}, \underline{y}) D_{uv}^L \left\{ [\Omega^{KL}(\underline{x}, D_{uv}^L \{ \underline{y} \})]_{cs} \right\} \right\} dy dx
\end{aligned} \tag{C5.15}$$

where:

$c, s = 1, 2, 3$ $c = \text{Cartesian coordinates index}$ $s = \text{triangle vertex index}$
--

The derivatives of the kernels  $g_i$  are defined as follows:

$$\begin{aligned}
 D_{uv}^L \{g_1(\underline{x}, D_{uv}^L \{\underline{y}\})\} &= \begin{bmatrix} \frac{\partial \phi(\underline{x}, \underline{y})}{\partial [\underline{y}]} D_{uv}^L \{\underline{y}\} \\ \frac{\partial \chi(\underline{x}, \underline{y})}{\partial [\underline{y}]} D_{uv}^L \{\underline{y}\} \end{bmatrix} \\
 D_{uv}^L \{g_2(\underline{x}, D_{uv}^L \{\underline{y}\})\} &= \begin{bmatrix} \frac{\partial \Gamma(\underline{x}, \underline{y})}{\partial [\underline{y}]} D_{uv}^L \{\underline{y}\} \\ \frac{\partial \phi(\underline{x}, \underline{y})}{\partial [\underline{y}]} D_{uv}^L \{\underline{y}\} \end{bmatrix} \quad (C5.16) \\
 D_{uv}^L \{g_3(\underline{x}, D_{uv}^L \{\underline{y}\})\} &= \begin{bmatrix} \frac{\partial \psi(\underline{x}, \underline{y})}{\partial [\underline{y}]} D_{uv}^L \{\underline{y}\} \end{bmatrix}
 \end{aligned}$$

### C5.3 SR3D Derivative of the Source Vector with Respect to the Mesh

The derivative of the second member of the linear system with respect to the mesh takes into account the sources defined inside the domain. As usual, we only consider for the moment the source reaction with one generic triangle (metallic or dielectric), so we obtain a  $6 S^K$  vector size as we can see from equation (C5.14). We consider an electric dipole as source for the scattering problem.

*C5.3.1 Derivative of Dipole Source:* for a dipole-type source, we consider the reaction between the source itself and a single triangle of the mesh since this is valuable for every triangle of the discretized structure. Here, we recall the equation (C3.5), in equation (C5.17), representing the coupling effects between a source dipole  $D_K$  and a triangle  $T_K$  of the mesh. As the dipole source depends on the geometry, then the derivative respect to the geometry is non zero.

$$\begin{bmatrix} S^K \end{bmatrix}_{2Cx1} = \begin{bmatrix} \begin{bmatrix} S_e^K \end{bmatrix}_{Cx1} \\ \begin{bmatrix} S_m^K \end{bmatrix}_{Cx1} \end{bmatrix} \quad (C5.17)$$

where:

$C, S = 3$
$C =$ number of cartesian coordinates
$S =$ number of triangle vertex
$e =$ electric reaction
$m =$ magnetic reaction

We assume the triangle  $T_K$  to be the reference triangle for the derivative calculation. Moreover, if the sub-linear system is taken into account, then a new derivative variable is considered instead of  $P_K$ . This new variable is defined as  $C_{uv}^K$ , where the  $K$  represents the dependency from the triangle  $T_K$ . The derivative of the source from equation (C5.17) is still defined by a 6 vector size.

$$\frac{\partial [S^K]}{\partial C_{uv}^K} \Big|_{2C_{x1}} = \begin{bmatrix} \frac{\partial [S_e^K]}{\partial C_{uv}^K} \Big|_{Cx1} \\ \frac{\partial [S_m^K]}{\partial C_{uv}^K} \Big|_{Cx1} \end{bmatrix} \quad (C5.18)$$

where:  $u, v =$  reference derivative point

As for the reaction matrix derivative, we can derive simple derivatives with respect to one vertex along one cartesian direction. For example, if we want the gradient with respect to  $C_1^K$  vertex along the  $y$  direction for a metallic structure, we only need to calculate:

$$\frac{\partial [S^K]}{\partial C_{21}^K} \Big|_{Cx1} = \begin{bmatrix} \frac{\partial [S_e^K]}{\partial C_{21}^K} \Big|_{Cx1} \\ \frac{\partial [S_m^K]}{\partial C_{21}^K} \Big|_{Cx1} \end{bmatrix} \quad (C5.19)$$

Let see Figure C5.3 for a visual description of the problem:

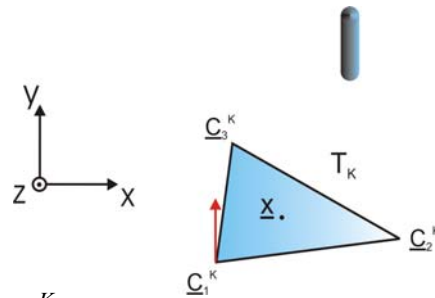


Figure C5.3:  $C_{21}^K$  gradient calculation for the sub-linear system  $S^K$

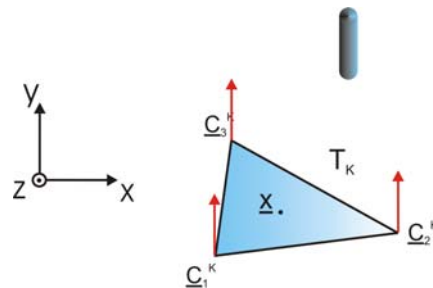


Figure C5.4: Gradient along  $y$  direction calculation for the sub-linear system  $S^K$

Otherwise, if we need the mesh gradient along  $y$  direction we must calculate three derivatives and sum them:

$$\frac{\partial [S^K]}{\partial y} \Big|_{2C_{x1}} = \frac{\partial [S^K]}{\partial C_{21}^K} \Big|_{2C_{x1}} + \frac{\partial [S^K]}{\partial C_{22}^K} \Big|_{2C_{x1}} + \frac{\partial [S^K]}{\partial C_{23}^K} \Big|_{2C_{x1}} \quad (C5.20)$$

Let see Figure C5.4 for a visual description of the problem.

The gradient of the source vector for a metallic structure is obtained through the source vector derivative with respect to every summit along every direction related to the reference triangle. The gradient is reported in equation C5.21.

$$\nabla_{\underline{C}^K} \left\{ \left[ S^K \right] \right\} \Big|_{(3C)x3} = \begin{bmatrix} \left. \frac{\partial S_e^K}{\partial C_{11}^K} \right|_{Cx1} & \left. \frac{\partial S_e^K}{\partial C_{12}^K} \right|_{Cx1} & \left. \frac{\partial S_e^K}{\partial C_{13}^K} \right|_{Cx1} \\ \left. \frac{\partial S_e^K}{\partial C_{21}^K} \right|_{Cx1} & \left. \frac{\partial S_e^K}{\partial C_{22}^K} \right|_{Cx1} & \left. \frac{\partial S_e^K}{\partial C_{23}^K} \right|_{Cx1} \\ \left. \frac{\partial S_e^K}{\partial C_{31}^K} \right|_{Cx1} & \left. \frac{\partial S_e^K}{\partial C_{32}^K} \right|_{Cx1} & \left. \frac{\partial S_e^K}{\partial C_{33}^K} \right|_{Cx1} \end{bmatrix} \quad (C5.21)$$

According to equation (C5.14) and equations (C3.22), (C3.24), we can define the source vector derivative with respect to the geometry:

$$\begin{aligned} \left[ D_{uv}^K \left\{ S_e^K(\underline{m}^D, \underline{y}^D) \right\} \right]_c &= -\mu H_K \oint_{T_K} D_{uv}^K \{ \phi(D_{uv}^K \{ \underline{x}, \underline{y}^D \}) \} \left[ -[B^K(\underline{x})]_c^t \underline{m}_t^D(\underline{x}, \underline{y}^D) + \right. \\ &\quad \left. \frac{1}{k \|\underline{x} - \underline{y}^D\|} \left( j - \frac{1}{k \|\underline{x} - \underline{y}^D\|} \right) \left( 2 [B^K(\underline{x})]_c^t \underline{m}^D - 3 [B^K(\underline{x})]_c^t \underline{m}_t^D(\underline{x}, \underline{y}^D) \right) \right] + \\ &\quad \phi(\underline{x}, \underline{y}^D) \left[ -D_{uv}^K \left\{ [B^K(D_{uv}^K \{ \underline{x} \})]_c^t \right\} \underline{m}_t^D(\underline{x}, \underline{y}^D) + [B^K(\underline{x})]_c^t D_{uv}^K \{ \underline{m}_t^D(D_{uv}^K \{ \underline{x}, \underline{y}^D \}) \} + \right. \\ &\quad \left. D_{uv}^K \left\{ \frac{1}{k \|\underline{x} - \underline{y}^D\|} \left( j - \frac{1}{k \|\underline{x} - \underline{y}^D\|} \right) \right\} \left( 2 [B^K(\underline{x})]_c^t \underline{m}^D - 3 [B^K(\underline{x})]_c^t \underline{m}_t^D(\underline{x}, \underline{y}^D) \right) + \right. \\ &\quad \left. \frac{1}{k \|\underline{x} - \underline{y}^D\|} \left( j - \frac{1}{k \|\underline{x} - \underline{y}^D\|} \right) \left( 2 D_{uv}^K \left\{ [B^K(D_{uv}^K \{ D_{uv}^K \{ \underline{x} \}) \}]_c^t \right\} \underline{m}^D - \right. \right. \\ &\quad \left. \left. 3 D_{uv}^K \left\{ [B^K(D_{uv}^K \{ \underline{x} \})]_c^t \right\} \underline{m}_t^D(\underline{x}, \underline{y}^D) - 3 [B^K(\underline{x})]_c^t D_{uv}^K \{ \underline{m}_t^D(D_{uv}^K \{ \underline{x}, \underline{y}^D \}) \} \right) \right] \Big] dx \\ \left[ D_{uv}^K \left\{ S_m^K(\underline{m}^D, \underline{y}^D) \right\} \right]_c &= -\mu H_K \oint_{T_K} D_{uv}^K \{ \psi(D_{uv}^K \{ \underline{x}, \underline{y}^D \}) \} \left[ \Upsilon^K(\underline{x}, \underline{y}^D) \right]_c + \\ &\quad \psi(\underline{x}, \underline{y}^D) D_{uv}^K \left\{ \left[ \Upsilon^K(D_{uv}^K \{ \underline{x}, \underline{y}^D \}) \right]_c \right\} dx \end{aligned} \quad (C5.22)$$

### C5.4 SR3D Derivative of the Discretized Reaction Matrix with Respect to the Mesh

Up to now, we have treated the theoretical issue from an analytic point of view. We want now to show the discretized forms for the  $A, D, T$  operators and  $Z_{xx}^{KL}$  terms with respect to the geometry. As for the classic SR3D code, the discretization is based on a seven-point Gauss discretization method (Annex 1). We recall that the Gauss weights  $\gamma_T$  for a generic discretization point are defined in equation (C3.25), the Green's function discrete form in equation (C3.26) and a discretized couple of triangles is reported in Figure C3.5.

So, according to equation (C3.28), the derivative of the discrete form with respect to the geometry of the  $A, D, T$  operators is given in equation (C5.23):

$$\begin{aligned} \left[ D_{uv}^L \{ A^{KL}(g_1) \} \right]_{cs} &= \frac{1}{4} \sum_k \sum_l \alpha_k \alpha_l \left\{ D_{uv}^L \left\{ \left[ g_1(x_k, D_{uv}^L \{y_l\}) \right]_c \right\} \left[ B^K(x_k) \right]_c' \left[ B^L(y_l) \right]_s + \right. \\ &\quad \left. g_1(x_k, y_l) \left[ B^K(x_k) \right]_c' D_{uv}^L \left\{ \left[ B^L(D_{uv}^L \{y_l\}) \right]_s \right\} \right\} \\ \left[ D_{uv}^L \{ D^{KL}(g_2) \} \right]_{cs} &= \frac{1}{4} \sum_k \sum_l \alpha_k \alpha_l \left\{ D_{uv}^L \left\{ \left[ g_2(x_k, D_{uv}^L \{y_l\}) \right]_c \right\} \right\} \end{aligned} \quad (C5.23)$$

$$\begin{aligned} \left[ D_{uv}^L \{ T^{KL}(g_3) \} \right]_{cs} &= \frac{1}{4} \sum_k \sum_l \alpha_k \alpha_l \left\{ D_{uv}^L \left\{ \left[ g_3(x_k, D_{uv}^L \{y_l\}) \right]_c \right\} \left[ \Omega^{KL}(x_k, y_l) \right]_{cs} + \right. \\ &\quad \left. g_3(x_k, y_l) D_{uv}^L \left\{ \left[ \Omega^{KL}(x_k, D_{uv}^L \{y_l\}) \right]_{cs} \right\} \right\} \end{aligned}$$

where:

$$\begin{aligned} D_{uv}^L \left\{ \left[ g_1(x_k, D_{uv}^L \{y_l\}) \right]_c \right\} &= \begin{bmatrix} \frac{\partial \phi(x_k, y_l)}{\partial [y_l]_c} D_{uv}^L \{ [y_l]_c \} \\ \frac{\partial \chi(x_k, y_l)}{\partial [y_l]_c} D_{uv}^L \{ [y_l]_c \} \end{bmatrix}, \quad D_{uv}^L \left\{ \left[ g_2(x_k, D_{uv}^L \{y_l\}) \right]_c \right\} = \begin{bmatrix} \frac{\partial \Gamma(x_k, y_l)}{\partial [y_l]_c} D_{uv}^L \{ [y_l]_c \} \\ \frac{\partial \phi(x_k, y_l)}{\partial [y_l]_c} D_{uv}^L \{ [y_l]_c \} \end{bmatrix} \\ D_{uv}^L \left\{ \left[ g_3(x_k, D_{uv}^L \{y_l\}) \right]_c \right\} &= \left[ \frac{\partial \psi(x_k, y_l)}{\partial [y_l]_c} D_{uv}^L \{ [y_l]_c \} \right] \end{aligned}$$

Finally, the discrete forms for the  $Z_{xx}^{KL}$  derivative terms are given by:

$$\begin{aligned} \left[ D_{uv}^L \{ Z_{ee}^{KL} \} \right]_{cs} &= \mu \left\{ \left[ D_{uv}^L \{ A^{KL}(\phi) \} \right]_{cs} + \left[ D_{uv}^L \{ D^{KL}(\Gamma) \} \right]_{cs} \right\} I_{se_{cs}} \\ \left[ D_{uv}^L \{ Z_{em}^{KL} \} \right]_{cs} &= \left[ D_{uv}^L \{ T^{KL}(\psi) \} \right]_{cs} I_{se_{cs}} \\ \left[ D_{uv}^L \{ Z_{me}^{KL} \} \right]_{cs} &= \left[ D_{uv}^L \{ T^{KL}(\psi) \} \right]_{cs} I_{se_{cs}} \\ \left[ D_{uv}^L \{ Z_{mm}^{KL} \} \right]_{cs} &= \frac{1}{\mu} \left\{ \left[ D_{uv}^L \{ A^{KL}(\chi) \} \right]_{cs} - 4 \left[ D_{uv}^L \{ D^{KL}(\phi) \} \right]_{cs} \right\} I_{sm_{cs}} \end{aligned} \quad (C5.24)$$

### C5.5 SR3D Derivative of the Discretized Source Vector with Respect to the Mesh

As for the reaction matrix, we want now to derive the discretized derivative form with respect to the geometry for the  $S$  vector. Once again the discretization is based on a seven-point Gauss method (Annex 1). We consider an electric dipole as source for the scattering problem.

*C5.5.1 Implementation of the Derivative of the Dipole Source Vector:* we can apply the Gauss method discretization to all the terms reported in equation C5.22, according to equations (C3.25) and (C3.26). The dipole  $D_K$  and the triangle  $T_K$  discrete form with a seven-point Gauss method representation in reported in Figure C3.6.

So, in equation (C5.25) the derivative of the discrete form for the dipole source vector with respect to the geometry is given by:

$$\begin{aligned}
\left[ D_{uv}^K \left\{ S_e^K(\underline{m}^D, \underline{y}^D) \right\} \right]_c &= -\frac{\mu}{2} \sum_k \alpha_k \left\{ D_{uv}^K \left\{ \left[ \phi(D_{uv}^K \{ \underline{x}_k \}, \underline{y}^D) \right]_c \right\} \left[ -[B^K(\underline{x}_k)]_c^t \underline{m}_t^D(\underline{x}_k, \underline{y}^D) + \right. \right. \\
&\quad \left. \left. \frac{1}{k \|\underline{x}_k - \underline{y}^D\|} \left( j - \frac{1}{k \|\underline{x}_k - \underline{y}^D\|} \right) \left( 2 [B^K(\underline{x}_k)]_c^t \underline{m}^D - 3 [B^K(\underline{x}_k)]_c^t \underline{m}_t^D(\underline{x}_k, \underline{y}^D) \right) \right] + \right. \\
&\quad \left. \phi(\underline{x}_k, \underline{y}^D) \left[ -D_{uv}^K \left\{ [B^K(D_{uv}^K \{ \underline{x}_k \})]_c^t \right\} \underline{m}_t^D(\underline{x}_k, \underline{y}^D) + [B^K(\underline{x}_k)]_c^t D_{uv}^K \nu \{ \underline{m}_t^D(D_{uv}^K \{ \underline{x}_k \}, \underline{y}^D) \} + \right. \right. \\
&\quad \left. \left. D_{uv}^K \left\{ \frac{1}{k \|\underline{x}_k - \underline{y}^D\|} \left( j - \frac{1}{k \|\underline{x}_k - \underline{y}^D\|} \right) \right\} \left( 2 [B^K(\underline{x}_k)]_c^t \underline{m}^D - 3 [B^K(\underline{x}_k)]_c^t \underline{m}_t^D(\underline{x}_k, \underline{y}^D) \right) + \right. \right. \tag{C5.25} \\
&\quad \left. \left. \frac{1}{k \|\underline{x}_k - \underline{y}^D\|} \left( j - \frac{1}{k \|\underline{x}_k - \underline{y}^D\|} \right) \left( 2 D_{uv}^K \left\{ [B^K(D_{uv}^K \{ \underline{x}_k \})]_c^t \right\} \underline{m}^D - 3 D_{uv}^K \left\{ [B^K(D_{uv}^K \{ \underline{x}_k \})]_c^t \right\} \underline{m}_t^D(\underline{x}_k, \underline{y}^D) - \right. \right. \\
&\quad \left. \left. \left. 3 [B^K(\underline{x}_k)]_c^t D_{uv}^K \{ \underline{m}_t^D(D_{uv}^K \{ \underline{x}_k \}, \underline{y}^D) \} \right\} \right] \right\} \\
\left[ D_{uv}^K \left\{ S_m^K(\underline{m}^D, \underline{y}^D) \right\} \right]_c &= -\frac{\mu}{2} \sum_k \left\{ D_{uv}^K \left\{ \left[ \psi(D_{uv}^K \{ \underline{x}_k \}, \underline{y}^D) \right]_c \right\} \left[ \Upsilon^K(\underline{x}_k, \underline{y}^D) \right]_c + \right. \\
&\quad \left. \psi(\underline{x}_k, \underline{y}^D) D_{uv}^K \left\{ \left[ \Upsilon^K(D_{uv}^K \{ \underline{x}_k \}, \underline{y}^D) \right]_c \right\} \right\}
\end{aligned}$$

**CHAPTER 6:**  
**SR3D MESH DERIVATIVE IMPLEMENTATION**

## Chapter 6 - SR3D Mesh Derivative Implementation

In Chapter 5, we have explained how to define the derivative with respect to geometry of the MoM linear system equations, detailing the reaction between a single couple of triangles for the reaction matrix and the reaction between a triangle of the mesh and a point source with respect to the source vector (or second member of the linear system). See equations C5.7 and C5.14 as equation references. In this chapter, we want to show how to numerically implement these discrete equations. The numerical code has been developed entirely in Fortran 77 language.

We have also developed two numerical techniques in order to calculate the expressions given in equation C3.29 and C3.31, as done for the normal SR3D reaction in Chapter 3. For the first one, we have the Full-Numerical (FN) technique of the reaction integrals using the Gauss discretization method. The second technique is based on the Semi-Numerical (SN) method where one of the two reaction integrals is calculated analytically and, for the second one, we use the Gauss discretization method. In the following, a preliminary description of these two techniques, is reported:

*Full-Numerical Technique:* this technique is used when the triangles of the couple  $T_K T_L$  are electrically far from each other. It is called FAR configuration. The FN technique cannot be applied when the triangles are too close due to the fact that it will produce an increase of computational burden for the integral computation or, in a worse case, when the two triangles are superimposed, a singularity inside the Green's function kernels (see equation C3.17) will appear making even impossible the use of the technique.

The FN implementation is also used for the computation of the source vector, since no singularity appears as the source may be defined on a side of the triangles for a voltage source or outside the structure surface in case of an electrical dipole.

*Semi-Numerical Technique:* the SN implementation has been developed in order to be able to treat both electrical CLOSE configurations, for accelerating the computation of the integrals, and SINGULAR configurations, when the couple of triangles is superimposed (i.e.  $T_K \equiv T_L$  and  $\underline{r} = (\underline{x}_l - \underline{x}_k) = 0$ , see equation C3.5 for reference). In this development, the SN technique can be only applied to coplanar couple of triangles.

The SN technique is convenient since it is faster than the FN implementation for CLOSE configuration; that's because as the distance between two triangles decreases, the number of discretization Gauss points raises in order to maintain the same accuracy for FN technique. It is clear that if the Gauss points number starts to be large, so the computational speed will decrease critically; that's why in that case, we prefer to use the SN implementation.

On the other hand, the SN technique is strictly needed when the triangles are superimposed. In the SUPERIMPOSED case, the SN implementation operates on the Green's function kernels factorization in order to separate the singular part from the regular one. The singular part is treated with a special analytic reduction method whereas for the regular part a Taylor expansion is used. No SN implementation is used for the computation of the source vector, since no singularity is present.

The derivative with respect to the geometry of the  $T_K, T_L$  reaction terms is more complicated than the normal reaction one. Nothing changes about the electrical distances, where the FN and SN technique are still used. For the derivative geometry reaction, we must also take care about the number and the order of the triangles  $T_K, T_L$  common vertices. In fact, if the  $T_K$  and  $T_L$  triangles have a common vertex then the derivative of  $T_K$  over  $T_L$  and the derivative of  $T_L$  over  $T_K$  with respect to the common vertices must be taken both into account. As for the normal reaction, we fix a threshold, called  $D$ , in order to choose which technique to be used between the FN and the SN ones. We use this threshold with respect to the barycenters  $\underline{b}$  of triangles (see Figures below).

We consider the triangle common vertices configuration we are interested in applying the SN technique for the electrical CLOSE and SUPERIMPOSED cases. We can find these cases in Figure C6.1 in which the two common vertices reaction (Red), the single common vertex (Orange) and the three common vertices (Green) are shown.

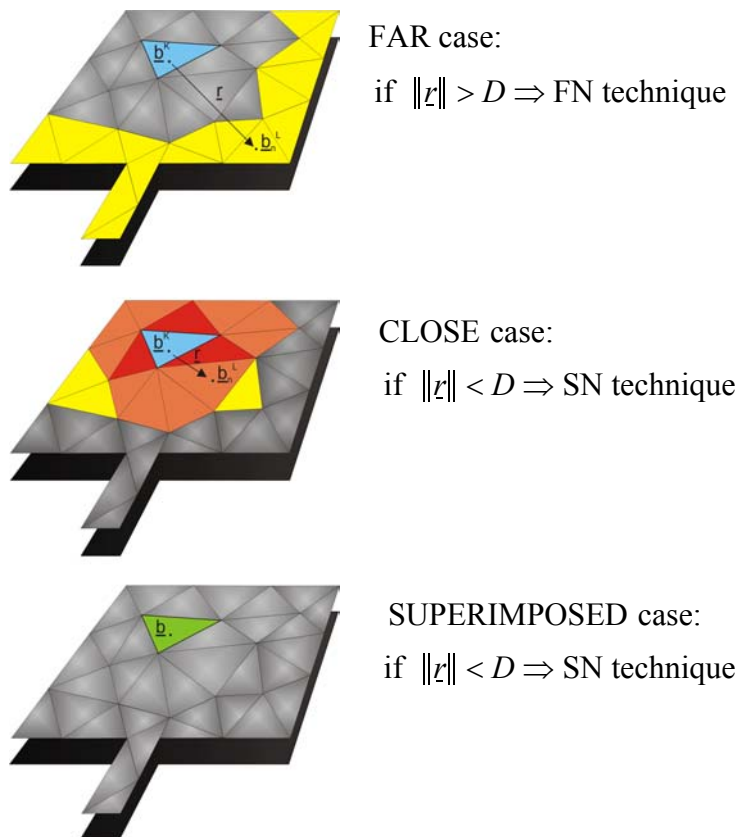


Figure C6.1: Definition of the relative distance for triangles  $T_K T_L$  for the reaction matrix derivative calculation

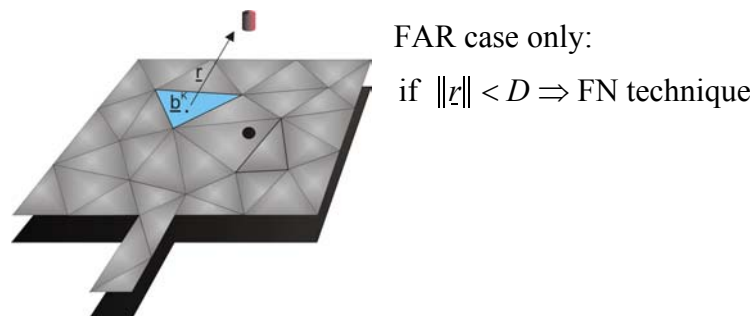


Figure C6.2: Definition of the relative distance for triangle  $T_K$  and a source point for the source vector calculation

We must point out for the derivative of the common vertex case that a special solution has to be taken into account. Let's consider the next examples, where the reference for the derivative triangle is still  $T_L$  :

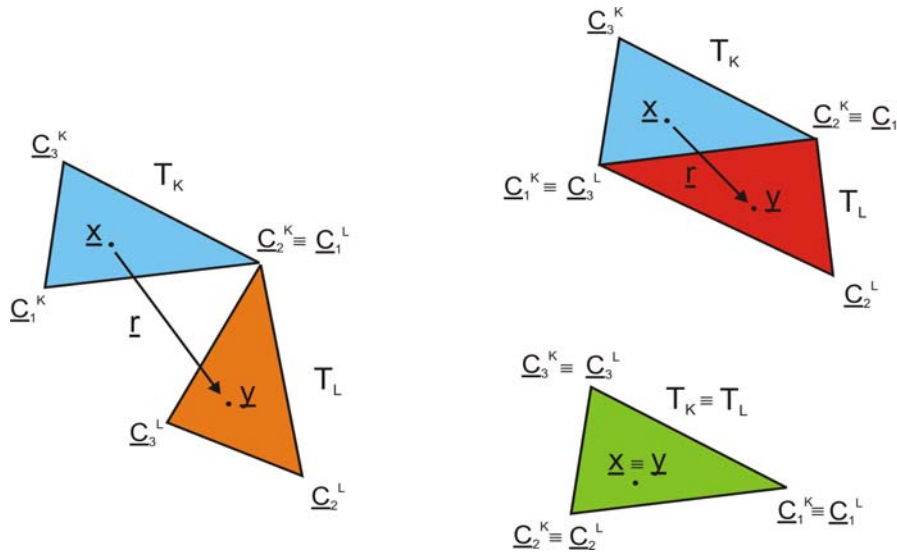


Figure C6.3: Common vertex case in a generic 3 dimensional space

According to equation C3.8, if we consider the left case, in the Figure above, and we desire to calculate the reaction derivative with respect to  $C_2^L$  and  $C_3^L$ , along every direction, the normal SN derivative case can be used, since there are not  $T_K$  common vertices with respect to  $T_L$ . Instead, if we desire the reaction derivative with respect to  $C_{21}^L$ , i.e. along  $y$  direction, both the reaction derivatives with respect to  $T_L$  and  $T_K$  must be taken into account for this vertex. This means that the total reaction derivative for the vertex  $C_{21}^L$  will be the sum of the derivatives of the reaction with respect to  $C_{21}^L$  and  $C_{22}^K$  both. If we consider a metallic structure, then the matrix reaction derivative will be:

$$\left. \frac{\partial [Z^{KL}]}{\partial C_{21}^L} \right|_{CxS} = \left. \frac{\partial [Z_{ee}^{KL}]}{\partial C_{21}^L} \right|_{CxS} + \left. \frac{\partial [Z_{ee}^{KL}]}{\partial C_{22}^K} \right|_{CxS} \quad (C6.1)$$

What has been said is valid for each common vertex case. It doesn't matter the number of common vertices are defined for a couple of triangles ( $T_K, T_L$ ).

### C6.1 Full-Numerical Technique

In Chapter 5, we gave the expressions of both the derivative with respect to the geometry for the reaction matrix and source vector. Now we want to describe the numerical implementation of equations C5.23, C5.24 and C5.25 for the Full-Numerical technique.

*C6.1.1 Reaction Matrix Derivative:* we want now describe the derivative reaction terms of equation C5.24 between a single couple of triangles using the Full-Numerical technique. According to Figure C3.5, equations C3.8, C5.15 and referring to equations C5.23 and C5.24 (also reported in equation C6.2), we will describe the derivative of the terms forming the  $A, D, T$  operators. This technique is quite linear to apply as all the terms appearing in equation C6.2 are defined and we only need to perform a double summation for each operator.

$$\begin{aligned}
 \left[ D_{uv}^L \{ A^{KL}(g_1) \} \right]_{cs} &= \frac{1}{4} \sum_k \sum_l \alpha_k \alpha_l \left\{ D_{uv}^L \left\{ \left[ g_1(\underline{x}_k, D_{uv}^L \{ \underline{y}_l \}) \right]_c \right\} \left[ B^K(\underline{x}_k) \right]_c^t \left[ B^L(\underline{y}_l) \right]_s + \right. \\
 &\quad \left. g_1(\underline{x}_k, \underline{y}_l) \left[ B^K(\underline{x}_k) \right]_c^t D_{uv}^L \left\{ \left[ B^L(D_{uv}^L \{ \underline{y}_l \}) \right]_s \right\} \right\} \\
 \left[ D_{uv}^L \{ D^{KL}(g_2) \} \right]_{cs} &= \frac{1}{4} \sum_k \sum_l \alpha_k \alpha_l \left\{ D_{uv}^L \left\{ \left[ g_2(\underline{x}_k, D_{uv}^L \{ \underline{y}_l \}) \right]_c \right\} \right\} \quad (C6.2) \\
 \left[ D_{uv}^L \{ T^{KL}(g_3) \} \right]_{cs} &= \frac{1}{4} \sum_k \sum_l \alpha_k \alpha_l \left\{ D_{uv}^L \left\{ \left[ g_3(\underline{x}_k, D_{uv}^L \{ \underline{y}_l \}) \right]_c \right\} \left[ \Omega^{KL}(\underline{x}_k, \underline{y}_l) \right]_{cs} + \right. \\
 &\quad \left. g_3(\underline{x}_k, \underline{y}_l) D_{uv}^L \left\{ \left[ \Omega^{KL}(\underline{x}_k, D_{uv}^L \{ \underline{y}_l \}) \right]_{cs} \right\} \right\}
 \end{aligned}$$

Where the derivatives of the kernels  $g_i$  are defined as follows:

$$\begin{aligned}
 D_{uv}^L \left\{ \left[ g_1(\underline{x}_k, D_{uv}^L \{ \underline{y}_l \}) \right]_c \right\} &= \begin{bmatrix} \frac{\partial \phi(\underline{x}_k, \underline{y}_l)}{\partial [\underline{y}_l]_c} D_{uv}^L \{ [\underline{y}_l]_c \} \\ \frac{\partial \chi(\underline{x}_k, \underline{y}_l)}{\partial [\underline{y}_l]_c} D_{uv}^L \{ [\underline{y}_l]_c \} \end{bmatrix} \\
 D_{uv}^L \left\{ \left[ g_2(\underline{x}_k, D_{uv}^L \{ \underline{y}_l \}) \right]_c \right\} &= \begin{bmatrix} \frac{\partial \Gamma(\underline{x}_k, \underline{y}_l)}{\partial [\underline{y}_l]_c} D_{uv}^L \{ [\underline{y}_l]_c \} \\ \frac{\partial \phi(\underline{x}_k, \underline{y}_l)}{\partial [\underline{y}_l]_c} D_{uv}^L \{ [\underline{y}_l]_c \} \end{bmatrix} \quad (C6.3) \\
 D_{uv}^L \left\{ \left[ g_3(\underline{x}_k, D_{uv}^L \{ \underline{y}_l \}) \right]_c \right\} &= \begin{bmatrix} \frac{\partial \psi(\underline{x}_k, \underline{y}_l)}{\partial [\underline{y}_l]_c} D_{uv}^L \{ [\underline{y}_l]_c \} \end{bmatrix}
 \end{aligned}$$

According to equations from C4.2 to C4.5, the derivative terms in expressions C6.2 and C6.3 will be explained in the following. For more details see Annex 4.

As everything depends on the Gauss points, in expression C6.4, we will give first the derivative with respect to the geometry for a generic Gauss point  $\underline{w}$  defined in a generic triangle  $T$  geometry (see Annex 1).

$$\begin{aligned}
 \left[ D_{u1}^T \{ \underline{w} \} \right]_c &= (1 - \zeta_{1c} - \zeta_{2c}) \delta_c^u \\
 \left[ D_{u2}^T \{ \underline{w} \} \right]_c &= (\zeta_{1c}) \delta_c^u \\
 \left[ D_{u3}^T \{ \underline{w} \} \right]_c &= (\zeta_{2c}) \delta_c^u \quad (C6.4)
 \end{aligned}$$

$$\text{with: } \boxed{\left[ D_{uv}^L \{ \underline{w} \} \right]_c = 0 \text{ if } c \neq u}$$

According to equation C3.13, we give now the expression of  $B$  matrix derivative with respect to the triangle  $L$  geometry:

$$\begin{aligned} \left[ D_{uv}^L \left\{ B^L(D_{uv}^L \{ \underline{y}_l \}) \right\} \right]_{cs} &= \left[ \left[ D_{uv}^L \{ \underline{y}_l \} \right]_{cs} \middle| \left[ D_{uv}^L \{ \underline{y}_l \} \right]_{cs} \middle| \left[ D_{uv}^L \{ \underline{y}_l \} \right]_{cs} \right] - \\ &\left[ \left[ D_{uv}^L \{ \underline{C}^L \} \right]_{c3} \middle| \left[ D_{uv}^L \{ \underline{C}^L \} \right]_{c1} \middle| \left[ D_{uv}^L \{ \underline{C}^L \} \right]_{c2} \right] \end{aligned} \quad (\text{C6.5})$$

Then, according to equation C3.14, we now give the expression of  $\Omega$  determinant derivative with respect to the triangle  $L$  geometry:

$$\begin{aligned} \left[ D_{uv}^L \left\{ \Omega^{KL}(\underline{x}_k, D_{uv}^L \{ \underline{y}_l \}) \right\} \right]_{cs} &= \det \begin{pmatrix} \left[ D_{uv}^L \left\{ B^L(D_{uv}^L \{ \underline{y}_l \}) \right\} \right]_{1s} & 0 & \left[ D_{uv}^L \{ \underline{y}_l \} \right]_1 \\ \left[ B^L \{ \underline{y}_l \} \right]_{2s} & \left[ B^K \{ \underline{x}_k \} \right]_{2s} & \left[ \underline{y}_l - \underline{x}_k \right]_2 \\ \left[ B^L \{ \underline{y}_l \} \right]_{3s} & \left[ B^K \{ \underline{x}_k \} \right]_{3s} & \left[ \underline{y}_l - \underline{x}_k \right]_3 \end{pmatrix} + \\ &\det \begin{pmatrix} \left[ B^L \{ \underline{y}_l \} \right]_{1s} & \left[ B^K \{ \underline{x}_k \} \right]_{1s} & \left[ \underline{y}_l - \underline{x}_k \right]_1 \\ \left[ D_{uv}^L \left\{ B^L(D_{uv}^L \{ \underline{y}_l \}) \right\} \right]_{2s} & 0 & \left[ D_{uv}^L \{ \underline{y}_l \} \right]_2 \\ \left[ B^L \{ \underline{y}_l \} \right]_{3s} & \left[ B^K \{ \underline{x}_k \} \right]_{3s} & \left[ \underline{y}_l - \underline{x}_k \right]_3 \end{pmatrix} + \\ &\det \begin{pmatrix} \left[ B^L \{ \underline{y}_l \} \right]_{1s} & \left[ B^K \{ \underline{x}_k \} \right]_{1s} & \left[ \underline{y}_l - \underline{x}_k \right]_1 \\ \left[ B^L \{ \underline{y}_l \} \right]_{2s} & \left[ B^K \{ \underline{x}_k \} \right]_{2s} & \left[ \underline{y}_l - \underline{x}_k \right]_2 \\ \left[ D_{uv}^L \left\{ B^L(D_{uv}^L \{ \underline{y}_l \}) \right\} \right]_{3s} & 0 & \left[ D_{uv}^L \{ \underline{y}_l \} \right]_3 \end{pmatrix} \end{aligned} \quad (\text{C6.6})$$

According to equations C3.8 and C3.14, we give the Green's function kernel derivatives with respect to the triangle  $L$  geometry. First, in equation C6.7, we will give the expressions of the Green's function kernel derivatives with respect to the direction  $c$  of the Gauss point  $y$  defined on triangle  $L$ . For the sake of simplicity, we use the variables  $r = \left\| \underline{y}_l - \underline{x}_k \right\|$  and  $r_c = \left[ \underline{y}_l - \underline{x}_k \right]_c$ .

$$\begin{aligned}
\frac{\partial \phi(\underline{x}_k, \underline{y}_l)}{\partial [\underline{y}_l]_c} &= \frac{e^{jkr}}{r} [r]_c [jkr - 1], & \frac{\partial \Gamma(\underline{x}_k, \underline{y}_l)}{\partial [\underline{y}_l]_c} &= -\frac{4}{k^2} \frac{e^{jkr}}{r} [r]_c [jkr - 1], \\
\frac{\partial \psi(\underline{x}_k, \underline{y}_l)}{\partial [\underline{y}_l]_c} &= \frac{e^{jkr}}{r} [r]_c [3 - 3jkr - (kr)^2], & \frac{\partial \chi(\underline{x}_k, \underline{y}_l)}{\partial [\underline{y}_l]_c} &= k^2 \frac{e^{jkr}}{r} [r]_c [jkr - 1]
\end{aligned} \tag{C6.7}$$

Finally, we will show the Green's function kernel derivatives with respect to the triangle  $L$  geometry in equation C6.8.

$$\begin{aligned}
D_{uv}^L \left\{ \phi(\underline{x}_k, D_{uv}^L \{ \underline{y}_l \}) \right\} &= \frac{e^{jkr}}{r^2} [r]_c [jkr - 1] (D_{uv}^L \{ [\underline{y}_l]_c \}) \\
D_{uv}^L \left\{ \psi(\underline{x}_k, D_{uv}^L \{ \underline{y}_l \}) \right\} &= \frac{e^{jkr}}{r^5} [r]_c [3 - 3jkr - (kr)^2] (D_{uv}^L \{ [\underline{y}_l]_c \}) \\
D_{uv}^L \left\{ \Gamma(\underline{x}_k, D_{uv}^L \{ \underline{y}_l \}) \right\} &= -\frac{4}{k^2} \frac{e^{jkr}}{r^2} [r]_c [jkr - 1] (D_{uv}^L \{ [\underline{y}_l]_c \}) \\
D_{uv}^L \left\{ \chi(\underline{x}_k, D_{uv}^L \{ \underline{y}_l \}) \right\} &= k^2 \frac{e^{jkr}}{r^2} [r]_c [jkr - 1] (D_{uv}^L \{ [\underline{y}_l]_c \})
\end{aligned} \tag{C6.8}$$

*C6.1.2 Source Vector Derivative:* let's show now how to implement the source vector derivative with respect to the geometry reported in equation C5.25 for the Full-Numerical technique. According to Figure C3.6 and equations from C4.2 to C4.11 and referring to equation C5.25 (here reported in equation C6.9) we will describe the  $S$  term derivative. This technique is quite linear to apply as once all the terms appearing in equation C6.9 are defined, we only need to perform a single summation for each operator. For more details, see Annex 4.

$$\begin{aligned}
\left[ D_{uv}^K \left\{ S_e^K(\underline{m}^D, \underline{y}^D) \right\} \right]_c &= \frac{\mu}{2} \sum_k \alpha_k \left\{ D_{uv}^K \left\{ \left[ \phi(D_{uv}^K \{ \underline{x}_k \}, \underline{y}^D) \right]_c \right\} \left[ -[B^K(\underline{x}_k)]_c^t \underline{m}_t^D(\underline{x}_k, \underline{y}^D) + \right. \right. \\
&\quad \left. \frac{1}{k \|\underline{x}_k - \underline{y}^D\|} \left( j - \frac{1}{k \|\underline{x}_k - \underline{y}^D\|} \right) \left( 2 [B^K(\underline{x}_k)]_c^t \underline{m}^D - 3 [B^K(\underline{x}_k)]_c^t \underline{m}_t^D(\underline{x}_k, \underline{y}^D) \right) \right] + \\
&\quad \left. \phi(\underline{x}_k, \underline{y}^D) \left[ -D_{uv}^K \left\{ [B^K(D_{uv}^K \{ \underline{x}_k \})]_c^t \right\} \underline{m}_t^D(\underline{x}_k, \underline{y}^D) + [B^K(\underline{x}_k)]_c^t D_{uv}^K \{ \underline{m}_t^D(D_{uv}^K \{ \underline{x}_k \}, \underline{y}^D) \} + \right. \right. \\
&\quad \left. \left. D_{uv}^K \left\{ \frac{1}{k \|\underline{x}_k - \underline{y}^D\|} \left( j - \frac{1}{k \|\underline{x}_k - \underline{y}^D\|} \right) \left\{ \left( 2 [B^K(\underline{x}_k)]_c^t \underline{m}^D - 3 [B^K(\underline{x}_k)]_c^t \underline{m}_t^D(\underline{x}_k, \underline{y}^D) \right) + \right. \right. \right. \right. \\
&\quad \left. \left. \frac{1}{k \|\underline{x}_k - \underline{y}^D\|} \left( j - \frac{1}{k \|\underline{x}_k - \underline{y}^D\|} \right) \left( 2 D_{uv}^K \left\{ [B^K(D_{uv}^K \{ \underline{x}_k \})]_c^t \right\} \underline{m}^D - \right. \right. \\
&\quad \left. \left. \left. \left. 3 D_{uv}^K \left\{ [B^K(D_{uv}^K \{ \underline{x}_k \})]_c^t \right\} \underline{m}_t^D(\underline{x}_k, \underline{y}^D) - 3 [B^K(\underline{x}_k)]_c^t D_{uv}^K \{ \underline{m}_t^D(D_{uv}^K \{ \underline{x}_k \}, \underline{y}^D) \} \right\} \right\} \right] \right\}
\end{aligned} \tag{C6.9}$$

$$\left[ D_{uv}^K \left\{ S_m^K(\underline{m}^D, \underline{y}^D) \right\} \right]_c = -\frac{\underline{m}}{2} \sum_k \left\{ D_{uv}^L \left\{ \left[ \Psi(D_{uv}^K \{ \underline{x}_k \}, \underline{y}^D) \right]_c \right\} \left[ \Upsilon^K(\underline{x}_k, \underline{y}^D) \right]_c + \right. \\ \left. \Psi(\underline{x}_k, \underline{y}^D) D_{uv}^K \left\{ \left[ \Upsilon^K(D_{uv}^K \{ \underline{x}_k \}, \underline{y}^D) \right]_c \right\} \right\} \quad (C6.9)$$

Where the derivatives of the kernels  $g_i$  are defined as follows:

$$D_{uv}^K \left\{ \left[ \phi(D_{uv}^K \{ \underline{x}_k \}, \underline{y}^D) \right]_c \right\} = \frac{\partial \phi(\underline{x}_k, \underline{y}^D)}{\partial [\underline{x}_k]_c} D_{uv}^L \{ [\underline{x}_k]_c \} \\ D_{uv}^K \left\{ \left[ \Psi(D_{uv}^K \{ \underline{x}_k \}, \underline{y}^D) \right]_c \right\} = \frac{\partial \Psi(\underline{x}_k, \underline{y}^D)}{\partial [\underline{x}_k]_c} D_{uv}^L \{ [\underline{x}_k]_c \} \quad (C6.10)$$

The  $B^K$  matrix derivatives are defined in equation C6.11 as:

$$\left[ D_{uv}^K \{ B^K(D_{uv}^K \{ \underline{x}_k \}) \} \right]_{cs} = \left[ \left[ D_{uv}^K \{ \underline{x}_k \} \right]_{cs} \left| \left[ D_{uv}^K \{ \underline{x}_k \} \right]_{cs} \left| \left[ D_{uv}^K \{ \underline{x}_k \} \right]_{cs} \right. \right] - \\ \left[ \left[ D_{uv}^K \{ \underline{C}^K \} \right]_{c3} \left| \left[ D_{uv}^K \{ \underline{C}^K \} \right]_{c1} \left| \left[ D_{uv}^K \{ \underline{C}^K \} \right]_{c2} \right. \right] \quad (C6.11)$$

The expression of the dipole moment  $\underline{m}^D$  does not depend on the geometry; instead, according to equation C3.22, the transversal dipolar moment  $\underline{m}_t^D$  derivative is defined as:

$$D_{uv}^K \{ \underline{m}_t^D(\underline{r}) \} = -\frac{1}{r^2} \left[ D_{uv}^K \left\{ \left[ \underline{m}^D \cdot \underline{r} \right] \right\} \cdot \underline{r} + \left[ \underline{m}^D \cdot \underline{r} \right] \cdot D_{uv}^K \left\{ \underline{r} \right\} + \right. \\ \left. r^2 D_{uv}^K \left\{ \frac{1}{r^2} \right\} \left[ \underline{m}^D \cdot \underline{r} \right] \cdot \underline{r} \right] \quad (C6.12)$$

$$\text{where: } \underline{r} = (\underline{x}_k - \underline{y}^D)$$

Finally, we have the mixed product defined by the term  $\Upsilon^K$  derivative reported in equation C6.13:

$$\left[ D_{uv}^K \{ \Upsilon^K(D_{uv}^K \{ \underline{x}_k \}, \underline{y}^D) \} \right]_c = \det \left( \begin{array}{ccc} \left[ D_{uv}^K \{ B^K(D_{uv}^K \{ \underline{x}_k \}) \} \right]_{1c} & 0 & \left[ D_{uv}^K \{ \underline{x}_k \} \right]_1 \\ \left[ B^K(\underline{x}_k) \right]_{2s} & \left[ \underline{m}^D \right]_2 & \left[ (\underline{x}_k - \underline{y}^D) \right]_2 \\ \left[ B^K(\underline{x}_k) \right]_{3s} & \left[ \underline{m}^D \right]_3 & \left[ (\underline{x}_k - \underline{y}^D) \right]_3 \end{array} \right) + \quad (C6.13)$$

$$\det \begin{pmatrix} [B^K(x_k)]_{1s} & [m^D]_1 [x_k - y^D]_1 \\ [D_{uv}^K \{B^K(D_{uv}^K \{x_k\})\}]_{2s} & 0 [D_{uv}^K \{x_k\}]_2 \\ [B^K(x_k)]_{3s} & [m^D]_3 [x_k - y^D]_3 \end{pmatrix} + \det \begin{pmatrix} [B^K(x_k)]_{1s} & [m^D]_1 [x_k - y^D]_1 \\ [B^K(x_k)]_{2s} & [m^D]_2 [x_k - y^D]_2 \\ [D_{uv}^K \{B^K(D_{uv}^K \{x_k\})\}]_{3s} & 0 [D_{uv}^K \{x_k\}]_3 \end{pmatrix} \quad (C6.13)$$

Once these terms are calculated, we are able to find the FN reaction terms derivative reported in equation C3.31.

## C6.2 Semi-Numerical Technique

In Chapter 5, we gave the expressions of both the derivative with respect to the geometry for the reaction matrix and source vector. Now, we want to describe the numerical implementation of equations C5.23, C5.24 and C5.25 for the Semi-Numerical technique.

We also assume to work with planar structures only, so even if reduces the field of application of SR3D it notably simplifies the optimization procedure. Under this hypothesis and according to equation C2.28, we can say that if we consider the reaction between two planar structures, defined on the  $\gamma$  plane, then:

$$\Omega^{KL} = (\nabla_{L'} G \times \underline{\alpha}) \cdot \underline{\beta}^{test} \Big|_{\underline{\alpha}, \underline{\beta} \in \gamma} = 0 \quad (C6.14)$$

This lead to obtain a zero value of the  $R_2$  term in equation C2.28 and consequently a zero value for  $T$  operator reported in equation C3.28. As said this hypothesis simplifies the model but only planar structures can be treated.

*C6.2.1 Reaction Matrix Derivative:* the goal is to calculate the reaction terms of equation C5.24 between a single couple of triangles using the Semi-Numerical technique. According to Figure C3.5, equations C3.8, C5.15 and referring to equations C5.23 and C5.24, under the hypothesis of equation C6.14), we will describe the terms forming the  $A, D$  operator derivatives. As the equations defined in the following need a quite complex mathematical treatment, it has been reported in Annex 4; in this chapter we only report the main theory with the final expressions of all the terms which are defined inside the reduced  $A, D$  operators. As we treat the SN technique, we take into account only coplanar  $T_K, T_L$  reaction as we are under the hypothesis defined in equation C6.14 for  $A, D, T$  operators.

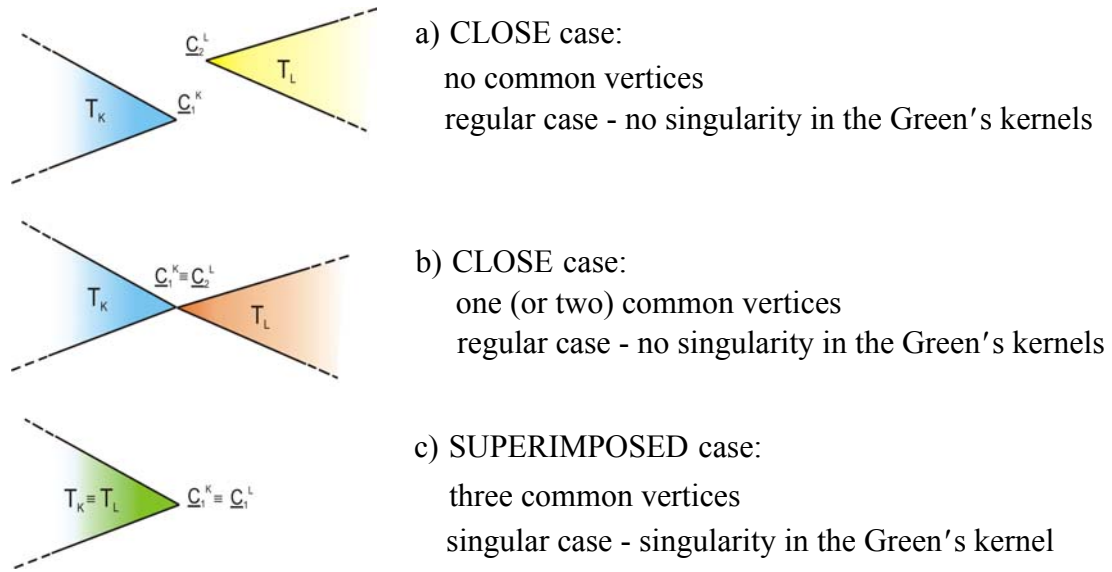


Figure C6.4: Common vertices derivative variables

There is a substantial difference between the SN reaction technique and the SN derivative reaction one. The difference lies inside the derivation variable  $\underline{C}^L$ . In fact, here we must discriminate the SN regular case *a)*, from the SN regular case with common vertices *b)* and from the SN singular case *c)* as shown in Figure C6.4.

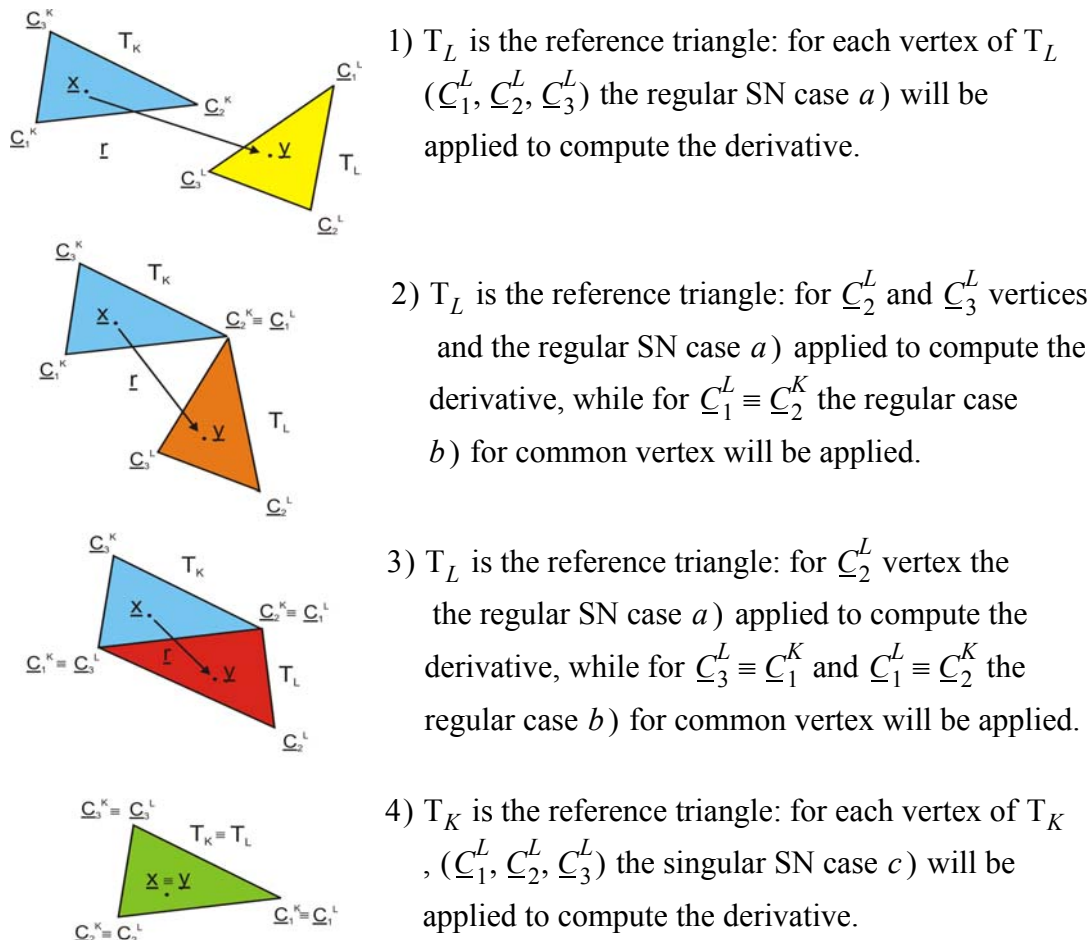


Figure C6.5: All the SN technique cases with respect to the derivation vertex

That means for each configuration defined in Figure C6.4, different derivative expressions will be given. Let's define every possible case that can occurs using the SN technique in Figure C6.5.

Let's give now the derivative expressions for the  $A, D$  operators with respect to the Figures C6.4 and examples of Figure C6.5. As many variables depend on both the triangles  $T_K, T_L$ , we will specify also the derivative of the variables arguments.

a) *Regular case with no common vertices,  $T_K \neq T_L$ .* According to equations from C4.16 to C4.22 and Annex 4, we show the  $A, D$  operator derivatives with respect to the geometry.

$$\begin{aligned} \left[ D_{uv}^L \{A^{KL}(g^\infty)\} \right]_{cs} &= \frac{1}{4} \sum_k \sum_l \alpha_k \alpha_l \left\{ D_{uv}^L \{t_0^L(x_k)\} \left[ B^K(x_k) \right]_c^t \left[ B^L(x_l) \right]_s + t_0^L(x_k) \left[ B^K(x_k) \right]_c^t D_{uv}^L \left\{ \left[ B^L(x_l) \right]_s \right\} + \right. \\ &\quad \left. \left[ B^K(x_k) \right]_c^t \left[ D_{uv}^L \{t_1^L(x_k)\} \right] \left[ D_{uv}^L \{t_1^L(x_k)\} \right] \left[ D_{uv}^L \{t_1^L(x_k)\} \right]_s \right\} + \\ &\quad \frac{1}{4} \sum_k \sum_l \alpha_k \alpha_l \left\{ \left[ B^K(x_k) \right]_c^t D_{uv}^L \left\{ \left[ B^L(y_l) \right]_s \right\} g^\infty(x_k, y_l) + \left[ B^K(x_k) \right]_c^t \left[ B^L(y_l) \right]_s D_{uv}^L \left\{ g^\infty(x_k, D_{uv}^L \{y_l\}) \right\} \right\} \\ \left[ D_{uv}^L \{D^{KL}(g^\infty)\} \right]_{cs} &= \frac{1}{4} \sum_k \sum_l \alpha_k \alpha_l D_{uv}^L \{t_0^L(x_k)\} + \frac{1}{4} \sum_k \sum_l \alpha_k \alpha_l g^\infty(x_k, x_l) \end{aligned} \quad (C6.15)$$

b) *Regular case with common vertices,  $T_K \neq T_L$ .* According to equations from C4.16 to C4.22 and Annex 4, we show the  $A, D$  operator derivatives with respect to the geometry. We want now to solve the most complicate case for the SN technique. We have almost the same expression than the regular case with no common vertices. In fact, due to the dependancy of the derivative on the common vertex  $\underline{C}^K \equiv \underline{C}^L$ , we must change the expression of the  $A, D$  operator derivative expressions. So, if we define the vertices  $\underline{C}_A^K \equiv \underline{C}_B^L = \underline{C}_v^T$ , where  $A$  and  $B$  are the vertex index number for  $T_K$  and  $T_L$  respectively. We obtain:

$$\begin{aligned} \left[ D_{uv}^T \{A^{KL}(g^\infty)\} \right]_{cs} &= \frac{1}{4} \sum_k \sum_l \alpha_k \alpha_l \left\{ D_{uB}^L \{t_0^L(D_{uA}^K \{x_k\})\} \left[ B^K(x_k) \right]_c^t \left[ B^L(x_l) \right]_s + \right. \\ &\quad \left. t_0^L(x_k) D_{uA}^K \left\{ \left[ B^K(D_{uA}^K \{x_k\}) \right]_c^t \left[ B^L(x_l) \right]_s + t_0^L(x_k) \left[ B^K(x_k) \right]_c^t D_{uB}^L \left\{ \left[ B^L(D_{uA}^K \{x_l\}) \right]_s \right\} \right\} + \\ &\quad D_{uA}^K \left\{ \left[ B^K(D_{uA}^K \{x_k\}) \right]_c^t \left[ t_1^L(x_k) \right] \left[ t_1^L(x_k) \right] \left[ t_1^L(x_k) \right]_s \right\} + \\ &\quad \left. \left[ B^K(x_k) \right]_c^t \left[ D_{uB}^L \{t_1^L(D_{uA}^K \{x_k\})\} \right] \left[ D_{uB}^L \{t_1^L(D_{uA}^K \{x_k\})\} \right] \left[ D_{uB}^L \{t_1^L(D_{uA}^K \{x_k\})\} \right]_s \right\} + \quad (C6.16) \\ &\quad \frac{1}{4} \sum_k \sum_l \alpha_k \alpha_l \left\{ D_{uA}^K \left\{ \left[ B^K(D_{uA}^K \{x_k\}) \right]_c^t \left[ B^L(y_l) \right]_s \right\} g^\infty(x_k, y_l) + \left[ B^K(x_k) \right]_c^t D_{uB}^L \left\{ \left[ B^L(D_{uB}^L \{y_l\}) \right]_s \right\} g^\infty(x_k, y_l) + \right. \\ &\quad \left. \left[ B^K(x_k) \right]_c^t \left[ B^L(y_l) \right]_s D_{uA}^K \left\{ g^\infty(D_{uA}^K \{x_k\}, y_l) \right\} + \left[ B^K(x_k) \right]_c^t \left[ B^L(y_l) \right]_s D_{uB}^L \left\{ g^\infty(x_k, D_{uB}^L \{y_l\}) \right\} \right\} \\ \left[ D_{uv}^T \{D^{KL}(g^\infty)\} \right]_{cs} &= \frac{1}{4} \sum_k \sum_l \alpha_k \alpha_l D_{uB}^L \{t_0^L(D_{uA}^K \{x_k\})\} + \\ &\quad \frac{1}{4} \sum_k \sum_l \alpha_k \alpha_l \left\{ D_{uA}^K \left\{ g^\infty(D_{uA}^K \{x_k\}, y_l) \right\} + D_{uB}^L \left\{ g^\infty(x_k, D_{uB}^L \{y_l\}) \right\} \right\} \end{aligned}$$

c) *Singular case with all common vertices*,  $T_K \equiv T_L$ . According to equations from C4.16 to C4.22 and Annex 4, we show the  $A, D$  operator derivatives with respect to the geometry. If we define the vertices  $\underline{C}_A^K \equiv \underline{C}_A^L = \underline{C}_v^T$ , where  $A$  and  $B$  are the vertex index number for  $T_K$  and  $T_L$  respectively. We obtain:

$$\begin{aligned}
\left[ D_{uv}^K \{A^{KL}(\mathbf{g}^\infty)\} \right]_{cs} &= \frac{1}{4} \sum_k \sum_l \alpha_k \alpha_l \left\{ D_{uv}^K \{t_0^K(D_{uv}^K \{\mathbf{x}_k\})\} \left[ B^K(\mathbf{x}_k) \right]_c^t \left[ B^K(\mathbf{x}_l) \right]_s + \right. \\
& \quad t_0^K(\mathbf{x}_k) D_{uv}^K \left\{ \left[ B^K(D_{uv}^K \{\mathbf{x}_k\}) \right]_c^t \left[ B^K(\mathbf{x}_l) \right]_s + t_0^K(\mathbf{x}_k) \left[ B^K(\mathbf{x}_k) \right]_c^t D_{uv}^K \left\{ \left[ B^K(D_{uv}^K \{\mathbf{x}_l\}) \right]_s \right\} + \\
& \quad D_{uv}^K \left\{ \left[ B^K(D_{uv}^K \{\mathbf{x}_k\}) \right]_c^t \left\{ t_1^K(\mathbf{x}_k) \left| t_1^K(\mathbf{x}_k) \right| t_1^K(\mathbf{x}_k) \right\}_s + \right. \\
& \quad \left. \left[ B^K(\mathbf{x}_k) \right]_c^t \left[ D_{uv}^K \{t_1^K(D_{uv}^K \{\mathbf{x}_k\})\} \left| D_{uv}^K \{t_1^K(D_{uv}^K \{\mathbf{x}_k\})\} \right| D_{uv}^K \{t_1^K(D_{uv}^K \{\mathbf{x}_k\})\} \right]_s \right\} + \tag{C6.17} \\
& \quad \frac{1}{4} \sum_k \sum_l \alpha_k \alpha_l \left\{ D_{uv}^K \left\{ \left[ B^K(D_{uv}^K \{\mathbf{x}_k\}) \right]_c^t \left[ B^K(\mathbf{x}_l) \right]_s \mathbf{g}^\infty(\mathbf{x}_k, \mathbf{x}_l) + \left[ B^K(\mathbf{x}_k) \right]_c^t D_{uv}^K \left\{ \left[ B^K(D_{uv}^K \{\mathbf{x}_l\}) \right]_s \right\} \mathbf{g}^\infty(\mathbf{x}_k, \mathbf{x}_l) + \right. \\
& \quad \left. \left[ B^K(\mathbf{x}_k) \right]_c^t \left[ B^K(\mathbf{x}_l) \right]_s D_{uv}^K \{ \mathbf{g}^\infty(D_{uv}^K \{\mathbf{x}_k\}, \mathbf{x}_l) \} + \left[ B^K(\mathbf{x}_k) \right]_c^t \left[ B^K(\mathbf{x}_l) \right]_s D_{uv}^K \{ \mathbf{g}^\infty(\mathbf{x}_k, D_{uv}^K \{\mathbf{x}_l\}) \} \right\} \quad k \neq l \\
\left[ D_{uv}^K \{D^{KL}(\mathbf{g}^\infty)\} \right]_{cs} &= \frac{1}{4} \sum_k \sum_l \alpha_k \alpha_l D_{uv}^K \{ t_0^K(D_{uv}^K \{\mathbf{x}_k\}) \} + \\
& \quad \frac{1}{4} \sum_k \sum_l \alpha_k \alpha_l \{ D_{uv}^K \{ \mathbf{g}^\infty(D_{uv}^K \{\mathbf{x}_k\}, \mathbf{x}_l) \} + D_{uv}^K \{ \mathbf{g}^\infty(\mathbf{x}_k, D_{uv}^K \{\mathbf{x}_l\}) \} \} \quad k \neq l
\end{aligned}$$

**CHAPTER 7:**  
**OPTIMIZATION**

## Chapter 7 - Optimization

The optimization algorithm is defined in order to find the optimal position of a certain number of metallic objects inside the domain  $\Gamma$ , illuminated by a certain number of electric dipoles. In Figure C7.1, we report a scenario with  $K$  objects,  $M$  electric dipoles and  $N$  measurement points. The optimization variables are the positions of the objects and the cost functional is based on the scattered electric field data.

The optimization algorithm will be able to find the optimal position of these objects, inside  $\Omega$ , translating them in order to find out the desired scattered electric field in a certain number of measurement points.

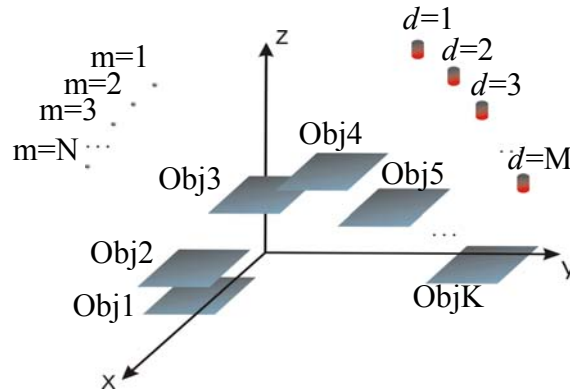


Figure C7.1: General geometry problem

The flow chart in Figure C7.2 resumes the whole optimization method. We want to show the main parts of the optimization procedure; for sake of simplicity, we want to point the attention on three parts: direct problem solution (Chapter 4), inverse problem solution (Chapter 6) and cost functional definition (Annex 5). Once these problems are solved, we can use any optimization algorithm, requiring the calculation of the gradient of the cost functional.

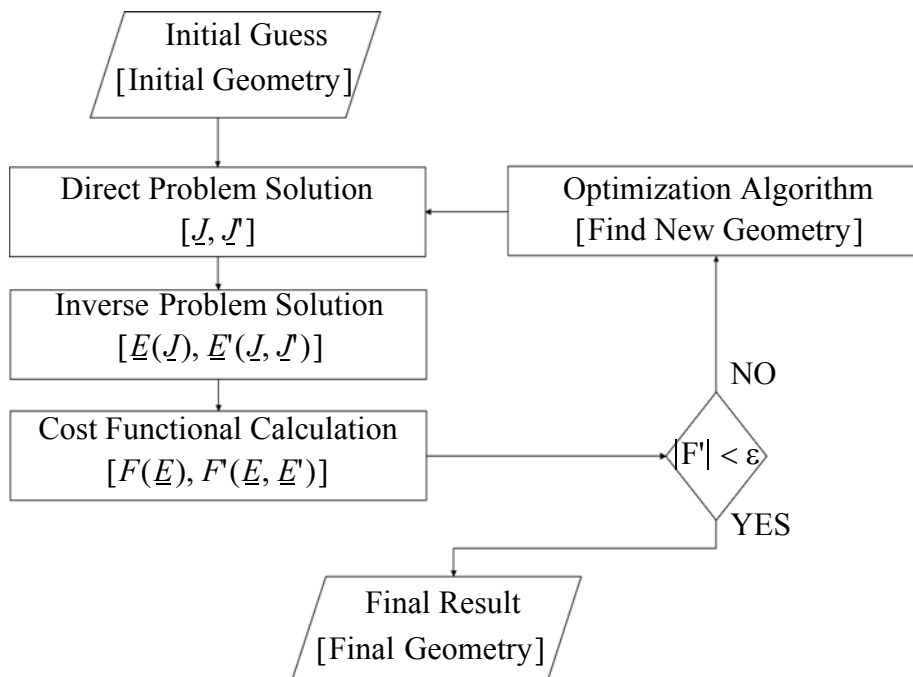


Figure C7.2: Optimization method flow chart

In Figure C7.2, we define the surface electric currents as  $\underline{J}$ , the electric scattered field as  $\underline{E}$  and the cost functional of the criteria as  $F$ ; the terms  $\underline{J}'$ ,  $\underline{E}'$  and  $F'$  are, respectively, the derivative with respect to the geometry.

## C7.1 Optimization Terms Calculation

In this paragraph, we will describe how to solve the direct and the inverse problem and how to compute the cost functional. As already seen in Chapter 4 and Chapter 6, the direct and the inverse problems are solved using a numerical method based on a time harmonic integral formulation. The unknowns are the electromagnetic density of currents on the boundary surfaces of the sub-domains of the structure, The numerical model is based on a surface discretization, using triangular finite elements.

*C7.1.1 Direct Problem:* we are considering mixed metallic and dielectric planar antennas illuminated by a certain number of plane waves or dipoles and using a time-harmonic Combined Field Integral Equation (CFIE) integral formulation  $\underline{E}$ ,  $\underline{H}$  for the 3D or 2D radiating structures.

$$\begin{aligned}\underline{E}(r) &= \underline{E}^{inc}(r) + j\omega\mu \oint_{\Omega} G(r, r') \underline{J}(r') d\Omega + \\ &\quad \frac{j}{\omega\epsilon} \oint_{\Omega} \underline{\nabla}_{r'} G(r, r') \underline{\nabla}_{\Omega} \cdot \underline{J}(r') d\Omega - \underline{\nabla} \times \oint_{\Omega} G(r, r') \underline{M}(r') d\Omega \\ \underline{H}(r) &= \underline{H}^{inc}(r) + j\omega\epsilon \oint_{\Omega} G(r, r') \underline{M}(r') d\Omega + \\ &\quad \frac{j}{\omega\mu} \oint_{\Omega} \underline{\nabla}_{r'} G(r, r') \underline{\nabla}_{\Omega} \cdot \underline{M}(r') d\Gamma - \underline{\nabla} \times \oint_{\Omega} G(r, r') \underline{J}(r') d\Gamma\end{aligned}\quad (C7.1)$$

$$\text{where: } \boxed{\Omega = \bigcup_{k=1}^N \Omega_k \quad \text{and} \quad G(r, r') = \frac{e^{jk\|r-r'\|}}{4\pi\|r-r'\|}}$$

$\underline{J}$  and  $\underline{M}$  design the electric and magnetic density surface currents on  $\Omega$  (surface of the scatterers or planar antennas). The numerical solution is based on a moment method or equivalently a variational integral formulation (Rumsey reaction concept or reciprocity principle). The unknowns electric and magnetic fluxes,  $\Phi_J$  and  $\Phi_M$ , of  $\underline{J}$  and  $\underline{M}$  surface density currents are solution of the linear system of equation (C7.2) (see Chapter 3).

$$[\underline{Z}] [\underline{\Phi}] = [\underline{S}] \quad (C7.2)$$

$$\text{where: } \boxed{[\underline{\Phi}] = \begin{bmatrix} \Phi_J \\ \Phi_M \end{bmatrix}}$$

Once the unknown fluxes have been calculated, we are able to find out their derivative with respect to the geometry. In order to do that, we need to define the linear system derivative:

$$\left[ \frac{\partial \underline{Z}}{\partial \Omega} \right] [\underline{\Phi}] + [\underline{Z}] \left[ \frac{\partial \underline{\Phi}}{\partial \Omega} \right] = \left[ \frac{\partial \underline{S}}{\partial \Omega} \right] \quad (C7.3)$$

Then, we need to solve this new linear system passing through equation (C7.4):

$$[Z] \left[ \frac{\partial \Phi}{\partial \Omega} \right] = \left[ \frac{\partial S}{\partial \Omega} \right] - \left[ \frac{\partial Z}{\partial \Omega} \right] [\Phi] \quad (C7.4)$$

Finally, we have the expression of the derivative with respect to the geometry of the linear system of equation (C7.2). The expression of the terms of equation (C7.5) are defined in Chapter 5.

$$\left[ \frac{\partial \Phi}{\partial \Omega} \right] = [Z]^{-1} \left\{ \left[ \frac{\partial S}{\partial \Omega} \right] - \left[ \frac{\partial Z}{\partial \Omega} \right] [\Phi] \right\} \quad (C7.5)$$

If now, we multiply the fluxes and its derivatives with respect to the geometry, with the vector basis as reported in equation (A2.5), we find out the surface currents and its derivatives.

$$\begin{aligned} \underline{J} &= \Phi_{J_1} \cdot \underline{j}_1 + \Phi_{J_2} \cdot \underline{j}_2 + \Phi_{J_3} \cdot \underline{j}_3 \\ \underline{M} &= \Phi_{M_1} \cdot \underline{m}_1 + \Phi_{M_2} \cdot \underline{m}_2 + \Phi_{M_3} \cdot \underline{m}_3 \end{aligned} \quad (C7.6)$$

where:  $\underline{j}, \underline{m}$  are the vector basis of the method of moment

*C7.1.2 Inverse Problem and Cost Functional:* the inverse scattering problem consists in retrieving the position of planar antennas when they are illuminated successively by a certain number  $L$  of plane waves or dipoles and when the radiation far-field or near-field patterns are measured in a certain region of the domain. The computed scattered electric field  $\underline{E}_{comp}^s$  is calculated using the results of the direct problem and it is reported in of equation (C7.7):

$$\underline{E}_{comp}^s = [G] [J] \quad (C7.7)$$

Then, we can also calculating the derivative of the computed scattered electric field with respect to the mesh. The expression of the terms of equations (C7.7) and (C7.8) are defined in Annex 5.

$$\frac{\partial \underline{E}_{comp}^s}{\partial \Omega} = \left[ \frac{\partial G}{\partial \Omega} \right] [J] + \left[ \frac{\partial J}{\partial \Omega} \right] [G] \quad (C7.8)$$

where:  $\left[ \frac{\partial J}{\partial \Omega} \right]$  current derivative with respect to mesh  
 $\left[ \frac{\partial G}{\partial \Omega} \right]$  Green's function derivative with respect to mesh

Given the measured or synthetic desired scattered electric field  $\underline{E}_{meas}^s$ , then the cost functional  $F$  is given by:

$$F = \sum_{l=1}^L \left\| \underline{E}_{meas}^s - \underline{E}_{comp}^s \right\|^2 \quad (C7.9)$$

The gradient of the cost functional  $F$  with respect to the vertices of the different triangular cells of the mesh is given by:

$$\frac{\partial F}{\partial \Omega} = 2 \sum_{l=1}^L \Re \{ \underline{E}_{meas}^s - \underline{E}_{comp}^s \} \frac{\partial \underline{E}_{comp}^s}{\partial \Omega} \quad (C7.10)$$

## C7.2 Optimization Routine

The flow chart of the optimization routine is reported in Figure C7.2. We want to give below a short resume of the entire procedure.

1. We start defining the synthetic or measured scattered field data related to the desired geometry. We call this data  $\underline{E}_{meas}^s$ .
2. We solve the direct problem obtaining the surface density currents  $\underline{J}$  and its derivatives with respect to the mesh  $\frac{\partial \underline{J}}{\partial \Omega}$ .
3. We solve the inverse problem obtaining the computed scattered field  $\underline{E}_{comp}^s$  and its derivatives with respect to the mesh  $\frac{\partial \underline{E}_{comp}^s}{\partial \Omega}$ . Then we can compute the cost functional  $F$  and its derivatives with respect to the mesh  $\frac{\partial F}{\partial \Omega}$ . The goal of the optimization is to reach the minimum of the cost functional  $F$ ; in order to do that we must satisfy the condition reported in equation (C7.11).

$$F = \min \left\{ \sum_{l=1}^L \left\| \underline{E}_{meas}^s - \underline{E}_{comp}^s \right\|^2 \right\} \Rightarrow \frac{\partial F}{\partial \Omega} = 0 \quad (C7.11)$$

4. If the condition in equation (C7.11) is not satisfied we must pass through the optimization algorithm and find a new geometry and then do again the loop.
5. Otherwise the optimization routine will stop, giving the final geometry.

**CHAPTER 8:**  
**CODE VALIDATION**

## Chapter 8 - Code Validation

We have described all the optimization procedure, explaining in details the numerical method used to solve the direct and the inverse problem. We have also introduced the SR3D in which this method has been implemented. As seen in Chapter 3 and Chapter 4, the SR3D main core has been revised and validated with respect to the old version. Since the old version is stable, we did not show any validation results for it.

We want to concentrate the attention to the validation of the new part, i.e. the derivative calculation with respect to the geometry of the reaction matrix and the source vector and the gradient of the cost functional.

### C8.1 Validation of the Derivative of the Linear System Elements

In Chapter 4, we have found the expressions of the reaction matrix and the source vector concerning the MoM linear system. We have found in Chapter 7 the expression of the surface density currents (see equation (C7.2) and equation (A2.5)). The derivative of the the surface density currents with respect to the geometry has been explained in Chapter 7 (see equation (C7.5) and equation (A2.5)), using the results obtained from Chapter 6. In order to validate the surface density currents with respect to the geometry, we define a test-case with a two-patches structure with one electric dipole placed between them, (Figure C8.1).

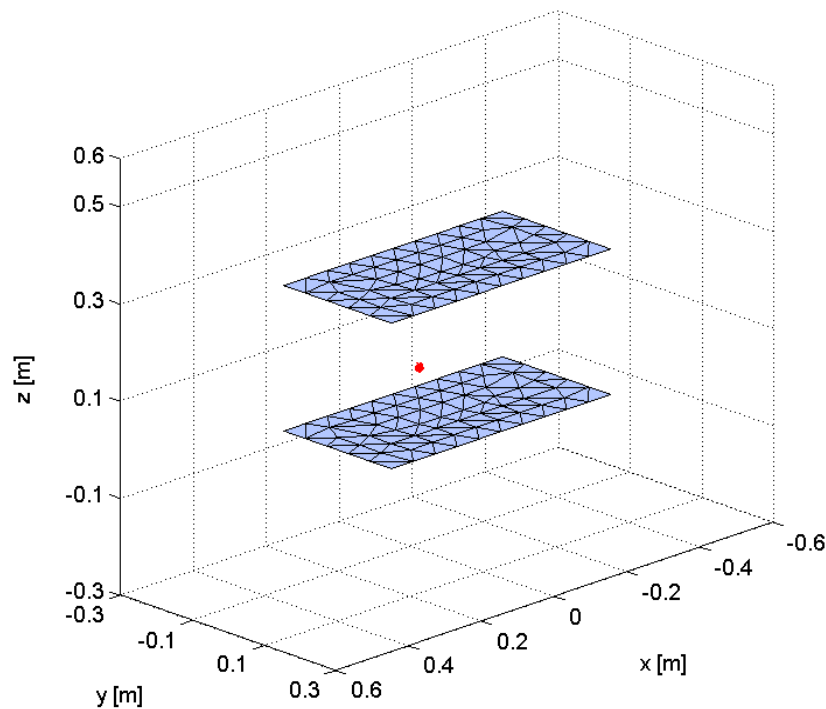


Figure C8.1: Surface density currents derivative validation case-test

The electric dipole is placed between the plates with the electric center placed at the point  $(x, y, z) = (0.15, 0.075, 0.15)$  m. The dipole moment is defined as  $(d_x, d_y, d_z) = (1, 1, 1)$  and the working frequency is 1 GHz ( $\lambda = 0.3$  m). The two identical parallel thin metallic plates have the dimensions of 0.3 m ( $\lambda$ ) of length along the y-axis and 0.6 m ( $2\lambda$ ) toward the x-axis and they are at a distance of 0.3 m ( $\lambda$ ) along the z-axis.

After the mesh generation, we obtain 228 triangles with a total of 312 degrees of freedom (considering that we have some triangles with common sides). We recall that the degrees of freedom represent the number of the current fluxes flowing through the sides of the triangles (see Figure A2.3). As we want to perform the derivative of the upper patch with respect to the lower one

and vice-versa, we consider a double number of degrees of freedom, i.e. 624. Once the structure has been defined, we computed the derivative of the surface density currents derivative with respect to the mesh and we have compared them using a sixth-order forward finite-difference derivative method. Of course, the terms used to compute the finite-difference derivative have been obtained by the SR3D code.

In Figure C8.2, we show the relative error percentage between the analytic and the numerical derivatives considering the shift of the plates along the x,y and z direction. The samples from 0 to 312 are relative to the derivative of the lower plate with respect to the fixed upper plate and the sample from 313 to 624 are relative to the derivative of the upper plate with respect to the fixed lower plate.

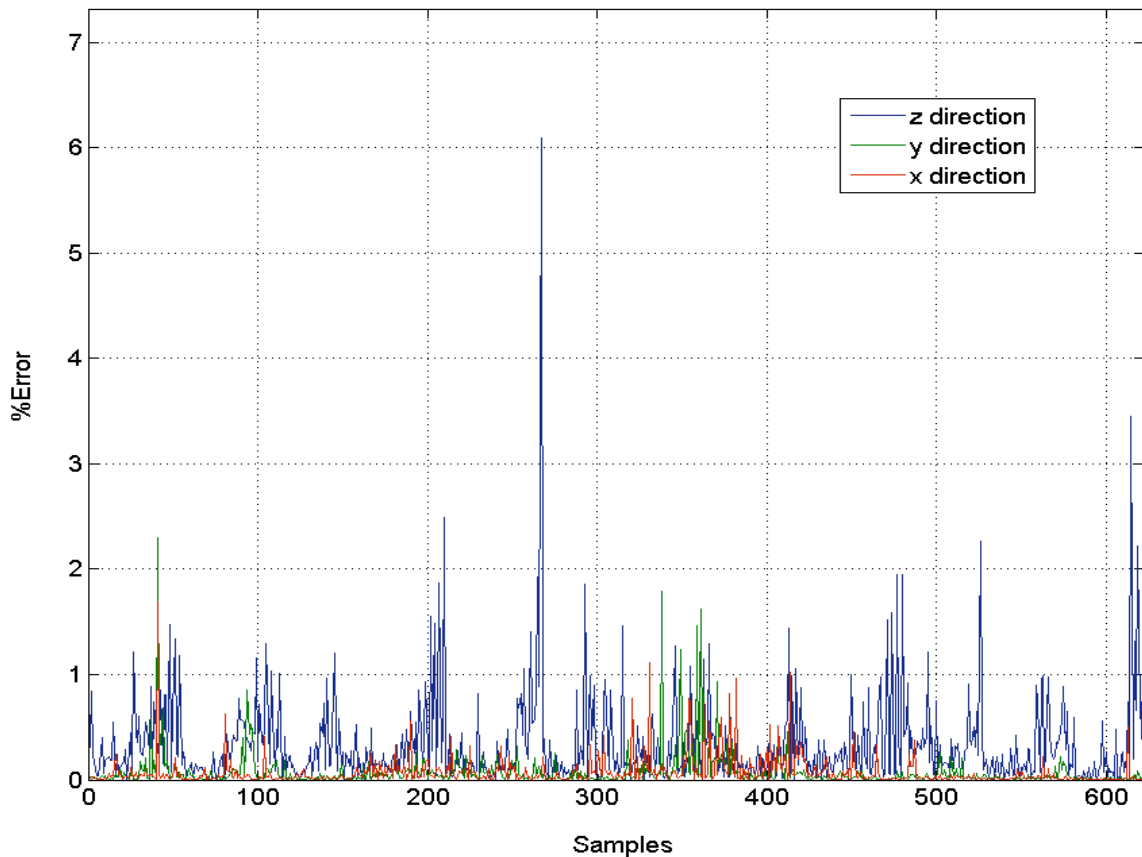


Figure C8.2: Percentage relative error for the surface density currents derivative

As we can see, the average error is quite small considering that we should increase the finite-difference method order to obtain a better convergence to the analytic values. Finally, we obtain:

Direction	Maximum Relative Error [%]	Average Relative Error [%]
x	1.685	0.075
y	2.301	0.076
z	6.100	0.331

Once derivative of the surface density current has been validated, we can also assert that the reaction matrix and the source vector derivative have been validated.

## C8.2 Cost Functional Gradient Derivative Validation

Since an optimization algorithm is involved in our code, then a cost functional has to be defined, as seen in Chapter 7 (see equation (C7.9)). Moreover, in order to understand the evolution of the optimization process, we have also defined the cost functional derivative with respect to the geometry (see equation (C7.10)).

We have to validate this gradient using a second-order forward finite-difference derivative method. In order to do that, we have chosen a trivial structure composed by three square metallic plates defined on the same x-y plane as shown in Figure C8.3.

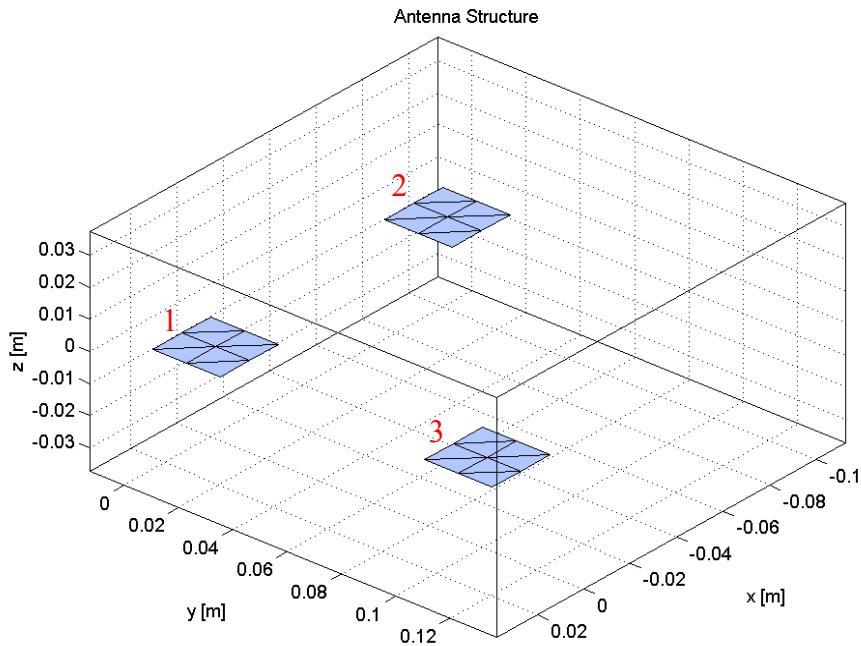


Figure C8.3: Cost functional derivative validation case-test

We have three electric dipoles placed around the structure at the following coordinate points: dipole 1 at  $(x_1, y_1, z_1) = (0.125, -0.07, 0.07)$  m, dipole 2 at  $(x_2, y_2, z_2) = (0.125, 0.07, 0.07)$  m and dipole 3 at  $(x_3, y_3, z_3) = (0, 0.0625, -0.1)$  m. The dipole moment is the same for all the dipoles and is defined as  $(d_x, d_y, d_z) = (1, 1, 1)$  while the working frequency is 3 GHz ( $\lambda = 0.1$  m). So each square thin plate has the side dimension of 0.025 m ( $\lambda/4$ ). The plate 1 is placed in the center of the coordinate system, then the plate 2 is at  $\lambda$  from the plate 1 along the x-axis in the negative direction while the plate 3 is at  $\lambda$  from the plate 1 along the y-axis in the positive direction.

We shifted the plate 1 along x and y directions with respect to a certain number of positions in order to find a map of the cost functional gradient and of its derivative with respect to the geometry (see Figure C8.4 and Figure C8.5). Normally, this technique is used to understand the behaviour of the functions and to set a convenient strategy for the optimization process; in this case, we are just interested in retrieving the shape of the cost functional and the cost functional derivative. We created a grid of values shifting only the plate 1 toward the x positive direction and the y negative direction with a step of 0.001 m, retrieving 30 samples for each axis (900 samples total).

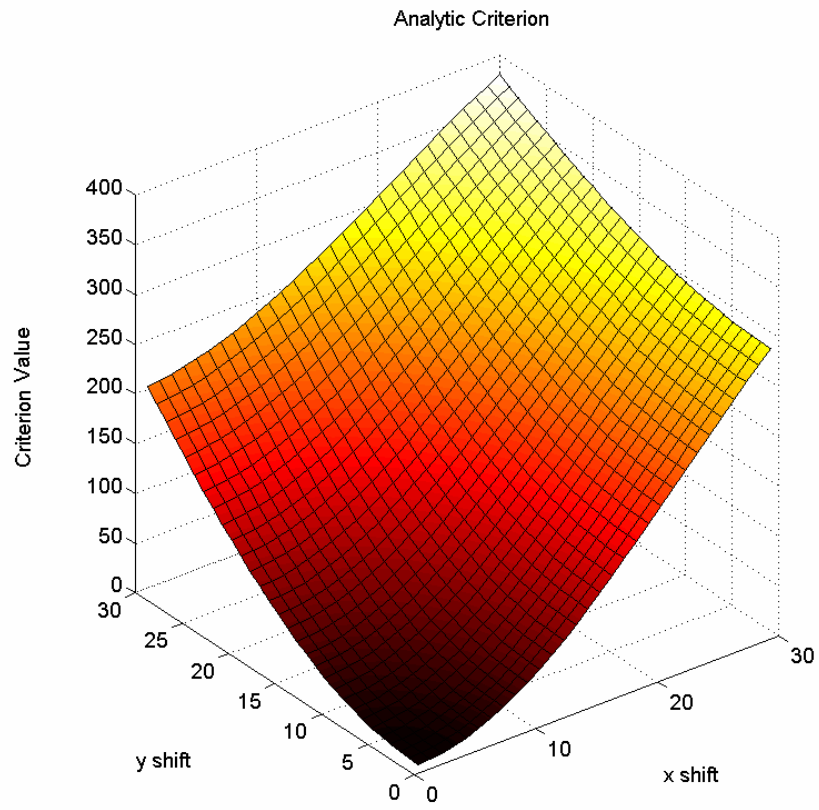


Figure C8.4: Map of the cost functional for plate 1 shift

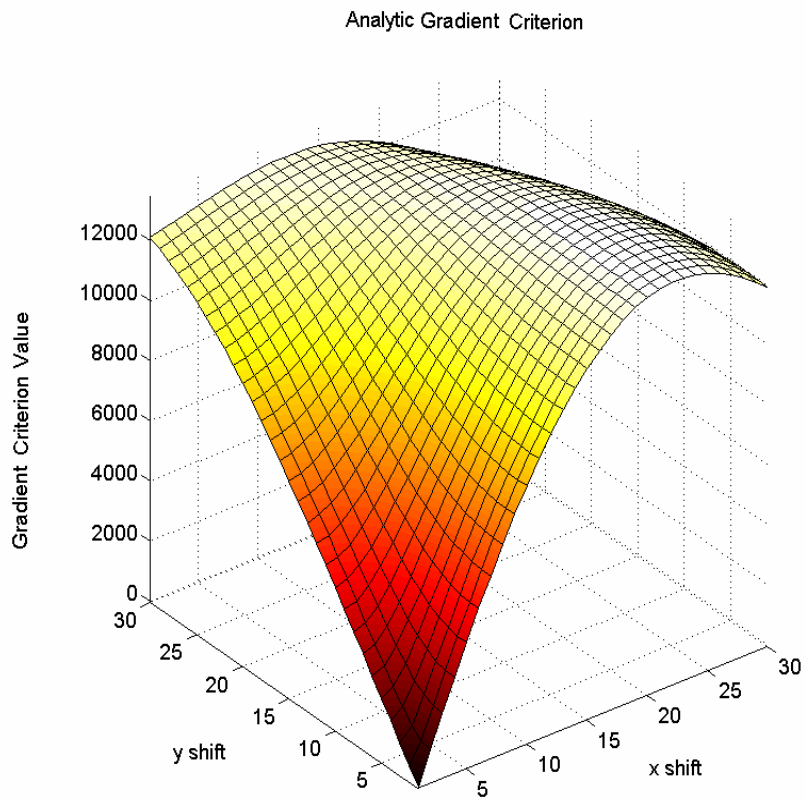


Figure C8.5: Map of the cost functional derivative for plate 1 shift

Then we have calculated the numerical derivative with respect to the plate 1 shifted along the x axis while the y shift remains fixed and the same for the plate 1 shifted toward the y direction while the x shift remains fixed. The results are reported, respectively, in Figure C8.6 and Figure C8.7.

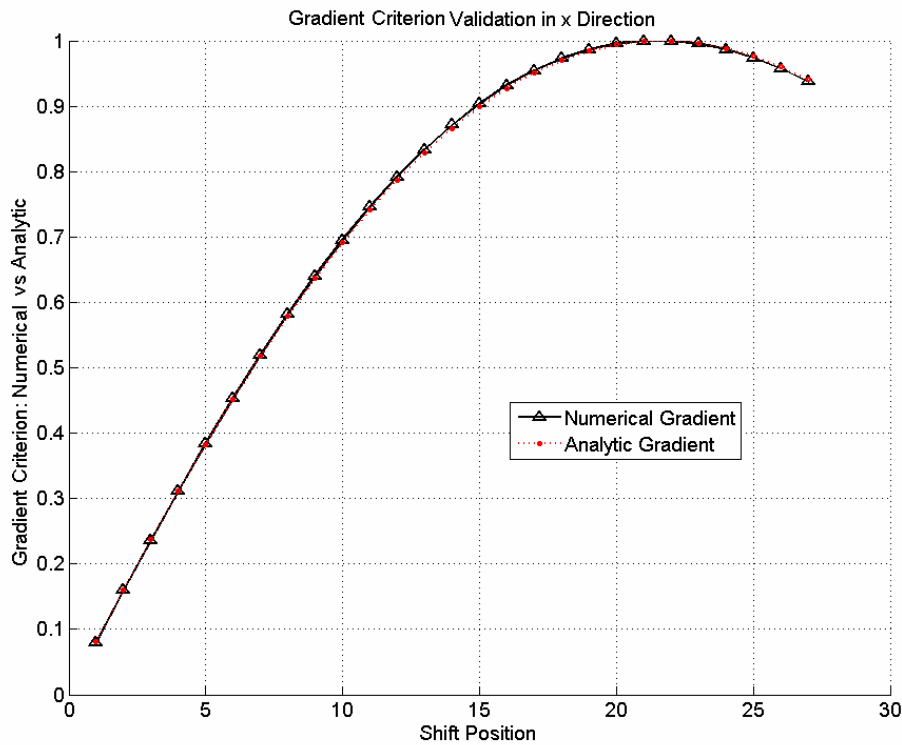


Figure C8.6: cost functional gradient validation along x direction for plate 1 shifting

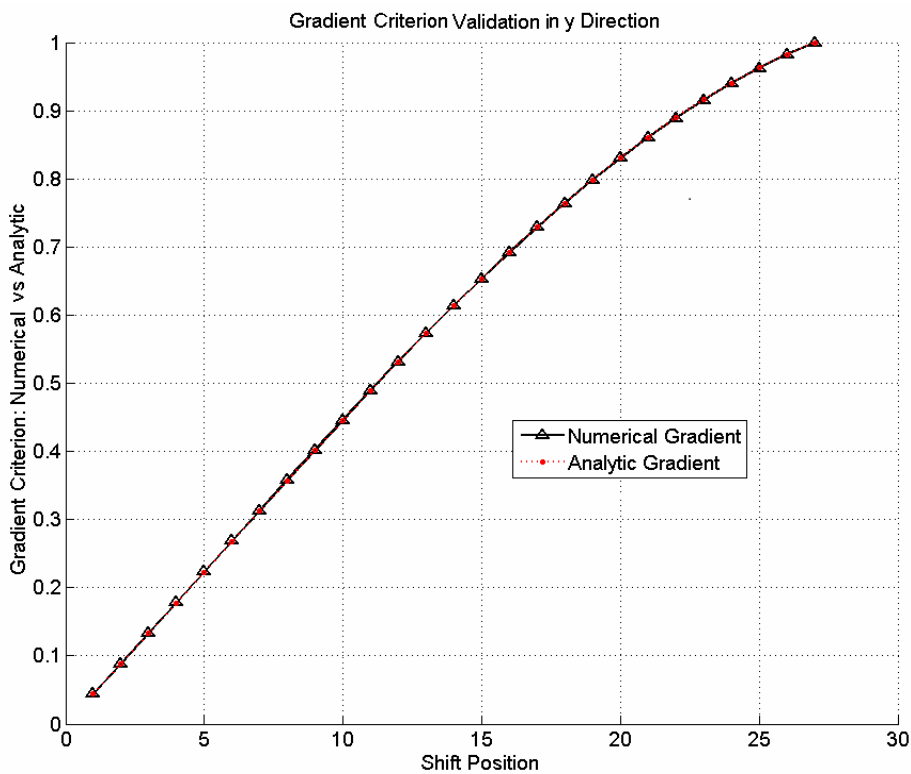


Figure C8.7: Cost functional gradient validation along y direction for plate 1 shifting

Finally, the percentage relative error between the numerical and the analytic gradient data is reported in the table:

Direction	Maximum Relative Error [%]	Average Relative Error [%]
x	0.892	0.510
y	0.740	0.536

### C8.3 First Example: Optimization Pattern Over the Criterion Map

For the first optimization example, we chose the structure previously used and reported in Figure C8.3. We use the same basic example configuration. In order to able to apply the optimization algorithm one initial guess must be defined. We chose to shift the first metallic plate of 0.02 m ( $\lambda/5$ ) along the x axis in the positive direction and of 0.02 m ( $\lambda/5$ ) along the y axis in the positive direction. If we consider the Figure C8.8, in red we have the geometry initial guess, in blue the final geometry and in green the desired geometry.

The optimization algorithm is able to optimize the location of a certain number of metallic objects using a cost function gradient, that is defined through the scattered field variable. So, we can define the desired geometry by simply calculating the synthetic scattered field data related to the desired configuration and use it inside the optimization procedure.

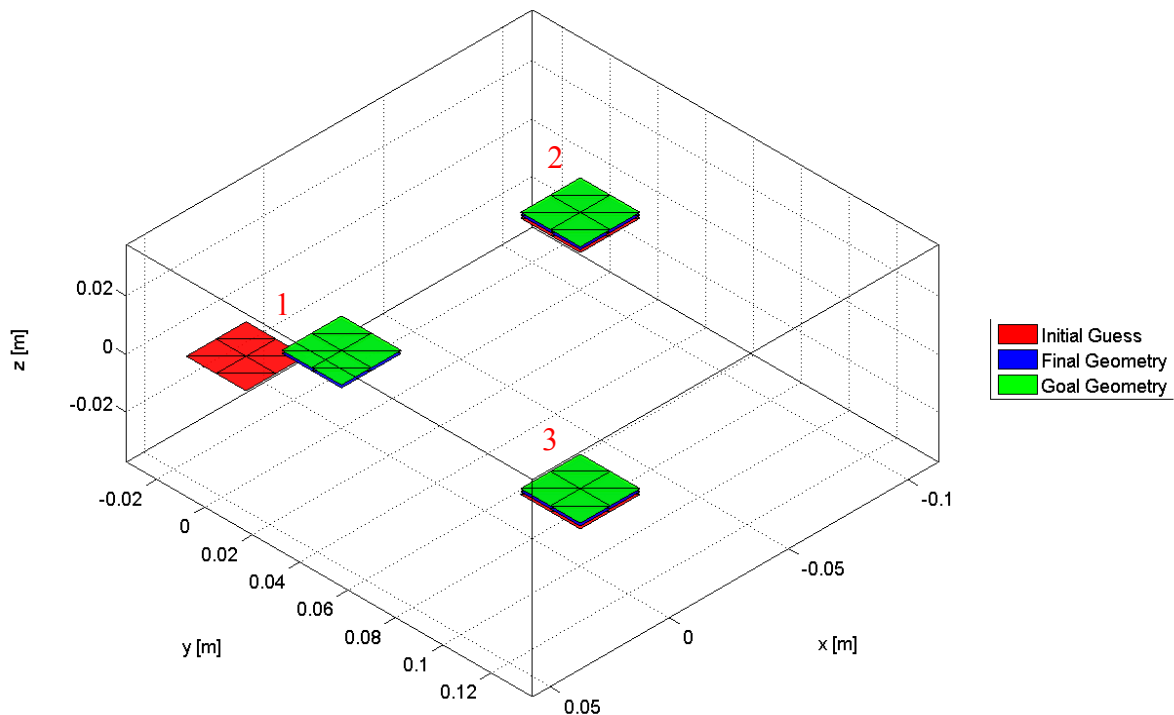


Figure C8.8: Initial guess, desired and final geometry

As constraints, we fix the plate 2 and 3 in their initial positions in order to have only one degree of freedom inside the optimization problem, represented by the position of the plate 1. Under this assumption we have obtained the follow results: in Figure C8.9 we have a representation of the criterion evolution map (the same as Figure C8.4) with all the optimization step points.

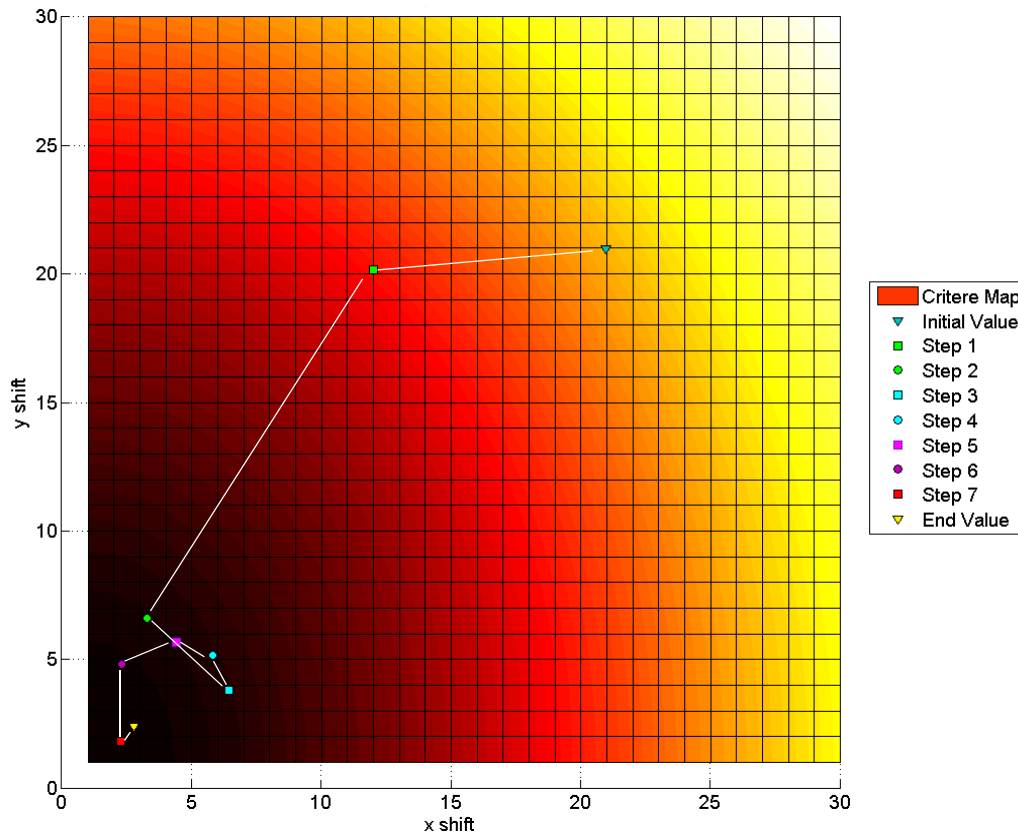


Figure C8.9: 2D Criterion map with optimization step points (9)

Finally we present the criterion convergence diagram in Figure C8.10. As we can see the convergence is obtained after 9 iterations with an excellent final value.

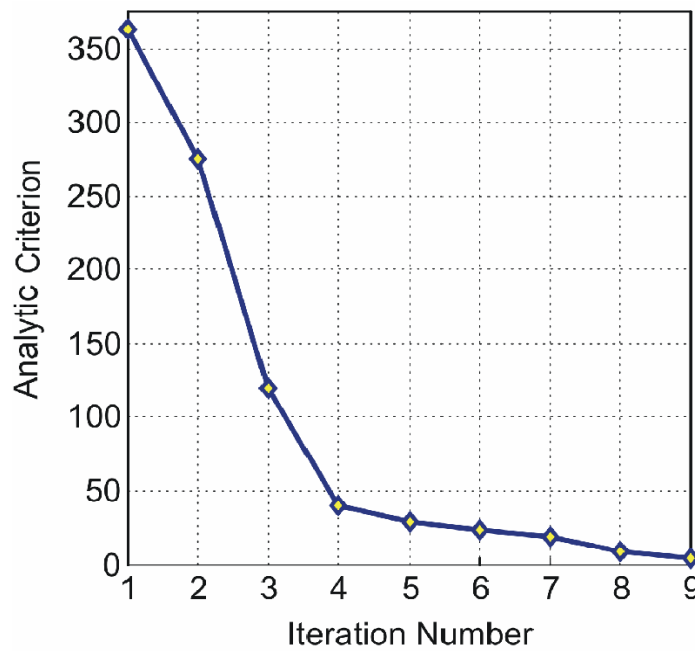


Figure C8.10: Criterion convergence

The start criterion value is of 363.9732 and the final criterion value is obtained after 9 iterations and its value is 3.7698 for a criterion improvement of about 98.96%.

## C8.4 Second Example: Scattered Field Evolution

In the previous example, we have shown the behaviour of the optimization algorithm over the criterion map of Figure C8.4. In this second example we consider the same structure in terms of location of the metallic plates and location of the dipole sources, but this time we are interested in observing the scattered field evolution, during the optimization process. We rise the measurement points number we choosing to equally distribute 361 measurement points over a sphere of 1m diameter.

In Figures C8.11, C8.12 and C8.13, we show the normalized radiation pattern of the structure respectively for the desired structure, the initial guess structure and the final structure.

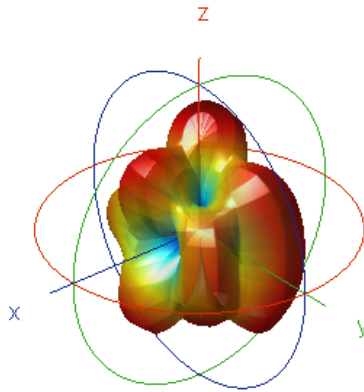


Figure C8.11: Normalized radiation pattern for the desired structure

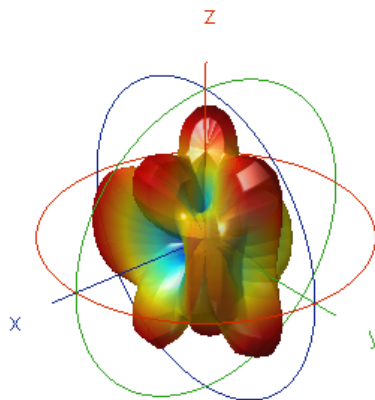


Figure C8.12: Normalized radiation pattern for the initial structure

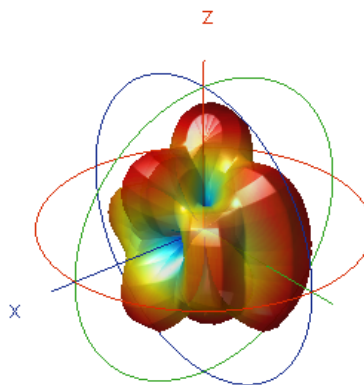


Figure C8.13: Normalized radiation pattern for the final structure

In Figure C8.14 and C8.15 we report, respectively, the cuts at  $\pi = 0^\circ$  and at  $\pi = 90^\circ$ , where we can see the differences between the initial diagram and the final one.

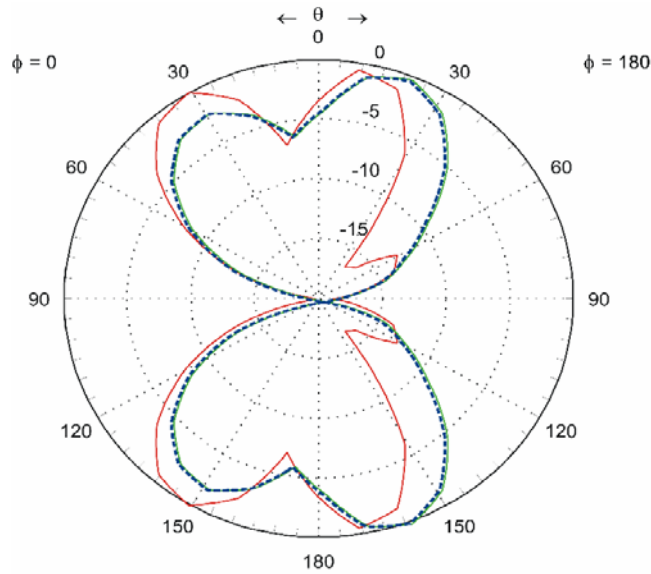


Figure C8.14: Radiation diagrams cut at  $\pi = 0^\circ$  (red initial, blue final, green desired)

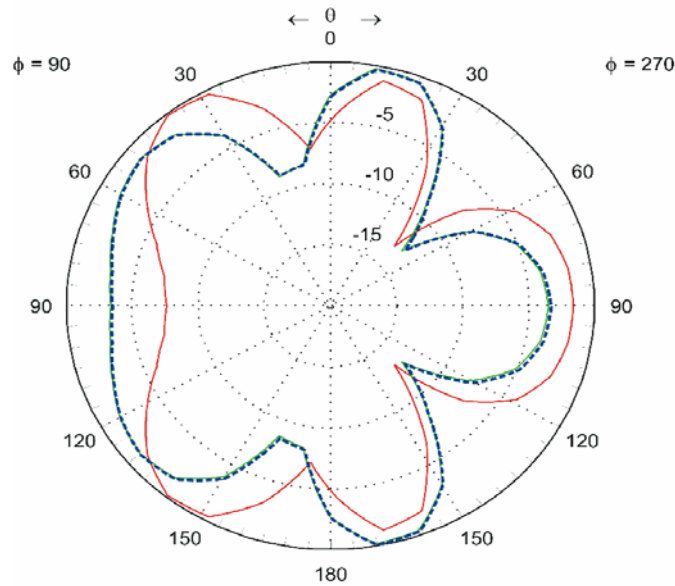


Figure C8.15: Radiation diagrams cut at  $\pi = 90^\circ$  (red initial, blue final, green desired)

Finally, we report the criterion convergence in Figure C8.16; this time the convergence is obtained after 3 optimization steps and also the final criterion value is lower with respect to the previous example. That is owing to the fact that an higher number of measurement points have been used, giving more information on the scattered field to the optimization algorithm.

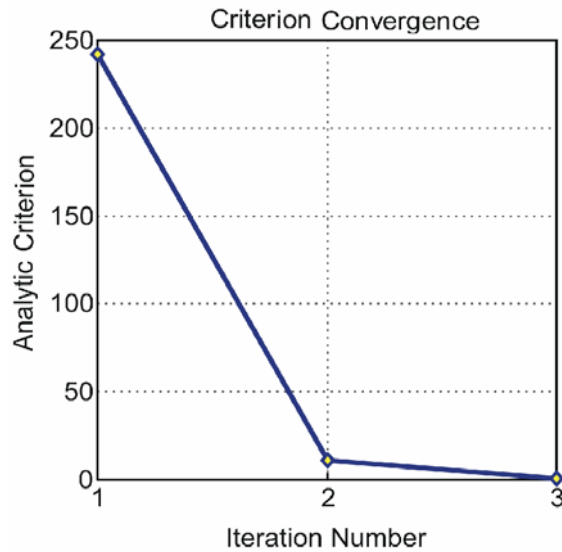


Figure C8.16: Criterion convergence

The start criterion value is of 242.2680 and the final criterion value is obtained after 3 iterations and its value is 0.07841 for a criterion improvement of about 99.96%.

### C8.5 Conclusion and Further Steps

This chapter demonstrates the robustness of the optimization environment where SR3D code and the optimization algorithm implemented in. Paragraph C8.1 and C8.2 validate the surface density current gradient with respect to the geometry and of the criterion gradient with respect to the geometry. Then, in the paragraphs C8.3 and C8.4 we show a simple application with different conditions, for the new-developed optimization tool with excellent results.

We want to apply this method to more complicate structures as, for example, a ground plane with a couple of small element located above it. We can also apply to the optimization of the location of the elements in linear and planar array [20]. Another interesting example should be retrieving the optimal location of some coupling element with respect to a ground plane in order to obtain a certain desired scattered field [3].

**CHAPTER 9:**  
**NUMERICAL EXPERIMENTS**

## Chapter 9 - Numerical Experiments

In Chapter 9, we present some numerical experiments for different antenna configurations. In these examples, we consider only planar and metallic structures and we want to retrieve the optimal location of certain elements with respect to a aimed synthetic scattered field. The objects inside the domain are illuminated by a certain number of electric dipoles

The working frequency is 3GHz ( $\lambda_0 = 0.1\text{m}$ ). The scattered field is computed over a 19x19 - point measurement set, defined over the surface of a sphere, of 10m-radius.

We consider only a spatial constraint on the position of a certain number of elements in the domain or by requiring the displacement direction. The contents of the presented graphical results are as follows:

- Original structure geometry
- Initial vs final structure geometry
- Radiation pattern of the original structure geometry (3D, xy plane, xz plane, yz plane)
- Radiation pattern of the initial structure geometry (3D, xy plane, xz plane, yz plane)
- Radiation pattern of the final structure geometry (3D, xy plane, xz plane, yz plane)
- Radiation pattern of the original vs final vs initial geometry cross-section  $\phi = [0, \pi]$
- Radiation pattern of the original vs final vs initial geometry cross-section  $[\pi/2, (3\pi/4)]$
- Convergence of the cost functional

We defined 8 examples in order to test the robustness and accuracy of the optimization procedure, trying, at the same time, to point out the generality of the method. Hereafter is shown a table reporting the list of the different numerical examples:

<i>Example</i>	<i>Structure Description</i>	<i>Ground Plane</i>	<i>Number of Sources</i>	<i>Measurement Points</i>
1	Planar Array I	No	1	19x19 (361)
2	Planar Array II	No	1	19x19 (361)
3	Linear Array I	No	6	19x19 (361)
4	Parasitic Elements I	Yes	6	19x19 (361)
5	Parasitic Elements II	Yes	2	19x19 (361)
6	Parasitic Elements III	Yes	2	19x19 (361)
7	Passive Antennas I	Yes	2	19x19 (361)
8	Passive Antennas II	Yes	2	19x19 (361)

## C9.1 Planar Array I

In this first numerical example, we want to retrieve the geometry for a basic 9-element planar array in a classic broadside configuration. Each patch element is defined with a  $\lambda/4$  side. In Figure C9.1 the original geometry is shown.

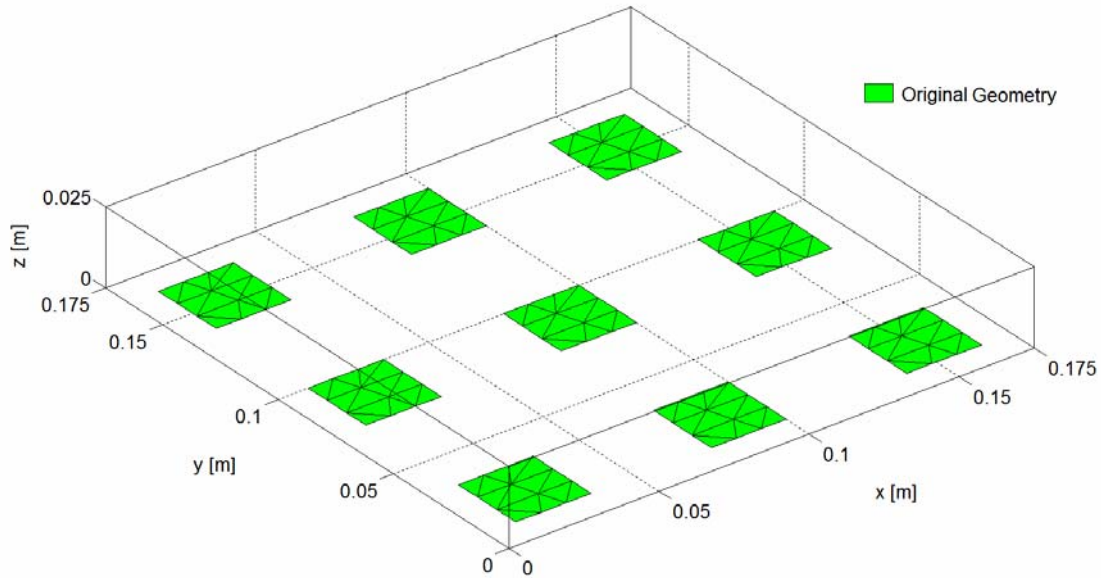


Figure C9.1: Original geometry

The positions of the elements of the original structure is reported in the table as follows:

Element	x [m]	y [m]	z [m]
1	0.01000	0.01000	0.00000
2	0.07500	0.01000	0.00000
3	0.14000	0.01000	0.00000
4	0.01000	0.07500	0.00000
5 (FIXED)	0.07500	0.07500	0.00000
6	0.14000	0.07500	0.00000
7	0.00000	0.14000	0.00000
8	0.07500	0.14000	0.00000
9	0.14000	0.14000	0.00000

For the incident field, we use one electric dipole defined in the Cartesian coordinates  $(x, y, z)$

Dipole N#	Dipole Moment	x [m]	y [m]	z [m]
1	(0,1,0)	0.08750	0.08750	10.0000

The dipole is placed far enough, in order to obtain about the same density currents over all the patches of the planar array. This example is aimed to show how to optimize the radiation pattern of the planar array, starting with an initial configuration in which secondary lobes are present. The optimization procedure is able find an optimal geometry configuration to eliminate the un-

desired lobes. The radiation pattern for the original structure configuration is shown in Figure C9.2.

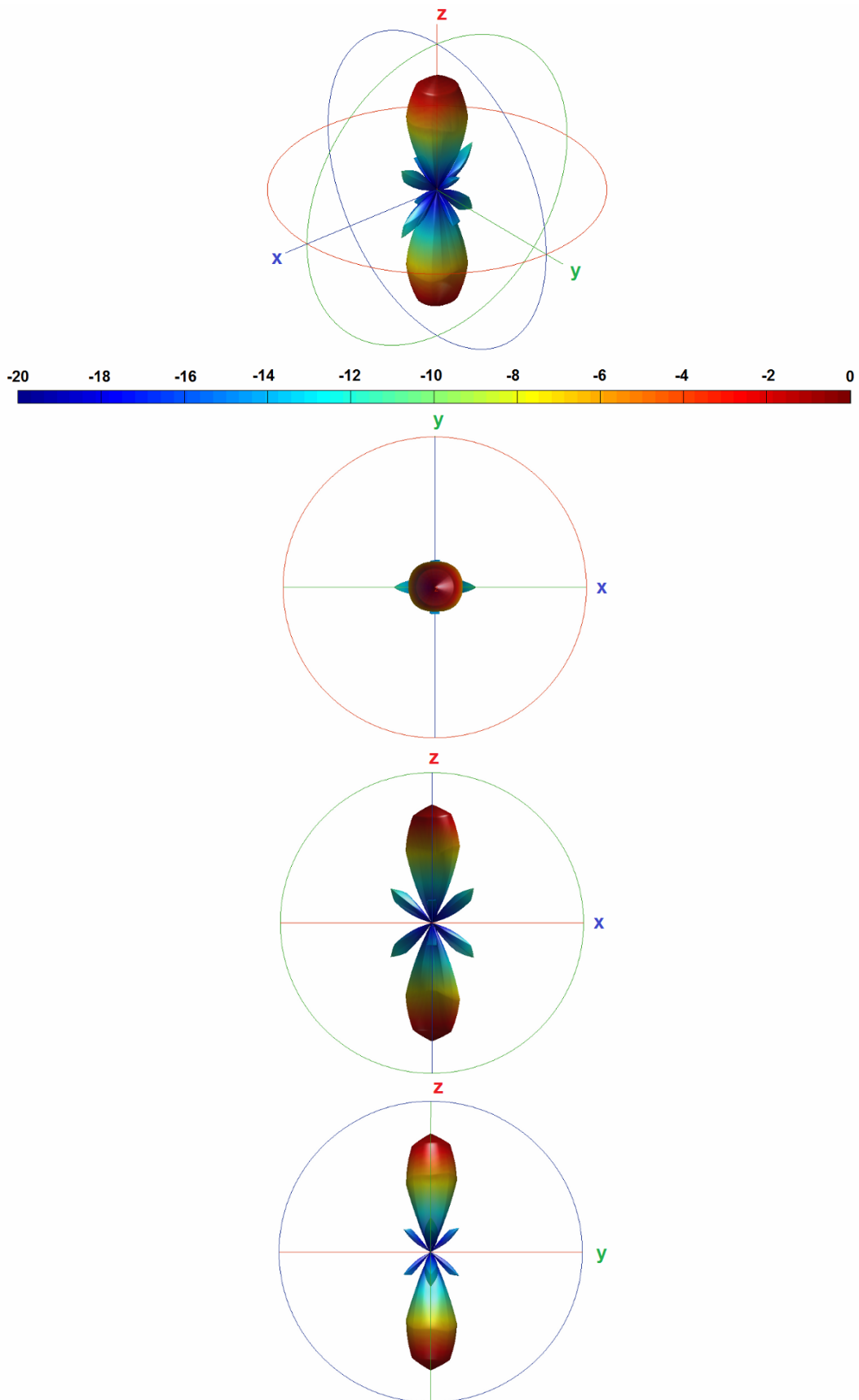


Figure C9.2: Radiation pattern of the original geometry

In order to define an initial guess, the patches have been moved away as shown in Figure C9.3, the initial structure is represented in red color while, the final structure geometry is represented in blue. The center element of the array, at the Cartesian origin, is remained fixed during the optimization procedure.

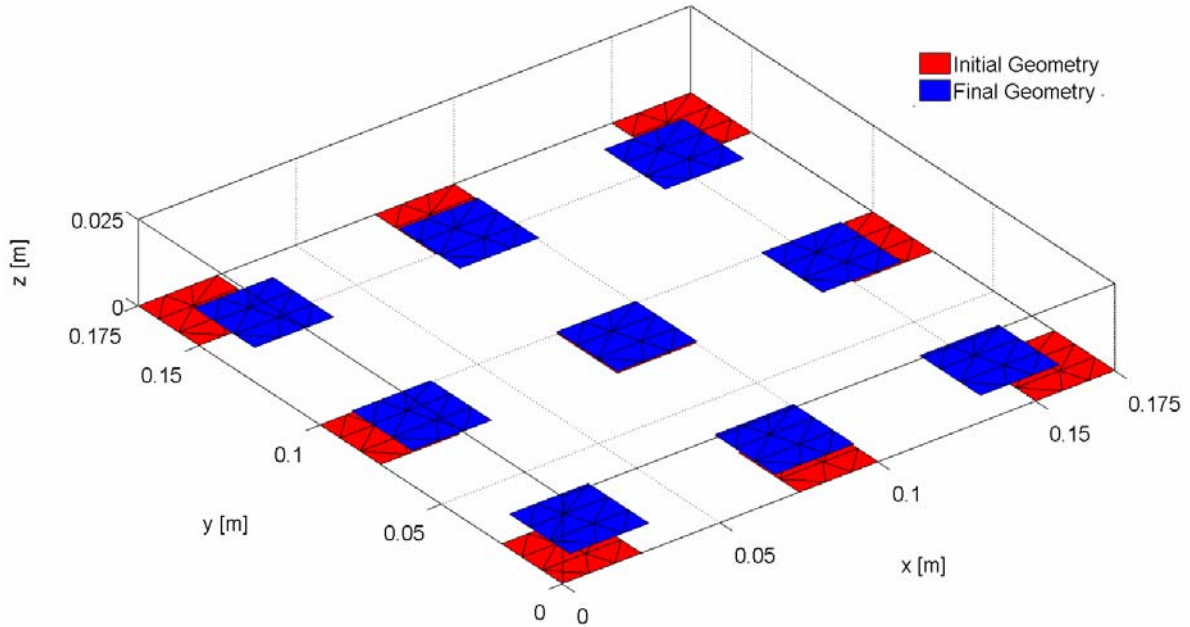


Figure C9.3: Initial vs final geometry

The positions of the elements of the initial and the final structures are reported in the table as follows:

Element	Initial Structure			Final Structure		
	x [m]	y [m]	z [m]	x [m]	y [m]	z [m]
1	0.00000	0.00000	0.00000	0.01005	0.00996	0.00000
2	0.07500	0.00000	0.00000	0.07507	0.01000	0.00000
3	0.15000	0.00000	0.00000	0.14006	0.01003	0.00000
4	0.00000	0.07500	0.00000	0.01000	0.07493	0.00000
5 (FIXED)	0.07500	0.07500	0.00000	0.07500	0.07500	0.00000
6	0.15000	0.07500	0.00000	0.13998	0.07507	0.00000
7	0.00000	0.15000	0.00000	0.009949	0.13998	0.00000
8	0.07500	0.15000	0.00000	0.074930	0.13999	0.00000
9	0.15000	0.15000	0.00000	0.139963	0.14004	0.00000

The radiation pattern of the initial structure is reported in Figure C9.4, while the radiation pattern for the final structure is reported in Figure C9.5.

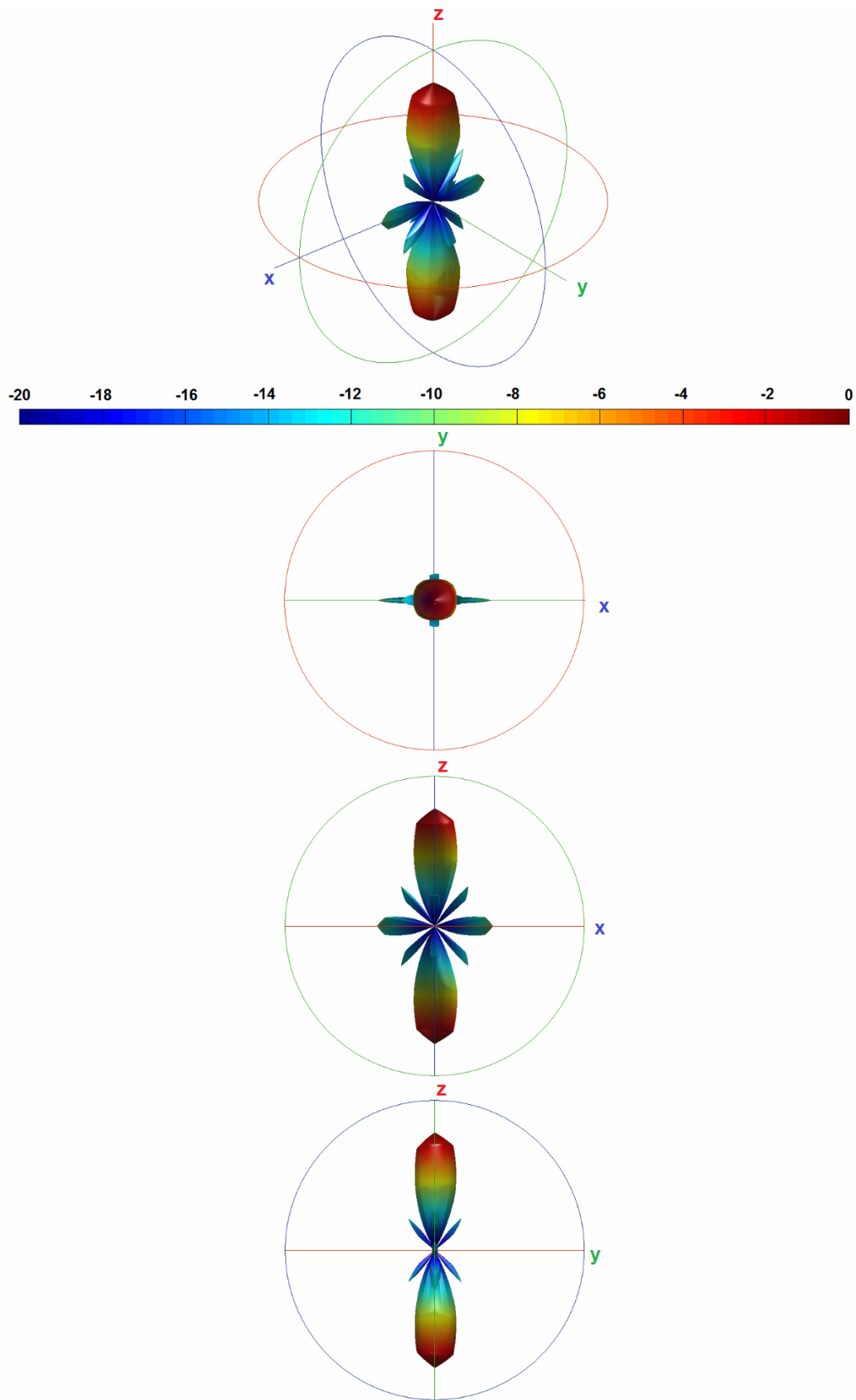


Figure C9.4: Radiation pattern of the initial geometry

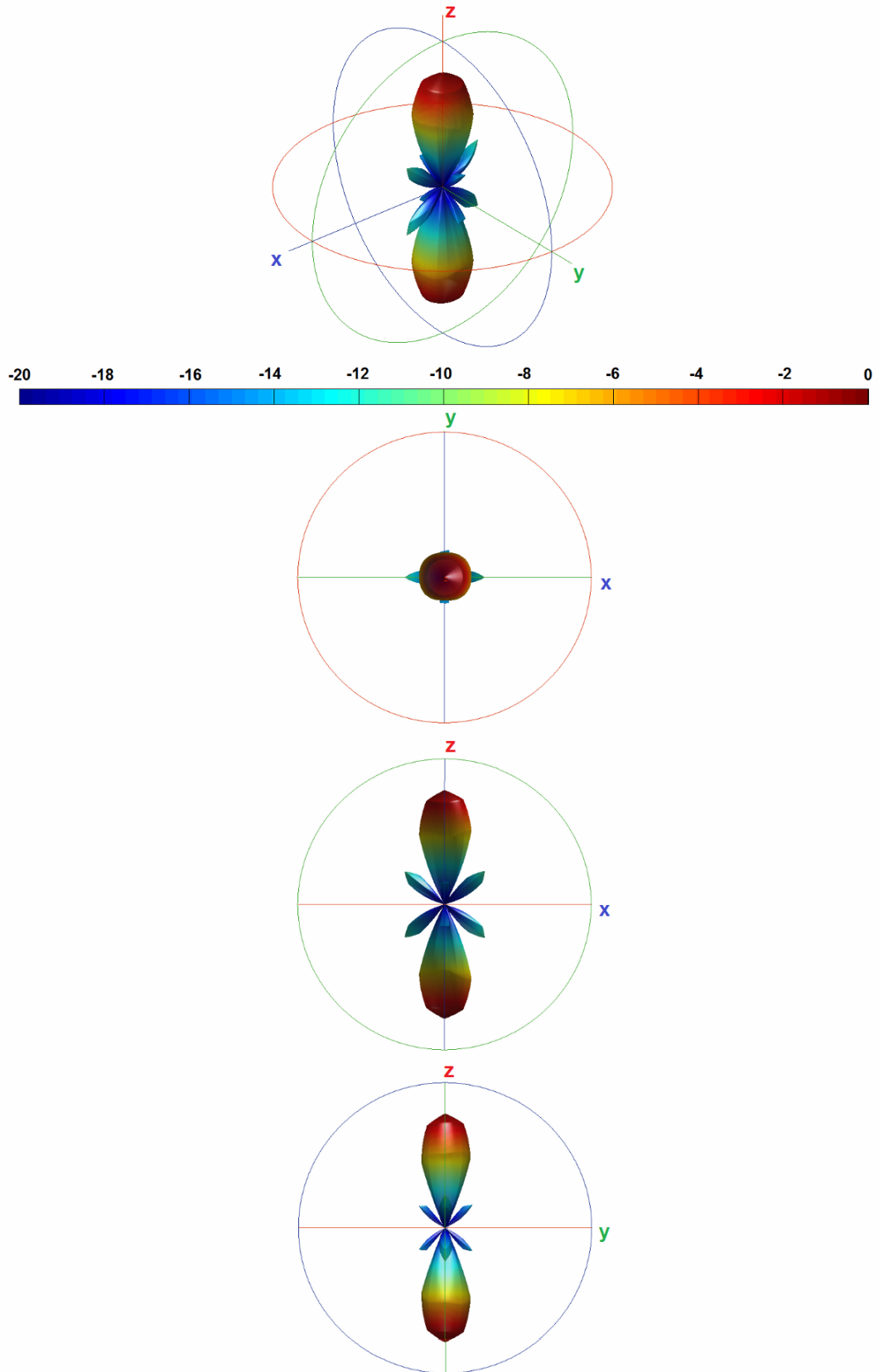


Figure C9.5: Radiation pattern of the final geometry

In Figure C9.6, we show the cross-sections of the radiation pattern with respect to main axes.

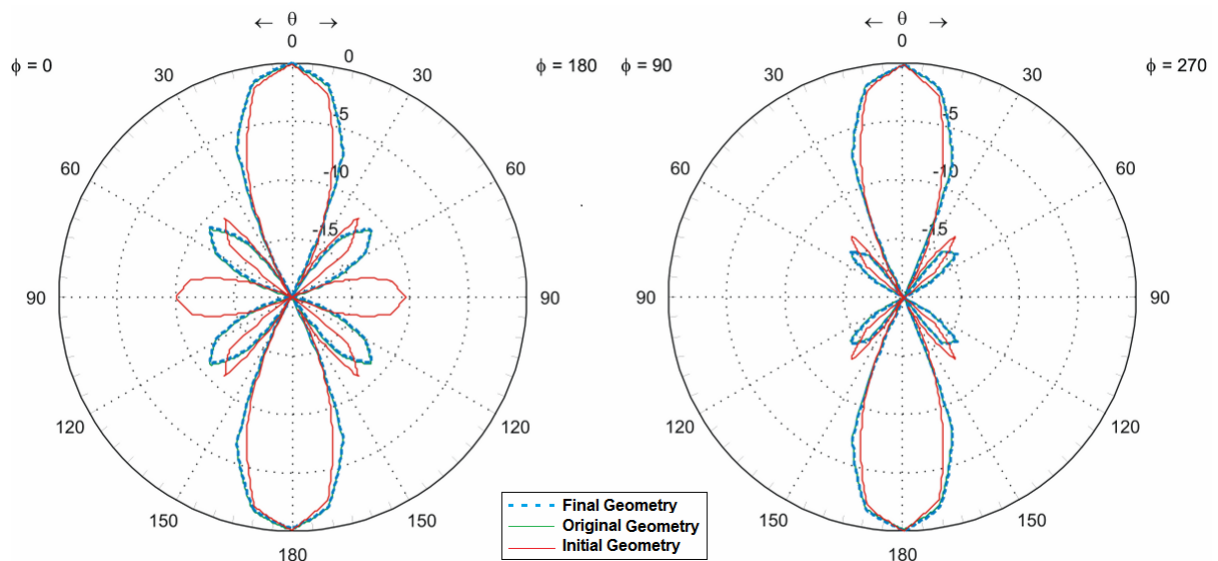


Figure C9.6: Radiation pattern cross-sections

Finally, we show the convergence of the cost functional (criterion), in Figure C9.7.

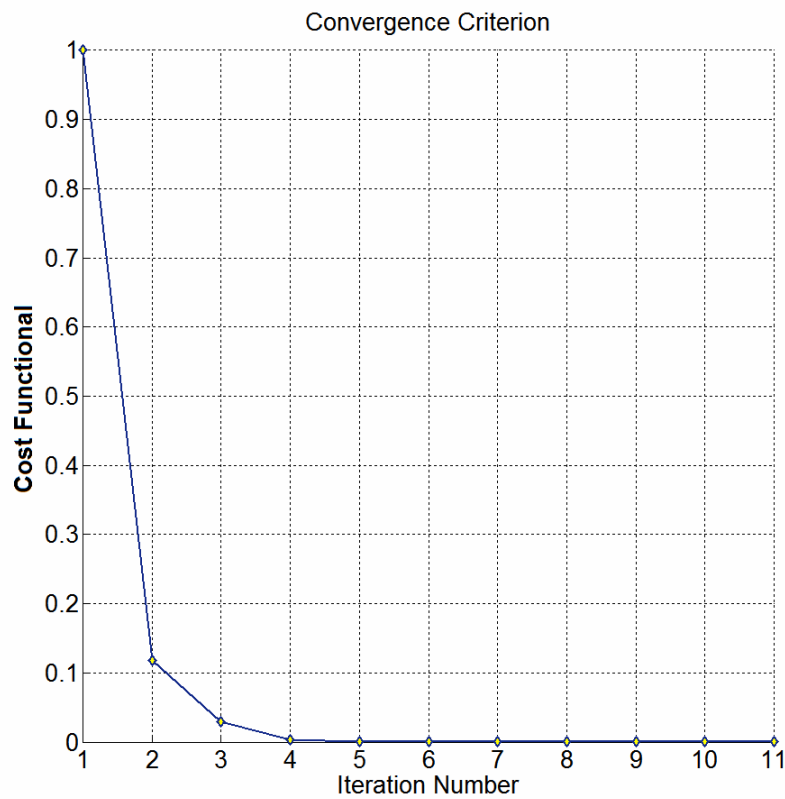


Figure C9.7: Normalized convergence of the cost functional

The convergence of the criterion is reached after 11 iterations, starting from an absolute value of  $8.9 \times 10^{-5}$  decreasing till a value of  $1.03 \times 10^{-8}$ . The reconstruction of the planar array has been achieved with a good agreement, considering a structure with 9 optimization variables and 126 degrees of freedom.

## C9.2 Planar Array II

For this second example, the geometry is the same basic 9-element planar array as in the paragraph 1, but, the electric dipole is shifted along the x-axis in order to illuminate the patch with an angle of incidence of  $10^\circ$ . The side of the patch element is  $\lambda/4$ . In Figure C9.2 the original geometry is shown.

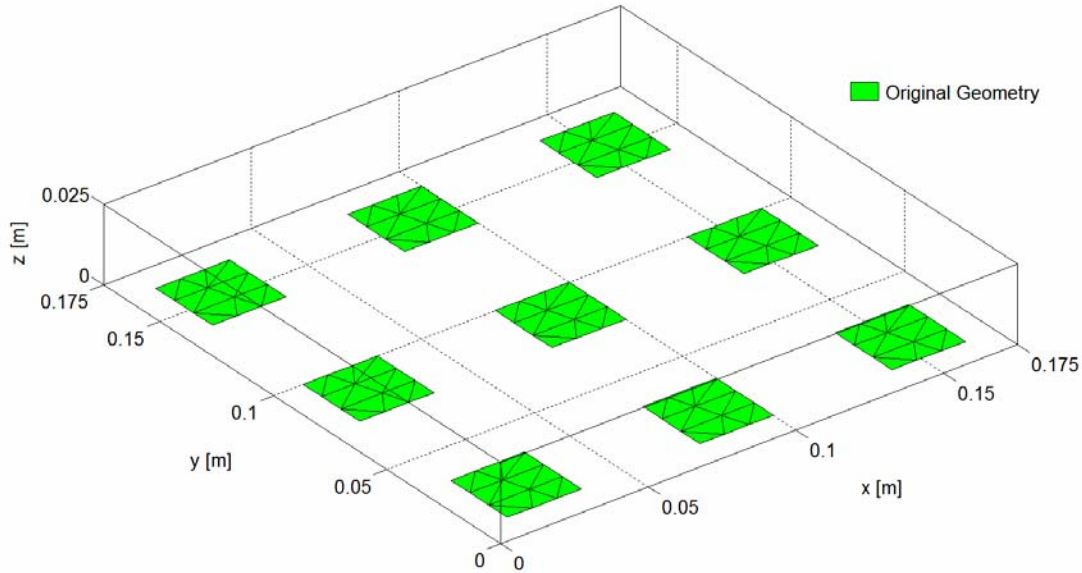


Figure C9.8: Original geometry

The positions of the objects of the original structure is reported in the table as follows:

Element	x [m]	y [m]	z [m]
1	0.01000	0.01000	0.00000
2	0.07500	0.01000	0.00000
3	0.14000	0.01000	0.00000
4	0.01000	0.07500	0.00000
5 (FIXED)	0.07500	0.07500	0.00000
6	0.14000	0.07500	0.00000
7	0.00000	0.14000	0.00000
8	0.07500	0.14000	0.00000
9	0.14000	0.14000	0.00000

For the incident field, we use one electric dipole defined in the Cartesian coordinates  $(x, y, z)$

Dipole N#	Dipole Moment	x [m]	y [m]	z [m]
1	(0,1,0)	1.74988	0.08750	10.0000

The dipole is placed far enough, in order to obtain about the same density currents over all the patches of the planar array. This example is aimed to show how to optimize the radiation pattern of the planar array, with a configuration for which a strong secondary lobe is present. The opti-

mization procedure will find an optimal geometry configuration in order to eliminate the undesired secondary lobe. The radiation pattern for the original structure is represented in Figure C9.9.

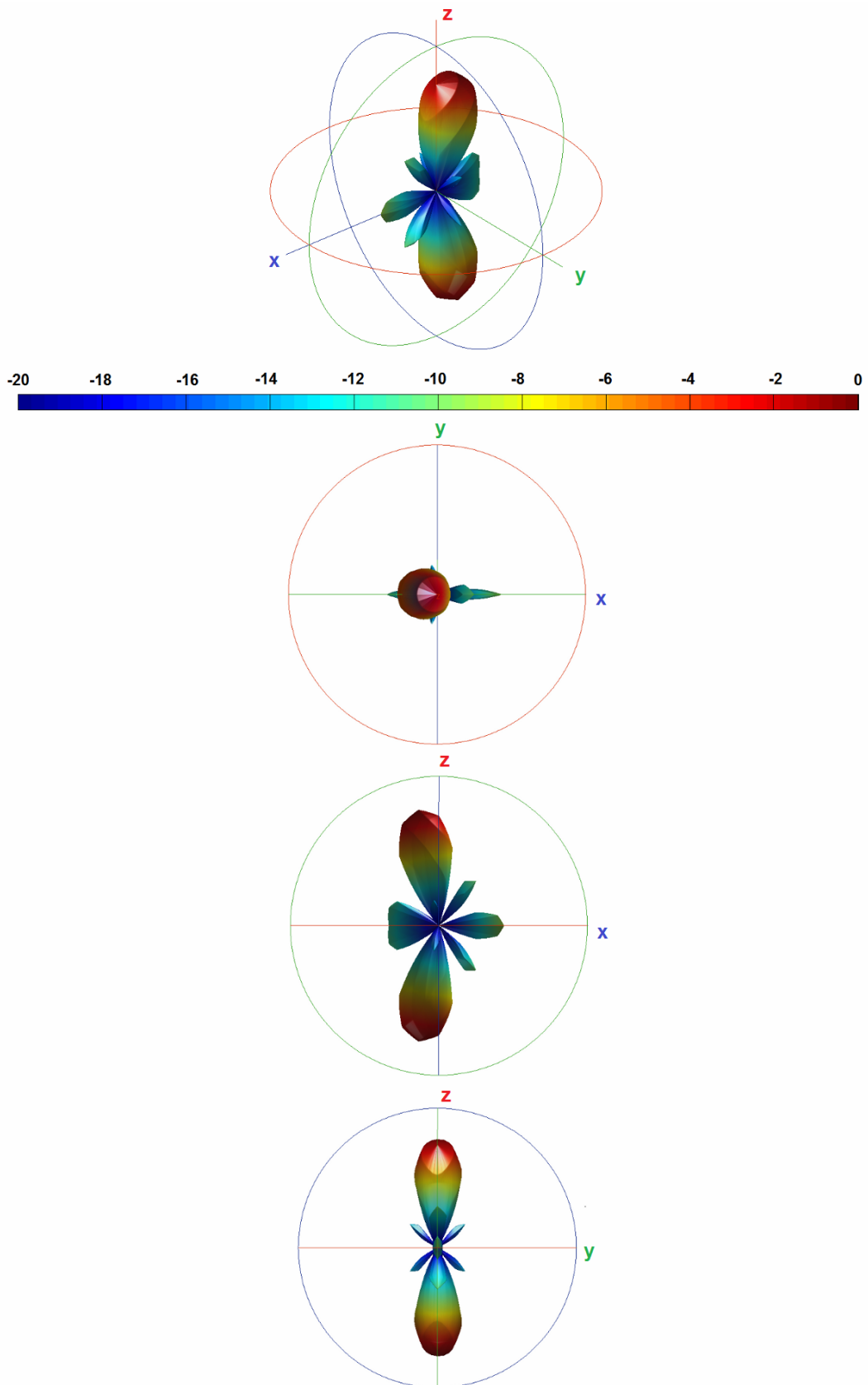


Figure C9.9: Radiation pattern of the original geometry

In order to define an initial guess, the patches have been moved away outwards as shown in Figure C9.10, the initial guess structure is represented in red color while, and the final structure geometry is represented in blue. The center element of the array, at the origin of the cartesian coordinates, is remained fixed during the optimization procedure.

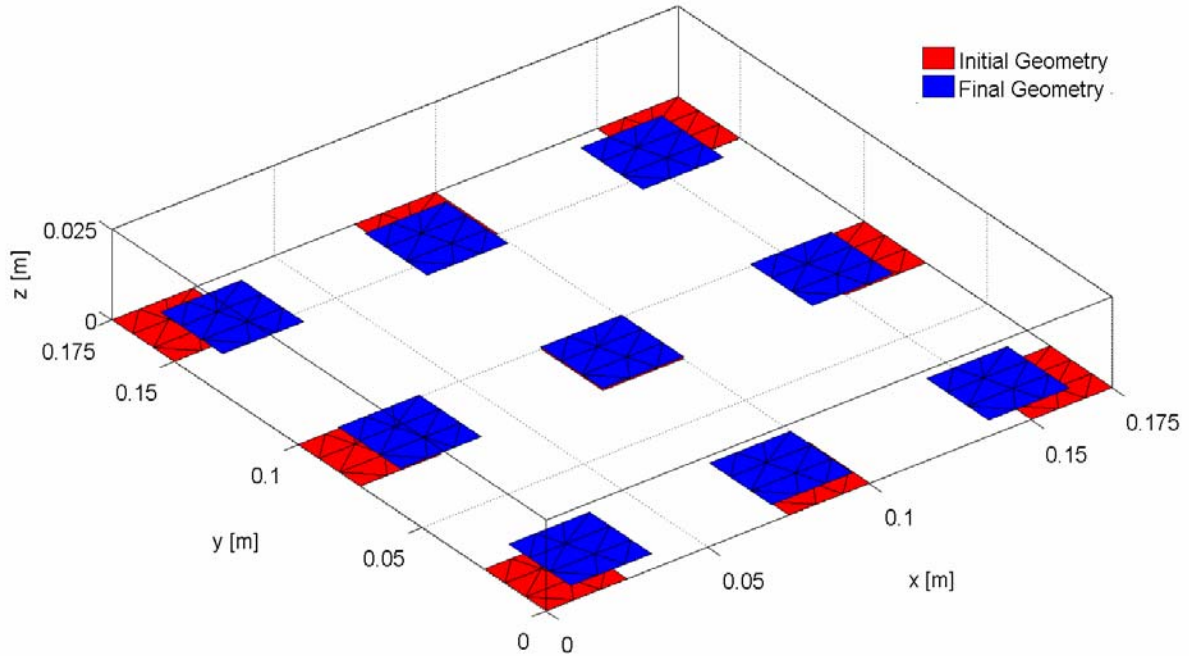


Figure C9.10: Initial vs final geometry

The positions of the elements of the initial and the final structures are reported in the table as follows:

Element	Initial Structure			Final Structure		
	x [m]	y [m]	z [m]	x [m]	y [m]	z [m]
1	0.00000	0.00000	0.00000	0.01151	0.00518	0.00000
2	0.07500	0.00000	0.00000	0.07411	0.00583	0.00000
3	0.15000	0.00000	0.00000	0.14094	0.00546	0.00000
4	0.00000	0.07500	0.00000	0.01233	0.07491	0.00000
5 (FIXED)	0.07500	0.07500	0.00000	0.07500	0.07500	0.00000
6	0.15000	0.07500	0.00000	0.13991	0.07512	0.00000
7	0.00000	0.15000	0.00000	0.01116	0.14499	0.00000
8	0.07500	0.15000	0.00000	0.07378	0.14423	0.00000
9	0.15000	0.15000	0.00000	0.14065	0.14448	0.00000

The radiation pattern for the initial structure is reported in Figure C9.11, while the radiation pattern for the final structure is reported in Figure C9.12.

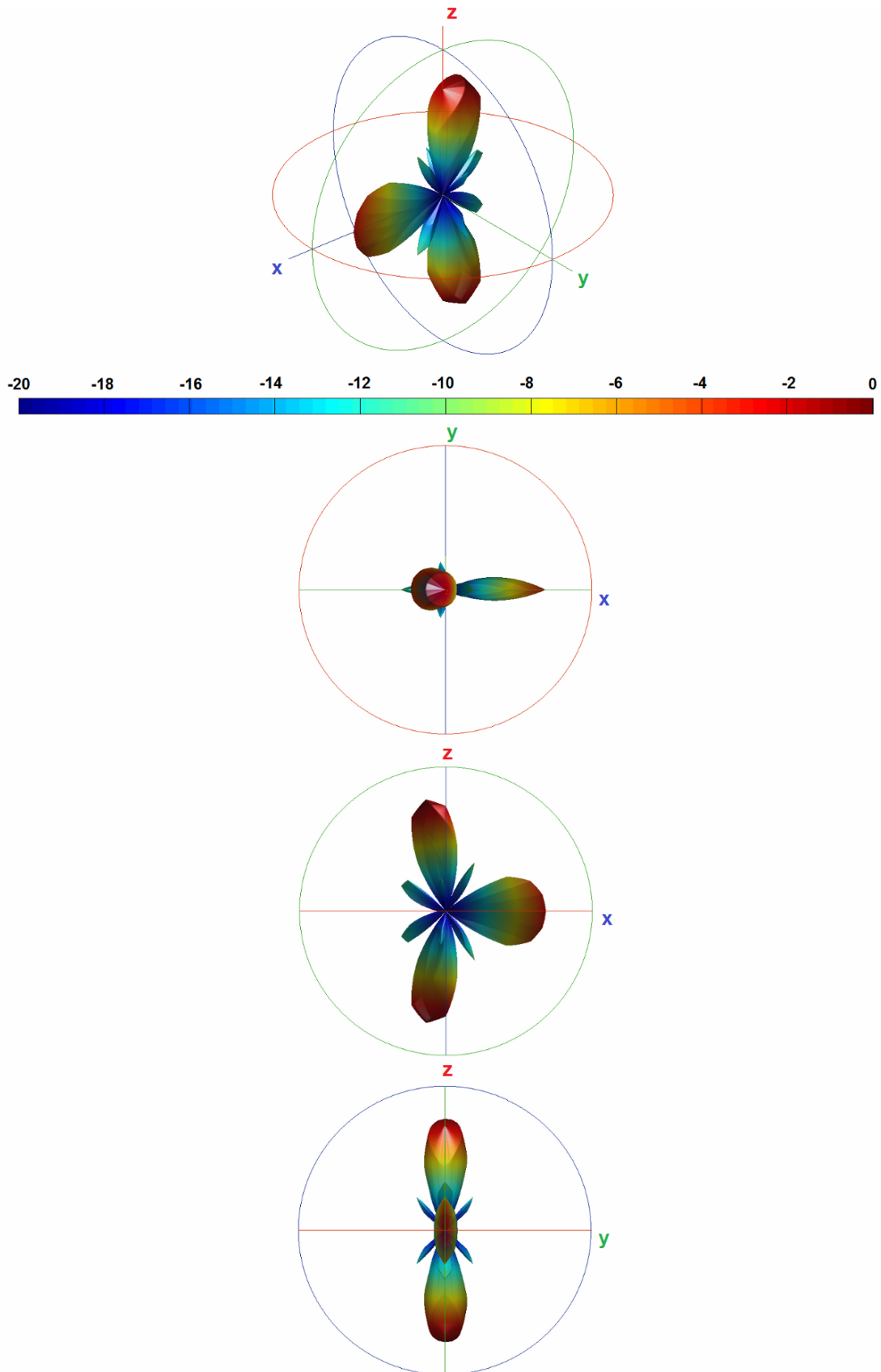


Figure C9.11: Radiation pattern of the initial geometry

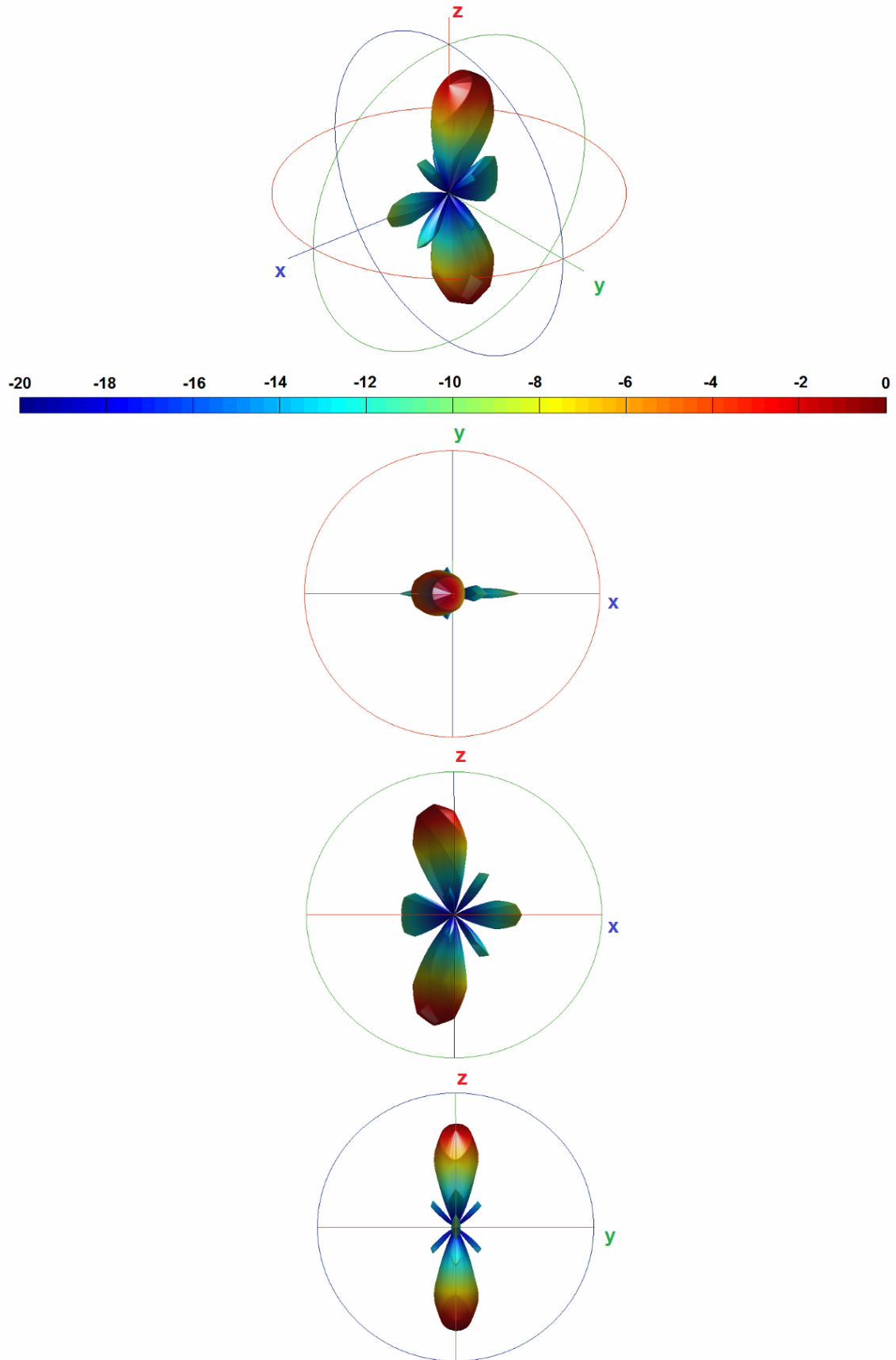


Figure C9.12: Radiation pattern of the final geometry

In Figure C9.13, we show the cross-sections of the radiation pattern with respect to main axes.

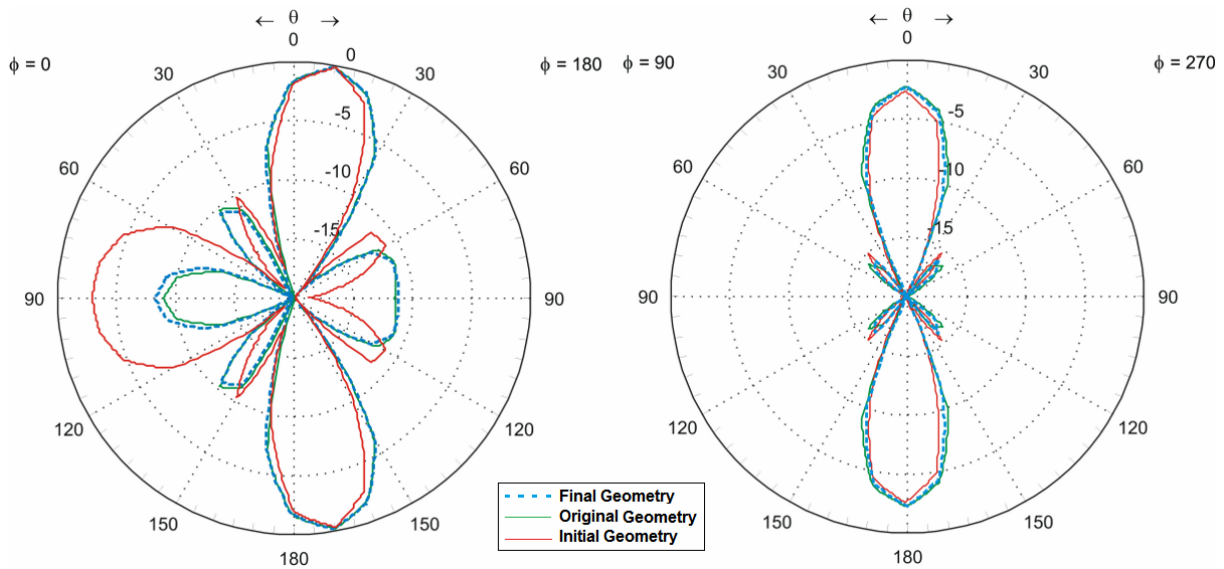


Figure C9.13: Radiation pattern cross-section

Finally, we show the convergence of the cost functional (criterion), in Figure C9.14.

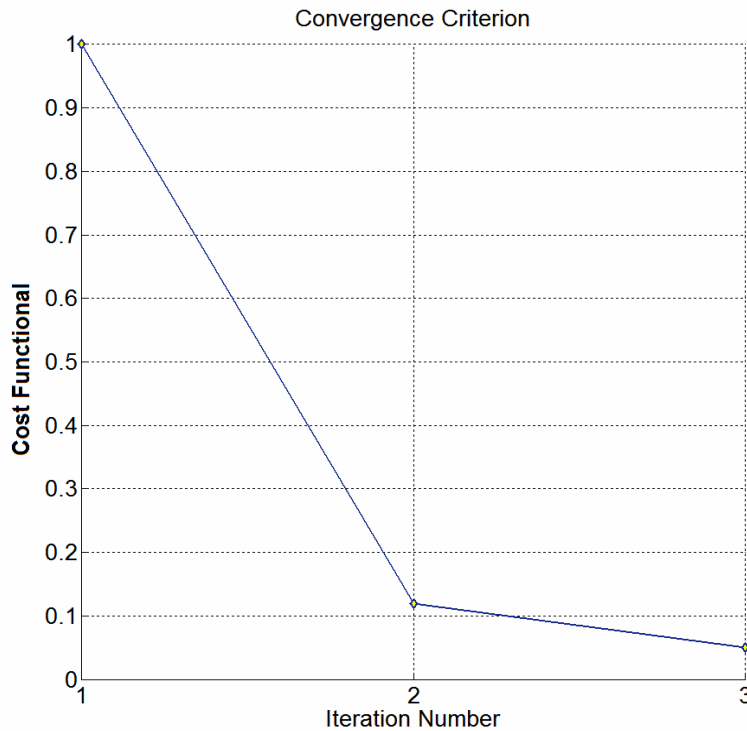


Figure C9.14: Normalized criterion convergence

The convergence of the criterion is reached after 3 iterations, starting from an absolute value of  $1.1 \times 10^{-2}$  decreasing till a value of  $5.5 \times 10^{-4}$ . The reconstruction of the planar array has been achieved with a lower agreement than the previous example, but the result it is still quite good, considering a structure with 9 optimization variables and 126 degrees of freedom. We observe from Figure C9.10, and from the final criterion value, that the global convergence has not been reached. Anyway, the discrepancy from the original radiation pattern and the final one is not so large as we can see from Figure C9.13.

### C9.3 Linear Array I

A linear array has been studied in this example. The array is composed of 5 cross-shaped elements with  $\lambda/2$  arm-length and placed along the z axis. In Figure C9.15, the original geometry is shown.

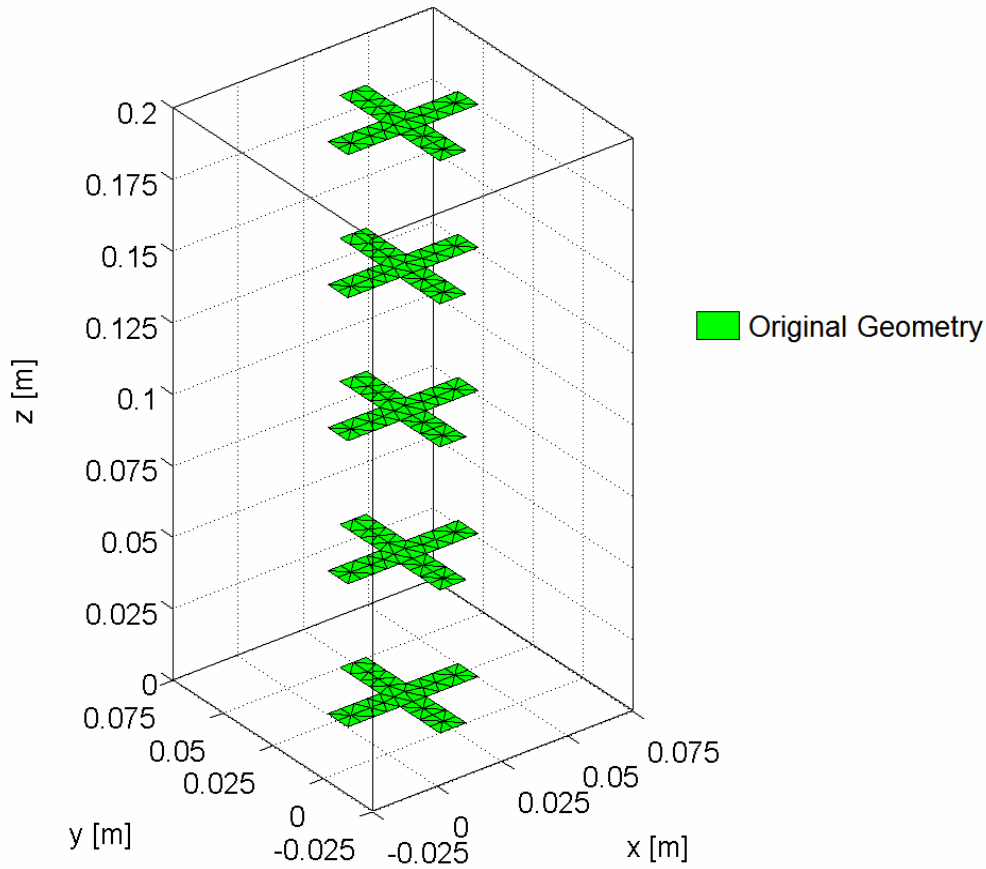


Figure C9.15: Original geometry

The positions of the elements of the original structure is reported in the table as follows:

Element	x [m]	y [m]	z [m]
1	0.00000	0.00000	0.00000
2	0.00000	0.00000	0.05000
3 (FIXED)	0.00000	0.00000	0.10000
4	0.00000	0.00000	0.15000
5	0.00000	0.00000	0.20000

For the incident field, we use 3 electric dipoles defined in the Cartesian coordinates  $(x, y, z)$

Dipole N#	Dipole Moment	x [m]	y [m]	z [m]
1	(1,1,0)	0.02500	0.02500	-0.50000
2	(1,1,0)	0.00000	0.05000	-0.50000
3	(1,1,0)	0.05000	0.00000	-0.50000

The radiation pattern for the original structure is shown in Figure C9.16.

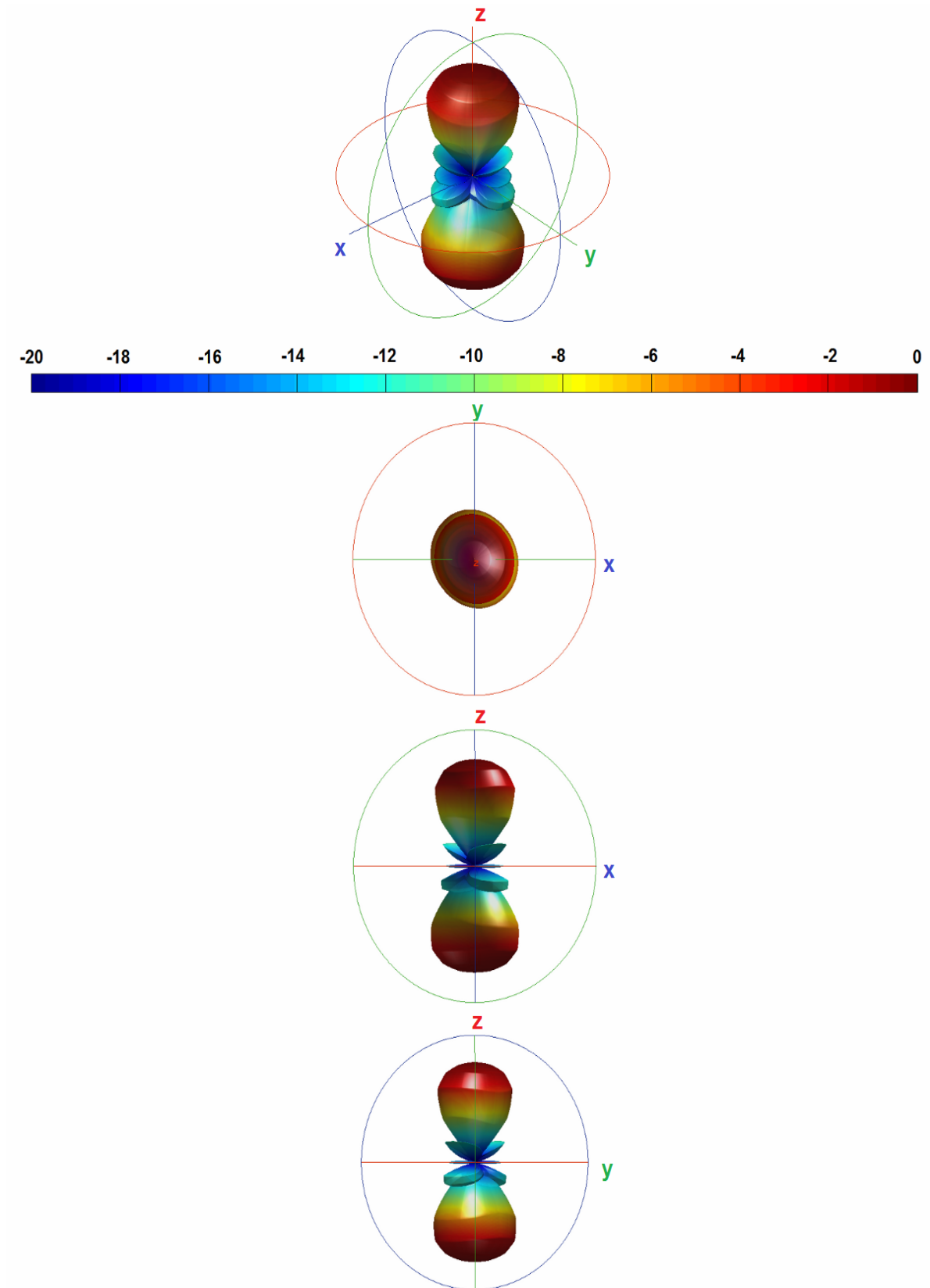


Figure C9.16: Radiation pattern of the original geometry

In order to define an initial guess, some cross-shaped elements have been moved inside the  $xy$  plane as shown in Figure C9.17, the initial guess structure is represented in red color while, the final structure geometry is represented in blue. The center element of the array is remained fixed, during the optimization procedure.

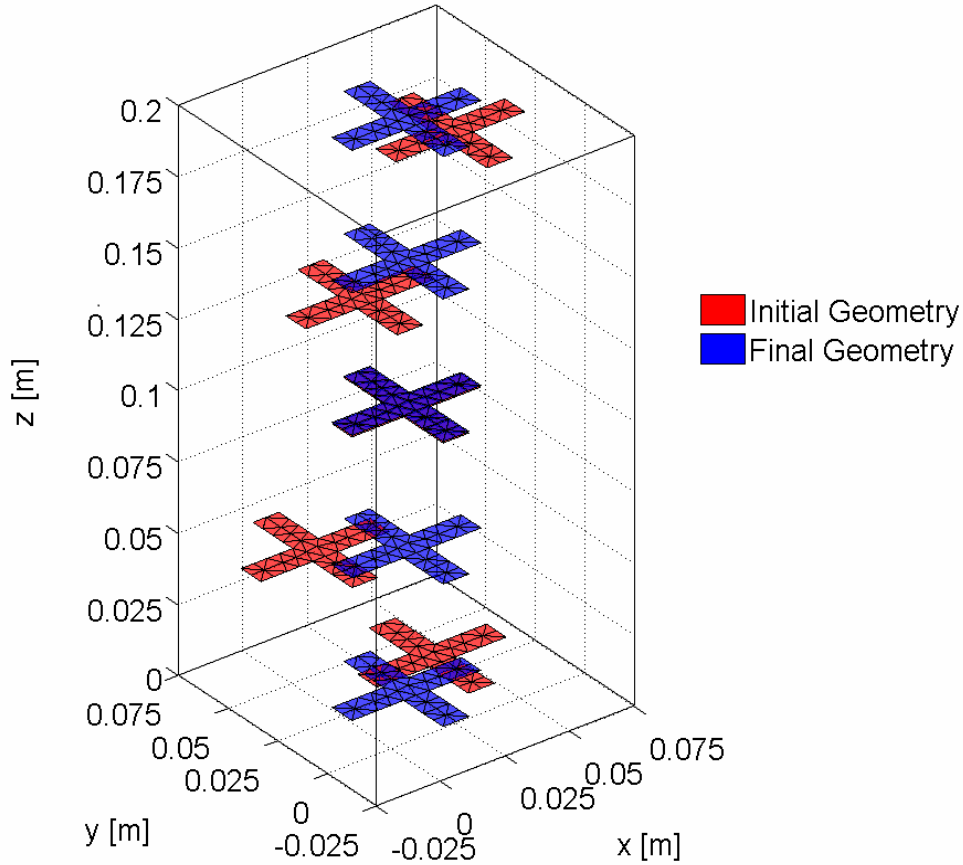


Figure C9.17: Initial vs final geometry

The positions of the elements of the initial and the final structures are reported in the table as follows:

Element	Initial Structure			Final Structure		
	x [m]	y [m]	z [m]	x [m]	y [m]	z [m]
1	0.01900	0.01200	0.00000	0.00001	-0.00002	0.00000
2	-0.02300	0.01600	0.05000	-0.00002	0.00005	0.05000
3 (FIXED)	0.00000	0.00000	0.00000	0.00000	0.00000	0.10000
4	-0.02400	-0.00800	0.15000	-0.00003	0.00001	0.15000
5	0.00700	-0.01300	0.20000	0.00001	-0.00003	0.20000

The radiation pattern for the initial structure is shown in Figure C9.18, while the radiation pattern for the final structure is shown in Figure C9.19.

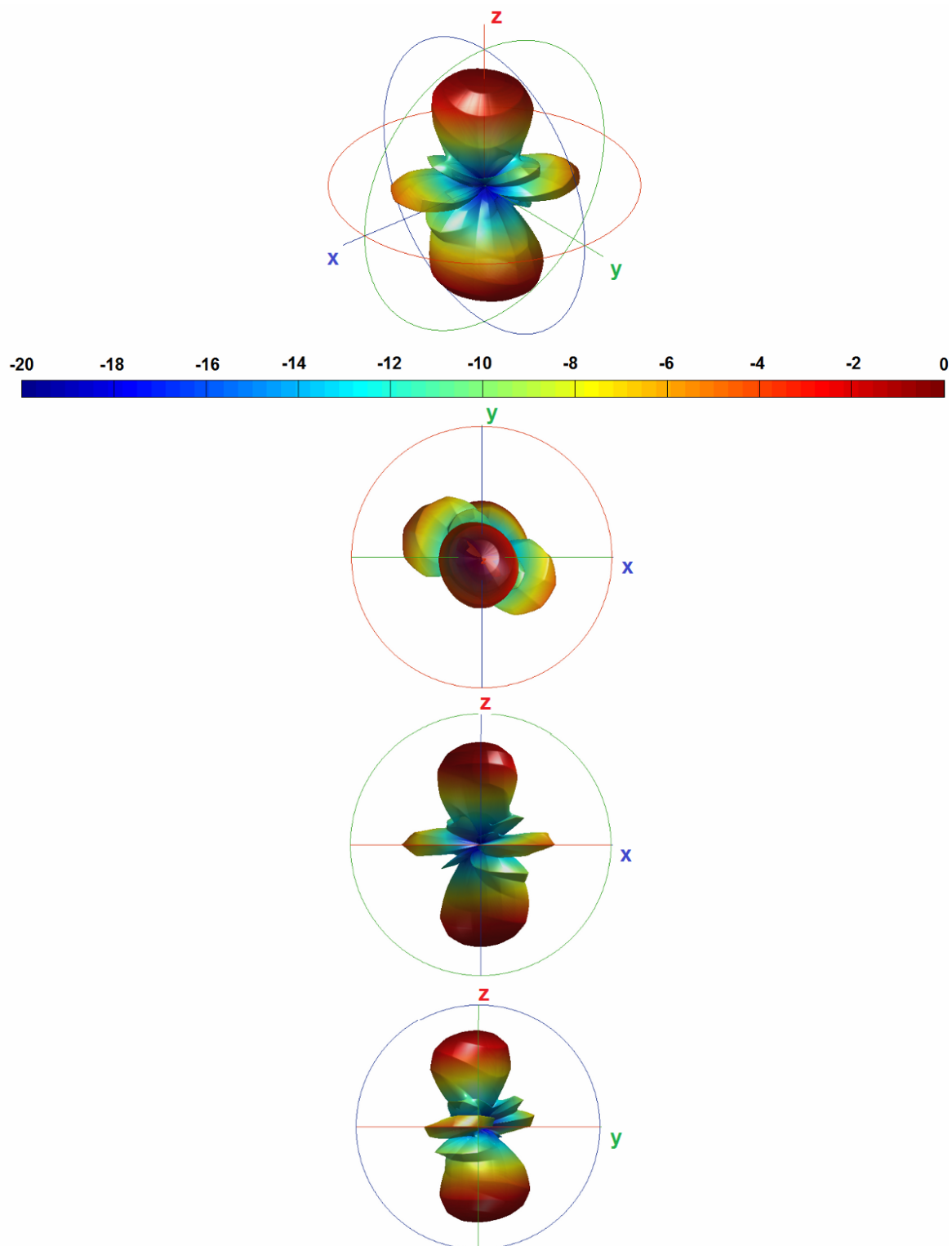


Figure C9.18: Radiation pattern of the initial geometry

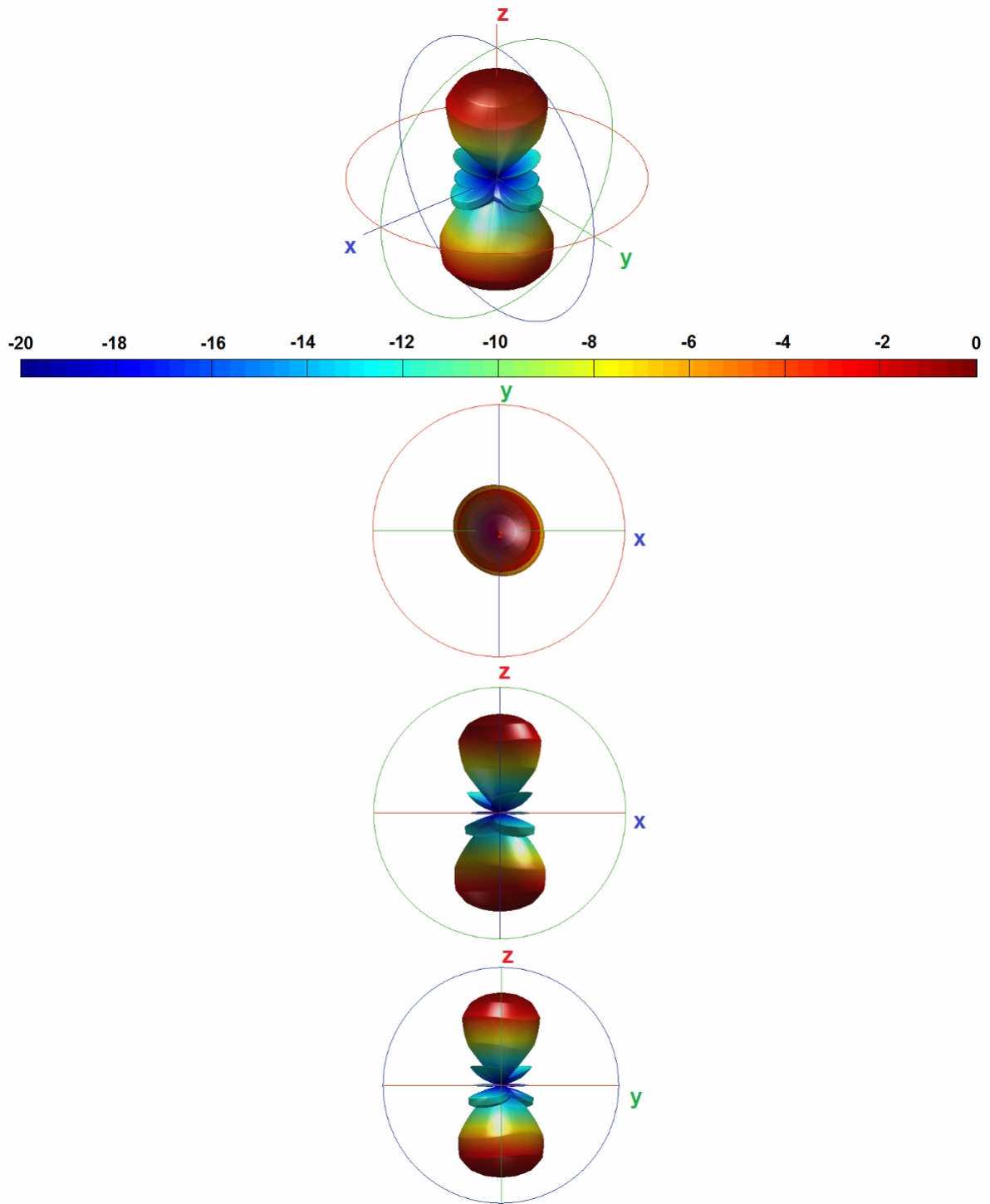


Figure C9.19: Radiation pattern of the final geometry

In Figure C9.20, we show the cross-sections of the radiation pattern with respect to main axes.

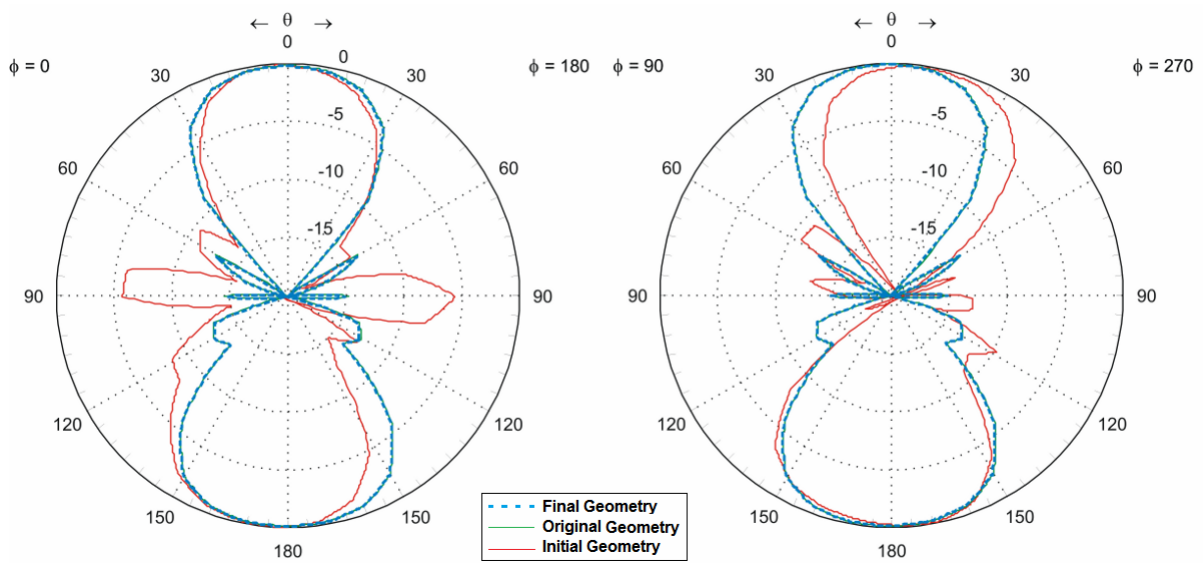


Figure C9.20: Radiation pattern cross-sections

Finally, we show the convergence of the cost functional (criterion), in Figure C9.21.

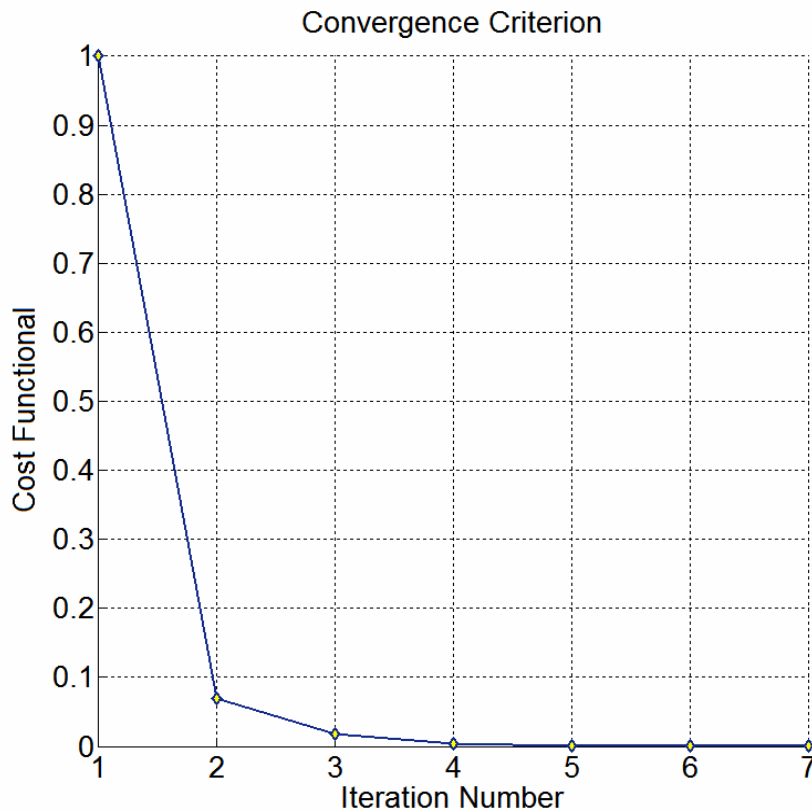


Figure C9.21: Normalized criterion convergence

The convergence of the criterion is reached after 7 iterations, starting from an absolute value of 305 decreasing till a value of 0.0035. The reconstruction of the linear array has been achieved with an excellent agreement, considering a structure with 5 optimization variables and 340 degrees of freedom.

### C9.4 Parasitic Elements I

We want now, to investigate how to find the optimal positions of 4 cubes considered as parasitic elements with  $\lambda/10$  side length, around a ground plane of  $\lambda \times 2\lambda$  length in x and y, respectively. In Figure C9.22, the original geometry is shown.

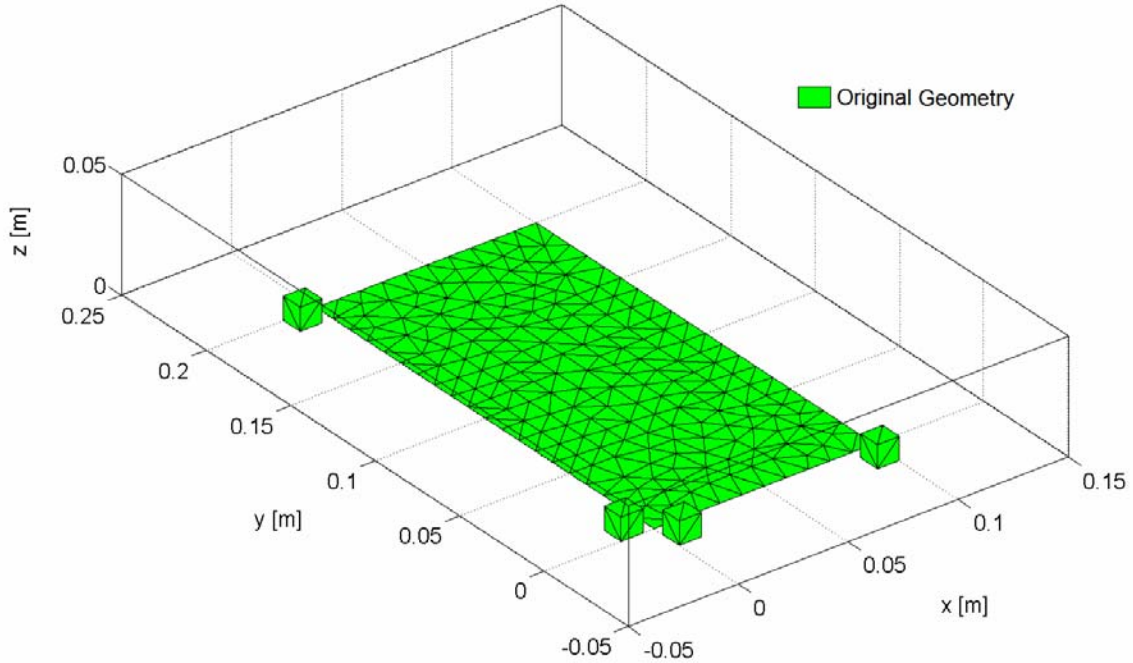


Figure C9.22: Original geometry

The position of the elements of the original structure is reported in the table as follows:

Element	x [m]	y [m]	z [m]
1 (FIXED GND)	0.00000	0.00000	0.00000
2	0.00000	-0.01500	0.00000
3	0.09000	-0.01500	0.00000
4	-0.01500	0.00000	0.00000
5	-0.01500	0.19000	0.00000

For the incident field, we use 5 electric dipoles defined in the Cartesian coordinates  $(x, y, z)$

Dipole N#	Dipole Moment	x [m]	y [m]	z [m]
1	(1,1,0)	0.05000	0.10000	0.50000
2	(1,0,0)	0.07500	0.10000	0.50000
3	(1,0,0)	0.02500	0.10000	0.50000
4	(0,1,0)	0.05000	0.12500	0.50000
5	(0,1,0)	0.02500	0.07500	0.50000

The radiation pattern for the original structure is shown in Figure C9.23.

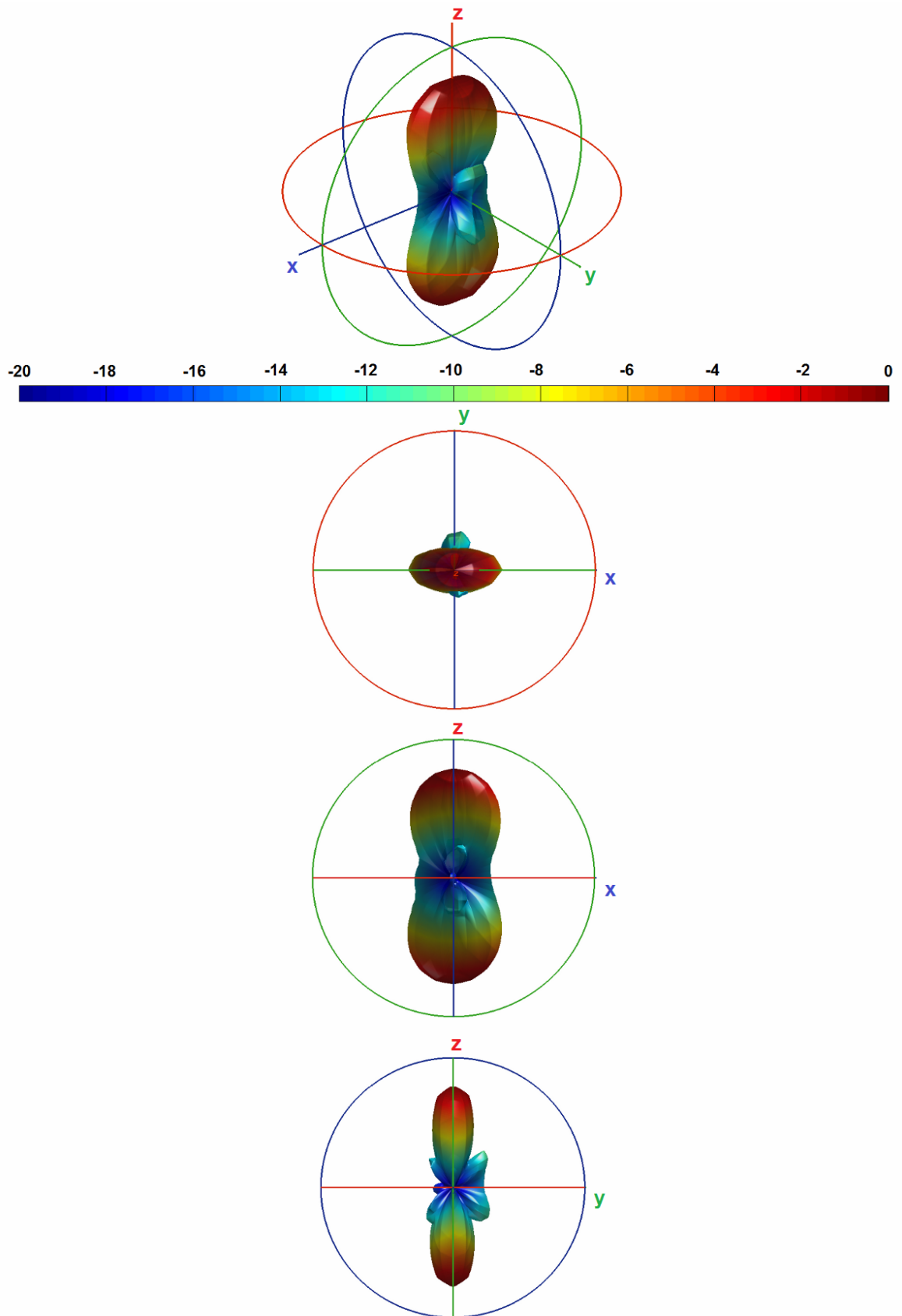


Figure C9.23: Radiation pattern of the original geometry

In order to define an initial guess, the cubes have been moved along the sides of the ground plane as shown in Figure C9.24. The initial guess structure is represented in red color while, the final structure geometry is represented in blue. In this example we choose to remain fixed only the position of the ground plane.

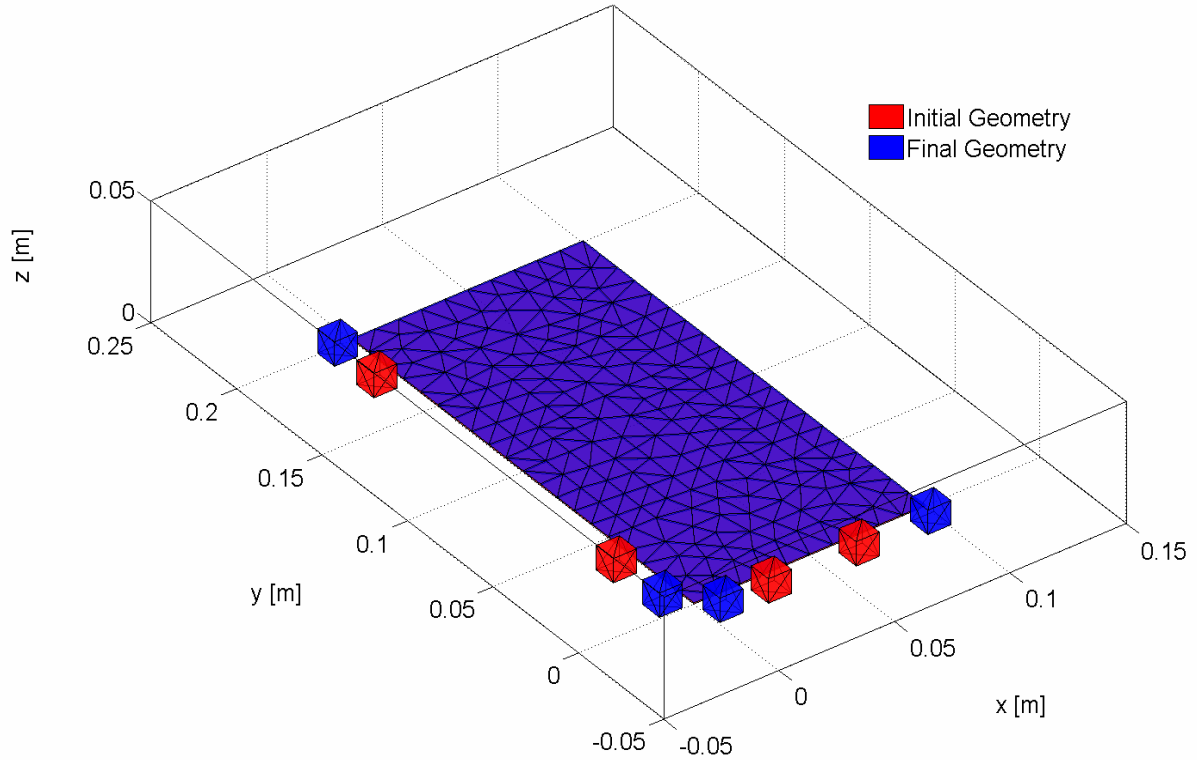


Figure C9.24: Initial vs final geometry

The positions of the objects of the initial and the final structures are reported in the table as follows:

Element	Initial Structure			Final Structure		
	x [m]	y [m]	z [m]	x [m]	y [m]	z [m]
1 (FIXED GND)	0.00000	0.00000	0.00000	0.00000	0.00000	0.00000
2	-0.02100	-0.01500	0.00000	0.00000	-0.01500	0.00000
3	0.05900	-0.01500	0.00000	0.08954	-0.01500	0.00000
4	-0.01500	0.02700	0.00000	-0.01500	0.00026	0.00000
5	-0.01500	0.16700	0.00000	-0.01500	0.19087	0.00000

The radiation pattern for the initial structure is shown in Figure C9.25, while the radiation pattern for the final structure is shown in Figure C9.26.

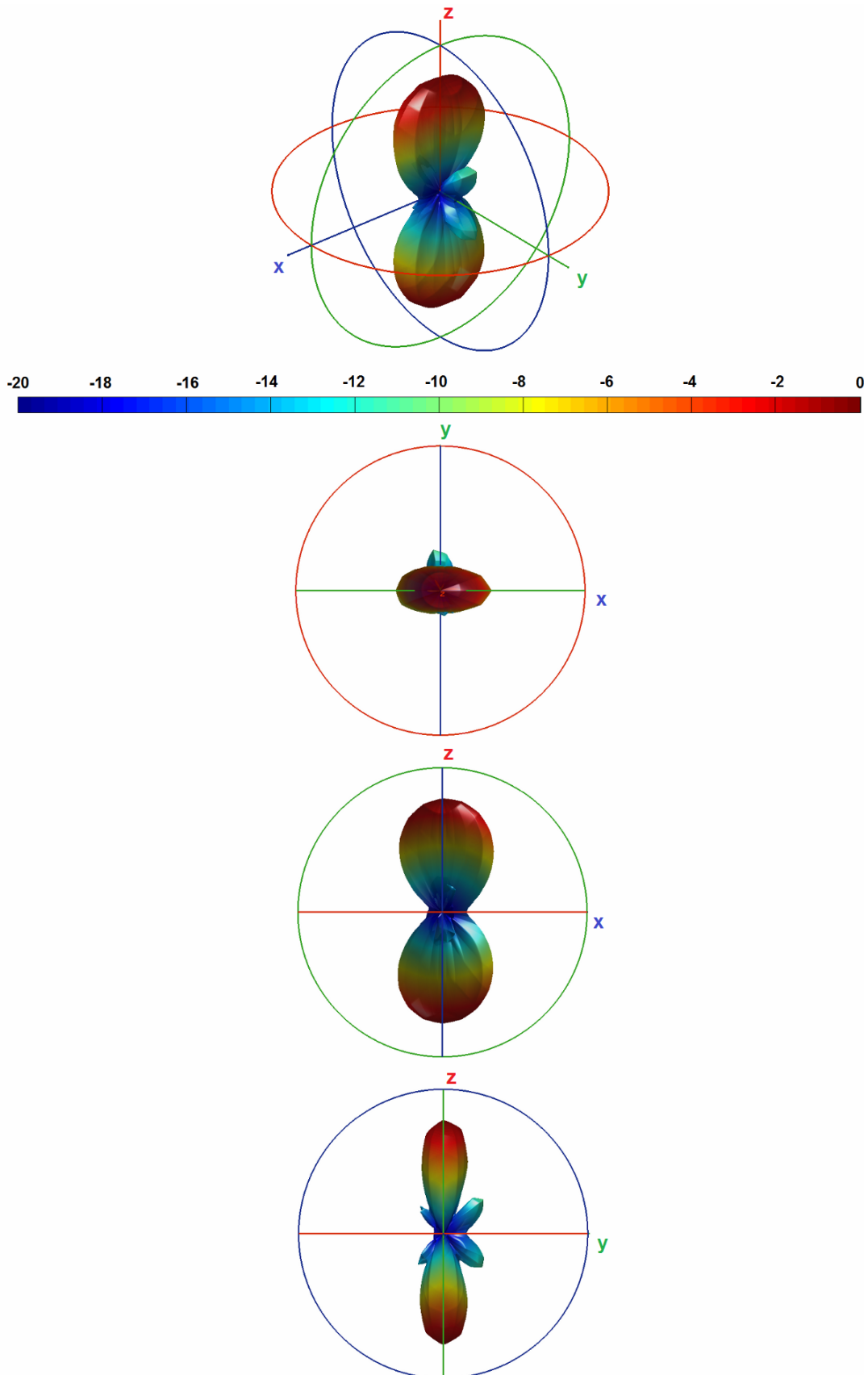


Figure C9.25: Radiation pattern of the initial geometry

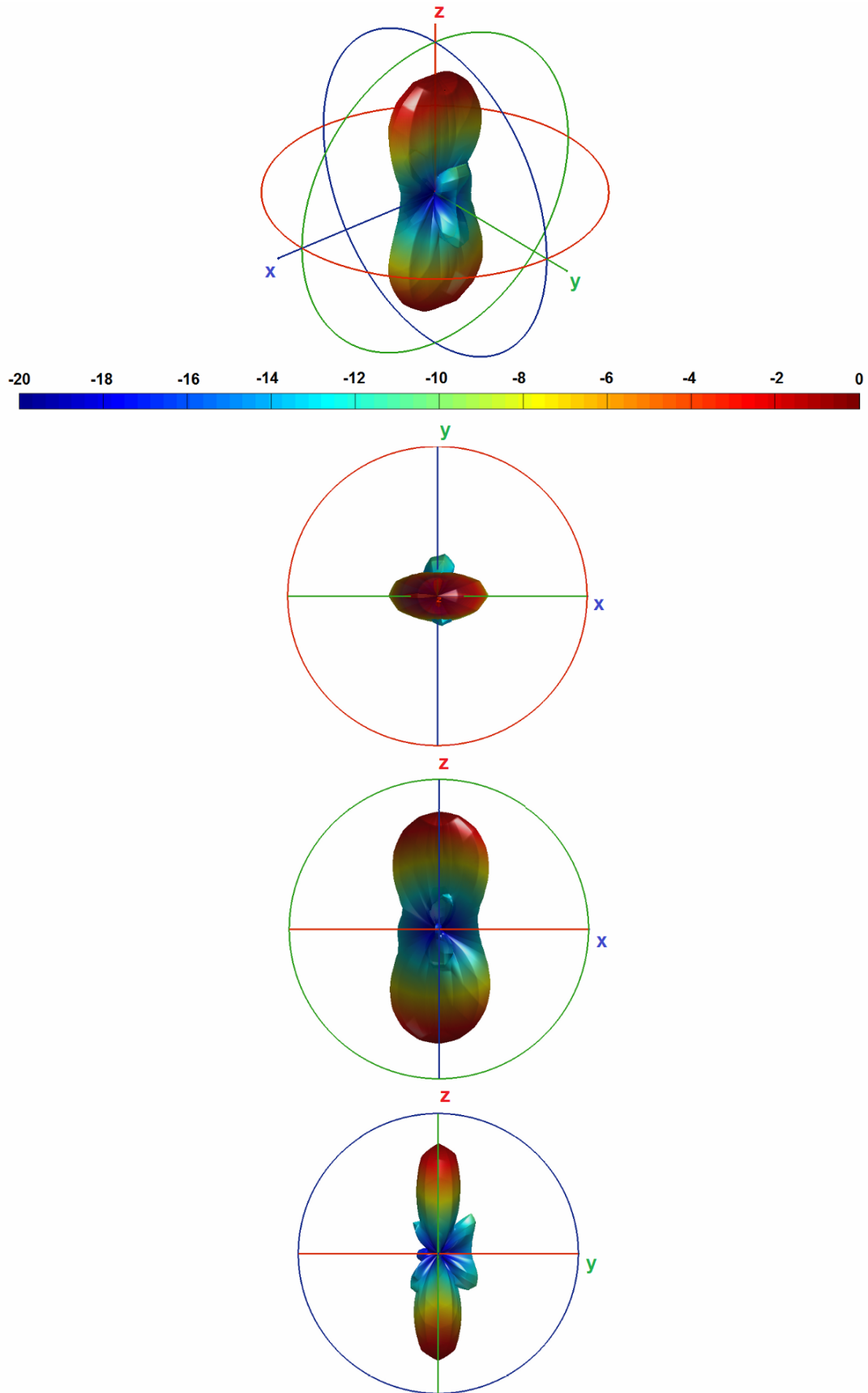


Figure C9.26: Radiation pattern of the final geometry

In Figure C9.27, we show the cross-sections of the radiation pattern with respect to main axes.

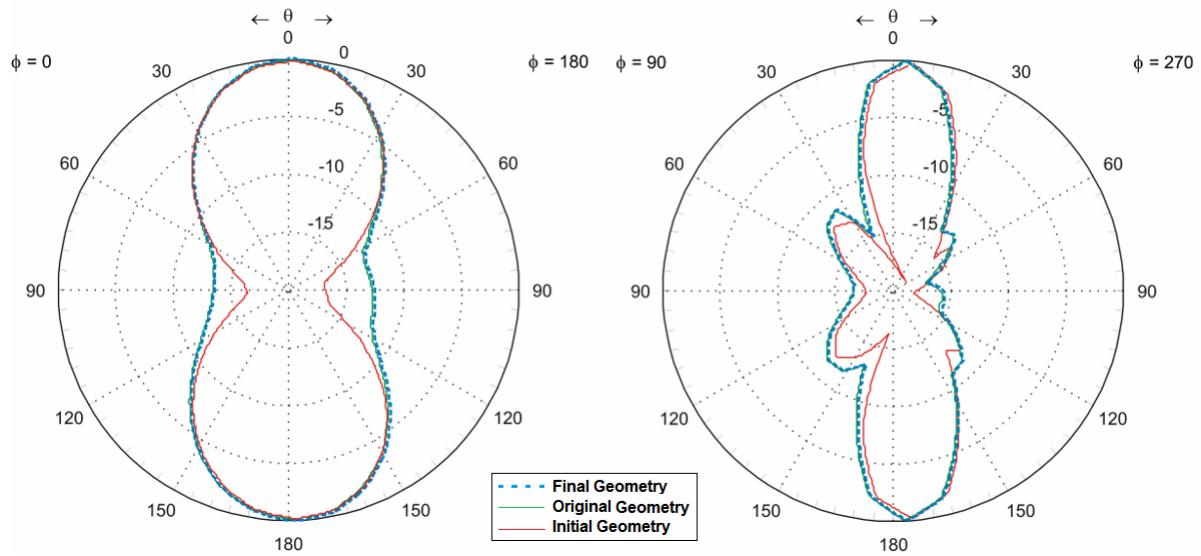


Figure C9.27: Radiation pattern cuts

Finally, we show the convergence of the cost functional (criterion), in Figure C9.28.

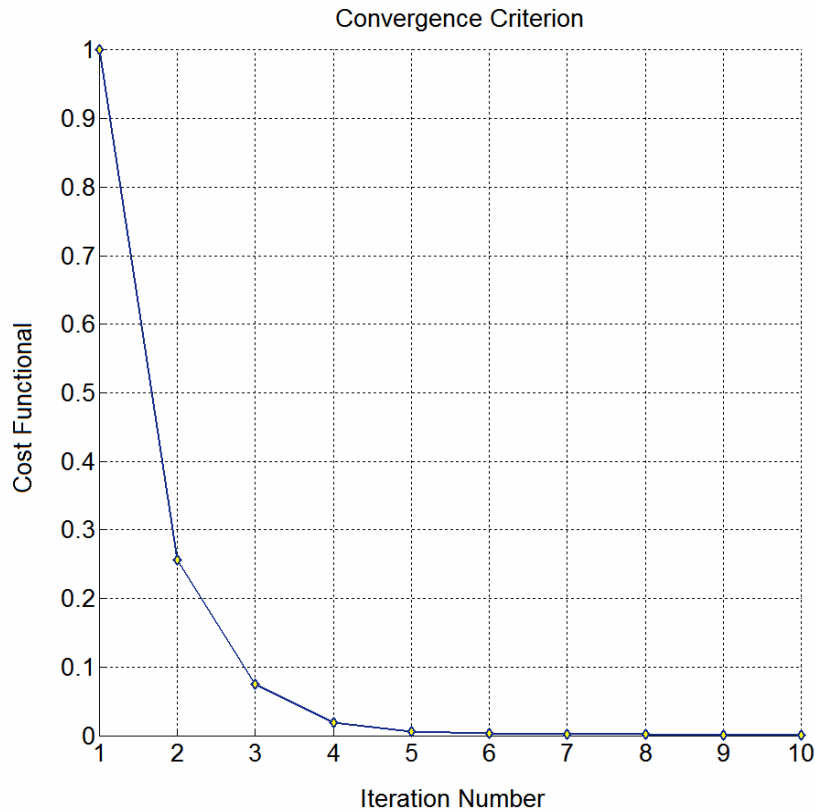


Figure C9.28: Normalized criterion convergence

The convergence of the criterion is reached after 7 iterations, starting from an absolute value of 304 decreasing till a value of 0.2015. The reconstruction of the linear array has been achieved with an excellent agreement, considering a structure with 5 optimization variables and 340 degrees of freedom.

## C9.5 Parasitic Elements II

We want to observe the behavior of the optimization algorithm when a parasitic element is present in the domain. The original structure is composed of a patch over a ground plane. The ground plane dimensions are  $\lambda \times \lambda$ , while the patch dimensions are  $\lambda/4 \times \lambda/4$ . The distance between the ground plane and the patch is  $\lambda/8$ . In Figure C9.29 the original geometry is shown.

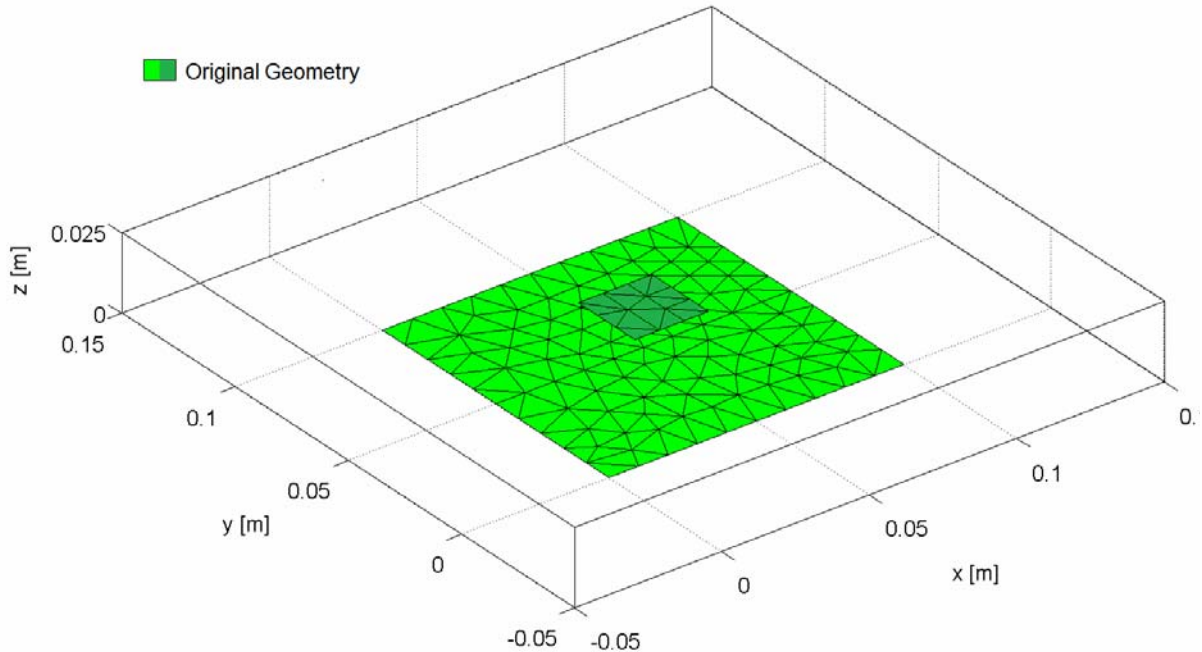


Figure C9.29: Original geometry

The position of the patch of the original structure is given in the table as follows:

Element	x [m]	y [m]	z [m]
1 (FIXED)	0.00000	0.00000	0.00000

For the incident field, we use 1 electric dipole defined in the Cartesian coordinates  $(x, y, z)$

Dipole N#	Dipole Moment	x [m]	y [m]	z [m]
1	(1,1,0)	0.05000	0.12500	0.50000

The radiation pattern of the original structure is shown in Figure C9.30.

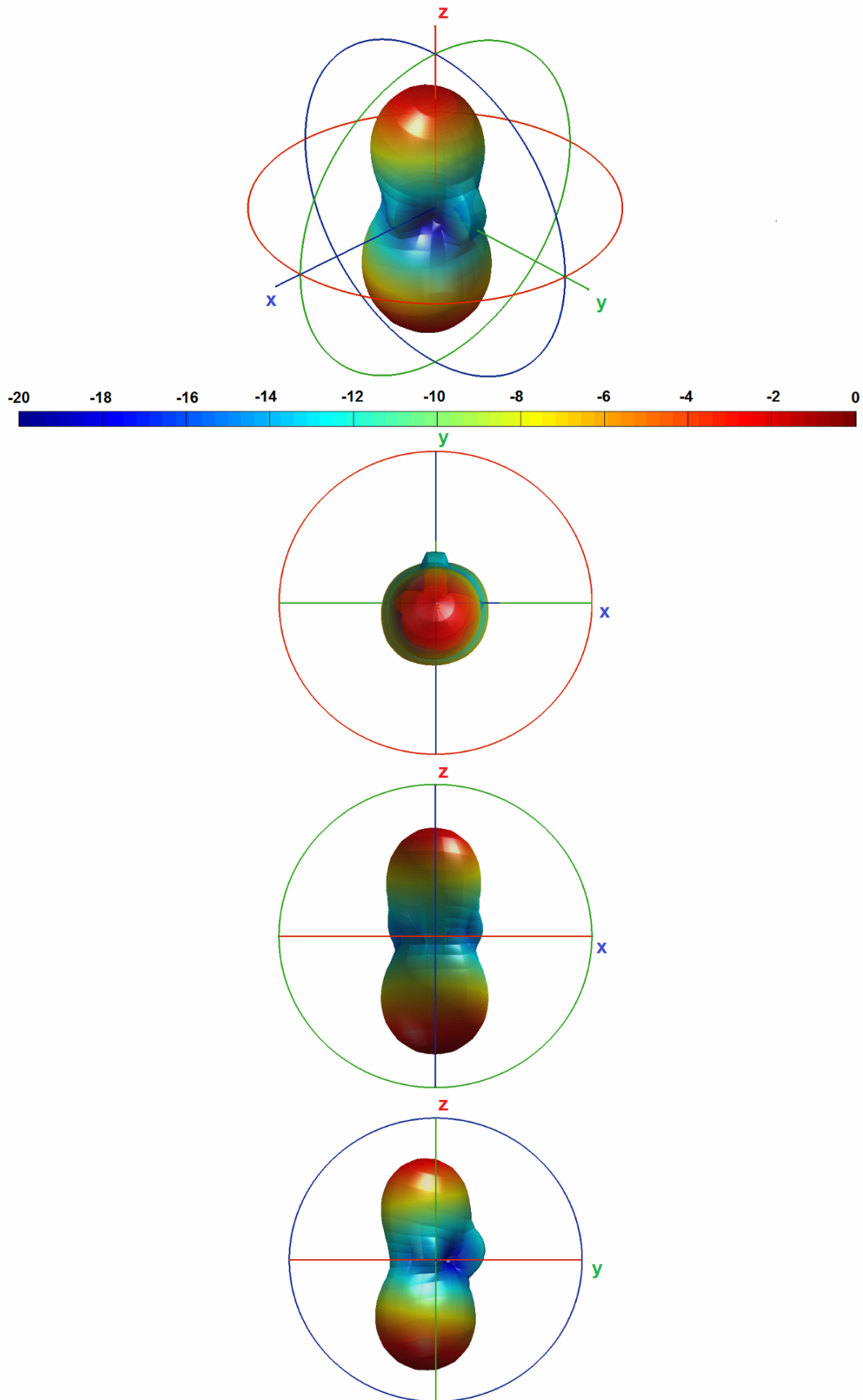


Figure C9.30: Radiation pattern of the original geometry

In order to define an initial guess, we are considering two identical objects, composed of a patch over a ground plane with a patch over it, in the domain, where the object 2 is the parasitic one, as shown in Figure C9.31. The initial guess structure is represented in red color, while, the final structure geometry, is represented in blue. In this example, we choose to remain fixed only the object 1 (reference antenna). The object 2, in the final geometry, has moved away too far, to be represented in this Figure (see red arrow).

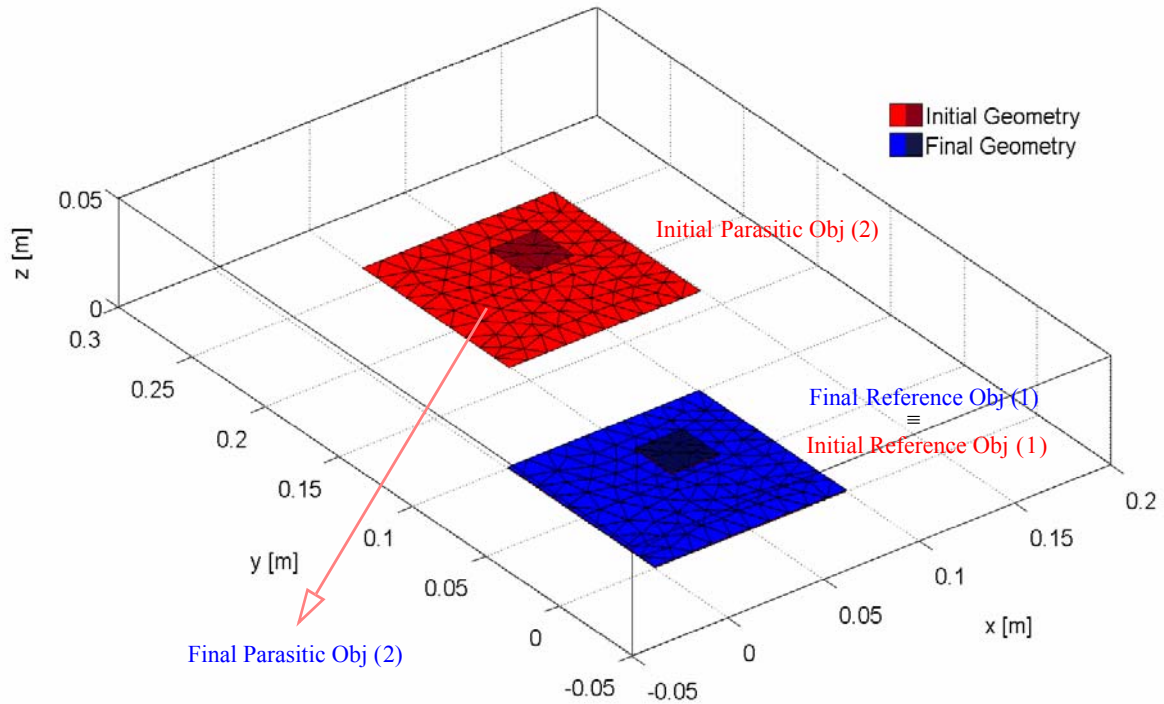


Figure C9.31: Initial vs final geometry

The positions of the objects of the initial and the final structures are reported in the table as follows:

Element	Initial Structure			Final Structure		
	x [m]	y [m]	z [m]	x [m]	y [m]	z [m]
1 (FIXED GND)	0.00000	0.00000	0.00000	0.00000	0.00000	0.00000
2	0.05000	0.16300	0.00000	-60000.0	-40000.0	0.00000

The radiation pattern for the initial structure is reported in Figure C9.32, while the radiation pattern for the final structure is reported in Figure C9.33.

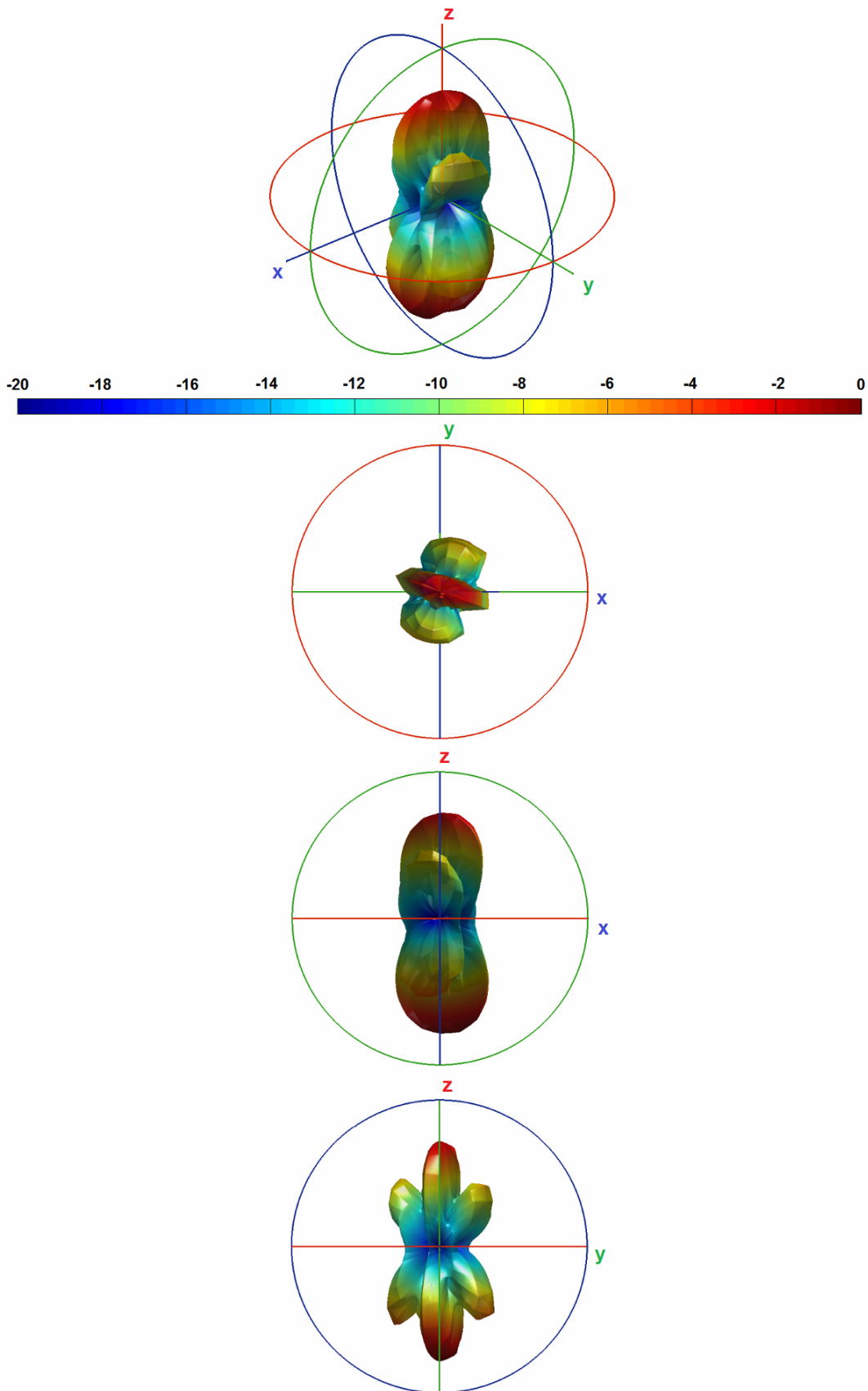


Figure C9.32: Radiation pattern of the initial geometry

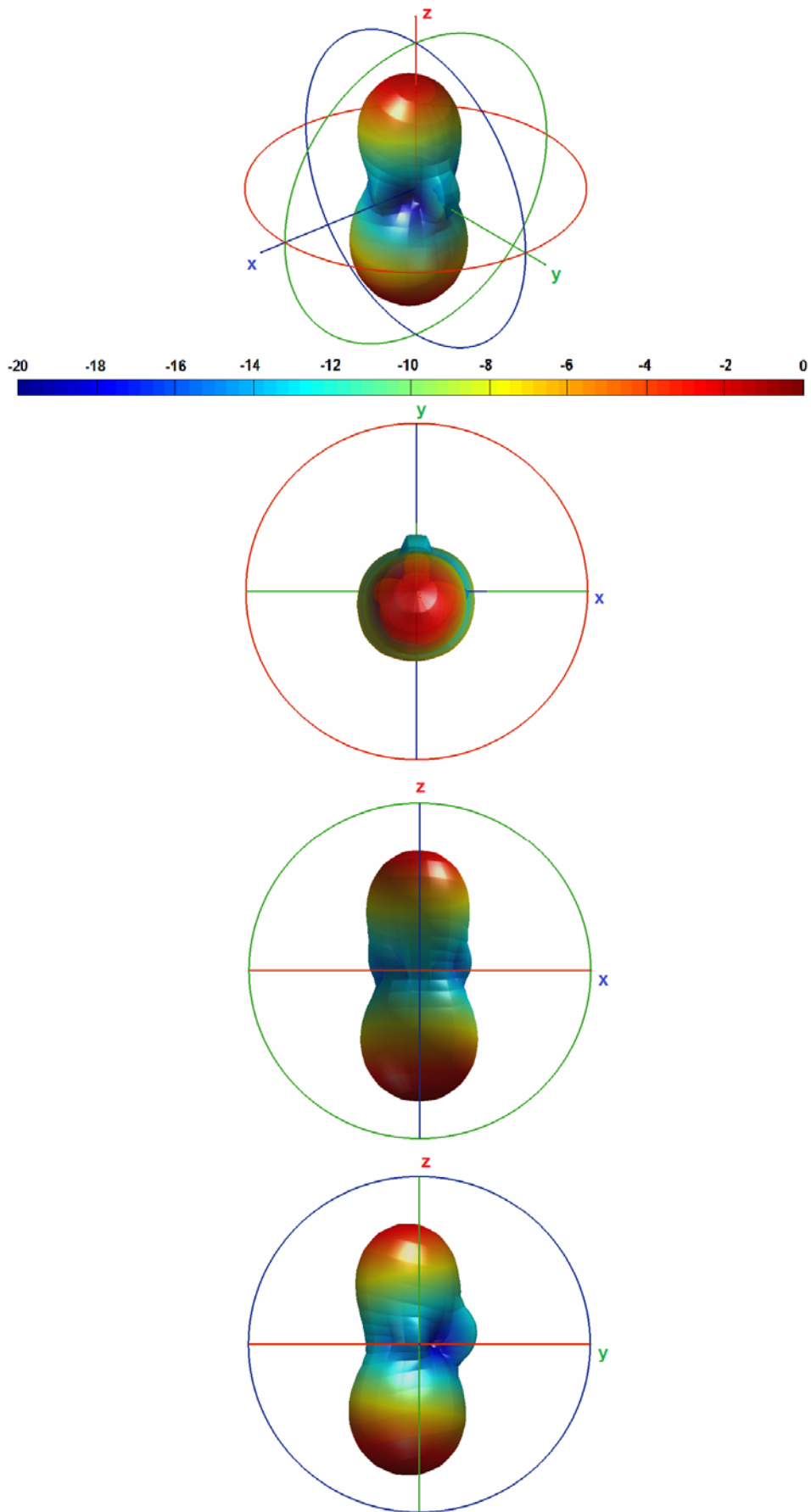


Figure C9.33: Radiation pattern of the final geometry

In Figure C9.34, we show the cross-sections of the radiation pattern with respect to main axes.

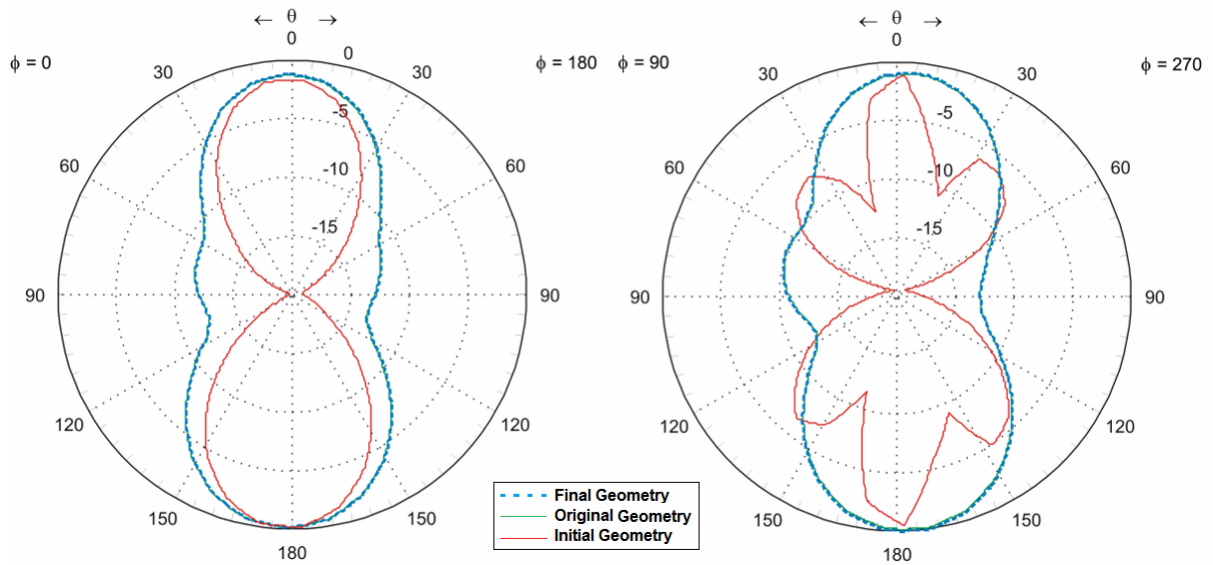


Figure C9.34: Radiation pattern cross-sections

Finally, we show the convergence of the cost functional (criterion), in Figure C9.35.

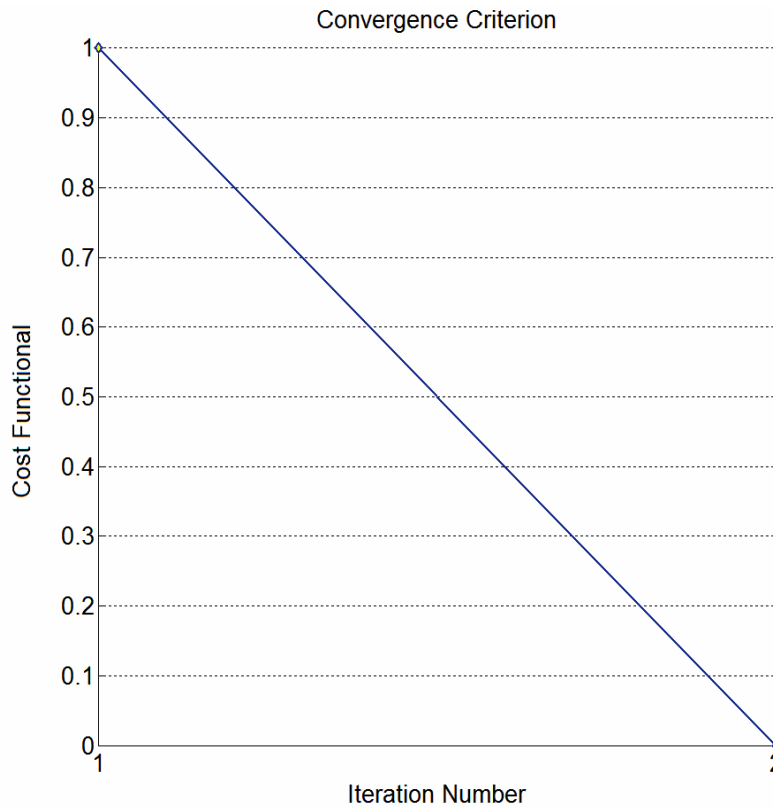


Figure C9.35: Normalized criterion convergence

The convergence of the criterion is reached after only 2 iterations, starting from an absolute value of 472 decreasing till a value of  $3.4 \times 10^{-12}$ . As we do not impose any spatial constraints, i.e., we do not put any limits for the shifting area in the  $xy$  plane, therefore the algorithm has moved immediately away the parasitic object as far as possible. As a result we assert then, that the algorithm is able to quickly recognize the disturbing object and handle it in the right way.

### C9.6 Parasitic Elements III

In this numerical example, we want to add to the domain small parasitic objects. In that way we would like to test the optimization algorithm behavior with respect to low coupled elements. We consider a patch with dimensions  $\lambda/4 \times \lambda/4$  over a ground plane with dimensions  $\lambda \times \lambda$ . The distance between the ground plane and the patch is  $\lambda/8$ . The parasitic elements are small  $\lambda/4$  length dipoles. In Figure C9.36, the original geometry is shown.

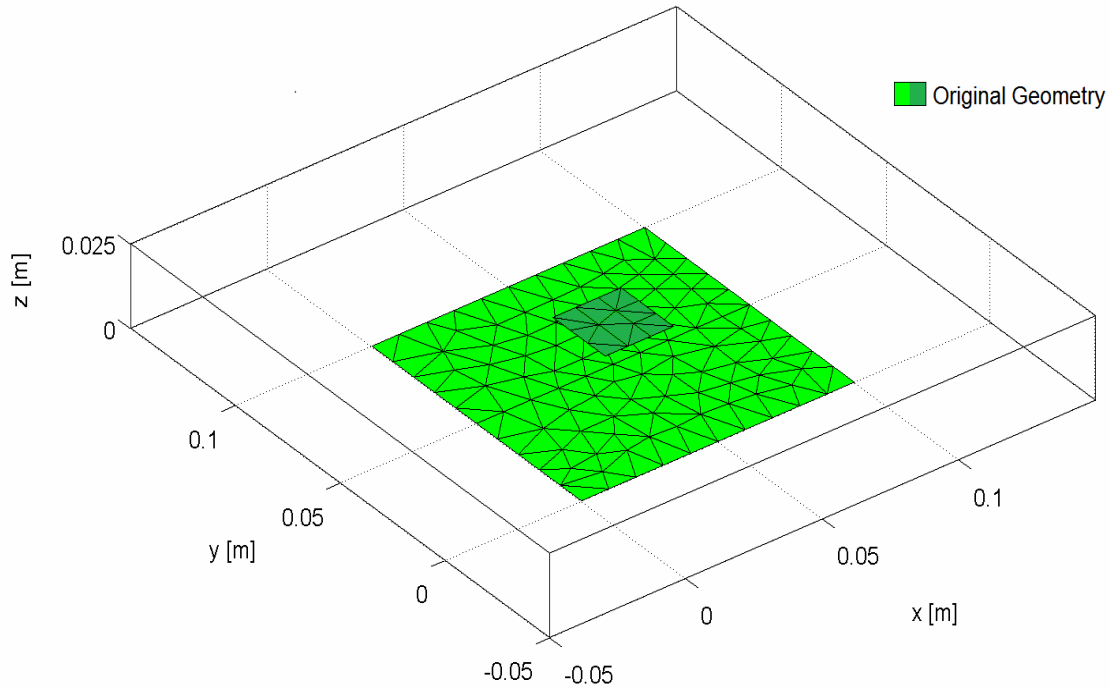


Figure C9.36: original geometry

The position of the object of the original structure is reported in the table as follows:

Element	x [m]	y [m]	z [m]
1 (FIXED)	0.00000	0.00000	0.00000

For the incident field, we use 1 electric dipole defined in the Cartesian coordinates  $(x, y, z)$

Dipole N#	Dipole Moment	x [m]	y [m]	z [m]
1	(1,1,0)	0.05000	0.12500	0.50000

The radiation pattern of the original structure is shown in Figure C9.37.

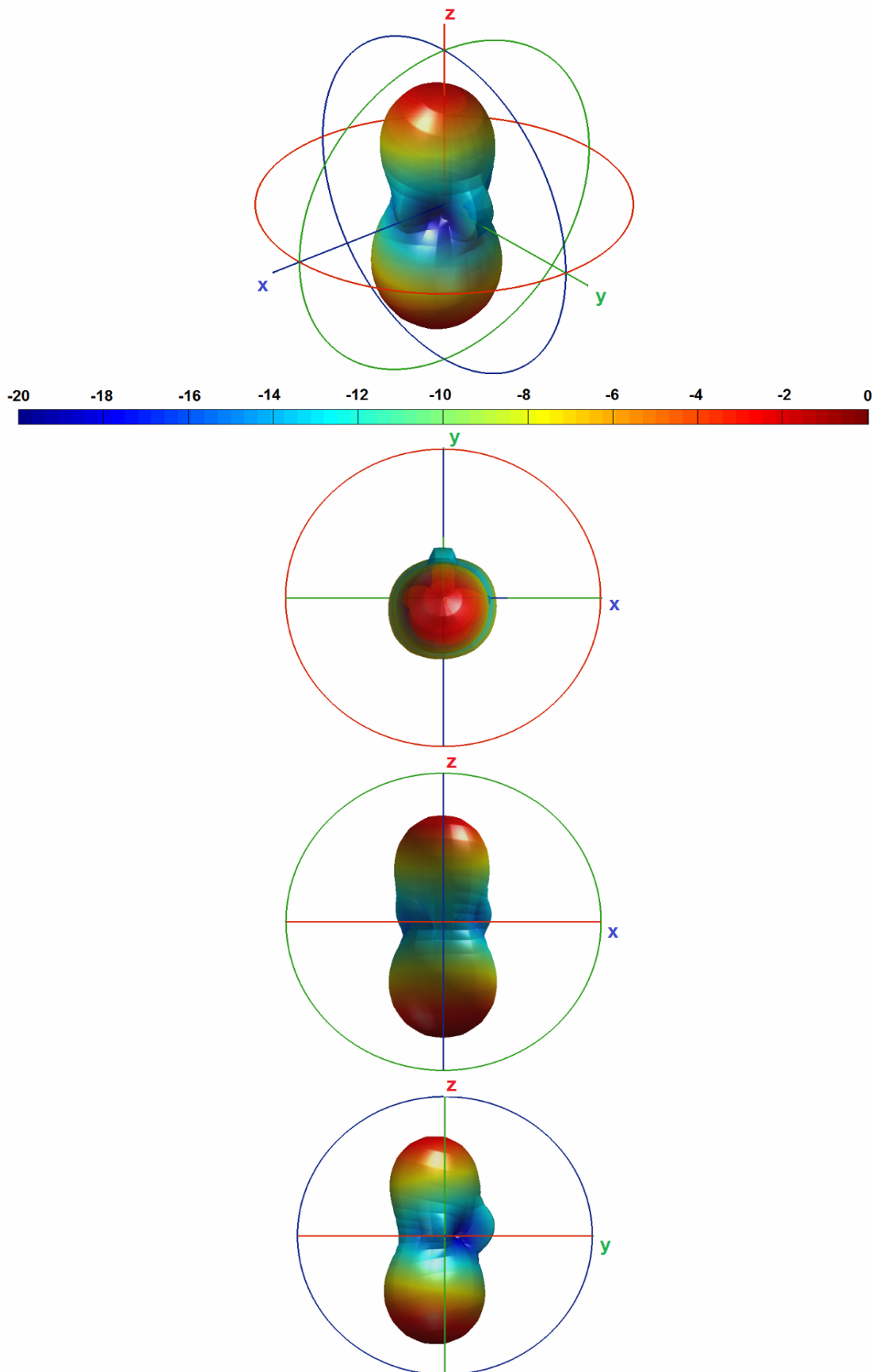


Figure C9.37: Radiation pattern of the original geometry

In order to define an initial guess, we place 4 small  $\lambda/4$  dipoles as shown in Figure C9.38. The initial guess structure is represented in red color while, the final structure geometry is represented in blue. In this example, we choose to remain fixed only the ground plane with the patch (reference object 1). The 4 dipoles (objects 2 to 5) have been moved away too far, in the final geometry, to be represented in the Figure C9.38 (see red arrows).

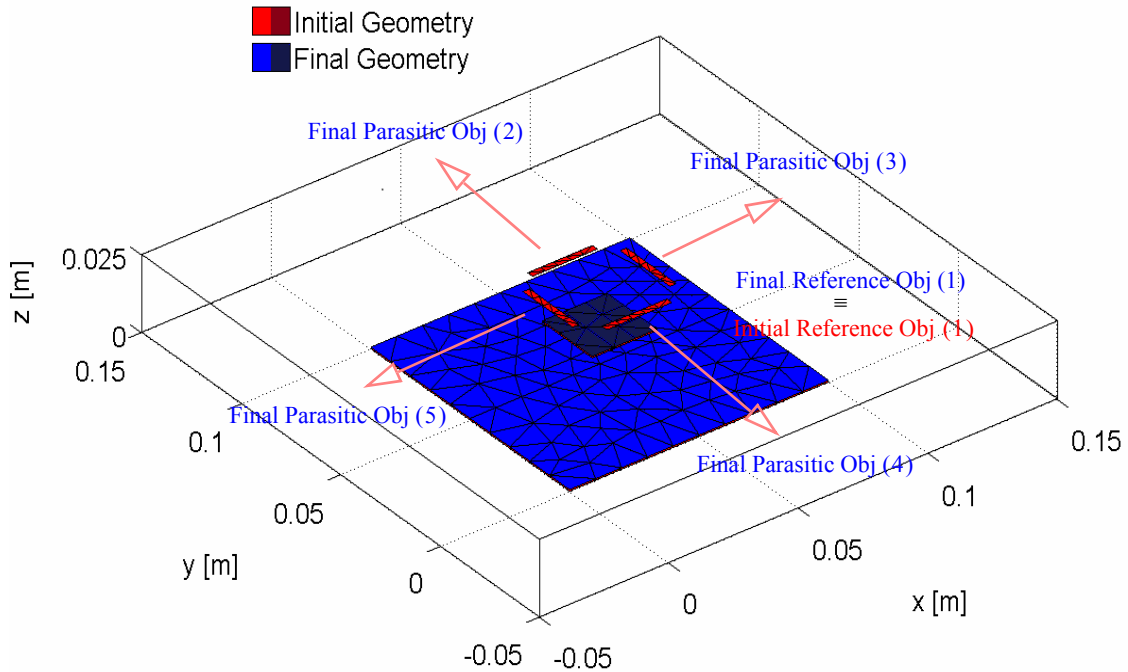


Figure C9.38: Initial vs final geometry

The positions of the objects of the initial and the final structures are reported in the table as follows:

Element	Initial Structure			Final Structure		
	x [m]	y [m]	z [m]	x [m]	y [m]	z [m]
1 (FIXED)	0.00000	0.00000	0.00000	0.00000	0.00000	0.00000
2	0.03000	0.03750	0.00000	-7703.00	-23254.0	0.00000
3	0.06750	0.03750	0.00000	-1187.00	15189.0	0.00000
4	0.03750	0.03000	0.00000	-13460.0	-5145.00	0.00000
5	0.03750	0.06750	0.00000	26617.0	-13495.0	0.00000

The radiation pattern of the initial structure is shown in Figure C9.39, while the radiation pattern of the final structure is shown in Figure C9.40.

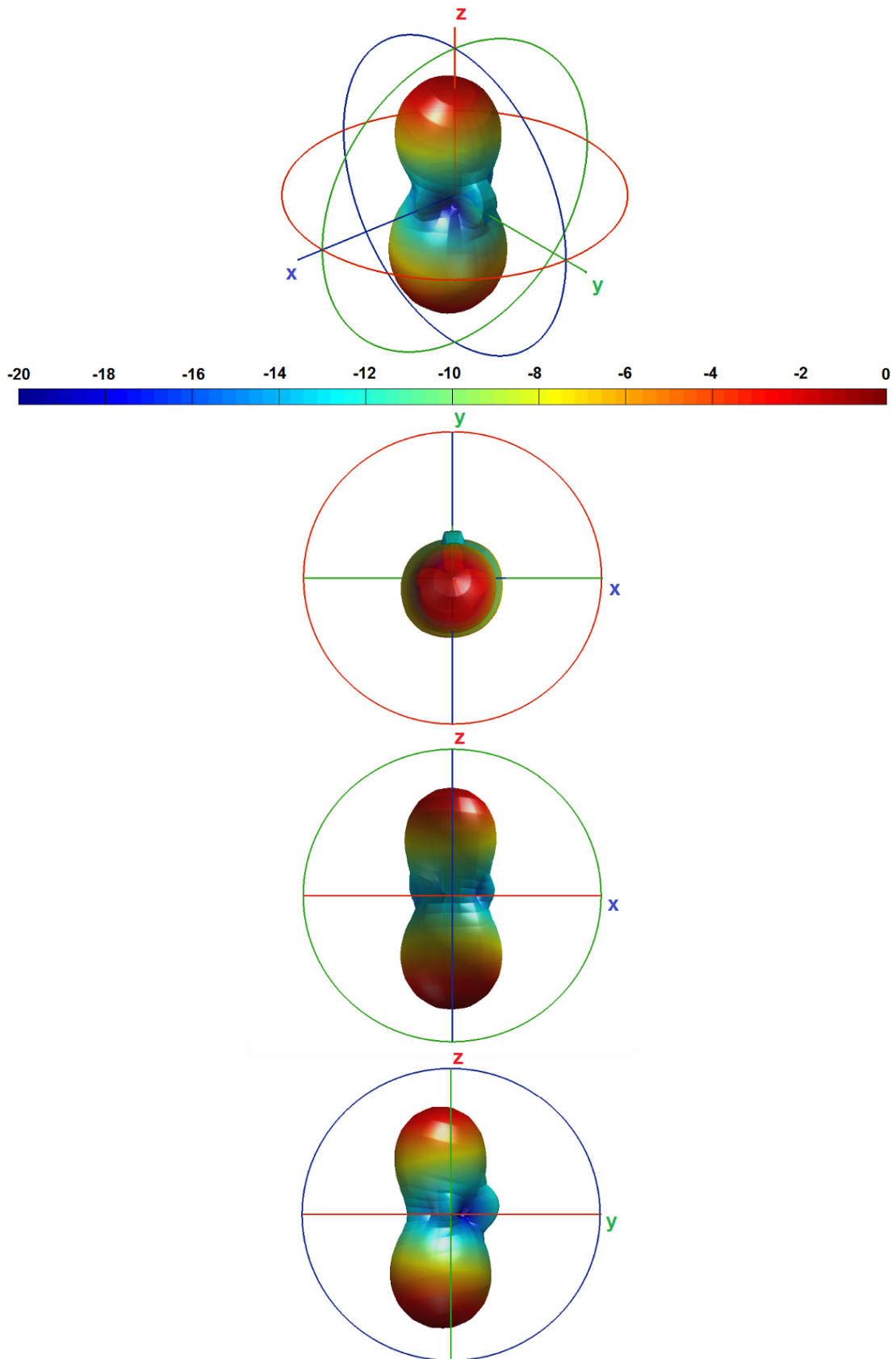


Figure C9.39: Radiation pattern of the initial geometry

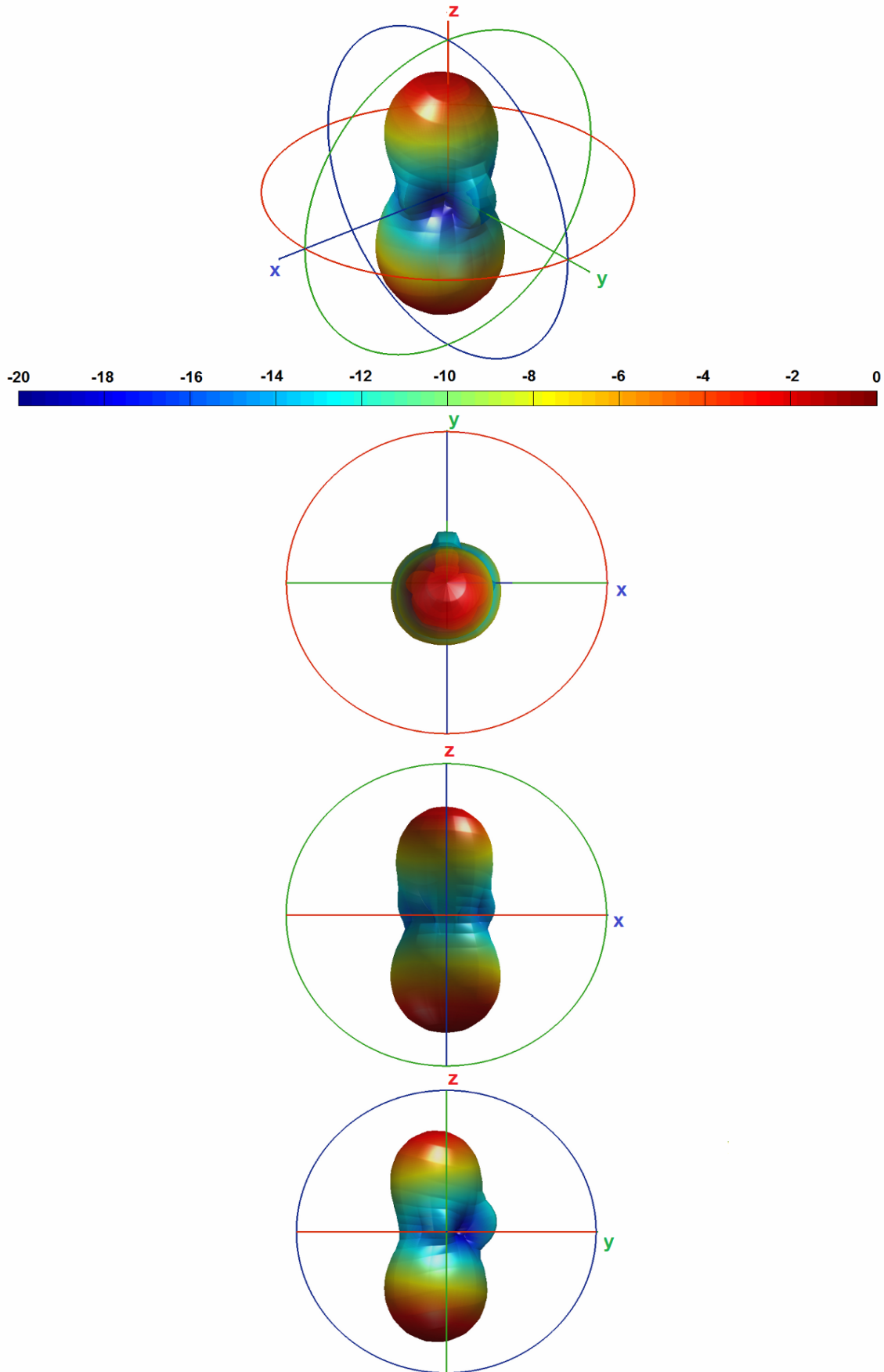


Figure C9.40: Radiation pattern of the final geometry

In Figure C9.41, we show the cross-sections of the radiation pattern with respect to main axes.

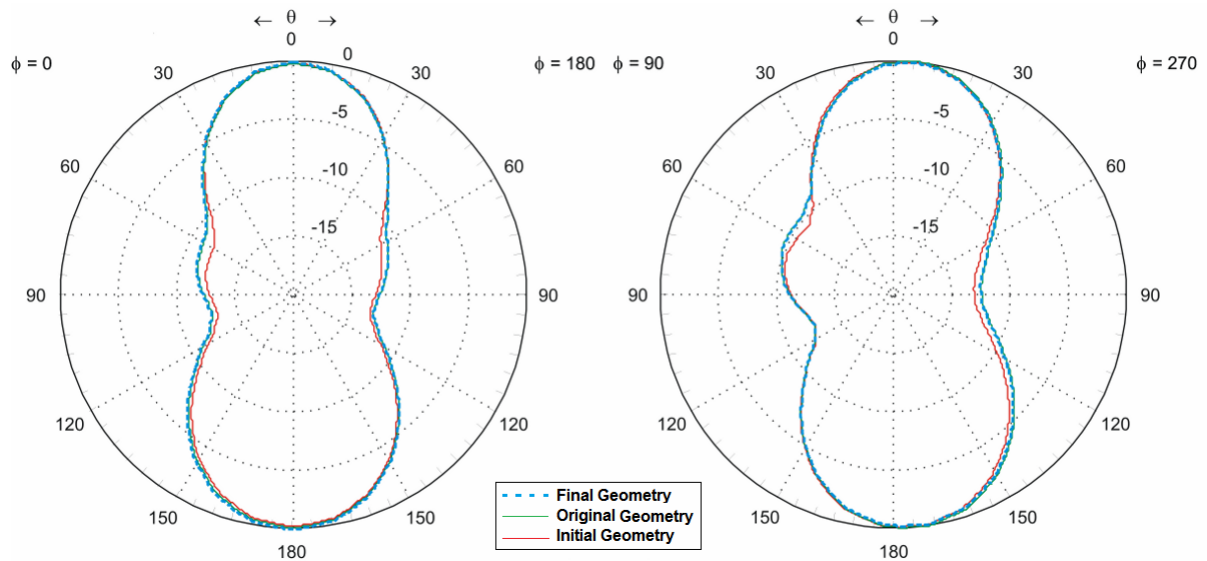


Figure C9.41: Radiation pattern cuts

Finally, we show the convergence of the cost functional (criterion), in Figure C9.42.

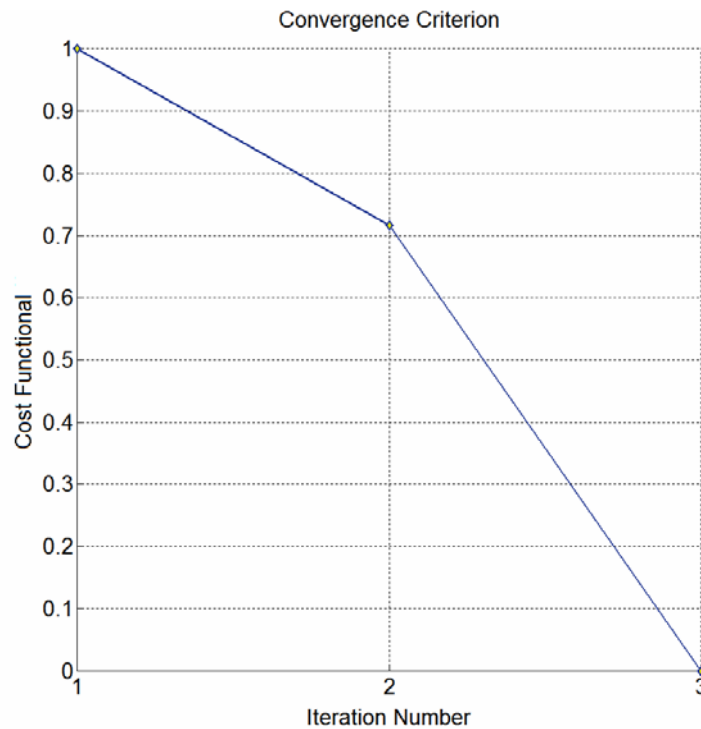


Figure C9.42: Normalized criterion convergence

The convergence of the criterion is reached after only 3 iterations, starting from an absolute value of 3.47 decreasing till a value of 3.38E-11. As we do not impose any spatial constraints, i.e., we do not put limits for the shifting area in the  $xy$  plane, therefore the algorithm has moved immediately away the parasitic objects as far as possible. We have the same behavior as in the previous example, but, this time, the coupling between the objects was very weak, involving that the algorithm has a deep sensitivity. We can see the weak coupling when comparing the Figures C9.39, C9.40 and C9.41, where we easily observe that the radiation pattern shape is almost the same for the three configurations.

### C9.7 Passive Antennas I

In this example, we want to reconstruct the original configuration of the objects composed of two patches located above their respective ground planes. Each ground plane has dimensions of  $\lambda \times \lambda$  and the patch above it has dimensions of  $\lambda/4 \times \lambda/4$ . The original distance between the two objects is shown in Figure C9.43.

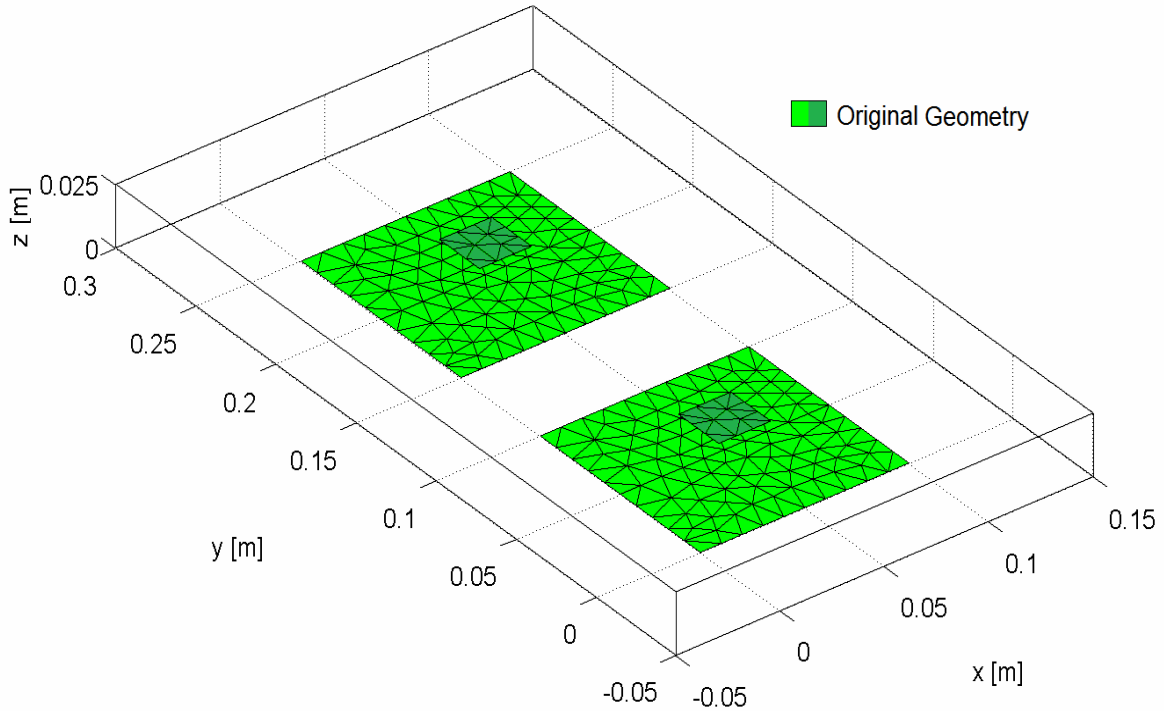


Figure C9.43: Original geometry

The positions of the objects of the original structure is reported in the table as follows:

Element	x [m]	y [m]	z [m]
1 (FIXED)	0.00000	0.00000	0.00000
2	0.00000	0.15000	0.00000

For the incident field, we use 1 electric dipole defined in the Cartesian coordinates  $(x, y, z)$

Dipole N#	Dipole Moment	x [m]	y [m]	z [m]
1	(1,1,0)	0.05000	0.10000	0.50000

The radiation pattern of the original structure is shown in Figure C9.44.

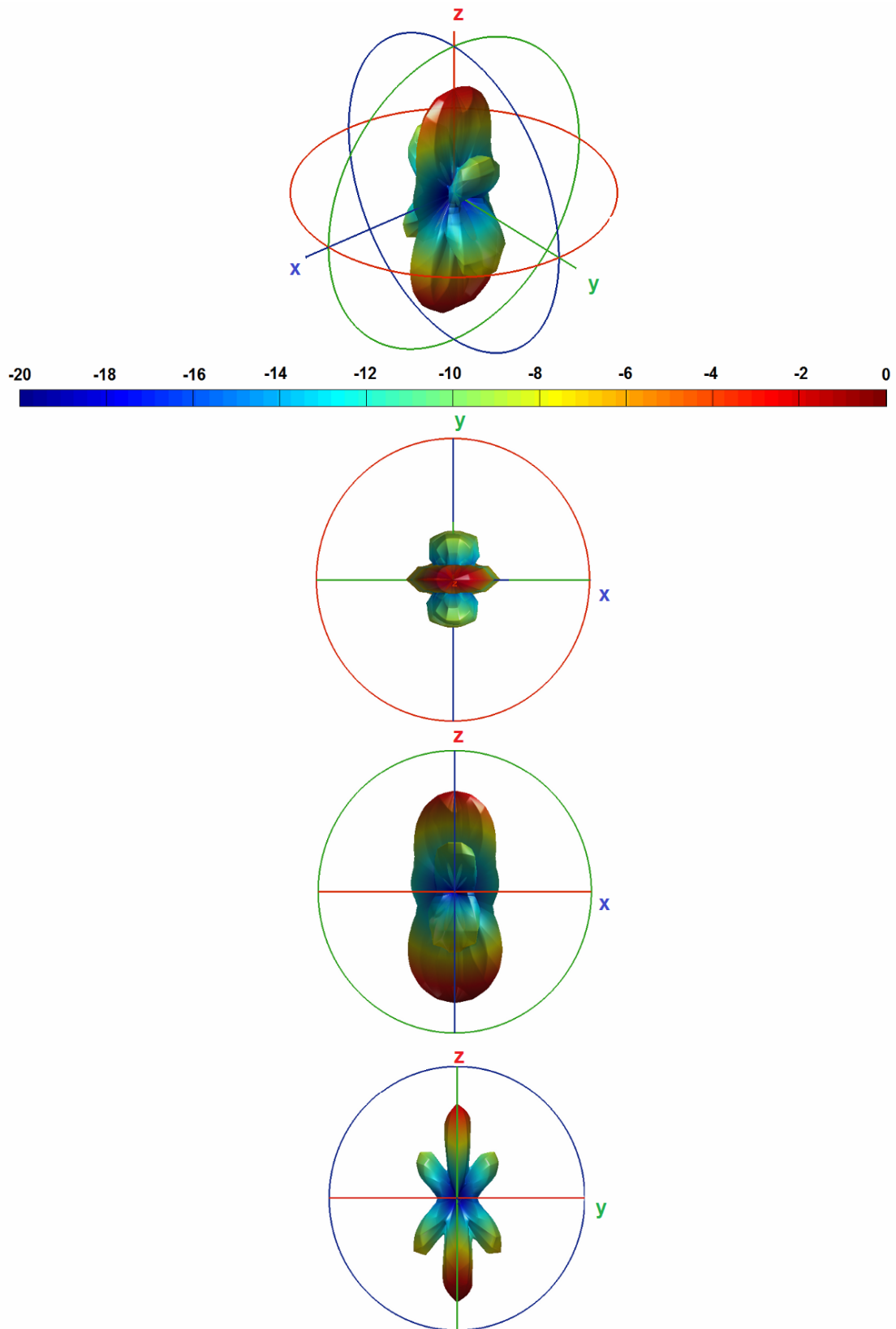


Figure C9.44: Radiation pattern of the original geometry

The initial guess structure is represented in red color while, the final structure geometry is represented in blue. In this example, we choose to remain fixed the reference object 1, as shown in Figure C9.45.

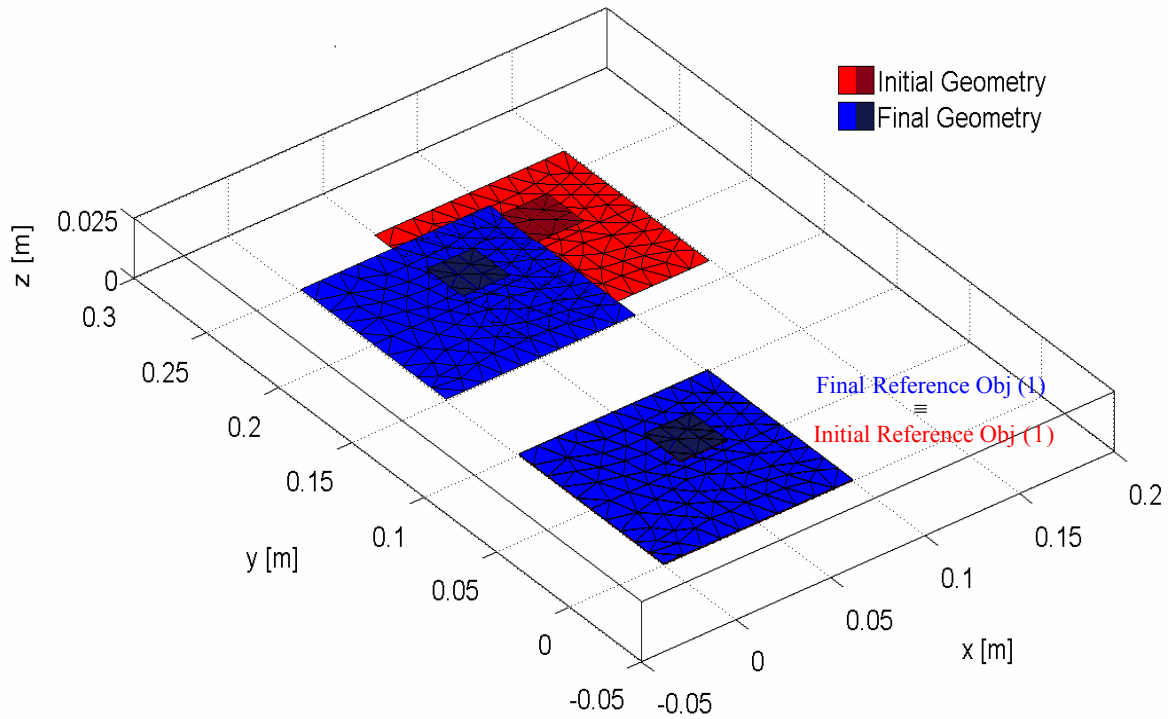


Figure C9.45: Initial vs final geometry

The positions of the objects of the initial and the final structures are reported in the table as follows:

Element	Initial Structure			Final Structure		
	x [m]	y [m]	z [m]	x [m]	y [m]	z [m]
1 (FIXED)	0.00000	0.00000	0.00000	0.00000	0.00000	0.00000
2	0.05000	0.1630	0.00000	0.00037	0.14989	0.00000

The radiation pattern of the initial structure is shown in Figure C9.46, while the radiation pattern of the final structure is shown in Figure C9.47.

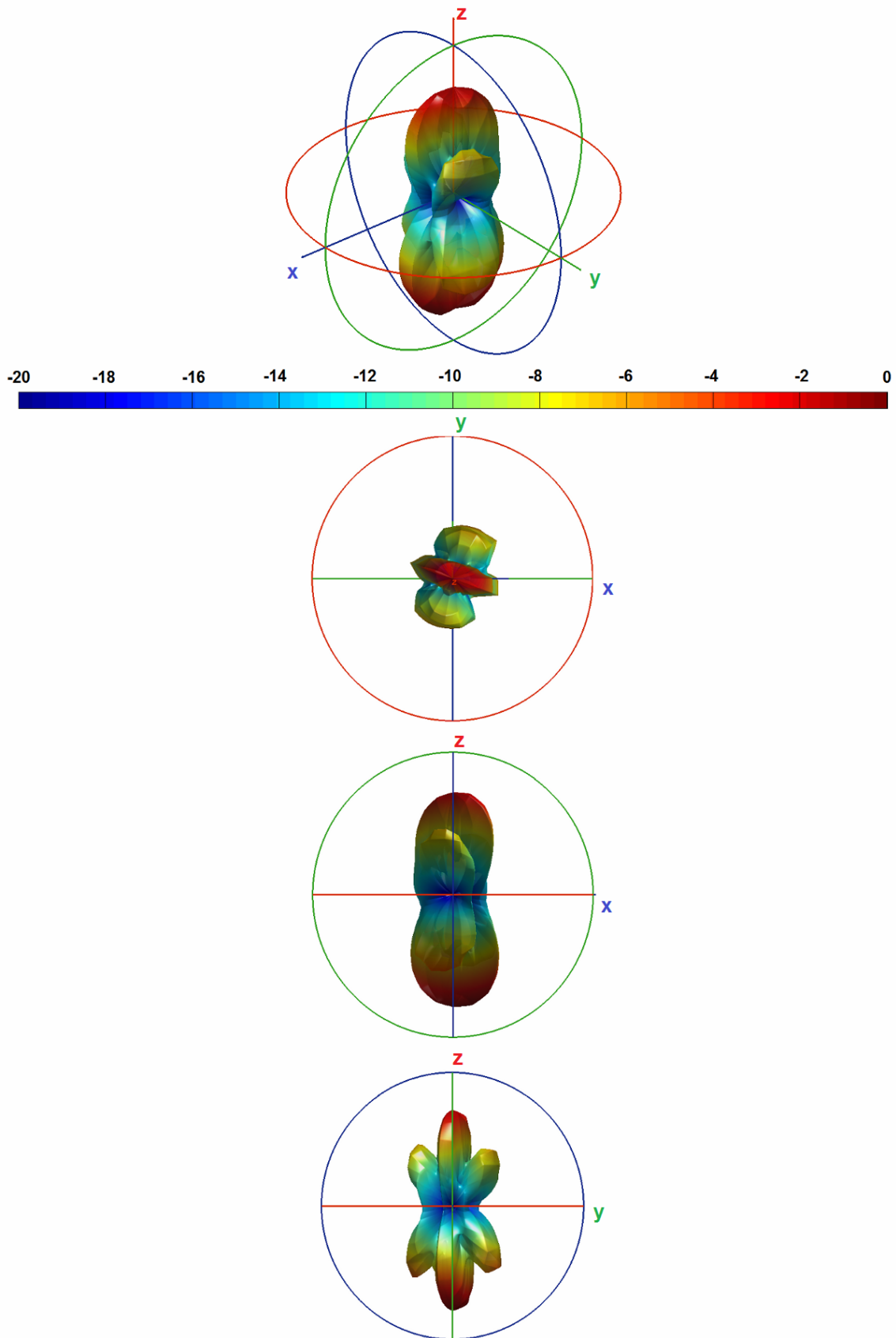


Figure C9.46: Radiation pattern of the initial geometry

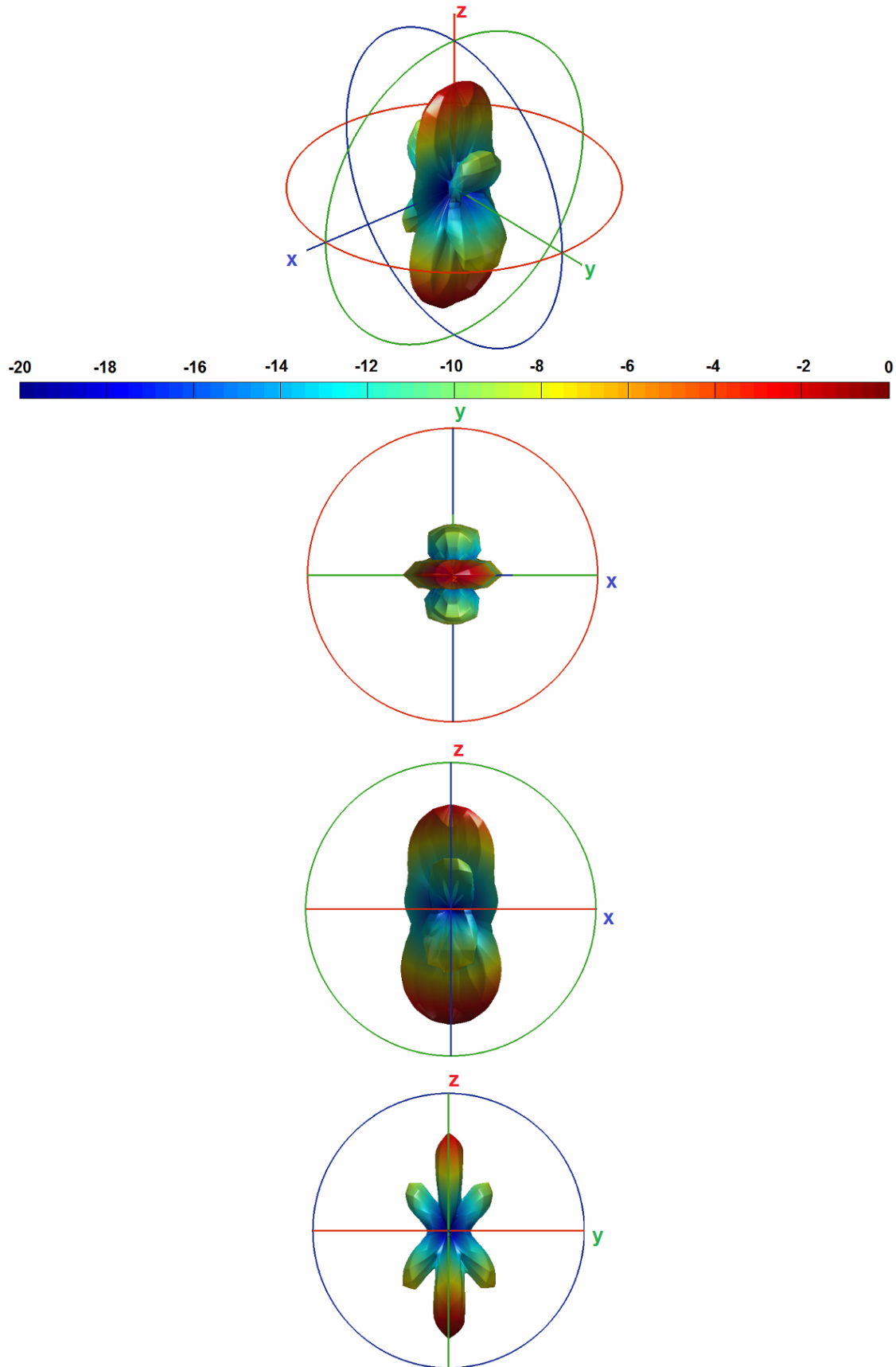


Figure C9.47: Radiation pattern of the final geometry

In Figure C9.48, we show the cross-sections of the radiation pattern with respect to main axes.

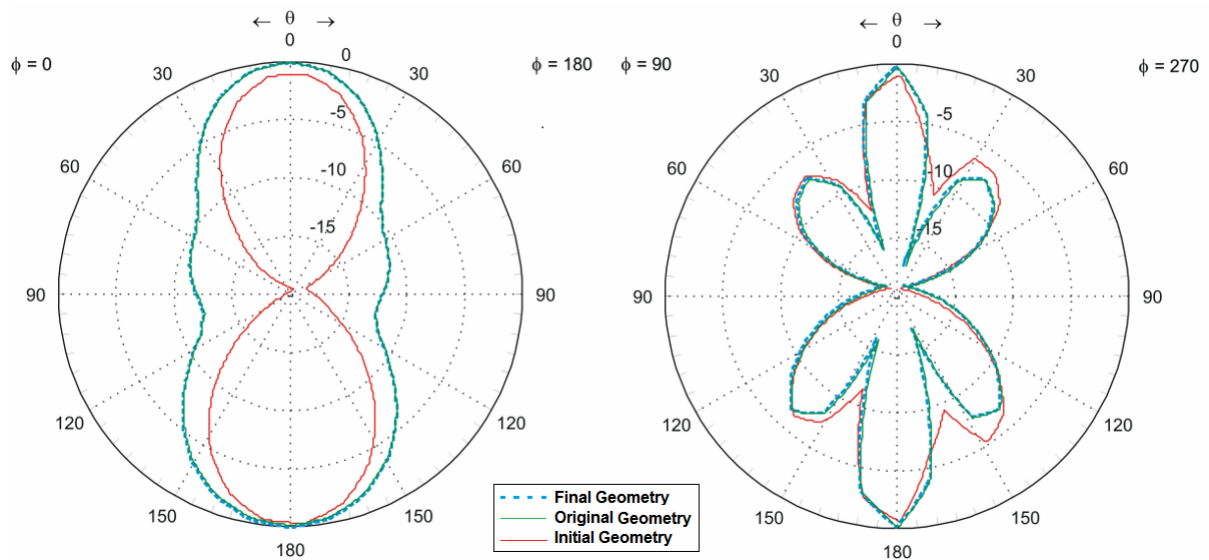


Figure C9.48: Radiation pattern cuts

As a result, we show the convergence of the cost functional (criterion), in Figure C9.49.

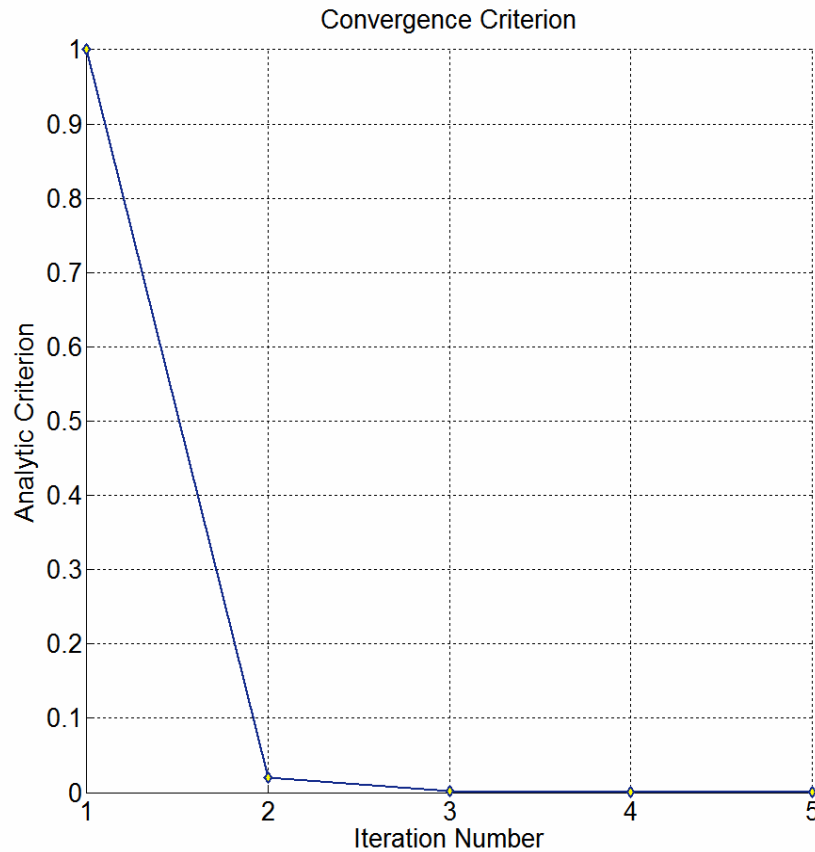


Figure C9.49: Normalized criterion convergence

The convergence of the criterion is reached after 5 iterations, starting from an absolute value of 267 decreasing till a value of 0.021. The reconstruction of the object position has been achieved with an excellent agreement, considering a structure with 2 optimization variables and 416 degrees of freedom.

## C9.8 Passive Antennas II

In this last example, we want to find the optimal position of two cross-shaped patches with  $\lambda/2$  arm-length, deployed above a ground plane. The ground plane has dimensions of  $2\lambda \times \lambda$ . The original distance between the two objects is shown in Figure C9.50.

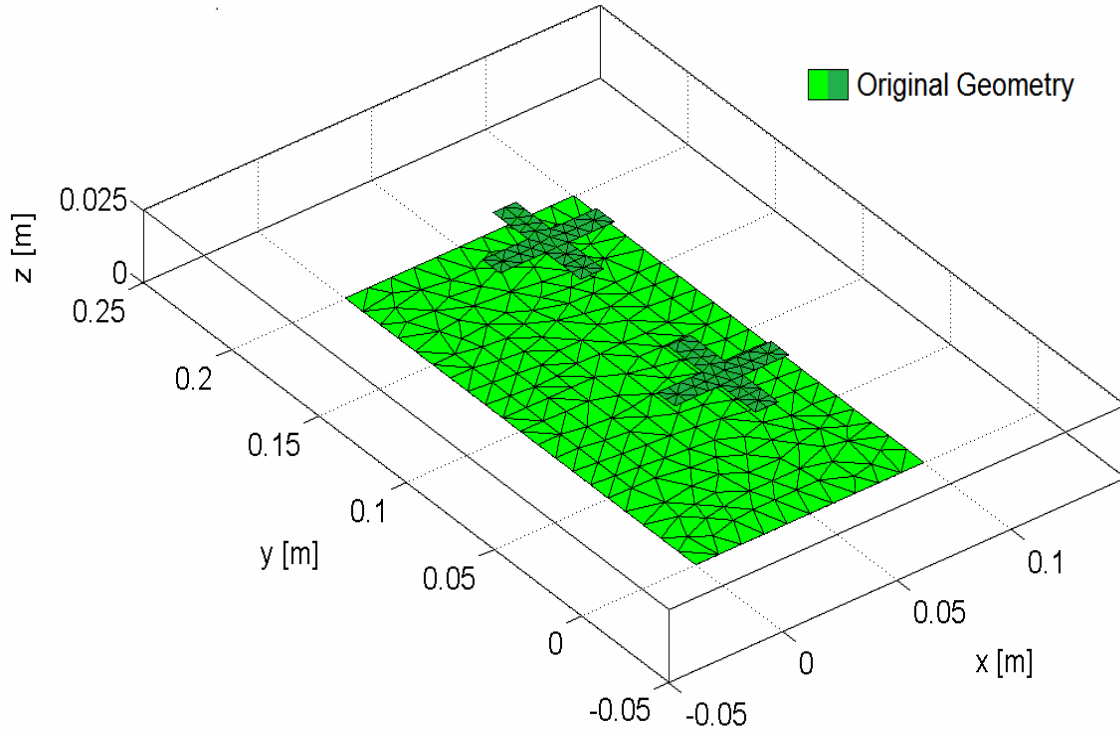


Figure C9.50: Original geometry

The positions of the objects of the original structure is reported in the table as follows:

Element	x [m]	y [m]	z [m]
1 (GND FIXED)	0.00000	0.00000	0.00000
2	0.02500	0.02500	0.02500
3	0.02500	0.12500	0.02500

For the incident field, we use one electric dipole defined in the Cartesian coordinates  $(x, y, z)$

Dipole N#	Dipole Moment	x [m]	y [m]	z [m]
1	(1,1,0)	0.00000	0.00000	0.25000

The radiation pattern of the original structure is shown in Figure C9.51.

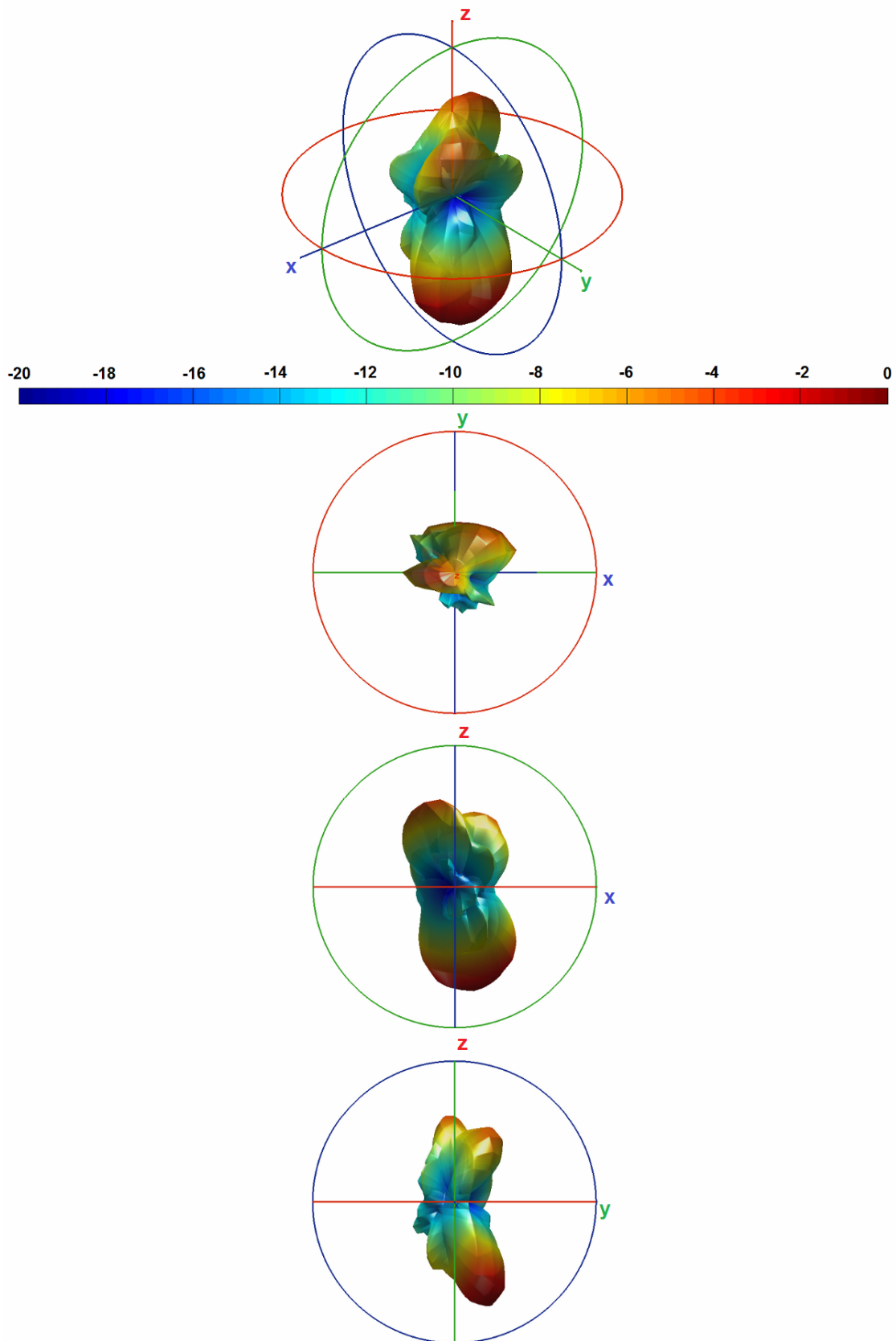


Figure C9.51: Radiation pattern of the original geometry

The initial guess structure is represented in red color while, the final structure geometry is represented in blue as shown in Figure C9.52. In this example, we choose to remain fixed only the ground plane

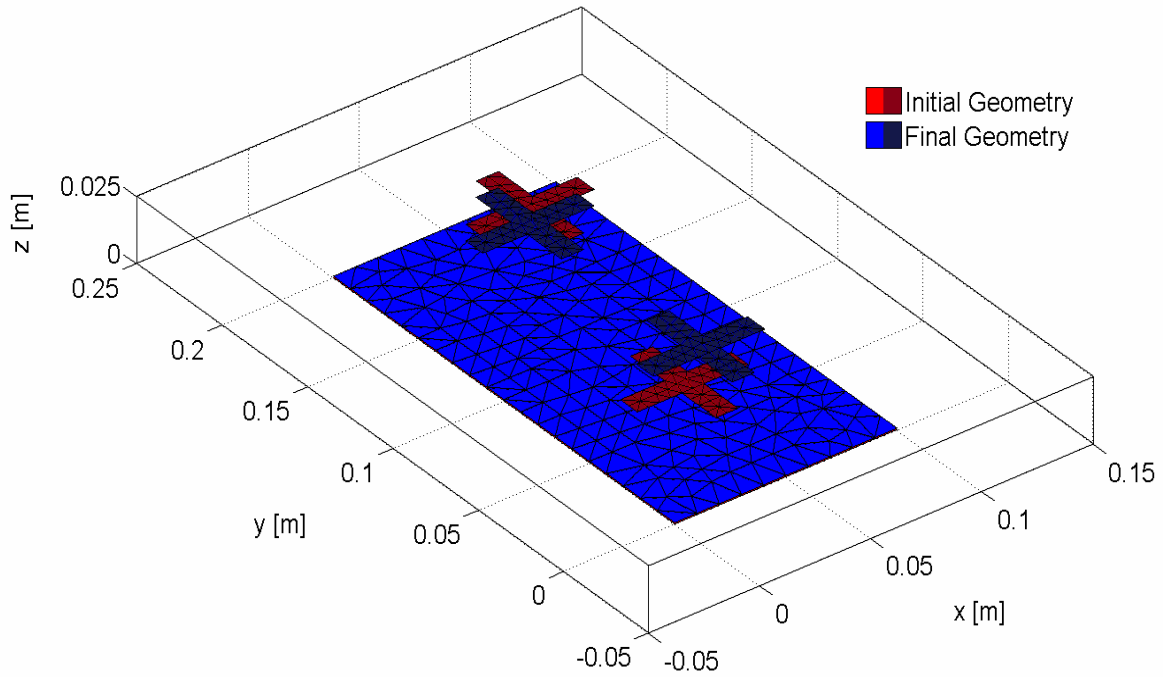


Figure C9.52: Initial vs final geometry

The positions of the objects of the initial and the final structures are reported in the table as follows:

Element	Initial Structure			Final Structure		
	x [m]	y [m]	z [m]	x [m]	y [m]	z [m]
1 (GND FIXED)	0.00000	0.00000	0.00000	0.00000	0.00000	0.00000
2	0.00700	0.01100	0.02500	0.02461	0.02488	0.02500
3	0.03200	0.13400	0.02500	0.02522	0.12536	0.02500

The radiation pattern of the initial structure is shown in Figure C9.53, while the radiation pattern of the final structure is shown in Figure C9.54.

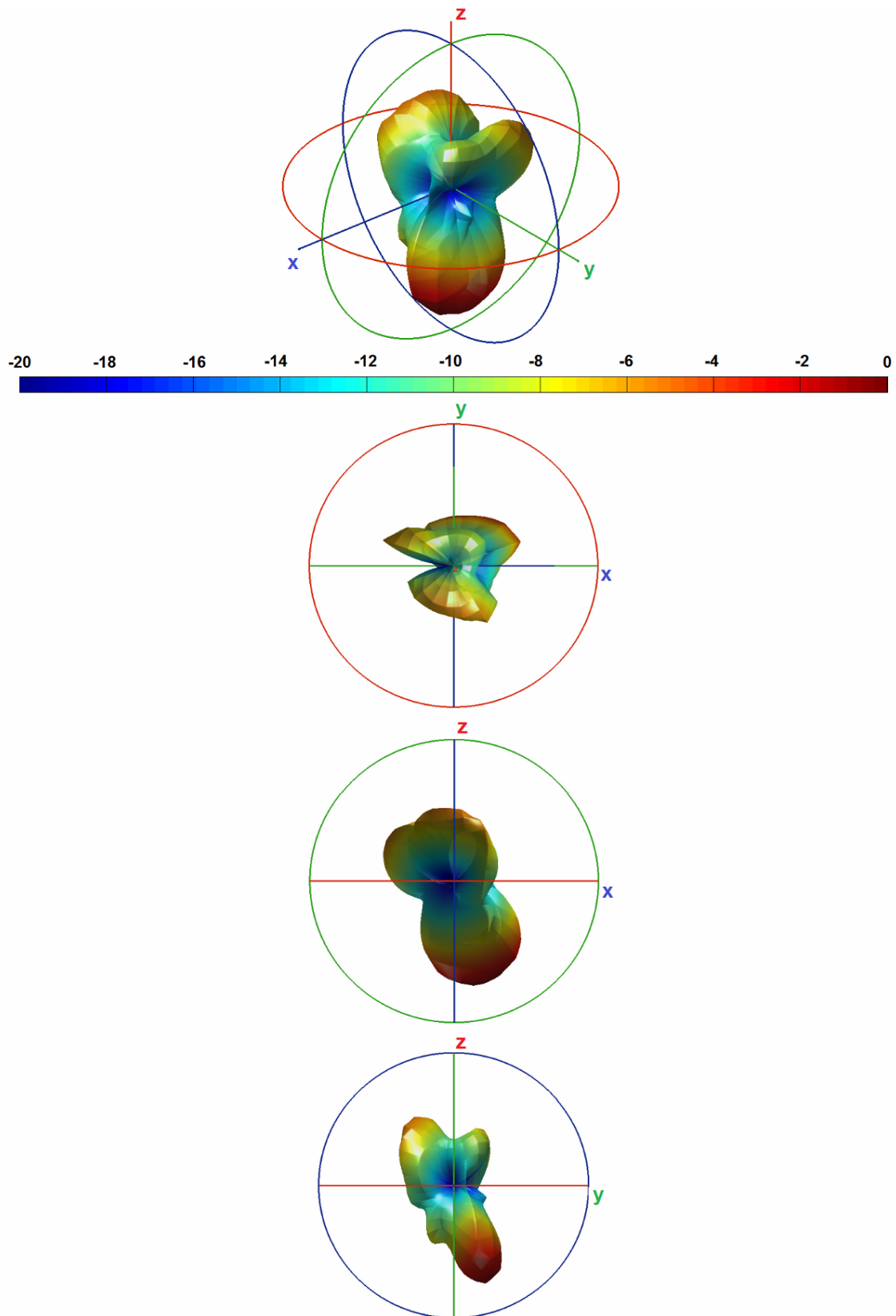


Figure C9.53: Radiation pattern of the initial geometry

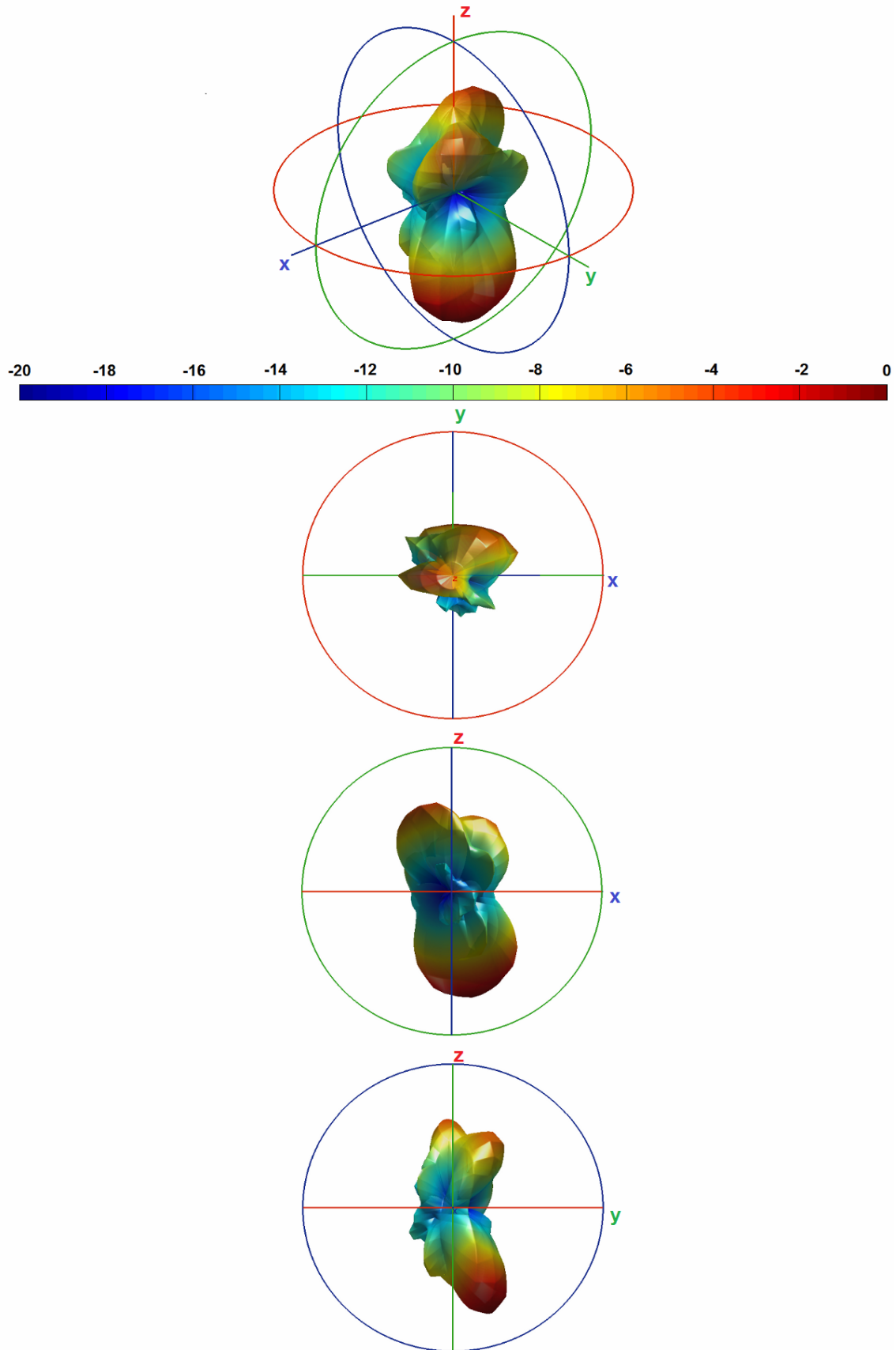


Figure C9.54: Radiation pattern of the final geometry

In Figure C9.55, we show the cross-sections of the radiation pattern with respect to main axes.

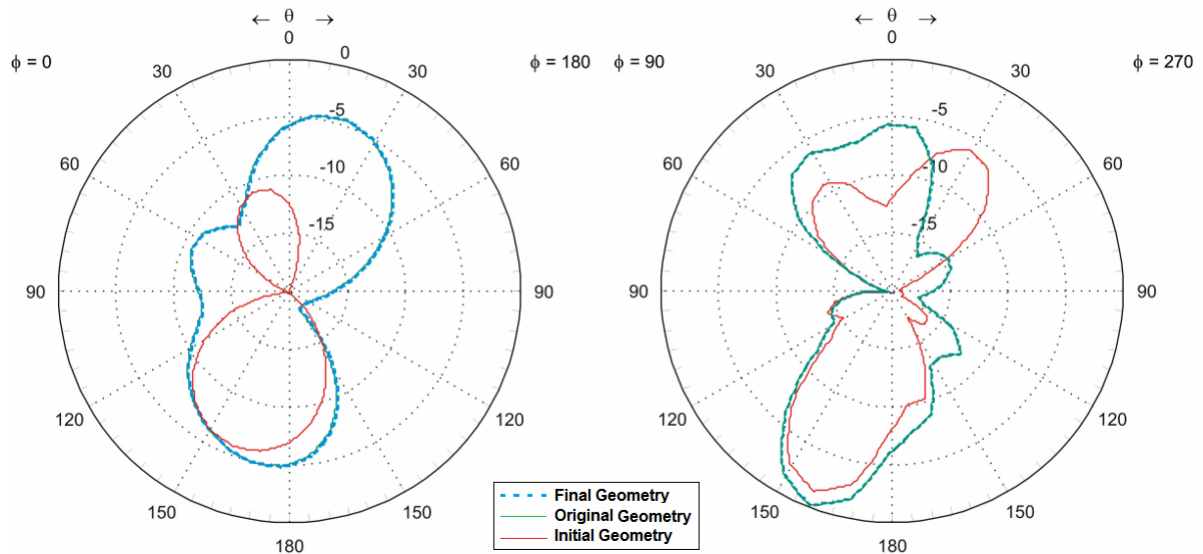


Figure C9.55: Radiation pattern cuts

Finally, we show the convergence of the cost functional (criterion), in Figure C9.56.

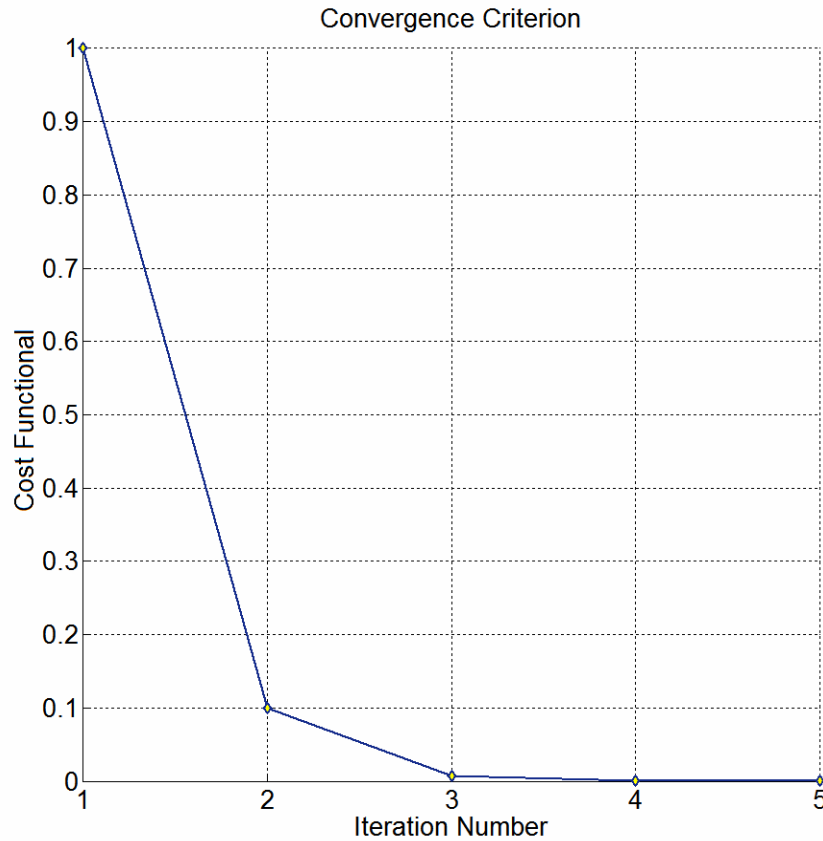


Figure C9.56: Normalized criterion convergence

The convergence of the criterion is reached after 5 iterations, starting from an absolute value of 867 decreasing till a value of 0.031. The reconstruction of the patches position has been achieved with an excellent agreement, considering a structure with 3 optimization variables and 520 degrees of freedom.

## **GENERAL CONCLUSION**

During this work, an inverse scattering method based on an integral formulation of the EM problem (SR3D code) has been developed. The aim was to find the optimal location of 3D or 2D multiple metallic objects or multiantenna systems from imposed constraints (e.g. radiation patterns).

As the results have shown, an efficient and accurate optimization procedure has successfully developed. The framework can be applied to a large number of electromagnetic problems due to the general character of the method.

The optimization is based on a gradient method algorithm which uses a cost functional that depends directly on the surface density currents, defined all over the electromagnetic structure. The innovation of this method consists in the calculation of the analytic derivative of the surface density currents, using the full-wave method. In that way, we obtain a high sensitivity with regard to the parameters we are interested in and considering that coupling effects between structures are taken into account.

It is of great interest to investigate more carefully how the derivation of the surface density currents with respect to the mesh has been calculated. When we talked about derivation with respect to the mesh, we defined for derivative variables, all the points of the mesh of the whole analyzed structure. Therefore, when we want to calculate the derivative of the surface density currents with respect to the mesh, we can choose which nodes are involved inside the computation. In other words, the numerical code developed during this work, is able to compute the variation of the surface density currents with respect to a desired set of mesh points. This is particularly interesting when, for example, we want to optimize the shape of an object, because we are able to compute the variation of the currents with respect to the mesh points that define the object contour. Moreover, we can choose not only the mesh points but also their direction in which we desire to compute the derivative, in the 3-dimensional space, obtaining the gradient of the structure with respect to all the points of the mesh. As the derivative is a linear operator, we can apply a linear combination of the results to define a custom direction of variation of the mesh points. In other words, we can compute the derivative of the surface density currents in the 3-dimensional space and as a consequence to be able to optimize the shape or the position of a set of metallic structures, using a full-wave method.

During this work, we have developed only an element position optimization, by computing the derivative of the surface density currents in the three main direction in a 3-dimensional Cartesian space. The conception of an element shape optimization will be carry out in future developments.

Numerical results, based on the element position optimization, have been achieved using a gradient-based algorithm within the optimization procedure. As we can observe from the numerical experiments, excellent results have been attained from scattered field data, thanks to the high sensitivity of the method. At present, the framework allows the user to remain fixed the position of a certain number of desired objects as imposed constraints.

The method combined with the SR3D code is modular, that is to say, it is possible, for future developments, to easily add constraints with respect to the cost functional, without modifying the main structure of the code.

A further step would be the implementation of the shape optimization of the elements, taking fully advantage of all the potentiality of the numerical modules developed during this work. It would also be possible to perform a multi-frequency study, by combining the cost functionals related to different frequency values.

Finally, a module able to compute the analytic derivation of the surface density currents, with respect to the frequency (first and second order), has been also developed and validated. So, further development could be aimed to combine the shape or position optimization with a frequency optimization obtaining a multi-parameter optimization framework.

## Annex 1 - Numerical Discretization Method

In order to compute the integral reaction expressions defined using the Rumsey's reaction theory, we have chosen a N-point Gauss method in order to discretize the mesh triangle surfaces. The reference discretization number is chosen as seven Gauss points for each triangle. But this number may vary with respect to the relative distance between two triangles.

Given a triangle  $T$  in the  $\mathfrak{R}^3$  domain, it is defined by its three summits  $s$ , and the 3 coordinates are expressed through the variable  $c$ :

$$T = \underline{C}_s^T = C_{cs}^T = [C_{1s}^T, C_{2s}^T, C_{3s}^T] \in \mathfrak{R}^3, \quad c, s = 1, 2, 3$$

In the following, the  $T$  dependancy of the summits will be omitted, for sake of simplicity. So, it is also possible to describe the same triangle by a single summit and two vectors:

$$T = \wp(\underline{C}_1, \underline{C}_1 \underline{C}_2, \underline{C}_1 \underline{C}_3) = \wp(C_1, \underline{u}_1, \underline{u}_2) = \{\underline{C}_1, \underline{C}_1 + \underline{u}_1, \underline{C}_1 + \underline{u}_2\}$$

The barycenter is defined as:

$$\underline{G} = \frac{1}{3} \cdot (\underline{C}_1 + \underline{C}_2 + \underline{C}_3)$$

We propose an approximate integration method on the triangle defining a linear form in the space of  $M + 1$  order derivable functions over  $T$ ;  $\mathfrak{I}$  is the value of the numerical integral using Gaussian quadrature:

$$\mathfrak{I}_T(f) = \Lambda(T) \cdot \sum_{i=1}^m \alpha_i \cdot f(\underline{w}_i)$$

with:	$\Lambda(T) = \int_T 1 dS,$	triangle T surface
	$\gamma_i = \alpha_i \Lambda(T),$	Gauss weights
	$\underline{w},$	generic Gauss point in $\mathfrak{R}^3$

as, if  $p_M$  is a polynomial with a degree less or equal then  $M$ , we have:

$$\mathfrak{I}_T(f) = \int_T p_M(\underline{w}) \cdot ds_w$$

So, if  $M = 5$  we have  $m = 7$  and then:

$$\begin{aligned} \underline{w}_j &= r \cdot \underline{C}_j + (1-r) \cdot \underline{G} & \alpha_j &= \frac{155 - \sqrt{15}}{1200} \\ \underline{w}_{j+3} &= s \cdot \underline{C}_j + (1-s) \cdot \underline{G} & \alpha_{j+3} &= \frac{155 + \sqrt{15}}{1200} \\ \underline{w}_7 &= \underline{G} & \alpha_7 &= \frac{9}{40} \end{aligned}$$

with:  $r = \frac{1 + \sqrt{15}}{7}, \quad s = \frac{1 - \sqrt{15}}{7}$   
 $j = 1, 2, 3$

In order to define the algorithm used to place the integration points ( $\underline{w}_j \in \mathfrak{R}^3$ ), we create the canonical triangle using the original triangle and two orthonormal vectors:

$$(\underline{e}_1, \underline{e}_2, \underline{e}_3) \text{ orthonormal base of } \mathfrak{R}^3 \quad T_0 = \wp(\underline{Q}, \underline{e}_1, \underline{e}_2)$$

This triangle is isomorphic with respect to unit triangle in  $\mathfrak{R}^2$ :  $\{\underline{Q}, (1, 0), (0, 1)\}$ . The summits of this triangle and the barycenter, are associated respectively to complex numbers as follows:

$$c_1 = 0 + i0 \quad c_2 = 1 + i0 \quad c_3 = 0 + i1 \quad g = \frac{1}{3} \cdot (1 + i1)$$

The Gauss quadrature points for the reference triangle are defined in complex coordinates (i.e.  $z_j \in C$ ) as follows:

$$\begin{aligned} z_j &= r \cdot c_j + \frac{(1-r)}{3} \cdot (1+i) & \alpha_i &= \frac{155 - \sqrt{15}}{1200} \\ z_{j+3} &= s \cdot c_j + \frac{(1-s)}{3} \cdot (1+i) & \alpha_{i+3} &= \frac{155 + \sqrt{15}}{1200} \\ z_7 &= \frac{1}{3} \cdot (1+i) & \alpha_7 &= \frac{9}{40} \end{aligned}$$

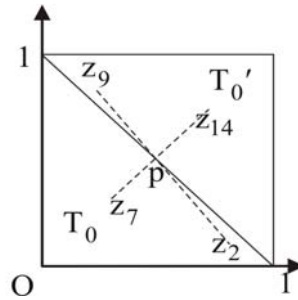
with:  $r = \frac{1 + \sqrt{15}}{7}, \quad s = \frac{1 - \sqrt{15}}{7}$   
 $j = 1, 2, 3$

or:

$$\begin{aligned} z_1 &= \frac{(1-r)}{3} \cdot (1+i) & z_4 &= \frac{(1-s)}{3} \cdot (1+i) \\ z_2 &= \frac{1+2r}{3} + i\left(\frac{1-r}{3}\right) & z_5 &= \frac{1+2s}{3} + i\left(\frac{1-s}{3}\right) \\ z_3 &= \frac{1-r}{3} + i\left(\frac{1+2r}{3}\right) & z_6 &= \frac{1-s}{3} + i\left(\frac{1+2s}{3}\right) & z_7 &= \frac{1+i}{3} \end{aligned}$$

It is possible, in a very simple way, to develop an approximated integration method on a unit square starting from the method previously shown:

$$\begin{aligned}
 p &= \frac{1+i}{2} \\
 T_0' &= S_p(T_0) \\
 S_p(z) &= p + (p-z) = 2p-z \\
 C_0 &= T_0 \cup T_0'
 \end{aligned}$$



$$\begin{aligned}
 z_8 &= p + (p - z_1) \\
 &\dots\dots \\
 z_{7+j} &= p + (p - z_j) \\
 &\dots\dots \\
 z_{14} &= p + (p - z_7) \\
 j &= 1, 2, 3
 \end{aligned}$$

Figure A1.1: Symmetric reference square

The  $T_0'$  triangle is the image of  $T_0$  through the centre  $p$  and the square is just the union of the two triangles. We have:

$$\int_{C_0} f(\underline{w}) ds_w = \int_{T_0} f(\underline{w}) ds_w + \int_{T_0'} f(\underline{w}) ds_w \Rightarrow \underline{\mathfrak{I}}_{C_0}(f) = \underline{\mathfrak{I}}_{T_0}(f) + \underline{\mathfrak{I}}_{T_0'}(f)$$

with:

$$\begin{aligned}
 \underline{\mathfrak{I}}_{T_0}(f) &= \frac{1}{2} \cdot \sum_{j=1}^m \alpha_j \cdot f(z_j) \\
 \underline{\mathfrak{I}}_{T_0'}(f) &= \frac{1}{2} \cdot \sum_{j=1}^m \alpha_j \cdot f(S_p(z_j))
 \end{aligned}$$

The integration points of the approximate method on the unit reference square are defined as:

$$S_p(z) = (1+i) - z$$

with:  $z_1, \dots, z_m, S_p(z_1), \dots, S_p(z_m)$

We can write:

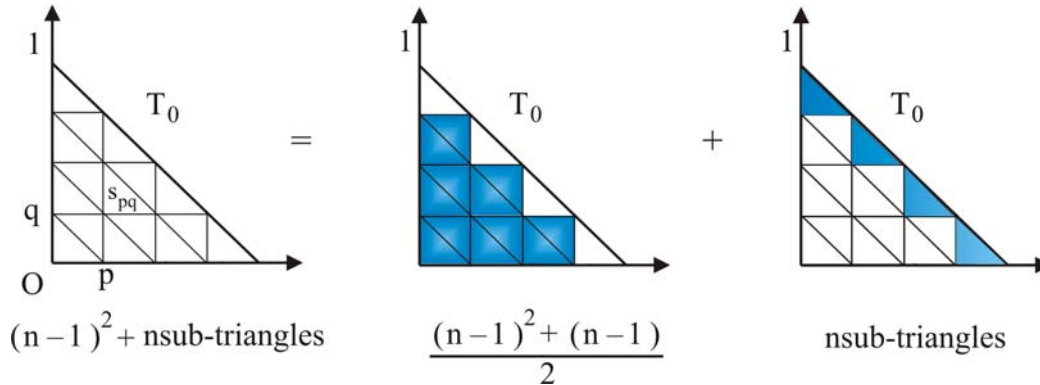
$$z_{j+m} = (1+i) - z_j \quad \alpha_{j+m} = \alpha_j$$

with:  $j = 1, \dots, m$

And the approximate integral on the unit square is defined as:

$$\underline{\mathfrak{I}}_{C_0}(f) = \frac{1}{2} \cdot \sum_{j=1}^{2m} \alpha_j \cdot f(z_j)$$

We consider now a new unit triangle  $T_0$  divided into a  $M$  sub-triangles partition obtained from the unit triangle  $T_0$  or from the symmetric triangle  $T_0'$ , using a  $1/n$  homothetic transformation followed by a translation. In order to avoid two different kinds of sub-triangles, we will group some of them together as squares and leave the border of sub-triangles as they are, as shown below:



The partition of unit triangle includes:

$$\frac{n(n-1)}{2} \text{ squares} \quad n \text{ triangles}$$

The position of the elements of the partition is defined through the  $s_{pq}$  points:

$$s_{pq} = h \cdot ((p-1) + i \cdot (q-1))$$

with:

$$\begin{aligned} h &= \frac{1}{n} \\ (q &= 1, \dots, n) \\ (p &= 1, \dots, n - q + 1) \end{aligned}$$

We define now the transformation of a unit square into the elements  $E_{pq}$  of the partition:

$$C_0 \rightarrow E_{pq} \quad z \rightarrow \zeta \quad \zeta = s_{pq} + h \cdot z$$

If we apply this transformation for the integration points of the approximate method on the unit square, we obtain:

$$z_j \in C_0 \rightarrow \zeta_j^{pq} \in E_{pq}, \quad z_i \in T_0 \rightarrow \zeta_i^{pq} \in E_{pq}$$

with:

$$\begin{aligned} i &= 1, \dots, m \\ j &= 1, \dots, 2m \end{aligned}$$

In order to simplify the algorithm, we must index the  $\zeta_j^{pq}$  family as follows:

$$\zeta_j^{pq} = \zeta_{\eta(p, q, j)}$$

$$\text{where: } \eta(p, q, j) = \sum_{k=1}^{q-1} ((n-k) \cdot 2m + m) + (p-1) \cdot 2m + j$$

So:

$$\eta(p, q, j) = m(q-1) + 2mn(q-1) - 2m \sum_{k=1}^{q-1} k + (p-1)2m + j$$

and since we has

$$\sum_{k=1}^{q-1} k = \frac{q \cdot (q-1)}{2}$$

we can finally write:

$$\eta(p, q, j) = m(q-1) \cdot (2n-q+1) + (p-1)2m + j$$

Let us define the composite method for unit triangle that is defined by a  $1/n$  element dimension partition, on which we apply a  $m$  point approximate method. So we have:

$$\begin{aligned} \mathfrak{I}_{T_0}^{nm}(f) &= A(T_0) \cdot \sum_{j=1}^N \beta_j \cdot f(\zeta_j) \\ \zeta_{\eta(p, q, j)} &= \frac{1}{n} \cdot (z_j + (p-1) + i \cdot (q-1)) \\ \beta_{\eta(p, q, j)} &= \frac{1}{n^2} \cdot \alpha_j \end{aligned}$$

with:

$N = mn^2,$	
$q = 1, \dots, n$	$p = 1, \dots, n - q + 1$
$j = 1, \dots, v_p$	$v_p = 2m$ if $p = 1, \dots, n - q$ $v_p = m$ if $p = n - q + 1$

Now we define the linear transformation that allows us to move from the triangle  $\{Q, (1, 0), (0, 1)\}$  to the triangle  $\{C_1, C_2, C_3\}$ :

$$T = \wp(\underline{C}_1, \underline{u}_1, \underline{u}_2), \quad \underline{u}_1 = \underline{C}_2 - \underline{C}_1, \quad \underline{u}_2 = \underline{C}_3 - \underline{C}_1$$

We define the transformation using the  $\{x_1, x_2\}$  generic unknowns:

$$(x_1, x_2, 0) \in \wp(Q, \underline{e}_1, \underline{e}_2) \rightarrow (w = \underline{C}_1 + x_1 \cdot \underline{u}_1 + x_2 \cdot \underline{u}_2) \in \wp(\underline{C}_1, \underline{u}_1, \underline{u}_2)$$

so:

$$\begin{pmatrix} w_1 \\ w_2 \\ w_3 \end{pmatrix} = \begin{bmatrix} u_{11} & u_{12} \\ u_{21} & u_{22} \\ u_{31} & u_{32} \end{bmatrix} \begin{pmatrix} x_1 \\ x_2 \end{pmatrix} + \begin{pmatrix} C_{11} \\ C_{21} \\ C_{31} \end{pmatrix}$$

Similarly, we have:

$$w_c = (1 - x_1 - x_2) \cdot C_{c1} + x_1 \cdot C_{c2} + x_2 \cdot C_{c3}$$

$$\text{or: } w_c = \sum_{s=1}^3 C_{cs} \cdot \chi_s(\underline{x})$$

$$\text{where: } \begin{cases} \chi_1 = 1 - x_1 - x_2 \\ \chi_2 = x_1 \\ \chi_3 = x_2 \end{cases}$$

The triangle  $T$  points are the images of triangle  $T_0$  points obtained by the linear transformation defined through the matrix product:

$$\underline{x} \in T_0 \rightarrow \underline{w} = [\underline{C}] \cdot \chi(\underline{x}) \in T$$

The points of the seven-point integration Gauss method, applied over every triangle are triangle summits linear functions. If the image of a triangle  $T$  obtained by an linear transformation  $\Phi$  is a triangle  $T'$ , then the integration points of triangle  $T'$ , are the images obtained by the tranformation  $\Phi$ , of integration points of triangle  $T$ :

$$\Phi T = \{\underline{C}_1, \underline{C}_2, \underline{C}_3\} = \wp(\underline{C}_1, \underline{u}_1, \underline{u}_2) \rightarrow T' = \{\underline{C}'_1, \underline{C}'_2, \underline{C}'_3\} = \wp(\underline{C}'_1, \underline{u}'_1, \underline{u}'_2)$$

$$\Phi(\underline{C}_s) = \underline{C}'_s$$

$$\Phi(\underline{C}_1 + x_1 \cdot \underline{u}_1 + x_2 \cdot \underline{u}_2) = \underline{C}'_1 + x_1 \cdot \underline{u}'_1 + x_2 \cdot \underline{u}'_2$$

$$\text{with: } \begin{cases} \underline{u}'_2 = \underline{C}'_1 \underline{C}'_3, & \underline{u}'_1 = \underline{C}'_1 \underline{C}'_2 \\ s = 1, 2, 3 \end{cases}$$

since:

$$X \in T \Leftrightarrow (\exists x_1, x_2 \quad x_1 \geq 0, x_2 \geq 0 \quad x_1 + x_2 \leq 1) \quad (\underline{C}_1 X = x_1 \cdot \underline{u}_1 + x_2 \cdot \underline{u}_2)$$

So, we have

$$X' = \Phi(X)$$

$$C_1' = \Phi(C_1)$$

$$X \in T \Rightarrow (\exists x_1, x_2 \quad x_1 \geq 0, x_2 \geq 0 \quad x_1 + x_2 \leq 1)(\underline{C}_1' X' = x_1 \cdot \underline{u}_1' + x_2 \cdot \underline{u}_2') \Rightarrow X' \in T'$$

We recall (see 2.2.1) that the integration points are defined by relation of the kind:

$$\underline{G} = \frac{1}{3} \cdot (\underline{C}_1 + \underline{C}_2 + \underline{C}_3)$$

$$\underline{X}_s = \omega \cdot \underline{C}_s + (1 - \omega) \cdot \underline{G}$$

$$\underline{X}_{s+3} = \omega \cdot \underline{C}_s + (1 - \omega) \cdot \underline{G}$$

in other words:

$$\underline{GX}_s = \omega \cdot \underline{GC}_s$$

$$\underline{C}_1 \underline{X}_s - \underline{C}_1 \underline{G} = \omega \cdot (\underline{C}_1 \underline{C}_s - \underline{C}_1 \underline{G})$$

So

$$\underline{C}_1 \underline{X}_s = \omega \cdot \underline{C}_1 \underline{C}_s + (1 - \omega) \cdot \underline{C}_1 \underline{G}$$

$$\underline{C}_1 \underline{X}_s = \omega \cdot \underline{C}_1 \underline{C}_s + \frac{(1 - \omega)}{3} \cdot (\underline{u}_1 + \underline{u}_2)$$

Since:

$$\underline{C}_1 \underline{C}_s = 0 \quad (s = 1)$$

$$\underline{C}_1 \underline{C}_s = \underline{u}_{s-1} \quad (s = 2, 3)$$

We have the same kind of relationships for any case:

$$\underline{C}_1 \underline{X}_s = a_{1s} \cdot \underline{u}_1 + a_{2s} \cdot \underline{u}_2$$

We have also:

$$\underline{X}_s' = \Phi(\underline{X}_s) \quad \underline{X}_s' = \underline{C}_1' + a_{1s} \cdot \underline{u}_1' + a_{2s} \cdot \underline{u}_2'$$

That yields:

$$\Phi(\underline{X}_s) = \omega \cdot \underline{C}_s' + (1 - \omega) \cdot \frac{1}{3} \cdot (\underline{C}_1' + \underline{C}_2' + \underline{C}_3')$$

So the integration point images are the integration points of the image triangle. We can also extend this result to the points of the composite method and obtain a very important result indeed. The images, defined by the linear application  $\Phi$  that transforms the unit triangle  $T_0$  into the triangle  $T$ , of the composite method points defined for  $T_0$ , give to us the points of a composite method defined for the triangle  $T$ . In this way, we can build a composite method for a triangle of the space using the following suite:

$$\begin{aligned} \underline{\mathfrak{I}}_T^{nm}(f) &= \Lambda(T) \cdot \sum_{j=1}^N \beta_j \cdot f(w_j) \\ \beta_{\eta(p,q,j)} &= \frac{1}{n} \cdot \alpha_j \end{aligned}$$

$$\text{with: } \boxed{N = mn^2}$$

and:

$$(\zeta_j = \zeta_{1j} + i \cdot \zeta_{2j}) \in T_0 \rightarrow (w_j = \Phi(\zeta_j)) \in T \quad w_j = \begin{bmatrix} u_{11} & u_{12} \\ u_{21} & u_{22} \\ u_{31} & u_{32} \end{bmatrix} \begin{pmatrix} \zeta_{1j} \\ \zeta_{2j} \end{pmatrix} + \begin{pmatrix} C_{11} \\ C_{21} \\ C_{31} \end{pmatrix}$$

$$\text{with: } \boxed{\begin{aligned} u_{c1} &= C_{c2} - C_{c1} \\ u_{c2} &= C_{c3} - C_{c1} \end{aligned}}$$

## Annex 2 - Basis Functions

As seen in Chapter 3, the old SR3D basis functions definition are not the best choice. In fact it is possible to simplify the basis definition reducing the complexity of the terms  $\Theta(\ )$ ,  $\Delta(\ )$ ,  $H$  reported in Annex 1, as follows.

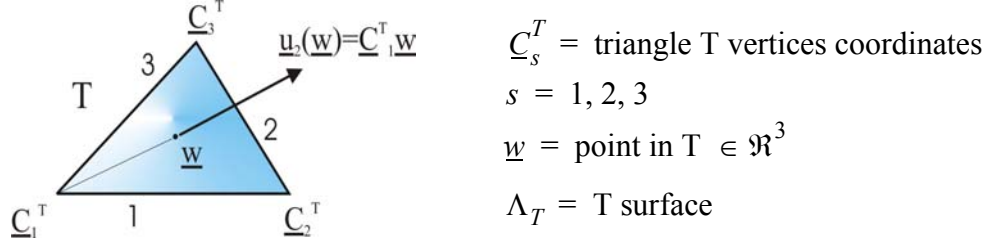


Figure A2.1: Geometry references of triangle

We want to calculate the fluxes of the basis vectors  $\underline{u}_s$  through the edges 1, 2, 3, of the triangle T itself, as reported in figure A2.1. We need to perform this operation in order to find the normalization coefficients of the vector basis. These coefficients are called fluxes and represented by the symbol  $I_s$ .

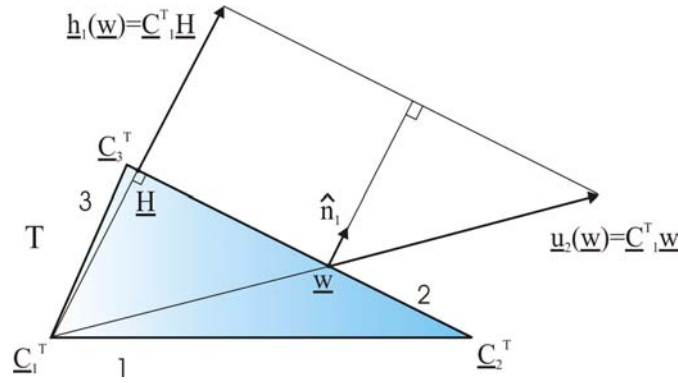


Figure A2.2:  $\underline{u}_s$  line integrals

For each vertex, we can write:

$$\begin{aligned}
 I_1(\underline{u}) &= \int_{\underline{C}_2^T \underline{C}_3^T} (\hat{n}_1 \cdot \underline{u}_2(\underline{w})) \cdot d\underline{C}_2^T \underline{C}_3^T = \left\| \underline{C}_2^T \underline{C}_3^T \right\| \left\| \underline{C}_1^T \underline{H} \right\| = 2\Lambda_T \\
 I_2(\underline{u}) &= \int_{\underline{C}_3^T \underline{C}_1^T} (\hat{n}_2 \cdot \underline{u}_3(\underline{w})) \cdot d\underline{C}_3^T \underline{C}_1^T = \left\| \underline{C}_3^T \underline{C}_1^T \right\| \left\| \underline{C}_2^T \underline{H} \right\| = 2\Lambda_T \quad (\text{A2.1}) \\
 I_3(\underline{u}) &= \int_{\underline{C}_1^T \underline{C}_2^T} (\hat{n}_3 \cdot \underline{u}_1(\underline{w})) \cdot d\underline{C}_1^T \underline{C}_2^T = \left\| \underline{C}_1^T \underline{C}_2^T \right\| \left\| \underline{C}_3^T \underline{H} \right\| = 2\Lambda_T
 \end{aligned}$$

We find out that all the three edge fluxes are equal to  $2\Lambda_T$ . Given  $\underline{v}$  a generic vectorial base, its normalization is written as follows:

$$\{\underline{v}_s(\underline{w}) = H\underline{u}_s(\underline{w}) \cup \Phi(\underline{v}_s(\underline{w})) = 1\} \Rightarrow H = \frac{1}{2\Lambda} \quad , \quad s = 1, 2, 3 \quad (\text{A2.2})$$

The normalization coefficient is equal to  $1/2\Lambda_T$  for each component of the vector basis. Since  $\underline{w} \in \mathcal{R}^3$  we have a three-vector basis to represent the triangle T. So we can define a vector basis through the  $\underline{u}_s$  vectors:

$$\underline{v}(\underline{w}) = \Phi_1 \cdot \underline{u}_1(\underline{w}) + \Phi_2 \cdot \underline{u}_2(\underline{w}) + \Phi_3 \cdot \underline{u}_3(\underline{w}) \quad (\text{A2.3})$$

where: $\Phi_s =$ weights of $\underline{v}$ vector base $s = 1, 2, 3$
---

Finally, the orthonormal vector basis  $\underline{u}$  is defined as follows, using the  $I_s$  fluxes found in equation A2.1:

$$\begin{aligned} \underline{u}_1(\underline{w}) &= H(\underline{C}_3 \underline{w}) \\ \underline{u}_2(\underline{w}) &= H(\underline{C}_1 \underline{w}) \\ \underline{u}_3(\underline{w}) &= H(\underline{C}_2 \underline{w}) \end{aligned} \quad (\text{A2.4})$$

Let us assume to analyze a mixed metallic and dielectric structure; in this case, we must define six degrees of freedom for each triangle of the structure mesh. In other words, we have an electric and a magnetic current flowing through each side of a triangle; each current is defined by the linear combination of the weights  $\Phi_s$  of equation (A2.3) and the orthonormal vector basis  $\underline{u}$  defined in equation A2.4. In case of a metallic structure, we have only three degrees of freedom since magnetic currents are not defined over metallic surfaces.

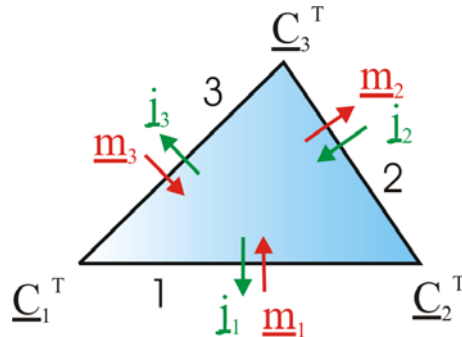


Figure A2.3: Degrees of freedom for a dielectric triangle of the mesh

In the full case (i.e. metal and dielectric structures) both electric and magnetic currents are needed, respectively  $\underline{j}$  and  $\underline{m}$ , with  $\underline{j}_s$  and  $\underline{m}_s$  the orthonormal base components:

$$\begin{aligned} \underline{j}(\underline{w}) &= J_1 \cdot \underline{j}_1(\underline{w}) + J_2 \cdot \underline{j}_2(\underline{w}) + J_3 \cdot \underline{j}_3(\underline{w}) \\ \underline{m}(\underline{w}) &= M_1 \cdot \underline{m}_1(\underline{w}) + M_2 \cdot \underline{m}_2(\underline{w}) + M_3 \cdot \underline{m}_3(\underline{w}) \end{aligned} \quad (\text{A2.5})$$

where: $\underline{j}_1(\underline{w}) = H(\underline{C}_3 \underline{w})$ $\underline{m}_1(\underline{w}) = H(\underline{C}_3 \underline{w})$ $\underline{j}_2(\underline{w}) = H(\underline{C}_1 \underline{w})$ $\underline{m}_2(\underline{w}) = H(\underline{C}_1 \underline{w})$ $\underline{j}_3(\underline{w}) = H(\underline{C}_2 \underline{w})$ $\underline{m}_3(\underline{w}) = H(\underline{C}_2 \underline{w})$
--

## Annex 3 - Semi-Numerical Technique

In Chapter 4, we described the main theory relative to the SN Technique. Hereafter we give the complete description of the calculations. In particular, we describe separately the  $A, D$  operators of equation (C4.13) (shown in equation (A3.1)) in order to understand how to obtain their final expressions given in equations (C4.16) and (C4.17).

$$\begin{aligned}
 A_{cs}^{KL}(g_1) &= \frac{1}{4} \sum_k \sum_l \alpha_k \alpha_l g_1(x_k, y_l) \left[ B^K(x_k) \right]_c^t \left[ B^L(y_l) \right]_s \\
 D_{cs}^{KL}(g_2) &= \frac{1}{4} \sum_k \sum_l \alpha_k \alpha_l g_2(x_k, y_l) \\
 T_{cs}^{KL}(g_3) &= 0
 \end{aligned} \tag{A3.1}$$

We also recall that both  $A$  and  $D$  operators have been splitted into a singular and a regular part according to equation (C4.14) (shown in equation (A3.2)):

$$\begin{aligned}
 A_{cs}^{KL}(g) &= A_{cs}^{KL}(g^0) + A_{cs}^{KL}(g^\infty) \\
 D_{cs}^{KL}(g) &= D_{cs}^{KL}(g^0) + D_{cs}^{KL}(g^\infty)
 \end{aligned} \tag{A3.2}$$

First, we show how to separate the singular part from the regular part from the Green's function kernels. The division into two different parts leads to the definition of two  $A, D$  operators parts as we will show in the following.

### A3.1 Green's Function Kernels for SN Technique

We can split the kernels in two parts as follows:

$$g(r) = g^0(r) + g^\infty(r) \tag{A3.3}$$

$$\text{where: } \boxed{
 \begin{aligned}
 g^0(r) &= \lim_{r \rightarrow 0} g(r) \\
 g^\infty(r) &= g(r) - g^0(r)
 \end{aligned}
 }$$

We recall the Green's function definition:

$$g_1(r) = \begin{bmatrix} \phi(r) \\ \chi(r) \end{bmatrix} \text{ along with: } g_2(r) = \begin{bmatrix} \Gamma(r) \\ \phi(r) \end{bmatrix} \tag{A3.4}$$

$$\text{with: } \boxed{
 \phi(r) = g(r) = \frac{e^{jkr}}{r}, \quad \Gamma(r) = -\frac{4}{k^2} g(r), \quad \chi(r) = k^2 g(r)
 }$$

The singular part  $g^0$  of the Green's function is given by the limit when  $r \rightarrow 0$ :

$$g^0(r) = \lim_{r \rightarrow 0} g(r) = \frac{1}{r} \quad (\text{A3.5})$$

For the regular part  $g^\infty$ , we make use of Taylor expansion series:

$$\frac{e^{jkr}}{r} = \frac{1}{r} + \sum_{n=1}^{\infty} \frac{(jkr)^n}{n!r} \quad (\text{A3.6})$$

We can write:

$$g^\infty(r) = [g(r) - g^0(r)] = jk \sum_{n=1}^{\infty} \frac{(jkr)^{(n-1)}}{n!} \quad (\text{A3.7})$$

We obtain the final expression of the Green's function  $g$ :

$$g(r) = [g^0(r) + g^\infty(r)] = \frac{1}{r} + jk \sum_{n=1}^{\infty} \frac{(jkr)^{(n-1)}}{n!} \quad (\text{A3.8})$$

### A3.2 Operator $A$ for Semi-Numerical Technique

Let's now consider the operator  $A$  relative to a generic couple of triangles  $T_K, T_L$  in the splitted representation of equation (A3.9):

$$A_{cs}^{KL}(g) = A_{cs}^{KL}(g^0) + A_{cs}^{KL}(g^\infty) \quad (\text{A3.9})$$

We can also write:

$$A_{cs}^{KL}(g) = A_{cs}^{KL}(r^{-1}) + A_{cs}^{KL}(g^\infty(r)) \quad (\text{A3.10})$$

where:	$A_{cs}^{KL}(r^{-1})$	operator A singular term
	$A_{cs}^{KL}(g^\infty(r))$	operator A regular term

The singular part needs a complex mathematical treatment, reported in following pages. According to equation (C3.14) and (C3.18) and recalling that  $r = \|\underline{y} - \underline{x}\|$ , we can write:

$$A_{cs}^{KL}(g) = H_K H_L \oint_{T_K} \oint_{T_L} g(\underline{x}, \underline{y}) \left( \left[ B^K(\underline{x}) \right]_c^t \left[ B^L(\underline{y}) \right]_s \right) dy dx \quad (\text{A3.11})$$

Using the results of equation (A3.8), we obtain:

$$A_{cs}^{KL}(g) = H_K H_L \oint_{T_K} [B^K(\underline{x})]_c^t \oint_{T_L} (g^0(\underline{x}, \underline{y}) + g^\infty(\underline{x}, \underline{y})) [B^L(\underline{y})]_s dy dx \quad (A3.12)$$

Then, we define function  $\mathfrak{G}^L$  :

$$\mathfrak{G}^L(g^0, \underline{x}) = \oint_{T_L} g^0(\underline{x}, \underline{y}) [B^L(\underline{y})]_s dy \quad (A3.13)$$

If we put this last equation inside equation (A3.12), we obtain:

$$A_{cs}^{KL}(g) = H_K H_L \left\{ \oint_{T_K} [B^K(\underline{x})]_c^t \mathfrak{G}^L(g^0, \underline{x}) dx + \oint_{T_K} \oint_{T_L} g^\infty(\underline{x}, \underline{y}) [B^K(\underline{x})]_c^t [B^L(\underline{y})]_s dy dx \right\} \quad (A3.14)$$

We modify now the  $\mathfrak{G}^L$  form as follows, obtaining this new form:

$$\begin{aligned} \mathfrak{G}^L(g^0, \underline{x}) = & \left[ \oint_{T_L} g^0(\underline{x}, \underline{y}) dy \right] \left[ \underline{x - C^L_3} \mid \underline{x - C^L_1} \mid \underline{x - C^L_2} \right] + \\ & + \left[ \oint_{T_L} (\underline{y - x}) g^0(\underline{x}, \underline{y}) dy \mid \oint_{T_L} (\underline{y - x}) g^0(\underline{x}, \underline{y}) dy \mid \oint_{T_L} (\underline{y - x}) g^0(\underline{x}, \underline{y}) dy \right] \end{aligned} \quad (A3.15)$$

where:

$$\begin{aligned} [B^L(\underline{y})] &= [\underline{y - x} \mid \underline{y - x} \mid \underline{y - x}] + [\underline{x - C^L_3} \mid \underline{x - C^L_1} \mid \underline{x - C^L_2}] \\ \underline{y - C^L_s} &= (\underline{y - x}) + (\underline{x - C^L_s}) \end{aligned}$$

According to equation (A3.15), we can now define one new matrix and two new functions:

$$\begin{aligned} [B^L(\underline{x})] &= [\underline{x - C^L_3} \mid \underline{x - C^L_1} \mid \underline{x - C^L_2}] \\ v_0^L(\underline{x}) &= \oint_{T_L} g^0(\underline{x}, \underline{y}) dy = \oint_{T_L} \frac{1}{\|\underline{y - x}\|} dy \quad (A3.16) \\ v_1^L(\underline{x}) &= \oint_{T_L} (\underline{y - x}) g^0(\underline{x}, \underline{y}) dy = \oint_{T_L} \frac{(\underline{y - x})}{\|\underline{y - x}\|} dy \end{aligned}$$

If we use now equation (A3.16) inside equation (A3.15), we find:

$$\mathfrak{g}^L(\mathbf{g}^0, \underline{x}) = v_0^L(\underline{x}) \left[ B^L(\underline{x}) \right] + \left[ v_1^L(\underline{x}) | v_1^L(\underline{x}) | v_1^L(\underline{x}) \right] \quad (\text{A3.17})$$

And finally, we obtain the forms for the singular and the regular parts of operator  $A$ :

$$\begin{aligned} A_{cs}^{KL}(\mathbf{g}^0) &= H_K H_L \left\{ \oint_{T_K} v_0^L(\underline{x}) \left[ B^K(\underline{x}) \right]_c^t \left[ B^L(\underline{x}) \right]_s dx + \right. \\ &\quad \left. + \oint_{T_K} \left[ B^K(\underline{x}) \right]_c^t \left[ v_1^L(\underline{x}) | v_1^L(\underline{x}) | v_1^L(\underline{x}) \right] dx \right\} \quad (\text{A3.18}) \\ A_{cs}^{KL}(\mathbf{g}^\infty) &= H_K H_L \oint_{T_K T_L} \mathfrak{g}^\infty(\underline{x}, \underline{y}) \left[ B^K(\underline{x}) \right]_c^t \left[ B^L(\underline{y}) \right]_s dy dx \end{aligned}$$

Then, we can calculate the operator  $A$  with respect to the correct Green's function kernels reported in equation (A3.4) for  $i = 1$ . This can be done owing to the linearity of the operator  $A$ .

$$\begin{aligned} A_{cs}^{KL}(\phi) &= A_{cs}^{KL}(\mathbf{g}^0) + A_{cs}^{KL}(\mathbf{g}^\infty) \\ A_{cs}^{KL}(\chi) &= A_{cs}^{KL}(k^2 \mathbf{g}^0) + A_{cs}^{KL}(k^2 \mathbf{g}^\infty) \end{aligned} \quad (\text{A3.19})$$

### A3.3 Operator $D$ for Semi-Numerical Technique

The operator  $D$  relative to a generic couple of triangles  $T_K, T_L$  is much easier to analyse and it is represented in the splitted form in equation (A3.20):

$$D_{cs}^{KL}(\mathbf{g}) = D_{cs}^{KL}(\mathbf{g}^0) + D_{cs}^{KL}(\mathbf{g}^\infty) \quad (\text{A3.20})$$

We can also write:

$$D_{cs}^{KL}(\mathbf{g}) \cong D_{cs}^{KL}(r^{-1}) + D_{cs}^{KL}(R^\infty(r)) \quad (\text{A3.21})$$

where:	$D_{cs}^{KL}(r^{-1})$	operator D singular term
	$D_{cs}^{KL}(R^\infty(r))$	operator D regular term

According to equation (A3.8), we obtain the final form for the singular and the regular parts of the operator  $D$ :

$$\begin{aligned} D_{cs}^{KL}(\mathbf{g}^0) &= H_K H_L \oint_{T_K} v_0^L(\underline{x}) dx \\ D_{cs}^{KL}(\mathbf{g}^\infty) &= H_K H_L \oint_{T_K T_L} \mathfrak{g}^\infty(\underline{x}, \underline{y}) dy dx \end{aligned} \quad (\text{A3.22})$$

Then, we can calculate the operator  $D$  with respect to the correct Green's function kernels reported in equation (A3.4) for  $i = 2$ . This can be done owing to the linearity of the operator  $D$ .

$$\begin{aligned} D_{cs}^{KL}(\phi) &= D_{cs}^{KL}(g^0) + D_{cs}^{KL}(g^\infty) \\ D_{cs}^{KL}(\Gamma) &= D_{cs}^{KL}\left(-\frac{4}{k^2}g^0\right) + D_{cs}^{KL}\left(-\frac{4}{k^2}g^\infty\right) \end{aligned} \quad (\text{A3.23})$$

### A3.5 $v_0$ and $v_1$ Functions

The  $v_0^L$  and  $v_1^L$  functions, appearing in equation (A3.16) and , are defined according to Figure (A3.1). Note that the point  $\underline{x} \in \mathfrak{R}^3$ , so it could be also contained inside  $T_L$ . On the other hand, this treatment is done in order to eliminate the possible singularity, so we don't care where the  $\underline{x}$  point is placed.

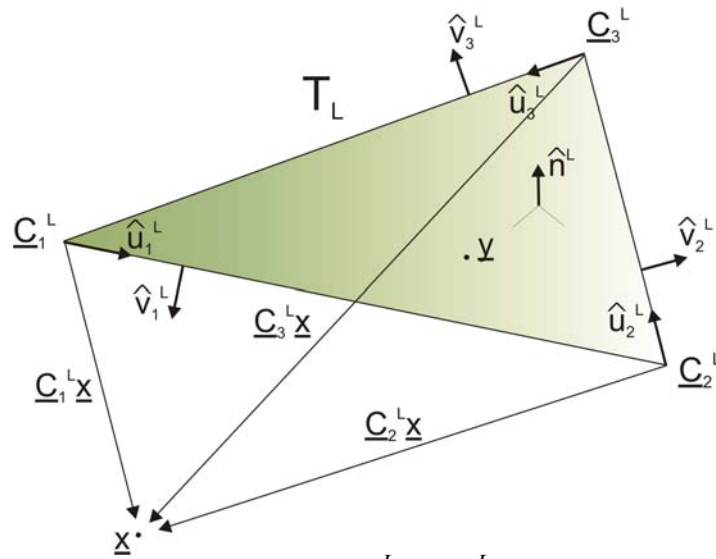


Figure A3.1: function  $v_0^L$  and  $v_1^L$  references

We also define three common functions in equation (A3.24):

$$\begin{aligned} a(\underline{x}) &= (\underline{C}_1^L \underline{x}) \times \hat{n}^L \\ \Omega_{AS}(\underline{x}, T_L) &= \text{solid angle between } T_K \text{ and } T_L \\ L_\sigma^L(\underline{x}) &= \log \left( \frac{\| \underline{C}_{\sigma+1}^L \underline{x} \| + (\hat{u}_\sigma^L | (\underline{C}_{\sigma+1}^L \underline{x}))}{\| \underline{C}_\sigma^L \underline{x} \| + (\hat{u}_\sigma^L | (\underline{C}_\sigma^L \underline{x}))} \right) \end{aligned} \quad (\text{A3.24})$$

A3.5.1  $v_0$  Function Definition: it is defined in equation (A3.25) in its complete form.

$$v_0^L(\underline{x}) = \oint_{T_L} \frac{1}{\| \underline{y} - \underline{x} \|} dy = -a(\underline{x})\Omega_{AS}(\underline{x}, T_L) + \sum_{\sigma=1}^3 ((\underline{C}_\sigma^L \underline{x}) | \hat{v}_\sigma^L) L_\sigma^L(\underline{x}) \quad (\text{A3.25})$$

We recall that we only treat the triangles  $T_K, T_L$  in the coplanar case. This means that the solid angle  $\Omega_{AS}$  or the  $a(\underline{x})$  has a zero value and so we obtain:

$$v_0^L(\underline{x}) = \oint_{T_L} \frac{1}{\|\underline{y}-\underline{x}\|} dy = \sum_{\sigma=1}^3 ((\underline{C}_{\sigma}^L \underline{x}) | \hat{v}_{\sigma}^L) L_{\sigma}^L(\underline{x}) \quad (\text{A3.26})$$

A3.5.2  $v_1$  Function Definition: it is defined in equation A3.27.

$$\begin{aligned} v_1^L(\underline{x}) = & a^2(\underline{x}) \Omega_{AS}(\underline{x}, T_L) \hat{n}^L - a(\underline{x}) \hat{n}^L \sum_{\sigma=1}^3 ((\underline{C}_{\sigma}^L \underline{x}) | \hat{v}_{\sigma}^L) L_{\sigma}^L(\underline{x}) + \\ & - \frac{1}{2} \sum_{\sigma=1}^3 \hat{v}_{\sigma}^L \left\{ (\hat{u}_{\sigma}^L | (\underline{C}_{\sigma+1}^L \underline{x})) \|\underline{C}_{\sigma+1}^L \underline{x}\| - (\hat{u}_{\sigma}^L | (\underline{C}_{\sigma}^L \underline{x})) \|\underline{C}_{\sigma}^L \underline{x}\| + \right. \\ & \left. + (\|\underline{C}_{\sigma}^L \underline{x}\|^2 - (\hat{u}_{\sigma}^L | (\underline{C}_{\sigma}^L \underline{x}))^2) L_{\sigma}^L(\underline{x}) \right\} \end{aligned} \quad (\text{A3.27})$$

Once again, the solid angle  $\Omega_{AS}$  or the  $a(\underline{x})$  has a zero value, so we obtain:

$$\begin{aligned} v_1^L(\underline{x}) = & \oint_{T_L} \frac{(\underline{y}-\underline{x})}{\|\underline{y}-\underline{x}\|} dy = -\frac{1}{2} \sum_{\sigma=1}^3 \hat{v}_{\sigma}^L \left\{ (\hat{u}_{\sigma}^L | (\underline{C}_{\sigma+1}^L \underline{x})) \|\underline{C}_{\sigma+1}^L \underline{x}\| + \right. \\ & \left. - ((\hat{u}_{\sigma}^L | (\underline{C}_{\sigma}^L \underline{x})) \|\underline{C}_{\sigma}^L \underline{x}\|) + (\|\underline{C}_{\sigma}^L \underline{x}\|^2 - (\hat{u}_{\sigma}^L | (\underline{C}_{\sigma}^L \underline{x}))^2) L_{\sigma}^L(\underline{x}) \right\} \end{aligned} \quad (\text{A3.28})$$

### A3.6 Numerical Implementation Issues for SN Technique

As said, it is possible to apply the SN technique even when the singularity does not occur, thanks to the generality of the method. In this case, a numerical implementation issue will appear. We have this case only inside a specific configuration with two distinct triangles, when the Gauss point  $\underline{x}$  is located on the line traced by the generic couple of the vertex points  $(\underline{C}_{i+1}^L, \underline{C}_i^L)$  of the triangle  $T_L$  (see Figure A3.2 with  $i=1$ ).

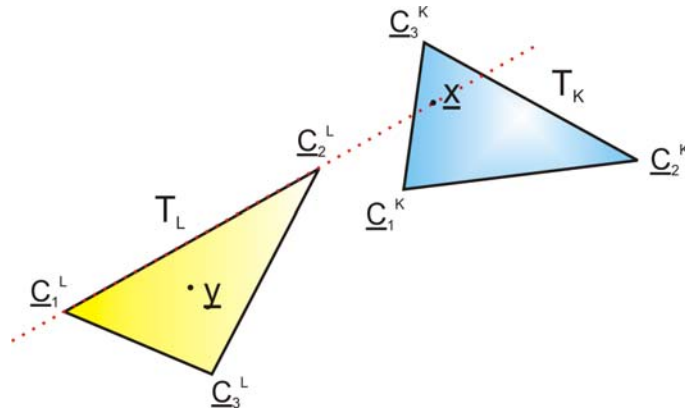


Figure A3.2: Special point-configuration case in the SN technique

In this special configuration, we need to replace the logarithmic approximation of the function  $L_{\sigma}^L$  of equation (A3.24):

$$L_{\sigma}^L(x) = \log\left(\frac{\|C_{\sigma+1}^L x\| + (\hat{u}_{\sigma}^L | (C_{\sigma+1}^L x))}{\|C_{\sigma}^L x\| + (\hat{u}_{\sigma}^L | (C_{\sigma}^L x))}\right) \quad (\text{A3.28})$$

with the following function:

$$L_{\sigma}^L(x) = -\log\left(\frac{\|C_{\sigma+1}^L x\|}{\|C_{\sigma}^L x\|}\right) \quad (\text{A3.29})$$

## Annex 4 - Derivative Calcululations

In Annex 4, we describe all the calculations needed to obtain the expressions reported in Chapter 6. First, we give the expressions for the the Full-Numerical and the Semi-Numerical technique. We recall that the derivative variables are the triangle vertices of the mesh  $\underline{C}^T$  (see equations C3.6, C3.8, C3.25, C3.26, C5.14).

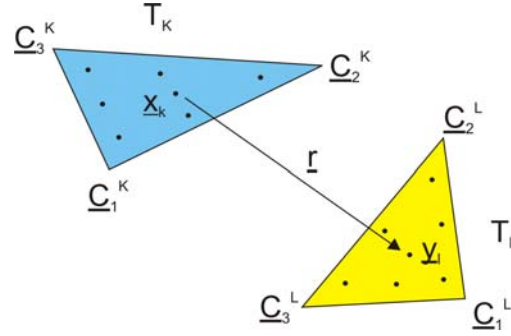


Figure A4.1: Generic couple of mesh triangles reaction

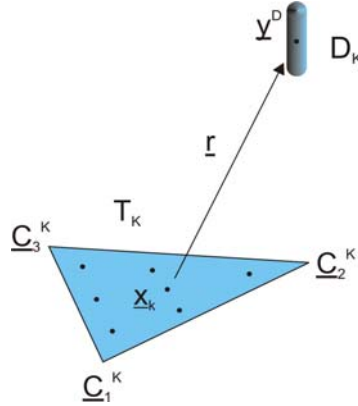


Figure A4.2: Generic mesh triangle - dipole reaction

### A4.1. FN Technique Derivative Calcululations: Derivative of the Reaction Matrix

The derivative is expressed with respect to the reference triangle  $T_L$ .

*A4.1.1. Basis Functions B*: let's start from the expression of equation C6.5. The basis function expression is reported in equation A4.1.

$$B^L(y_l) = \left[ \underline{C_3^L y_l} \mid \underline{C_1^L y_l} \mid \underline{C_2^L y_l} \right] \quad (\text{A4.1})$$

In equation A4.2, we have the following derivative form.

$$\left[ D_{uv}^L \left\{ B^L(D_{uv}^L \{y_l\}) \right\} \right]_{cs} = \left[ \left[ D_{uv}^L \{y_l\} \right]_{cs} \mid \left[ D_{uv}^L \{y_l\} \right]_{cs} \mid \left[ D_{uv}^L \{y_l\} \right]_{cs} \right] - \left[ \left[ D_{uv}^L \{C^L\} \right]_{c3} \mid \left[ D_{uv}^L \{C^L\} \right]_{c1} \mid \left[ D_{uv}^L \{C^L\} \right]_{c2} \right] \quad (\text{A4.2})$$

A4.1.2. *Gauss Points*  $\underline{y}$ : the derivative versus Gauss points is reported in equation C6.4. In order use the global reference, an homothetic transformation has been performed (see figure A4.3). We define the complex coordinates  $\underline{\zeta}$  as:

$$\underline{\zeta} = \zeta_1 + i \cdot \zeta_2 \quad (\text{A4.3})$$

and  $\underline{y}_l$  is defined as:

$$\underline{y}_l = \eta_1 \underline{u}_1 + \eta_2 \underline{u}_2 \quad (\text{A4.4})$$

$$\text{where: } \underline{u}_1 = (\underline{C}_2^L - \underline{C}_1^L), \quad \underline{u}_2 = (\underline{C}_3^L - \underline{C}_1^L)$$

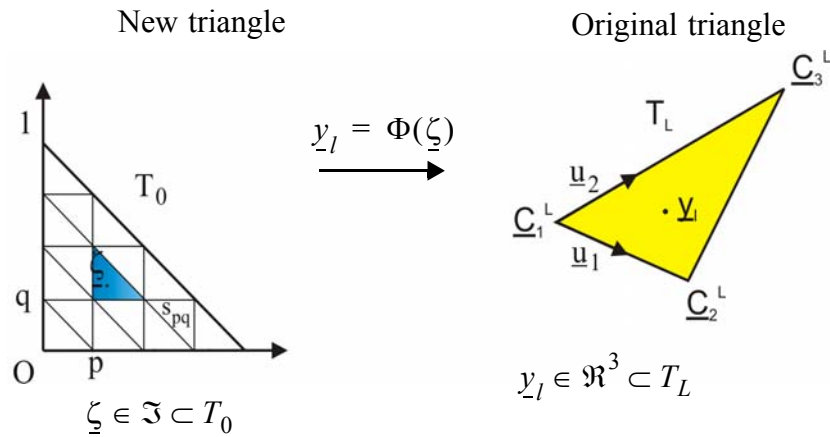


Figure A4.3: Global real reference from the complex one linear transformation  $\Phi(\ )$

Then, we apply a basis transformation:

$$\begin{aligned} \eta_1 &= a_{11} \zeta_1 + a_{12} \zeta_2 \\ \eta_2 &= a_{21} \zeta_1 + a_{22} \zeta_2 \end{aligned} \quad (\text{A4.5})$$

where  $a_{ij}$  are the unknowns. We can demonstrate, that the  $a_{ij}$  terms are defined as reported in equation A4.6:

$$\begin{cases} a_{11} = 0, a_{12} = 1 \\ a_{21} = 0, a_{22} = 1 \end{cases} \quad (\text{A4.6})$$

Since that we can also define  $\underline{y}_l$  in a different way:

$$\begin{cases} \eta_1 = \zeta_1 \\ \eta_2 = \zeta_2 \end{cases} \Rightarrow \underline{y}_l = \zeta_1 \underline{u}_1 + \zeta_2 \underline{u}_2 \quad (\text{A4.7})$$

$$\text{where: } \zeta_1 = \Re\{\underline{\zeta}\}, \quad \zeta_2 = \Im\{\underline{\zeta}\}$$

In other words, we obtain:

$$\underline{y}_l = \zeta_1(\underline{C}_2^L - \underline{C}_1^L) + \zeta_2(\underline{C}_3^L - \underline{C}_1^L) \quad (\text{A4.8})$$

Of course, for different Gauss points  $\underline{y}_l$  we have different values of complex coordinates  $\zeta$ . Finally, we can obtain the final form for a Gauss point  $\underline{y}_l$  (with respect to the cartesian coordinate  $c$ ), here shown in equation A4.9:

$$\begin{aligned} \left[ \underline{y}_l \right]_c &= \left[ (C_{c2}^L - C_{c1}^L) | (C_{c3}^L - C_{c1}^L) | (C_{c1}^L) \right] \begin{bmatrix} \zeta_1 \\ \zeta_2 \\ 1 \end{bmatrix} = \\ & \left[ C_{c2}^L | C_{c3}^L \right] \begin{bmatrix} \zeta_1 \\ \zeta_2 \end{bmatrix} + \left[ C_{c1}^L \right] (1 - \zeta_1 - \zeta_2) \end{aligned} \quad (\text{A4.9})$$

The derivative of equation A4.9 is defined in equation A4.10 and also reported in equation C6.4. The  $\delta_i^j$  is the Dirac function, so if  $i \Rightarrow j = \delta_i^j = 1$ , otherwise, its value is zero.

$$\begin{aligned} \left[ D_{u1}^T \{ \underline{y}_l \} \right]_c &= (1 - \zeta_{1c} - \zeta_{2c}) \delta_c^u \\ \left[ D_{u2}^T \{ \underline{y}_l \} \right]_c &= (\zeta_{1c}) \delta_c^u \\ \left[ D_{u3}^T \{ \underline{y}_l \} \right]_c &= (\zeta_{2c}) \delta_c^u \end{aligned} \quad (\text{A4.10})$$

*A4.1.3. Determinant  $\Omega$ :* the determinant  $\Omega$  derivative is defined in equation C6.6. First of all, we recall the determinant  $\Omega$  expression from equation C4.5:

$$\left[ \Omega^{KL}(\underline{x}_k, \underline{y}_l) \right]_{cs} = \det \left( \text{col}_s \left[ B^L(\underline{y}_l) \right] \mid \text{col}_c \left[ B^K(\underline{x}_k) \right] \mid \left[ \underline{y}_l - \underline{x}_k \right] \right) \quad (\text{A4.11})$$

We want to rewrite the determinant  $\Omega$  for a single couple of  $k, l$  Gauss points, obtaining:

$$\left[ \Omega^{KL}(\underline{x}_k, \underline{y}_l) \right]_{cs} = \det \begin{pmatrix} \left[ \underline{y}_l \right]_1 - \left[ \underline{C}^L \right]_p \left[ \underline{x}_k \right]_1 - \left[ \underline{C}^K \right]_q \left[ \underline{y}_l - \underline{x}_k \right]_1 \\ \left[ \underline{y}_l \right]_2 - \left[ \underline{C}^L \right]_p \left[ \underline{x}_k \right]_2 - \left[ \underline{C}^K \right]_q \left[ \underline{y}_l - \underline{x}_k \right]_2 \\ \left[ \underline{y}_l \right]_3 - \left[ \underline{C}^L \right]_p \left[ \underline{x}_k \right]_3 - \left[ \underline{C}^K \right]_q \left[ \underline{y}_l - \underline{x}_k \right]_3 \end{pmatrix} \quad (\text{A4.12})$$

$$\text{where: } \begin{cases} c=1 \\ c=2 \\ c=3 \end{cases} \Rightarrow \begin{cases} q=3 \\ q=1 \\ q=2 \end{cases}, \quad \begin{cases} s=1 \\ s=2 \\ s=3 \end{cases} \Rightarrow \begin{cases} p=3 \\ p=1 \\ p=2 \end{cases}$$

The reference triangle, for the derivative, is  $T_L$ . Moreover, it is possible to rewrite the determinant derivative considering that some terms are constant with respect to  $\underline{C}^L$ , afterwards, their derivative is equal to zero.

$$\begin{aligned}
\left[ D_{uv}^L \left\{ \Omega^{KL}(\underline{x}_k, D_{uv}^L \{y_l\}) \right\} \right]_{cs} &= \det \begin{pmatrix} \left[ D_{uv}^L \{y_l\} \right]_1 - \left[ D_{uv}^L \{C^L\} \right]_p & 0 & \left[ D_{uv}^L \{y_l\} \right]_1 \\ \left[ y_l \right]_2 - \left[ C^L \right]_p & \left[ x_k \right]_2 - \left[ C^K \right]_q & \left[ (y_l - x_k) \right]_2 \\ \left[ y_l \right]_3 - \left[ C^L \right]_p & \left[ x_k \right]_3 - \left[ C^K \right]_q & \left[ (y_l - x_k) \right]_3 \end{pmatrix} + \\
&\det \begin{pmatrix} \left[ y_l \right]_1 - \left[ C^L \right]_p & \left[ x_k \right]_1 - \left[ C^K \right]_q & \left[ (y_l - x_k) \right]_1 \\ \left[ D_{uv}^L \{y_l\} \right]_3 - \left[ D_{uv}^L \{C^L\} \right]_p & 0 & \left[ D_{uv}^L \{y_l\} \right]_2 \\ \left[ y_l \right]_3 - \left[ C^L \right]_p & \left[ x_k \right]_3 - \left[ C^K \right]_q & \left[ (y_l - x_k) \right]_3 \end{pmatrix} + \quad (A4.13) \\
&\det \begin{pmatrix} \left[ y_l \right]_1 - \left[ C^L \right]_p & \left[ x_k \right]_1 - \left[ C^K \right]_q & \left[ (y_l - x_k) \right]_1 \\ \left[ y_l \right]_2 - \left[ C^L \right]_p & \left[ x_k \right]_2 - \left[ C^K \right]_q & \left[ (y_l - x_k) \right]_2 \\ \left[ D_{uv}^L \{y_l\} \right]_3 - \left[ D_{uv}^L \{C^L\} \right]_p & 0 & \left[ D_{uv}^L \{y_l\} \right]_3 \end{pmatrix}
\end{aligned}$$

We can also write the equation A4.13 using the basis function definitions reported in equation A4.1. In that way, we obtain the results shown in equation C6.6.

$$\begin{aligned}
\left[ D_{uv}^L \left\{ \Omega^{KL}(\underline{x}_k, D_{uv}^L \{y_l\}) \right\} \right]_{cs} &= \det \begin{pmatrix} \left[ D_{uv}^L \left\{ B^L(D_{uv}^L \{y_l\}) \right\} \right]_{1s} & 0 & \left[ D_{uv}^L \{y_l\} \right]_1 \\ \left[ B^L \{y_l\} \right]_{2s} & \left[ B^K \{x_k\} \right]_{2s} & \left[ (y_l - x_k) \right]_2 \\ \left[ B^L \{y_l\} \right]_{3s} & \left[ B^K \{x_k\} \right]_{3s} & \left[ (y_l - x_k) \right]_3 \end{pmatrix} + \\
&\det \begin{pmatrix} \left[ B^L \{y_l\} \right]_{1s} & \left[ B^K \{x_k\} \right]_{1s} & \left[ (y_l - x_k) \right]_1 \\ \left[ D_{uv}^L \left\{ B^L(D_{uv}^L \{y_l\}) \right\} \right]_{2s} & 0 & \left[ D_{uv}^L \{y_l\} \right]_2 \\ \left[ B^L \{y_l\} \right]_{3s} & \left[ B^K \{x_k\} \right]_{3s} & \left[ (y_l - x_k) \right]_3 \end{pmatrix} + \quad (A4.14) \\
&\det \begin{pmatrix} \left[ B^L \{y_l\} \right]_{1s} & \left[ B^K \{x_k\} \right]_{1s} & \left[ (y_l - x_k) \right]_1 \\ \left[ B^L \{y_l\} \right]_{2s} & \left[ B^K \{x_k\} \right]_{2s} & \left[ (y_l - x_k) \right]_2 \\ \left[ D_{uv}^L \left\{ B^L(D_{uv}^L \{y_l\}) \right\} \right]_{3s} & 0 & \left[ D_{uv}^L \{y_l\} \right]_3 \end{pmatrix}
\end{aligned}$$

A4.1.4. *Green's Function Kernel*: according to figure A4.1 and equation A4.15, we now show the Green's kernel derivative calculations, in order to obtain equation C6.8.

$$\begin{aligned} r &= (y_l - x_k), \quad r_c = ([y_l]_c - [x_k]_c) \\ r &= \sqrt{\sum_c ([y_l]_c - [x_k]_c)^2} \quad c = 1, 2, 3 \end{aligned} \quad (\text{A4.15})$$

We can define the Green's kernel function derivatives as:

$$\begin{aligned} D_{uv}^L \left\{ \phi(x_k, D_{uv}^L \{y_l\}) \right\} &= \left( \frac{\partial \phi}{\partial r} \right) \left( \frac{\partial r}{\partial [y_l]_c} \right) (D_{uv}^L \{ [y_l]_c \}) \\ D_{uv}^L \left\{ \psi(x_k, D_{uv}^L \{y_l\}) \right\} &= \left( \frac{\partial \psi}{\partial r} \right) \left( \frac{\partial r}{\partial [y_l]_c} \right) (D_{uv}^L \{ [y_l]_c \}) \\ D_{uv}^L \left\{ \Gamma(x_k, D_{uv}^L \{y_l\}) \right\} &= \left( \frac{\partial \Gamma}{\partial r} \right) \left( \frac{\partial r}{\partial [y_l]_c} \right) (D_{uv}^L \{ [y_l]_c \}) \\ D_{uv}^L \left\{ \chi(x_k, D_{uv}^L \{y_l\}) \right\} &= \left( \frac{\partial \chi}{\partial r} \right) \left( \frac{\partial r}{\partial [y_l]_c} \right) (D_{uv}^L \{ [y_l]_c \}) \end{aligned} \quad (\text{A4.16})$$

$$\begin{aligned} \text{where:} \quad \phi(r) &= \frac{e^{jkr}}{r}, & \psi(r) &= (jkr - 1) \frac{e^{jkr}}{r^3}, \\ \Gamma(r) &= -\frac{4}{k^2} \frac{e^{jkr}}{r}, & \chi(r) &= k^2 \frac{e^{jkr}}{r} \end{aligned}$$

We define the Green's kernel function derivatives with respect to  $r$  as:

$$\begin{aligned} \frac{\partial \phi}{\partial r} &= \frac{e^{jkr}}{r} [jkr - 1], & \frac{\partial \psi}{\partial r} &= \frac{e^{jkr}}{r^4} [3 - 3jkr - (kr)^2] \\ \frac{\partial \Gamma}{\partial r} &= -\frac{4}{k^2} \frac{e^{jkr}}{r} [jkr - 1], & \frac{\partial \chi}{\partial r} &= k^2 \frac{e^{jkr}}{r} [r]_c [jkr - 1] \end{aligned} \quad (\text{A4.17})$$

The derivative of  $r$  with respect to a Gauss point is defined as:

$$\frac{\partial r}{\partial [y_l]_c} = \frac{[r]_c}{r} \quad (\text{A4.18})$$

So, if we combine the results of equations A4.17 and A4.18, we obtain the Green's function kernel derivatives with respect to variable  $\underline{C}^L$ :

$$\begin{aligned} D_{uv}^L \left\{ \phi(x_k, D_{uv}^L \{y_l\}) \right\} &= \frac{e^{jkr}}{r} [r]_c [jkr - 1] (D_{uv}^L \{ [y_l]_c \}) \\ D_{uv}^L \left\{ \psi(x_k, D_{uv}^L \{y_l\}) \right\} &= \frac{e^{jkr}}{r^4} [r]_c [3 - 3jkr - (kr)^2] (D_{uv}^L \{ [y_l]_c \}) \end{aligned} \quad (\text{A4.19})$$

$$\begin{aligned}
D_{uv}^L \left\{ \Gamma(\underline{x}_k, D_{uv}^L \{ \underline{y}_l \}) \right\} &= -\frac{4}{k^2} \frac{e^{jkr}}{r} [r]_c [jkr - 1] (D_{uv}^L \{ [y_l]_c \}) \\
D_{uv}^L \left\{ \chi(\underline{x}_k, D_{uv}^L \{ \underline{y}_l \}) \right\} &= k^2 \frac{e^{jkr}}{r} [r]_c [jkr - 1] (D_{uv}^L \{ [y_l]_c \})
\end{aligned} \tag{A4.19}$$

#### A4.2. FN Technique Derivative Calculations: Derivatives of the Source Vector

The derivative is done with respect to the reference triangle  $T_K$ .

*A4.2.1. Basis Functions  $B$* : the equation C6.11 is the same as the equation C6.5. The derivative calculations are the same as in equations A4.1 and A4.2.

*A4.2.2. Gauss Points  $\underline{x}$* : the derivative of the Gauss points is the same as in equations A4.3 to A4.10.

*A4.2.3. Determinant  $\Upsilon$* : the determinant  $\Upsilon$  derivative is defined in equation C6.13. First of all, we recall the determinant  $\Upsilon$  expression from equation C4.11. We want to rewrite the determinant  $\Upsilon$  for the  $k$  Gauss points, obtaining:

$$\begin{aligned}
\left[ \Upsilon^K(\underline{x}_k, \underline{y}^D) \right]_c &= \det \left( \text{col}_c \left[ B^K(\underline{x}_k) \right] \mid \underline{m}^D \mid \underline{x}_k - \underline{y}^D \right) \\
\left[ \Upsilon^K(\underline{x}_k, \underline{y}^D) \right]_c &= \det \begin{pmatrix} \left[ \underline{x}_k \right]_1 - \left[ \underline{C}^K \right]_q & \left[ \underline{m}^D \right]_1 & \left[ \underline{x}_k - \underline{y}^D \right]_1 \\ \left[ \underline{x}_k \right]_2 - \left[ \underline{C}^K \right]_q & \left[ \underline{m}^D \right]_2 & \left[ \underline{x}_k - \underline{y}^D \right]_2 \\ \left[ \underline{x}_k \right]_3 - \left[ \underline{C}^K \right]_q & \left[ \underline{m}^D \right]_3 & \left[ \underline{x}_k - \underline{y}^D \right]_3 \end{pmatrix}
\end{aligned} \tag{A4.20}$$

where:  $\begin{cases} c=1 \\ c=2 \\ c=3 \end{cases} \Rightarrow \begin{cases} q=3 \\ q=1 \\ q=2 \end{cases}$

The reference triangle, for the derivative, is  $T_K$ . Moreover, it is possible to rewrite the determinant derivative considering that some terms are constant with respect to  $\underline{C}^K$ , hence, their derivative is equal to zero.

$$\left[ D_{uv}^K \{ \Upsilon^K(\underline{x}_k, \underline{y}^D) \} \right]_c = \det \begin{pmatrix} \left[ D_{uv}^K \{ \underline{x}_k \} \right]_1 - \left[ D_{uv}^K \{ \underline{C}^K \} \right]_q & 0 & \left[ D_{uv}^K \{ \underline{x}_k \} \right]_1 \\ \left[ \underline{x}_k \right]_2 - \left[ \underline{C}^K \right]_q & \left[ \underline{m}^D \right]_2 & \left[ \underline{x}_k - \underline{y}^D \right]_2 \\ \left[ \underline{x}_k \right]_3 - \left[ \underline{C}^K \right]_q & \left[ \underline{m}^D \right]_3 & \left[ \underline{x}_k - \underline{y}^D \right]_3 \end{pmatrix} + \tag{A4.21}$$

$$\begin{aligned}
& \det \begin{pmatrix} [\underline{x}_k]_1 - [\underline{C}^K]_q & [\underline{m}^D]_1 \left[ \underline{(x_k - y^D)} \right]_1 \\ [D_{uv}^K \{ \underline{x}_k \}]_2 - [D_{uv}^K \{ \underline{C}^K \}]_q & 0 \quad [D_{uv}^K \{ \underline{x}_k \}]_2 \\ [\underline{x}_k]_3 - [\underline{C}^K]_q & [\underline{m}^D]_3 \left[ \underline{(x_k - y^D)} \right]_3 \end{pmatrix} + \\
& \det \begin{pmatrix} [\underline{x}_k]_1 - [\underline{C}^K]_q & [\underline{m}^D]_1 \left[ \underline{(x_k - y^D)} \right]_1 \\ [\underline{x}_k]_2 - [\underline{C}^K]_q & [\underline{m}^D]_2 \left[ \underline{(x_k - y^D)} \right]_2 \\ [D_{uv}^K \{ \underline{x}_k \}]_3 - [D_{uv}^K \{ \underline{C}^K \}]_q & 0 \quad [D_{uv}^K \{ \underline{x}_k \}]_3 \end{pmatrix} +
\end{aligned} \tag{A4.21}$$

We can also write the equation A4.21 using the basis function definitions as reported in A4.1. In that way, we obtain the results shown in equation C6.13.

$$\begin{aligned}
[D_{uv}^K \{ Y^K(D_{uv}^K \{ \underline{x}_k \}, y^D) \}]_c &= \det \begin{pmatrix} [D_{uv}^K \{ B^K(D_{uv}^K \{ \underline{x}_k \}) \}]_{1c} & 0 & [D_{uv}^K \{ \underline{x}_k \}]_1 \\ [B^K(\underline{x}_k)]_{2s} & [\underline{m}^D]_2 \left[ \underline{(x_k - y^D)} \right]_2 & \\ [B^K(\underline{x}_k)]_{3s} & [\underline{m}^D]_3 \left[ \underline{(x_k - y^D)} \right]_3 & \end{pmatrix} + \\
& \det \begin{pmatrix} [B^K(\underline{x}_k)]_{1s} & [\underline{m}^D]_1 \left[ \underline{(x_k - y^D)} \right]_1 \\ [D_{uv}^K \{ B^K(D_{uv}^K \{ \underline{x}_k \}) \}]_{2s} & 0 & [D_{uv}^K \{ \underline{x}_k \}]_2 \\ [B^K(\underline{x}_k)]_{3s} & [\underline{m}^D]_3 \left[ \underline{(x_k - y^D)} \right]_3 & \end{pmatrix} + \\
& \det \begin{pmatrix} [B^K(\underline{x}_k)]_{1s} & [\underline{m}^D]_1 \left[ \underline{(x_k - y^D)} \right]_1 \\ [B^K(\underline{x}_k)]_{2s} & [\underline{m}^D]_2 \left[ \underline{(x_k - y^D)} \right]_2 \\ [D_{uv}^K \{ B^K(D_{uv}^K \{ \underline{x}_k \}) \}]_{3s} & 0 & [D_{uv}^K \{ \underline{x}_k \}]_3 \end{pmatrix}
\end{aligned} \tag{A4.22}$$

A4.2.4. *Transversal Moment*  $\underline{m}_t^D$ : it is defined in equation C4.10, here reported in equation A4.23; instead its derivative is defined in equation C6.12

$$\underline{m}_t^D(\underline{x}_k, \underline{y}^D) = \underline{m}^D - \left[ [\underline{m}^D \cdot \underline{(x_k - y^D)}] \cdot \underline{(x_k - y^D)} \right] \left( \frac{1}{\| \underline{x_k - y^D} \|} \right)^2 \tag{A4.23}$$

Since the dipole moment  $\underline{m}^D$  term does not depend on the geometry of the structure, its derivative is zero. Therefore, we give the other derivative terms starting from the first scalar product:

$$D_{uv}^K \left\{ \underline{m}^D \cdot (\underline{x}_k - \underline{y}^D) \right\} = D_{uv}^K \left\{ \sum_c [\underline{m}^D]_c [\underline{r}]_c \right\} = [\underline{m}^D]_c \delta_u^c \left[ D_{uv}^K \{ \underline{x}_k \} \right]_c \quad (\text{A4.24})$$

then we have:

$$D_{uv}^K \left\{ (\underline{x}_k - \underline{y}^D) \right\} = \begin{bmatrix} \left[ D_{uv}^K \left\{ (\underline{x}_k - \underline{y}^D) \right\} \right]_1 \\ \left[ D_{uv}^K \left\{ (\underline{x}_k - \underline{y}^D) \right\} \right]_2 \\ \left[ D_{uv}^K \left\{ (\underline{x}_k - \underline{y}^D) \right\} \right]_3 \end{bmatrix} = \begin{bmatrix} \delta_1^c \left[ D_{uv}^K \{ \underline{x}_k \} \right]_1 \\ \delta_2^c \left[ D_{uv}^K \{ \underline{x}_k \} \right]_2 \\ \delta_3^c \left[ D_{uv}^K \{ \underline{x}_k \} \right]_3 \end{bmatrix} \quad (\text{A4.25})$$

And finally:

$$D_{uv}^K \left\{ \left( \frac{1}{\| \underline{x}_k - \underline{y}^D \|} \right)^2 \right\} = \frac{2}{\| \underline{x}_k - \underline{y}^D \|^3} \left( \frac{[\underline{x}_k - \underline{y}^D]_c \left[ D_{uv}^K \{ \underline{x}_k \} \right]_c}{\| \underline{x}_k - \underline{y}^D \|^2} \right) \quad (\text{A4.26})$$

Combining the results in equations A4.24, A4.25 and A4.26, we obtain the derivative in equation C6.12.

$$D_{uv}^K \{ \underline{m}_t^D(\underline{r}) \} = -\frac{1}{r^2} \left[ D_{uv}^K \left\{ [\underline{m}^D \cdot \underline{r}] \right\} \cdot \underline{r} + [\underline{m}^D \cdot \underline{r}] \cdot D_{uv}^K \left\{ \underline{r} \right\} \right] + r^2 D_{uv}^K \left\{ \frac{1}{r^2} \right\} [\underline{m}^D \cdot \underline{r}] \cdot \underline{r} \quad (\text{A4.27})$$

$$\text{where: } \underline{r} = (\underline{y}^D - \underline{x}_k)$$

### A4.3. SN Technique Derivative Calculations: Derivatives with Respect to the Triangle Dimension

The derivative is done with respect to the reference triangle  $T_L$ , for the SN regular case, otherwise, the reference triangle is  $T_K$ .

*A4.3.1. Geometry parameters in local reference:* in order to compute the reaction matrix derivatives using the semi-numerical technique, the geometrical dimensions of a triangle of the mesh have been used, and their derivatives with respect to the geometry as well. As we need to compute three times all of these parameters, we have shifted the order of the vertices; to do that a local reference has been defined in figure A4.4 (in this way a single Fortran routine will be used to compute all the parameters needed).

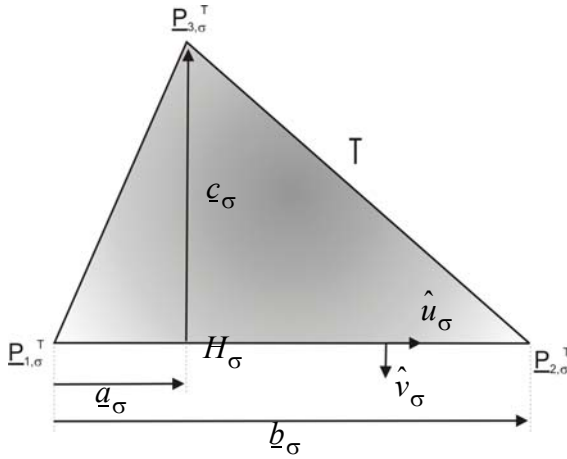


Figure A4.4: Mesh triangle geometry variables in the local reference

With:

$$C_{cs}^T = P_{cg,\sigma}^T = \begin{bmatrix} P_{1g,\sigma}^T \\ P_{2g,\sigma}^T \\ P_{3g,\sigma}^T \end{bmatrix} = \underline{P}_{g,\sigma}^T$$

Cartesian Coordinates:

$$c = 1, 2, 3$$

Vertex Number:

$$g, \sigma$$

The local summits  $\underline{P}_{g,\sigma}^T$  are defined as follows, according to figure A4.4:

$$\begin{aligned} (\sigma = 1) &\rightarrow \underline{C}_1^T = \underline{P}_{1,1}^T & \underline{C}_2^T &= \underline{P}_{2,1}^T & \underline{C}_3^T &= \underline{P}_{3,1}^T \\ (\sigma = 2) &\rightarrow \underline{C}_2^T = \underline{P}_{2,2}^T & \underline{C}_3^T &= \underline{P}_{3,2}^T & \underline{C}_1^T &= \underline{P}_{1,2}^T \\ (\sigma = 3) &\rightarrow \underline{C}_3^T = \underline{P}_{3,3}^T & \underline{C}_1^T &= \underline{P}_{1,3}^T & \underline{C}_2^T &= \underline{P}_{2,3}^T \end{aligned} \quad (\text{A4.28})$$

We first define the term  $\Pi_\sigma$ :

$$\Pi_\sigma = (\underline{P}_{1,\sigma}^T \underline{P}_{2,\sigma}^T) \cdot (\underline{P}_{1,\sigma}^T \underline{P}_{3,\sigma}^T) = \sum_{c=1}^3 (P_{c2,\sigma}^T - P_{c1,\sigma}^T)(P_{c3,\sigma}^T - P_{c1,\sigma}^T) \quad (\text{A4.29})$$

The  $\|\underline{a}_\sigma\|$ ,  $\|\underline{b}_\sigma\|$ ,  $\|\underline{c}_\sigma\|$  terms are defined as follows:

$$\|\underline{a}_\sigma\| = \frac{1}{\|\underline{b}_\sigma\|} \Pi_\sigma, \quad \|\underline{b}_\sigma\| = \left\| (\underline{P}_{1,\sigma}^T \underline{P}_{2,\sigma}^T) \right\|, \quad \|\underline{c}_\sigma\| = \sqrt{\left\| (\underline{P}_{1,\sigma}^T \underline{P}_{3,\sigma}^T) \right\|^2 - \|\underline{a}_\sigma\|^2} \quad (\text{A4.30})$$

Instead, the  $\underline{a}_\sigma$ ,  $\underline{b}_\sigma$ ,  $\underline{c}_\sigma$  are defined as follows:

$$\underline{a}_\sigma = \frac{\underline{b}_\sigma}{\|\underline{b}_\sigma\|} \|\underline{a}_\sigma\|, \quad \underline{b}_\sigma = (\underline{P}_{1,\sigma}^T \underline{P}_{2,\sigma}^T), \quad \underline{c}_\sigma = (\underline{P}_{1,\sigma}^T \underline{P}_{3,\sigma}^T) - \underline{a}_\sigma \quad (\text{A4.31})$$

The triangle surface is defined as:

$$\Lambda_\sigma = \frac{\|\underline{b}_\sigma\| \|\underline{c}_\sigma\|}{2} \quad (\text{A4.32})$$

Finally, we give the expressions of the unit vectors:

$$\hat{u}_\sigma = \frac{\underline{b}_\sigma}{\|\underline{b}_\sigma\|}, \quad \hat{v}_\sigma = -\frac{\underline{c}_\sigma}{\|\underline{c}_\sigma\|} \quad (\text{A4.33})$$

We will now give the derivatives with respect to the geometry of the expressions, reported in A4.29 to A4.33. As we are in the local reference, the derivative variable will be a  $\underline{P}_{g,\sigma}^T$  vertex point, as shown in equation A4.34.

$$\frac{\partial(\cdot)}{\partial \underline{P}_{uw,\sigma}^T} = D_{uw,\sigma}^T \{ \cdot \} \quad (\text{A4.34})$$

$$\begin{aligned} D_{uw,\sigma}^T \{ \Pi_\sigma \} &= \begin{bmatrix} \underline{P}_{1,\sigma}^T \delta_c^u & \underline{P}_{2,\sigma}^T \delta_c^u & \underline{P}_{3,\sigma}^T \delta_c^u \end{bmatrix} \begin{bmatrix} 2\delta_1^{w,\sigma} - \delta_2^{w,\sigma} - \delta_3^{w,\sigma} \\ \delta_3^{w,\sigma} - \delta_1^{w,\sigma} \\ \delta_2^{w,\sigma} - \delta_1^{w,\sigma} \end{bmatrix} \\ D_{uw,\sigma}^T \{ \|\underline{a}_\sigma\| \} &= -\frac{D_{uw,\sigma}^T \{ \|\underline{b}_\sigma\| \}}{\|\underline{b}_\sigma\|^2} \Pi_\sigma + \frac{1}{\|\underline{b}_\sigma\|} D_{uw,\sigma}^T \{ \Pi_\sigma \} \\ D_{uw,\sigma}^T \{ \|\underline{b}_\sigma\| \} &= \frac{(\underline{P}_{3,\sigma}^T - \underline{P}_{1,\sigma}^T) \delta_c^u}{\|\underline{b}_\sigma\|} (\delta_2^{w,\sigma} - \delta_1^{w,\sigma}) \\ D_{uw,\sigma}^T \{ \|\underline{c}_\sigma\| \} &= \frac{1}{\|\underline{c}_\sigma\|} (\delta_3^{w,\sigma} - \delta_1^{w,\sigma}) (\underline{P}_{3,\sigma}^T - \underline{P}_{1,\sigma}^T) \delta_c^u - \|\underline{a}_\sigma\| D_{uw,\sigma}^T \{ \|\underline{a}_\sigma\| \} \end{aligned} \quad (\text{A4.35})$$

Then, we have:

$$\begin{aligned} D_{uw,\sigma}^T \{ \underline{a}_\sigma \} &= D_{uw,\sigma}^T \{ \|\underline{a}_\sigma\| \hat{u}_\sigma \} = D_{uw,\sigma}^T \{ \|\underline{a}_\sigma\| \} \hat{u}_\sigma + \|\underline{a}_\sigma\| ( D_{uw,\sigma}^T \{ \hat{u}_\sigma \} ) \\ D_{uw,\sigma}^T \{ \underline{b}_\sigma \} &= (\delta_2^{w,\sigma} - \delta_1^{w,\sigma}) \begin{bmatrix} \delta_1^u \\ \delta_2^u \\ \delta_3^u \end{bmatrix} \\ D_{uw,\sigma}^T \{ \underline{c}_\sigma \} &= (\delta_3^{w,\sigma} - \delta_1^{w,\sigma}) \begin{bmatrix} \delta_1^u \\ \delta_2^u \\ \delta_3^u \end{bmatrix} \\ D_{uw,\sigma}^T \{ \hat{u}_\sigma \} &= \frac{1}{\|\hat{\underline{b}}_\sigma\|} \left( D_{uw,\sigma}^T \{ \underline{b}_\sigma \} - D_{uw,\sigma}^T \{ \|\underline{b}_\sigma\| \} \hat{u}_\sigma \right) \\ D_{uw,\sigma}^T \{ \hat{v}_\sigma \} &= \frac{1}{\|\hat{\underline{c}}_\sigma\|} \left( D_{uw,\sigma}^T \{ \underline{c}_\sigma \} - D_{uw,\sigma}^T \{ \|\underline{c}_\sigma\| \} \hat{v}_\sigma \right) \end{aligned} \quad (\text{A4.36})$$

Finally, the derivative of the triangle surface is:

$$D_{uw,\sigma}^T \{ \Lambda_L \} = \frac{(\|\underline{b}_\sigma\| D_{uw,\sigma}^T \{ \underline{c}_\sigma \} + \|\underline{c}_\sigma\| D_{uw,\sigma}^T \{ \underline{b}_\sigma \})}{2} \quad (\text{A4.37})$$

If we want to transform all the derivatives in equations, from A4.35 to A4.37, from the local to the global reference, we must use the linear transformation reported in equation A4.28, in order to obtain:

$$P_{cg, \sigma}^T \Rightarrow C_{cs}^T \quad (A4.38)$$

Then, in figure A4.5, we show the global reference parameters.

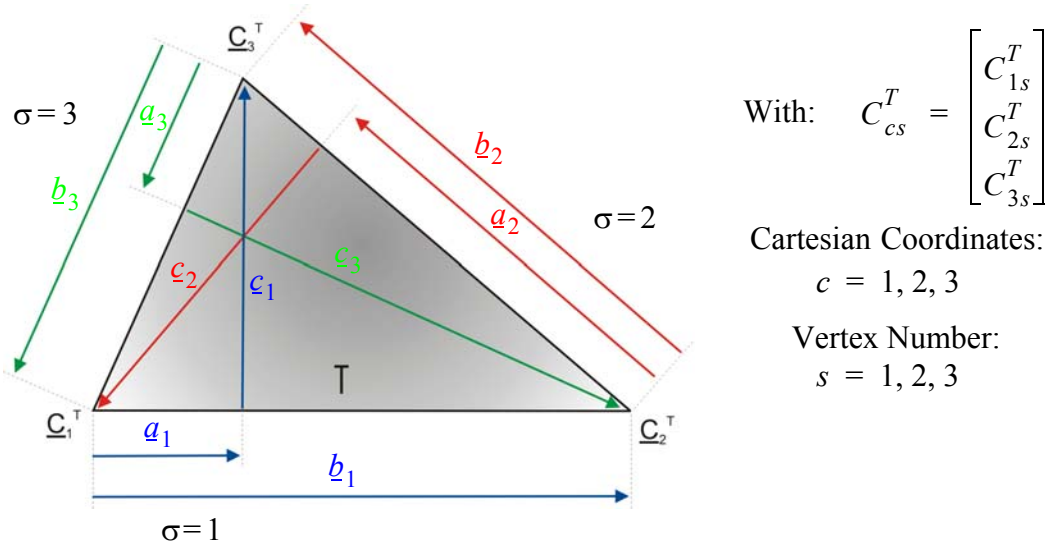


Figure A4.5: Mesh triangle geometry variables in the global reference

A4.3.2.  $t_0$  and  $t_1$  for regular SN case: we define now the derivative of the terms reported in expressions C6.15 and C6.16. We recall that we are treating the regular case for the SN technique, i.e., in this case we have  $T_K \neq T_L$  with  $x_k \notin T_L$ .

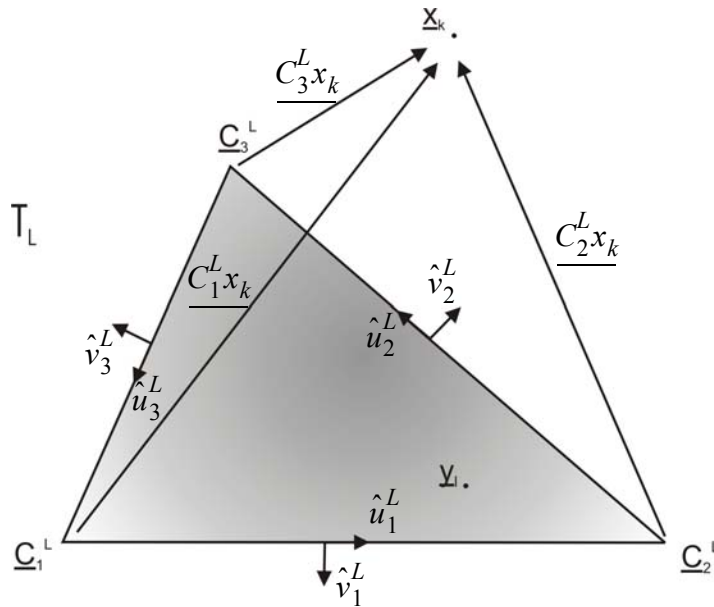


Figure A4.6: Mesh triangle geometry variables for  $t_0$  and  $t_1$  terms in global reference

First of all, according to figure A4.5 and A4.6, we define the  $v_0$  and  $v_1$  terms.

$$\begin{aligned}
v_0^L(\underline{x}_k) &= \sum_{s=1}^3 \left( (\underline{C}_s^L \underline{x}_k) \Big| \hat{v}_s^L \right) L_s^L(\underline{x}_k) \\
v_1^L(\underline{x}_k) &= \frac{1}{2} \sum_{s=1}^3 \hat{v}_s^L \left\{ \left( \hat{u}_s^L \Big| (\underline{C}_{(s+1)}^L \underline{x}_k) \right) \left\| \underline{C}_{(s+1)}^L \underline{x}_k \right\| - \left( \hat{u}_s^L \Big| (\underline{C}_s^L \underline{x}_k) \right) \left\| \underline{C}_s^L \underline{x}_k \right\| + \right. \\
&\quad \left. \left( \left\| \underline{C}_s^L \underline{x}_k \right\|^2 - (\hat{u}_s^L \Big| (\underline{C}_s^L \underline{x}_k))^2 \right) L_s^L(\underline{x}_k) \right\} = \frac{1}{2} \sum_{s=1}^3 \hat{v}_s^L \left\{ \underline{V}_{a1}^L(\underline{x}_k) - \underline{V}_{b1}^L(\underline{x}_k) + \underline{V}_{c1}^L(\underline{x}_k) \right\} \quad (\text{A4.39}) \\
\text{where: } L_s^L(\underline{x}_k) &= \log \left\{ \frac{\left\| \underline{C}_{(s+1)}^L \underline{x}_k \right\| + (\hat{u}_s^L \Big| (\underline{C}_{(s+1)}^L \underline{x}_k))}{\left\| \underline{C}_s^L \underline{x}_k \right\| + (\hat{u}_s^L \Big| (\underline{C}_s^L \underline{x}_k))} \right\}
\end{aligned}$$

We also give in equation A4.40 all the terms which appear in equation A4.39, recalling that we have already treated the terms  $\hat{u}_\sigma$  and  $\hat{v}_\sigma$  in equations A4.33 and A4.36:

$$\begin{aligned}
\left( (\underline{C}_s^L \underline{x}_k) \Big| \hat{v}_s^L \right) &= \sum_{c=1}^3 \left\{ \left[ \underline{x}_k \right]_c - \left[ \underline{C}_s^L \right]_c \right\} \hat{v}_s^L \\
\left\| \underline{C}_s^L \underline{x}_k \right\| &= \sqrt{\sum_{c=1}^3 \left\{ \left[ \underline{x}_k \right]_c - \left[ \underline{C}_s^L \right]_c \right\}^2}, \quad \left\| \underline{C}_{(s+1)}^L \underline{x}_k \right\| = \sqrt{\sum_{c=1}^3 \left\{ \left[ \underline{x}_k \right]_c - \left[ \underline{C}_{(s+1)}^L \right]_c \right\}^2} \\
\left( \hat{u}_s^L \Big| (\underline{C}_s^L \underline{x}_k) \right) &= \sum_{c=1}^3 \hat{u}_s^L \left\{ \left[ \underline{x}_k \right]_c - \left[ \underline{C}_s^L \right]_c \right\} \\
\left( \hat{u}_s^L \Big| (\underline{C}_{(s+1)}^L \underline{x}_k) \right) &= \sum_{c=1}^3 \hat{u}_s^L \left\{ \left[ \underline{x}_k \right]_c - \left[ \underline{C}_{(s+1)}^L \right]_c \right\} \quad (\text{A4.40}) \\
\underline{V}_{a1}^L(\underline{x}_k) &= \left( \hat{u}_s^L \Big| (\underline{C}_{(s+1)}^L \underline{x}_k) \right) \left\| \underline{C}_{(s+1)}^L \underline{x}_k \right\| \\
\underline{V}_{b1}^L(\underline{x}_k) &= \left( \hat{u}_s^L \Big| (\underline{C}_s^L \underline{x}_k) \right) \left\| \underline{C}_s^L \underline{x}_k \right\| \\
\underline{V}_{c1}^L(\underline{x}_k) &= \left( \left\| \underline{C}_s^L \underline{x}_k \right\|^2 - (\hat{u}_s^L \Big| (\underline{C}_s^L \underline{x}_k))^2 \right) L_s^L(\underline{x}_k)
\end{aligned}$$

According to equations from A4.35 to A4.37 and C5.14, we can define the derivatives with respect to the geometry of expressions, in A4.41

$$\begin{aligned}
D_{uv}^L \left\{ (\underline{C}_s^L \underline{x}_k) \Big| \hat{v}_s^L \right\} &= \sum_{c=1}^3 \left\{ D_{uv}^L \left\{ \left[ \underline{x}_k \right]_c - \left[ \underline{C}_s^L \right]_c \right\} v_{cs}^L + \left( \left[ \underline{x}_k \right]_c - \left[ \underline{C}_s^L \right]_c \right) \left[ D_{uv}^L \left\{ \hat{v}_s^L \right\} \right]_c \right\} \\
D_{uv}^L \left\{ \left\| \underline{C}_s^L \underline{x}_k \right\| \right\} &= \sum_{c=1}^3 \left\{ \frac{\left( \left[ \underline{x}_k \right]_c - \left[ \underline{C}_s^L \right]_c \right) \delta_c^u (-\delta_s^v)}{\left\| \underline{C}_s^L \underline{x}_k \right\|_c} \right\} \quad (\text{A4.41})
\end{aligned}$$

$$\begin{aligned}
D_{uv}^L \left\{ \left\| \underline{C}_{(s+1)x_k}^L \right\| \right\} &= \sum_{c=1}^3 \left\{ \frac{\left( \left[ \underline{x}_k \right]_c - \left[ \underline{C}_{(s+1)}^L \right]_c \right) \delta_c^u (-\delta_s^v)}{\left\| \underline{C}_{(s+1)x_k}^L \right\|_c} \right\} \\
D_{uv}^L \left\{ \hat{u}_s^L | \underline{C}_s^L x_k \right\} &= \sum_{c=1}^3 \left\{ \left( \left[ \underline{x}_k \right]_c - \left[ \underline{C}_s^L \right]_c \right) \left[ D_{uv}^L \{ \hat{u}_s^L \} \right]_c + \delta_c^u (-\delta_s^v) u_{cs}^L \right\} \\
D_{uv}^L \left\{ \hat{u}_s^L | \underline{C}_{(s+1)}^L x_k \right\} &= \sum_{c=1}^3 \left\{ \left( \left[ \underline{x}_k \right]_c - \left[ \underline{C}_{(s+1)}^L \right]_c \right) \left[ D_{uv}^L \{ \hat{u}_s^L \} \right]_c + \delta_c^u (-\delta_s^v) u_{cs}^L \right\} \\
D_{uv}^L \{ L_s^L(\underline{x}_k) \} &= \frac{D_{uv}^L \left\| \underline{C}_{(s+1)x_k}^L \right\| + D_{uv}^L \left( \hat{u}_s^L | \underline{C}_{(s+1)x_k}^L \right)}{\left\| \underline{C}_{(s+1)x_k}^L \right\| + \left( \hat{u}_s^L | \underline{C}_{(s+1)x_k}^L \right)} + \tag{A4.41} \\
&\quad \frac{D_{uv}^L \left\| \underline{C}_s^L x_k \right\| + D_{uv}^L \left( \hat{u}_s^L | \underline{C}_s^L x_k \right)}{\left\| \underline{C}_s^L x_k \right\| + \left( \hat{u}_s^L | \underline{C}_s^L x_k \right)} \\
D_{uv}^L \{ V_{a1}^L(\underline{x}_k) \} &= D_{uv}^L \left\{ \hat{u}_s^L | \underline{C}_{(s+1)x_k}^L \right\} \left\| \underline{C}_{(s+1)x_k}^L \right\| + \left( \hat{u}_s^L | \underline{C}_{(s+1)x_k}^L \right) D_{uv}^L \left\{ \left\| \underline{C}_{(s+1)x_k}^L \right\| \right\} \\
D_{uv}^L \{ V_{b1}^L(\underline{x}_k) \} &= D_{uv}^L \left\{ \hat{u}_s^L | \underline{C}_s^L x_k \right\} \left\| \underline{C}_s^L x_k \right\| + \left( \hat{u}_s^L | \underline{C}_s^L x_k \right) D_{uv}^L \left\{ \left\| \underline{C}_s^L x_k \right\| \right\} \\
D_{uv}^L \{ V_{c1}^L(\underline{x}_k) \} &= 2 \left\{ \left\| \underline{C}_s^L x_k \right\| D_{uv}^L \left\{ \hat{u}_s^L | \underline{C}_s^L x_k \right\} - \left( \hat{u}_s^L | \underline{C}_s^L x_k \right) D_{uv}^L \left\{ \left\| \underline{C}_s^L x_k \right\| \right\} \right\} L_s^L(\underline{x}_k) + \\
&\quad + \left\{ \left( \left\| \underline{C}_s^L x_k \right\|^2 - \left( \hat{u}_s^L | \underline{C}_s^L x_k \right)^2 \right) D_{uv}^L \{ L_s^L(\underline{x}_k) \} \right\}
\end{aligned}$$

We can now define the derivatives of the terms in A4.39:

$$\begin{aligned}
D_{uv}^L \{ v_0^L(\underline{x}_k) \} &= \sum_{s=1}^3 \left[ D_{uv}^L \left\{ \left( \underline{C}_s^L x_k \right) \hat{v}_s^L \right\} L_s^L(\underline{x}_k) + \left( \left( \underline{C}_s^L x_k \right) \hat{v}_s^L \right) D_{uv}^L \{ L_s^L(\underline{x}_k) \} \right] \\
D_{uv}^L \{ v_1^L(\underline{x}_k) \} &= -\frac{1}{2} \sum_{s=1}^3 \left\{ \hat{v}_s^L D_{uv}^L \{ V_{a1}^L(\underline{x}_k) \} + \left\| \underline{C}_{(s+1)x_k}^L \right\| \left( \hat{u}_s^L | \underline{C}_{(s+1)x_k}^L \right) D_{uv}^L \{ \hat{v}_s^L \} \right\} + \\
&\quad - \left\{ \hat{v}_s^L D_{uv}^L \{ V_{b1}^L(\underline{x}_k) \} + \left\| \underline{C}_s^L x_k \right\| \left( \hat{u}_s^L | \underline{C}_s^L x_k \right) D_{uv}^L \{ \hat{v}_s^L \} \right\} + \tag{A4.42} \\
&\quad + \left\{ \hat{v}_s^L D_{uv}^L \{ V_{c1}^L(\underline{x}_k) \} + \left( \left\| \underline{C}_s^L x_k \right\|^2 - \left( \hat{u}_s^L | \underline{C}_s^L x_k \right)^2 \right) L_s^L(\underline{x}_k) D_{uv}^L \{ \hat{v}_s^L \} \right\}
\end{aligned}$$

Finally, we give the expressions for the terms  $t_0$  and  $t_1$  and their derivatives:

$$t_0^L(\underline{x}_k) = \frac{v_0^L(\underline{x}_k)}{\Lambda_L}, \quad t_1^L(\underline{x}_k) = \frac{v_1^L(\underline{x}_k)}{\Lambda_L} \quad (\text{A4.43})$$

$$\begin{aligned} D_{uv}^L \{t_0^L(\underline{x}_k)\} &= \left( \frac{D_{uv}^L \{v_0^L(\underline{x}_k)\}}{\Lambda_L} - \frac{v_0^L(\underline{x}_k) D_{uv}^L \{\Lambda_L\}}{\Lambda_L^2} \right) \\ D_{uv}^L \{t_1^L(\underline{x}_k)\} &= \left( \frac{D_{uv}^L \{v_1^L(\underline{x}_k)\}}{\Lambda_L} - \frac{v_1^L(\underline{x}_k) D_{uv}^L \{\Lambda_L\}}{\Lambda_L^2} \right) \end{aligned} \quad (\text{A4.44})$$

*A4.3.3.  $t_0$  and  $t_1$  for singular SN case:* we define now the derivative of the terms reported in expression C6.17. We recall that are treating the singular case for the SN technique, i.e., in this case we have  $T_K \equiv T_L$ .

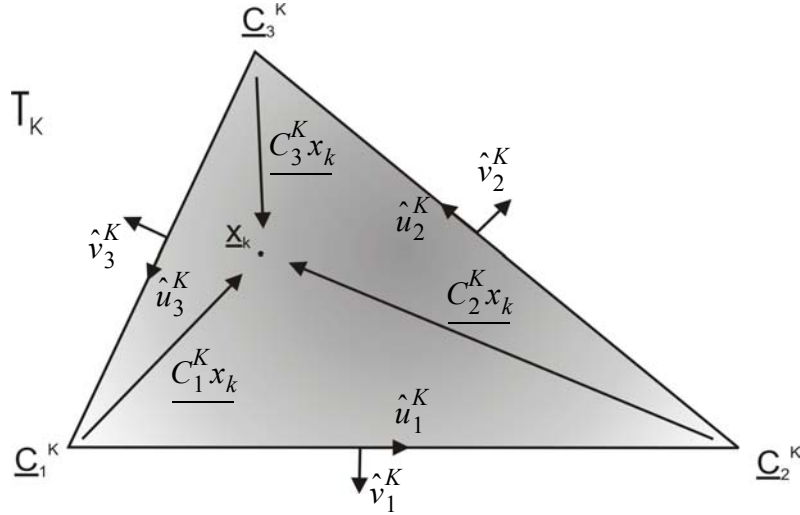


Figure A4.7: mesh triangle geometry variables for  $t_0$  and  $t_1$  terms in global reference

First of all, according to figure A4.5 and A4.7, we will define the  $v_0$  and  $v_1$  terms.

$$\begin{aligned} v_0^K(\underline{x}_k) &= \sum_{s=1}^3 \left( (C_s^K x_k) \middle| \hat{v}_s^K \right) L_s^K(\underline{x}_k) \\ v_1^K(\underline{x}_k) &= \frac{1}{2} \sum_{s=1}^3 \hat{v}_s^K \left\{ \left( \hat{u}_s^K \middle| (C_{(s+1)}^K x_k) \right) \left\| C_{(s+1)}^K x_k \right\| - \left( \hat{u}_s^K \middle| (C_s^K x_k) \right) \left\| C_s^K x_k \right\| + \right. \\ &\quad \left. \left( \left\| C_s^K x_k \right\|^2 - (\hat{u}_s^K \middle| (C_s^K x_k))^2 \right) L_s^K(\underline{x}_k) \right\} = \frac{1}{2} \sum_{s=1}^3 \hat{v}_s^K \left\{ V_{a1}^K(\underline{x}_k) - V_{b1}^K(\underline{x}_k) + V_{c1}^K(\underline{x}_k) \right\} \quad (\text{A4.45}) \\ \text{where: } L_s^K(\underline{x}_k) &= \log \left\{ \frac{\left\| C_{(s+1)}^K x_k \right\| + (\hat{u}_s^K \middle| (C_{(s+1)}^K x_k))}{\left\| C_s^K x_k \right\| + (\hat{u}_s^K \middle| (C_s^K x_k))} \right\} \end{aligned}$$

We also give in equation A4.46 all the terms which appear in equation A4.39, recalling that we have already treated the terms  $\hat{u}_\sigma$  and  $\hat{v}_\sigma$ , in equations A4.33 and A4.36:

$$\begin{aligned}
\left( (C_s^K x_k) \middle| \hat{v}_s^K \right) &= \sum_{c=1}^3 \left\{ \left[ \underline{x}_k \right]_c - \left[ \underline{C}_s^K \right]_c \right\} \hat{v}_s^K \\
\| C_s^K x_k \| &= \sqrt{\sum_{c=1}^3 \left\{ \left[ \underline{x}_k \right]_c - \left[ \underline{C}_s^K \right]_c \right\}^2} \quad \| C_{(s+1)}^K x_k \| = \sqrt{\sum_{c=1}^3 \left\{ \left[ \underline{x}_k \right]_c - \left[ \underline{C}_{(s+1)}^K \right]_c \right\}^2} \\
\left( \hat{u}_s^K \middle| (C_s^K x_k) \right) &= \sum_{c=1}^3 \hat{u}_s^K \left\{ \left[ \underline{x}_k \right]_c - \left[ \underline{C}_s^K \right]_c \right\} \\
\left( \hat{u}_s^K \middle| (C_{(s+1)}^K x_k) \right) &= \sum_{c=1}^3 \hat{u}_s^K \left\{ \left[ \underline{x}_k \right]_c - \left[ \underline{C}_{(s+1)}^K \right]_c \right\} \\
L_{a1}^K(x_k) &= \left( \hat{u}_s^K \middle| (C_{(s+1)}^K x_k) \right) \| C_{(s+1)}^K x_k \| \\
L_{b1}^K(x_k) &= \left( \hat{u}_s^K \middle| (C_s^K x_k) \right) \| C_s^K x_k \| \\
L_{c1}^K(x_k) &= \left( \| C_s^K x_k \|^2 - (\hat{u}_s^K \middle| (C_s^K x_k))^2 \right) L_s^K(x_k)
\end{aligned} \tag{A4.46}$$

According to equations from A4.35 to A4.37 and C5.14, we can define the derivatives with respect to the geometry (expressions in A4.47).

$$\begin{aligned}
D_{uv}^K \left\{ (C_s^K x_k) \middle| \hat{v}_s^K \right\} &= \sum_{c=1}^3 \left\{ D_{uv}^K \left\{ \left[ \underline{x}_k \right]_c - \left[ \underline{C}_s^K \right]_c \right\} v_{cs}^K + \left( \left[ \underline{x}_k \right]_c - \left[ \underline{C}_s^K \right]_c \right) \left[ D_{uv}^K \left\{ \hat{v}_s^K \right\} \right]_c \right\} \\
D_{uv}^K \left\{ \| C_s^K x_k \| \right\} &= \sum_{c=1}^3 \left\{ \frac{\left( \left[ \underline{x}_k \right]_c - \left[ \underline{C}_s^K \right]_c \right) \delta_c^u \left( \left[ D_{uv}^K \left\{ \underline{x}_k \right\} \right]_c - \delta_s^v \right)}{\left\| \underline{C}_s^L x_k \right\|_c} \right\} \\
D_{uv}^K \left\{ \| C_{(s+1)}^K x_k \| \right\} &= \sum_{c=1}^3 \left\{ \frac{\left( \left[ \underline{x}_k \right]_c - \left[ \underline{C}_{(s+1)}^L \right]_c \right) \delta_c^u \left( \left[ D_{uv}^K \left\{ \underline{x}_k \right\} \right]_c - \delta_s^v \right)}{\left\| \underline{C}_{(s+1)}^L x_k \right\|_c} \right\} \\
D_{uv}^K \left\{ \hat{u}_s^K \middle| (C_s^K x_k) \right\} &= \sum_{c=1}^3 \left\{ \left( \left[ \underline{x}_k \right]_c - \left[ \underline{C}_s^K \right]_c \right) \left[ D_{uv}^K \left\{ \hat{u}_s^K \right\} \right]_c + \delta_c^u \left( \left[ D_{uv}^K \left\{ \underline{x}_k \right\} \right]_c - \delta_s^v \right) u_{cs}^K \right\} \\
D_{uv}^K \left\{ \hat{u}_s^K \middle| (C_{(s+1)}^K x_k) \right\} &= \sum_{c=1}^3 \left\{ \left( \left[ \underline{x}_k \right]_c - \left[ \underline{C}_{(s+1)}^K \right]_c \right) \left[ D_{uv}^K \left\{ \hat{u}_s^K \right\} \right]_c + \delta_c^u \left( \left[ D_{uv}^K \left\{ \underline{x}_k \right\} \right]_c - \delta_s^v \right) u_{cs}^K \right\}
\end{aligned} \tag{A4.47}$$

$$\begin{aligned}
D_{uv}^K \{L_s^K(\underline{x}_k)\} &= \frac{D_{uv}^K \left\| \underline{C}_{(s+1)}^K \underline{x}_k \right\| + D_{uv}^K (\hat{u}_s^K | \underline{C}_{(s+1)}^K \underline{x}_k)}{\left\| \underline{C}_{(s+1)}^K \underline{x}_k \right\| + (\hat{u}_s^K | \underline{C}_{(s+1)}^K \underline{x}_k)} + \\
&\quad - \frac{D_{uv}^K \left\| \underline{C}_s^K \underline{x}_k \right\| + D_{uv}^K (\hat{u}_s^K | \underline{C}_s^K \underline{x}_k)}{\left\| \underline{C}_s^K \underline{x}_k \right\| + (\hat{u}_s^K | \underline{C}_s^K \underline{x}_k)} \\
D_{uv}^K \{V_{a1}^K(\underline{x}_k)\} &= D_{uv}^K \left\{ \hat{u}_s^K | \underline{C}_{(s+1)}^K \underline{x}_k \right\} \left\| \underline{C}_{(s+1)}^K \underline{x}_k \right\| + (\hat{u}_s^K | \underline{C}_{(s+1)}^K \underline{x}_k) D_{uv}^K \left\{ \left\| \underline{C}_{(s+1)}^K \underline{x}_k \right\| \right\} \\
D_{uv}^K \{V_{b1}^K(\underline{x}_k)\} &= D_{uv}^K \left\{ \hat{u}_s^K | \underline{C}_s^K \underline{x}_k \right\} \left\| \underline{C}_s^K \underline{x}_k \right\| + (\hat{u}_s^K | \underline{C}_s^K \underline{x}_k) D_{uv}^K \left\{ \left\| \underline{C}_s^K \underline{x}_k \right\| \right\} \quad (A4.47) \\
D_{uv}^K \{V_{c1}^K(\underline{x}_k)\} &= 2 \left\{ \left\| \underline{C}_s^K \underline{x}_k \right\| D_{uv}^K \left\{ \hat{u}_s^K | \underline{C}_s^K \underline{x}_k \right\} - (\hat{u}_s^K | \underline{C}_s^K \underline{x}_k) D_{uv}^K \left\{ \left\| \underline{C}_s^K \underline{x}_k \right\| \right\} \right\} L_s^K(\underline{x}_k) + \\
&\quad + \left\{ \left( \left\| \underline{C}_s^K \underline{x}_k \right\|^2 - (\hat{u}_s^K | \underline{C}_s^K \underline{x}_k)^2 \right) D_{uv}^K \{L_s^K(\underline{x}_k)\} \right\}
\end{aligned}$$

We can now define the derivatives of the terms, in A4.45:

$$\begin{aligned}
D_{uv}^K \{v_0^K(\underline{x}_k)\} &= \sum_{s=1}^3 \left[ D_{uv}^K \left\{ (\underline{C}_s^K \underline{x}_k) | \hat{v}_s^K \right\} L_s^K(\underline{x}_k) + \left( (\underline{C}_s^K \underline{x}_k) | \hat{v}_s^K \right) D_{uv}^K \{L_s^K(\underline{x}_k)\} \right] \\
D_{uv}^K \{v_1^K(\underline{x}_k)\} &= -\frac{1}{2} \sum_{s=1}^3 \left\{ \hat{v}_s^K D_{uv}^K \{V_{a1}^K(\underline{x}_k)\} + \left\| \underline{C}_{(s+1)}^K \underline{x}_k \right\| (\hat{u}_s^K | \underline{C}_{(s+1)}^K \underline{x}_k) D_{uv}^K \{ \hat{v}_s^K \} \right\} + \\
&\quad - \left\{ \hat{v}_s^K D_{uv}^K \{V_{b1}^K(\underline{x}_k)\} + \left\| \underline{C}_s^K \underline{x}_k \right\| (\hat{u}_s^K | \underline{C}_s^K \underline{x}_k) D_{uv}^K \{ \hat{v}_s^K \} \right\} + \\
&\quad + \left\{ \hat{v}_s^K D_{uv}^K \{V_{c1}^K(\underline{x}_k)\} + \left( \left\| \underline{C}_s^K \underline{x}_k \right\|^2 - (\hat{u}_s^K | \underline{C}_s^K \underline{x}_k)^2 \right) L_s^K(\underline{x}_k) D_{uv}^K \{ \hat{v}_s^K \} \right\} \quad (A4.48)
\end{aligned}$$

Finally, we give the expressions for the terms  $t_0$  and  $t_1$  and their derivatives:

$$t_0^K(\underline{x}_k) = \frac{v_0^K(\underline{x}_k)}{\Lambda_K}, \quad t_1^K(\underline{x}_k) = \frac{v_1^K(\underline{x}_k)}{\Lambda_K} \quad (A4.49)$$

$$\begin{aligned}
D_{uv}^K \{t_0^K(\underline{x}_k)\} &= \left( \frac{D_{uv}^K \{v_0^K(\underline{x}_k)\}}{\Lambda_K} - \frac{v_0^K(\underline{x}_k) D_{uv}^K \{\Lambda_K\}}{\Lambda_K^2} \right) \\
D_{uv}^K \{t_1^K(\underline{x}_k)\} &= \left( \frac{D_{uv}^K \{v_1^K(\underline{x}_k)\}}{\Lambda_K} - \frac{v_1^K(\underline{x}_k) D_{uv}^K \{\Lambda_K\}}{\Lambda_K^2} \right) \quad (A4.50)
\end{aligned}$$

A4.3.4.  $g_\infty$  Green's function: in C4.51 (see A3.4 also), we give the expression of the  $g_\infty$  function.

$$g_\infty(r) = jk \sum_{n=1}^N \frac{(jkr)^{(n-1)}}{n!} \quad (\text{A4.51})$$

Then, according to equation C4.14, the derivative of  $g_\infty$  function, i.e., using the Taylor's expansion, with respect to the geometry, is defined as follows:

$$D_{uv}^L \{g_\infty\} = \sum_{n=1}^N (jk)^n (n-1) \binom{n}{n} r^{(n-3)} \quad (\text{A4.52})$$

## Annex 5 - Scattered Field Derivative with Respect to the Mesh

In order to solve the inverse problem, we need to compute the scattered field from the currents found when solving the direct problem. We want show now the scattered field form and its derivative with respect to the mesh. First, we define:

$$\begin{aligned}
 x_p, \quad p = 1, \dots, n_p & \quad \text{measurement point} \\
 y_q, \quad q = 1, \dots, m_q & \quad \text{Gauss quadrature point} \\
 \Omega_n, \quad n = 1, \dots, N_\Omega & \quad \text{object defined by the position } g_n \in R^3
 \end{aligned} \tag{A5.1}$$

The scattered field  $\underline{E}(x_p)$  defined in the  $x_p$  point is the sum of the fields generated by each object  $\Omega_n$ , in the domain.

$$\underline{E}(x_p) = \sum_{n=1}^{N_\Omega} \underline{e}(\Omega_n, x_p) \tag{A5.2}$$

$$\begin{aligned}
 \text{with: } \underline{e}(\Omega_n, \underline{j}, x_p) &= \alpha_t \int_{\Gamma_n} j(y) G(x_p, y) dy + \alpha_r \int_{\Gamma_n} \underline{\nabla}_\Gamma \cdot \underline{j}(y) \underline{\nabla}_x G(x_p, y) dy \\
 \underline{j}(y) &= \sum_{\tau \in \tau_{e\nu} = 1} \sum J_{I_d(\tau, \nu)} \underline{\phi}_{\tau\nu}(y)
 \end{aligned}$$

where:  $I_d(\tau, \nu)$  is the number of degrees of freedom  $\nu$  of an element of triangle  $T_\tau$   
 $\underline{\phi}_{\tau\nu}(y)$  is the basis function related to the edge  $\nu$  of an element of triangle  $\tau$

So we obtain:

$$\begin{aligned}
 \underline{e}(\Omega, J, x) = \sum_{\tau \in \{t | (T_t \in \Gamma)\}} \left\{ \alpha_t \sum_{\nu=1}^3 \left[ I_d(\tau, \nu) \int_{\Gamma_n} \underline{\phi}_{\tau\nu}(y) G(x, y) dy \right] + \right. \\
 \left. \alpha_r \sum_{\nu=1}^3 \left[ I_d(\tau, \nu) \int \underline{\nabla}_\Gamma \cdot \underline{\phi}_{\tau\nu}(y) \underline{\nabla}_x G(x, y) dy \right] \right\} \tag{A5.3}
 \end{aligned}$$

And we put:

$$\underline{e}(\Omega, J, x) = \sum_{\tau \in \{t | (T_t \in \Gamma)\}} \underline{e}(T_\tau, J, x) \tag{A5.4}$$

To obtain the scattered field at the  $x$  point, we have:

$$\underline{E}(x) = \sum_{n=1}^{N_\Omega} \sum_{\tau \in \{t | (T_t \in \Gamma)\}} \underline{e}(T_\tau, J, x) \tag{A5.5}$$

Considering the equation (A5.2), the electric field derivative with respect to the position  $g_n$  of each object is:

$$\frac{\partial E_{\Omega_p}(x, g_p)}{g_p} = \sum_{n=1}^{\infty} \frac{\partial \underline{e}(\Omega_n(g_p), J(g_p), x)}{g_p} = \frac{\partial \underline{e}(\Omega(g_p), J(g_p), x)}{g_p} + \sum_{n=1}^{N_\Omega} \frac{\partial \underline{e}(\Omega_n(g_p), J(g_p), x)}{g_p} \Big|_{n \neq p} \quad (\text{A5.6})$$

## Annex 6 - SR3D Frequency Derivatives

In parallel to the geometry derivative of SR3D integral formulation, another module has been developed and validated but not still integrated within the core of the optimization procedure. Anyway, in this annex we want to report the expressions of the derivatives (first and second order) with respect to the frequency of the  $Z$  reaction matrix (see equation C3.11 to recall their definitions). This module can be used with the cost functional definition (see Chapter 7) in order to optimize the electromagnetic structure within a certain bandwidth.

### A6.1 First Order Derivative of the Discrete Reaction Matrix with Respect to the Frequency

Let's start from the first order derivative with respect to the frequency. We calculate the derivatives according to the equations from C3.8 to C3.18.

*A6.1.1 - First Order Frequency Derivative for Regular Case:* in this case, it is sufficient to calculate the  $Z_{xx}^{KL}$  terms replacing the Green's function kernels functions with its derivatives with respect to  $k$ . These derivatives are reported in equation A6.1:

$$\begin{aligned} \frac{\partial}{\partial k} \phi(k) &= j e^{jkr}, & \frac{\partial}{\partial k} \psi(k) &= -k \frac{e^{jkr}}{r}, \\ \frac{\partial}{\partial k} \Gamma(k) &= 4 \frac{e^{jkr}}{k^2} \left( \frac{2}{kr} - j \right), & \frac{\partial}{\partial k} \chi(k) &= \frac{e^{jkr}}{r} (2k + jk^2 r) \end{aligned} \quad (\text{A6.1})$$

We obtain the derivative of  $Z_{xx}^{KL}$  terms with respect to the frequency, using the  $A, D, T$  operator form of equation C3.8 and just replacing the new Green's function kernels functions reported in A6.1.

$$\begin{aligned} \frac{\partial}{\partial k} \left[ Z_{ee}^{KL} \right]_{cs} &= \mu \left\{ \left[ A^{KL} \left( \frac{\partial}{\partial k} \phi(k) \right) \right]_{cs} + \left[ D^{KL} \left( \frac{\partial}{\partial k} \Gamma(k) \right) \right]_{cs} \right\} I_{se_{cs}} \\ \frac{\partial}{\partial k} \left[ Z_{em}^{KL} \right]_{cs} &= \left[ T^{KL} \left( \frac{\partial}{\partial k} \psi(k) \right) \right]_{cs} I_{se_{cs}} \\ \frac{\partial}{\partial k} \left[ Z_{me}^{KL} \right]_{cs} &= \left[ T^{KL} \left( \frac{\partial}{\partial k} \psi(k) \right) \right]_{cs} I_{sm_{cs}} \\ \frac{\partial}{\partial k} \left[ Z_{mm}^{KL} \right]_{cs} &= \frac{1}{\mu} \left\{ \left[ A^{KL} \left( \frac{\partial}{\partial k} \psi(k) \right) \right]_{cs} - 4 \left[ D^{KL} \left( \frac{\partial}{\partial k} \phi(k) \right) \right]_{cs} \right\} I_{sm_{cs}} \end{aligned} \quad (\text{A6.2})$$

*A6.1.2 - First Order Frequency Derivative for Singular Case:* at present, we have the problem to eliminate the singularity in the  $A, D, T$  operators. We assume to work with planar structures only. So this reduce, for the moment, the field of application of SR3D but notably simplifies the optimization procedure. Under this assumption and according to equation C2.28, we can say that if we consider the reaction between two planar structures, defined on the  $\gamma$  plane, then:

$$\Omega^{KL} = (\nabla_{\underline{r}'} G \times \underline{\alpha}) \cdot \underline{\beta}^{test} \Big|_{\underline{\alpha}, \underline{\beta} \in \gamma} = 0 \quad (\text{A6.3})$$

This leads to obtain a zero value for the  $R_2$  term in equation C2.28 and consequently to a zero value for  $T$  operator reported in equation C3.28.

$$\begin{aligned}
\frac{\partial}{\partial k} \left[ A^{KL}(\phi(k)) \right]_{cs} &= H_K H_L \oint_{T_K T_L} \oint j e^{jkr} \left[ B^K(\underline{x}) \right]_c^t \left[ B^L(\underline{y}) \right]_s dy dx = \left[ A^{KL} \left( \frac{\partial}{\partial k} \phi(k) \right) \right]_{cs} \\
\frac{\partial}{\partial k} \left[ A^{KL}(\chi(k)) \right]_{cs} &= H_K H_L 2k \oint_{T_K T_L} \oint \frac{e^{jkr}}{r} \left[ B^K(\underline{x}) \right]_c^t \left[ B^L(\underline{y}) \right]_s dy dx + \\
&\quad H_K H_L k^2 \oint_{T_K T_L} \oint j e^{jkr} \left[ B^K(\underline{x}) \right]_c^t \left[ B^L(\underline{y}) \right]_s dy dx = \left[ A^{KL} \left( \frac{\partial}{\partial k} \phi(k) \right) \right]_{cs} \quad (A6.4) \\
\frac{\partial}{\partial k} \left[ D^{KL}(\phi(k)) \right]_{cs} &= H_K H_L \oint_{T_K T_L} \oint j e^{jkr} dy dx = \left[ D^{KL} \left( \frac{\partial}{\partial k} \phi(k) \right) \right]_{cs} \\
\frac{\partial}{\partial k} \left[ D^{KL}(\Gamma(k)) \right]_{cs} &= H_K H_L \frac{8}{k^3} \oint_{T_K T_L} \oint \frac{e^{jkr}}{r} dy dx - H_K H_L \frac{4}{k^2} \oint_{T_K T_L} \oint j e^{jkr} dy dx = \left[ D^{KL} \left( \frac{\partial}{\partial k} \Gamma(k) \right) \right]_{cs}
\end{aligned}$$

If we define the  $\Delta_k$  function, we obtain:

$$\begin{aligned}
\Delta_k &= j e^{jkr} \\
\oint_{T_K T_L} \oint \frac{e^{jkr}}{r} \left[ B^K(\underline{x}) \right]_c^t \left[ B^L(\underline{y}) \right]_s dy dx &= A_{PHI\_SN} \quad (A6.5) \\
\oint_{T_K T_L} \oint \frac{e^{jkr}}{R} dT_L dT_K &= D_{PHI\_SN}
\end{aligned}$$

We obtain:

$$\begin{aligned}
\frac{\partial}{\partial k} \left[ A^{KL}(\phi(k)) \right]_{cs} &= H_K H_L \oint_{T_K T_L} \oint \Delta_k \left[ B^K(\underline{x}) \right]_c^t \left[ B^L(\underline{y}) \right]_s dy dx = D_{APHI\_SN} \\
\frac{\partial}{\partial k} \left[ A^{KL}(\chi(k)) \right]_{cs} &= 2k [A_{PHI\_SN}] + k^2 [D_{APHI\_SN}] = D_{AXI\_SN} \\
\frac{\partial}{\partial k} \left[ D^{KL}(\phi(k)) \right]_{cs} &= H_K H_L \oint_{T_K T_L} \oint \Delta_k dy dx = D_{DPHI\_SN} \\
\frac{\partial}{\partial k} \left[ D^{KL}(\Gamma(k)) \right]_{cs} &= \frac{4}{k^3} [D_{PHI\_SN}] - \frac{4}{k^2} [D_{DPHI\_SN}] = D_{DGAMMA\_SN}
\end{aligned} \quad (A6.6)$$

## A6.2 Second Order Derivative of the Discrete Reaction Matrix with Respect to the Frequency

Let's start from the first order derivative with respect to the frequency. We calculate the derivative according to the equations from C3.8 to C3.18.

*A6.2.1 - Second Order Frequency Derivative for Regular Case:* in this case, it is sufficient to calculate the  $Z_{xx}^{KL}$  terms replacing the Green's function kernels functions with its derivatives with respect to  $k$ . These derivatives are reported in equation A6.7:

$$\begin{aligned} \frac{\partial^2}{\partial k^2} \phi_k &= -r e^{jkr}, & \frac{\partial^2}{\partial k^2} \psi_k &= -e^{jkR} \left( \frac{1}{r} + jk \right), \\ \frac{\partial^2}{\partial k^2} \Gamma_k &= -\frac{4}{k^2} e^{jkr} \left( \frac{6}{k^2 r} - \frac{j4}{k} - r \right), & \frac{\partial^2}{\partial k^2} \chi_k &= -\frac{e^{jkR}}{r} \left( k^2 r - j4k - \frac{2}{r} \right) \end{aligned} \quad (\text{A6.7})$$

We obtain the derivatives of  $Z_{xx}^{KL}$  terms with respect to the frequency, using the  $A, D, T$  operator form of equation C3.8 and just replacing the new Green's function kernels functions reported in A6.7

$$\begin{aligned} \frac{\partial^2}{\partial k^2} [Z_{ee}^{KL}]_{cs} &= \mu \left\{ \left[ A^{KL} \left( \frac{\partial^2}{\partial k^2} \phi(k) \right) \right]_{cs} + \left[ D^{KL} \left( \frac{\partial^2}{\partial k^2} \Gamma(k) \right) \right]_{cs} \right\} I_{se_{cs}} \\ \frac{\partial^2}{\partial k^2} [Z_{em}^{KL}]_{cs} &= \left[ T^{KL} \left( \frac{\partial^2}{\partial k^2} \psi(k) \right) \right]_{cs} I_{se_{cs}} \\ \frac{\partial^2}{\partial k^2} [Z_{me}^{KL}]_{cs} &= \left[ T^{KL} \left( \frac{\partial^2}{\partial k^2} \psi(k) \right) \right]_{cs} I_{sm_{cs}} \\ \frac{\partial^2}{\partial k^2} [Z_{mm}^{KL}]_{cs} &= \frac{1}{\mu} \left\{ \left[ A^{KL} \left( \frac{\partial^2}{\partial k^2} \psi(k) \right) \right]_{cs} - 4 \left[ D^{KL} \left( \frac{\partial^2}{\partial k^2} \phi(k) \right) \right]_{cs} \right\} I_{sm_{cs}} \end{aligned} \quad (\text{A6.8})$$

*A6.2.2 - Second Order Frequency Derivative for Singular Case:* at present we have the problem to eliminate the singularity in the  $A, D, T$  operators. We assume to work with planar structures only. So this reduce, for the moment, the field of application of SR3D but notably simplifies the optimization procedure. Under this assumption and according to equation C2.28, we can say that if we consider the reaction between two planar structures, defined on the  $\gamma$  plane, then:

$$\Omega^{KL} = (\nabla_{r'} G \times \underline{\alpha}) \cdot \underline{\beta}^{test} \Big|_{\underline{\alpha}, \underline{\beta} \in \gamma} = 0 \quad (\text{A6.9})$$

This leads to obtain a zero value for the  $R_2$  term in equation C2.28 and consequently to a zero value for  $T$  operator reported in equation C3.28. As said this assumption simplifies the model but only planar structures can be treated. Let's see the other two terms (integral version):

$$\begin{aligned}
\frac{\partial^2}{\partial k^2} [A^{KL}(\phi(k))]_{cs} &= H_K H_L \oint_{T_K T_L} \oint -r e^{jkr} [B^K(x)]_c [B^L(y)]_s dy dx = \left[ A^{KL} \left( \frac{\partial^2}{\partial k^2} \phi(k) \right) \right]_{cs} \\
\frac{\partial^2}{\partial k^2} [A^{KL}(\chi(k))]_{cs} &= H_K H_L k^2 \oint_{T_K T_L} \oint -r e^{jkr} [B^K(x)]_c [B^L(y)]_s dy dx + \\
&\quad H_K H_L 4k \oint_{T_K T_L} \oint j e^{jkr} [B^K(x)]_c [B^L(y)]_s dy dx + \\
&\quad H_K H_L 2 \oint_{T_K T_L} \oint \frac{e^{jkr}}{r} [B^K(x)]_c [B^L(y)]_s dy dx = \left[ A^{KL} \left( \frac{\partial^2}{\partial k^2} \phi(k) \right) \right]_{cs} \\
\frac{\partial^2}{\partial k^2} [D^{KL}(\phi(k))]_{cs} &= H_K H_L \oint_{T_K T_L} \oint -r e^{jkr} dT_L dT_K = \left[ D^{KL} \left( \frac{\partial^2}{\partial k^2} \phi(k) \right) \right]_{cs} \quad (A6.10) \\
\frac{\partial^2}{\partial k^2} [D^{KL}(\Gamma(k))]_{cs} &= -H_K H_L \frac{4}{k^2} \oint_{T_K T_L} \oint -r e^{jkr} dT_L dT_K + \\
&\quad H_K H_L \frac{16}{k^3} \oint_{T_K T_L} \oint j e^{jkr} dT_L dT_K + \\
&\quad H_K H_L \frac{24}{k^4} \oint_{T_K T_L} \oint \frac{e^{jkr}}{r} dT_L dT_K = \left[ D^{KL} \left( \frac{\partial^2}{\partial k^2} \Gamma(k) \right) \right]_{cs}
\end{aligned}$$

If we define the function  $\theta_k = -r e^{jkr}$ , we obtain:

$$\begin{aligned}
\frac{\partial^2}{\partial k^2} [A^{KL}(\phi(k))]_{cs} &= H_K H_L \oint_{T_K T_L} \oint \theta_k [B^K(x)]_c [B^L(y)]_s dy dx = D2APHI\_SN \\
\frac{\partial^2}{\partial k^2} [A^{KL}(\chi(k))]_{cs} &= k^2 [D2APHI\_SN] + 4k [DAPHI\_SN] + \\
&\quad 2 [APHI\_SN] = D2AXI\_SN \\
\frac{\partial^2}{\partial k^2} [D^{KL}(\phi(k))]_{cs} &= H_K H_L \oint_{T_K T_L} \oint \theta_k dT_L dT_K = D2DPHI\_SN \\
\frac{\partial^2}{\partial k^2} [D^{KL}(\Gamma(k))]_{cs} &= -k^2 [D2DPHI\_SN] + \frac{16}{k^3} [DDPHI\_SN] + \\
&\quad -\frac{24}{k^4} [DPHI\_SN] = D2DGAMMA\_SN
\end{aligned} \quad (A6.11)$$

## **BIBLIOGRAPHY**

- [1] **Abramowitz M., Stegun I. A.**  
*"Handbook of Mathematical Functions"*  
Dover publications Inc., New York, 1965.
- [2] **Addaci R., Diallo A., Le Thuc P., Staraj R.**  
*"Evaluation of Diversity and MIMO Performance of a New High Port to Port Isolation Dual-Band System"*  
International Symposium on Antennas and Propagation and USNC/URSI National Radio Science Meeting, 2012, Chicago, IL USA, July 8 - 14 2012.
- [3] **Andùjar A., Anguera J., Puente C.**  
*"Ground Plane Boosters as a Compact Antenna Technology for Wireless Handheld Devices"*  
IEEE Transactions on Antennas and Propagation, Vol. 59, No.5, pp 1668-1677, May 2011.
- [4] **Arnold V.**  
*"Equations Différentielles Ordinaires"*  
Editions Mir, Moscou, 1996.
- [5] **Balannis C.A.**  
*"Antenna Theory. Analysis and Design"*  
Editions J. Wiley, New York, 1982.
- [6] **Bendali A.**  
*"Approximation par Eléments finis de Surface de Problèmes de Diffraction des Ondes Electromagnétiques"*  
Université P. et M. Curie, Paris VI, 1984.
- [7] **Bendali A.**  
*"Numerical Analysis of the Exterior Boundary Value Problem for the Time-Harmonic Maxwell Equation by a Boundary Finite Element Method"*  
Math. Comp., 43, pp 29-46, 1984.
- [8] **Bouix M.**  
*"Les Discontinuités du Rayonnement Electromagnétique"*  
Edition Dunod, Paris, 1966.
- [9] **Brachat P.**  
*"Principe d'Equivalence en Electromagnétisme"*  
Annales des Télécom., 48, n°5-6, pp 333-340, 1993.

- [10] **Charet G.**  
*"Cours d'Analyse Numérique"*  
Sedes-Informatique, 1975.
- [11] **Collin R.E., Zucker F.S.**  
*"Antennas Theory"*  
Inter-University Electronic Series, Vol. 7, Edition Mac Graw Hill, New York, 1969.
- [12] **Dauvignac J.Y.**  
*"Analyse Rigoureuse de Structures Rayonnantes à 3 Dimensions: Applications aux Antennes Planaires"*  
Thèse de doctorat en Electronique, Université de Nice - Sophia Antipolis, Janvier 1993.
- [13] **Dedeban C.**  
*"Gestion Par Blocs de la Matrice du Logiciel S.R.3D."*  
Communication Personnelle, Avril 1992.
- [14] **Dedeban C.**  
*"Implantation de la Méthode de Cholesky dans le Logiciel S.R.3D."*  
Communication Personnelle, Juin 1994.
- [15] **Dhat G., Touzot.**  
*"Une Présentation de la Méthode des Eléments Finis de Surface"*  
Editions Maloine S.A., Paris, 1981.
- [16] **Ferraye R.**  
*"Développement d'un Algorithme de Diffraction Inverse par Déformations Eulériennes de Courbes de Niveaux pour la Reconstruction d'Images Microondes. Application à l'Imagerie Radar"*  
Thèse de doctorat en Sciences Physiques, Université de Nice - Sophia Antipolis, Mars 2000.
- [17] **Kong J. A.**  
*"Electromagnetic Wave Theory"*  
Editions John Wiley & Sons, New York, 1986.
- [18] **Koziel S., Ogursov S.**  
*"Linear Antenna Array Synthesis Using Gradient-Based Optimization with Analytical Derivatives"*  
International Symposium on Antennas and Propagation and USNC/URSI National Radio Science Meeting, 2012, Chicago, IL USA, July 8 - 14 2012.

- [19] **Lindelli I. V.**  
*"Methods for Electromagnetic Field Analysis"*  
Editions Clarendon Press, Oxford, 1992.
- [20] **Majid M. Khodier, Christos G. Christodoulou**  
*"Linear Array Geometry Synthesis with Minimum Sidelobe Level and Null Control Using Particle Swarm Optimization"*  
IEEE Transactions on Antennas and Propagation, Vol. 53, No.8, pp 2674-2679, August 2005.
- [21] **Miller E.K.**  
*"A Selective Survey of Computational Electromagnetics"*  
IEEE-AP, Vol. 36, No.9, pp 1281-1305, September 1973.
- [22] **Nedelec J.C.**  
*"Computation of Eddy Currents on a Surface in  $\mathbb{R}^3$  By Finite Elements"*  
SIAM j. numer. anal. vol 15, n°3, pp580-594, 1978.
- [23] **Nedelec J.C., Bendali A., Devys C., Ziani A.**  
*"MAGELLAN: Code de Calcul"*  
Ecole Polytechnique, Paris, Octobre 1986.
- [24] **Pollak S.V.**  
*"Structured Fortran 77 Programming"*  
Boyd & Fraser, 1982.
- [25] **Pichot Ch., Dubard J.L., Dedeban C., Zoppi M.**  
*"Optimisation de forme par algorithmes génétiques et ensembles de niveaux (Level Sets)"*  
Atelier "Optimisation de Formes en Electromagnétisme pour la Conception d'Antennes et de Circuits Microondes", CNES-CCT Electromagnétisme et Circuits Microondes - CNRS GDR "Ondes Antennes et Circuits (GT4)", Toulouse, 7 Avril 2010.
- [26] **Press W. H., Teukolsky S.A., Vetterling W. T., Flannery B. P.**  
*"Numerical Recipes, the Art of Scientific Computing"*  
Cambridge University Press, Third Edition, 2007.
- [27] **Rao M. S., Wilton D. R., Glisson A. W.**  
*"Electromagnetic Scattering By Surfaces of Arbitrary Shape"*  
IEEE-AP, vol 30, n°3, pp 409-418, May 1982.

- [28] **Ratajczak P., Brachat P., Guiraud J. L.**  
*"Rigorous Analysis of Three Dimensional Structures Incorporating Dielectrics"*  
IEEE-AP, vol 42, n°8, pp 1077-1088, August 1994.
- [29] **Ratajczak P., Bousquet T., Brachat P., Dedeban C., Guiraud J. L.**  
*"Applications du Formalisme des Equations Intégrales à des Structures à 3 Dimensions Comportant des Dielectriques"*  
Actes du Congrès JINA'94, ISSN 1168-3848, pp 62-65, Nov. 1994.
- [30] **Ratajczak P.**  
*"Applications du Formalisme Rigoureux des Equations Intégrales à l'Etude de Structures 3D Inhomogènes Excitées par Mode Guidés"*  
Thèse de doctorat en Electronique, Université de Nice - Sophia Antipolis, Janvier 1995.
- [31] **Roubine E.**  
*"Antennes"* Tome 1  
Editions Masson, Paris, 1978.
- [32] **Rumsey V. H.**  
*"Reaction Concept in Electromagnetic Theory"*  
Physical Review, vol. 94, n°6, pp 1491-1493, Juin 1954.
- [33] **Stratton J. A.**  
*"Théorie de l'Electromagnétisme"*  
Editions Dunond, Paris, 1961.
- [34] **Stutzman W. L. Pereira C. S.**  
*"Antenna Theory and Desing"*  
Edition John Wiley and Sons, New York, 1981.
- [35] **Van den Berg F.**  
*"An Analysis of Particle Swarm Optimizers"*  
PhD. thesis, University of Pretoria etd, 2001.
- [36] **Van Bladel J.**  
*"Electromagnetics Fields"*  
Edition Springer Verlag, Berlin, revised printing, 1985.

- [37] **Zoppi M., Dedeban C., Pichot Ch., Selleri S., Pelosi G.,**  
*"Antenna Shape Synthesis of Various Planar Configurations using a Hybrid Conjugate Gradient Method"*  
IEEE ICWIT 2010, Honolulu Hawaii, August 28 - September 23, 2010.
- [38] **Zoppi M., Dedeban C., Pichot Ch., Selleri S., Pelosi, G.**  
*"Optimal Location of Multi-antenna Systems Using a Conjugate Gradient Method"*  
CEM'11 Computational Electromagnetics International Workshop, Izmir, Turkey, August 10 - 13, 2011.
- [39] **Zoppi M., Dedeban C., Pichot Ch., Selleri S., Pelosi, G.**  
*"Optimal Location of Multiple Objects or Multi-Systems"*  
International Symposium on Antennas and Propagation and USNC/URSI National Radio Science Meeting, 2012, Chicago, IL USA, July 8 - 14, 2012.

## **ABSTRACT**

The aim of the present work is the development of an optimization method for electromagnetic structures (objects and planar antennas) under constraints (scattered field, radiation pattern, S parameters, ...).

A gradient-based optimization technique is applied to a rigorous mixed-integral formulation of the electromagnetic field (Combined Field Integral Equation or CFIE) coupling the electric and magnetic field formulations over the surface (external boundary) of the objects analyzed. The scattered or the radiation problem is led to the solution of a linear system. The optimization problem under constraints is defined through the minimization of a non linear functional (cost functional) measuring the deviation between the measured data (scattered field, radiation diagram, S parameters, ...) and the data obtained with the rigorous integral formulation defined in numerical form.

In order to apply an optimization technique based on a descent gradient algorithm, the calculation of the cost functional derivatives is needed. This calculation is performed in an analytical way with respect to every magnitude (incident field, scattered field, surface currents,...) that affects the cost functional. This calculation gives to the present study a very general orientation concerning the analysis of any type of antenna configuration.

The applications of interest concern the planar antennas systems (multi-antenna systems) illuminated by one or several incident waves or feeded by one or more ways with regard to the antennas location optimization framework within the multi-antenna arrays or within the MIMO multi-receiver antennas.

### **Keywords:**

- Optimization method
- Rigorous mixed-integral formulation
- Method of moments
- Analytic derivative with respect to the geometry
- Derivative of surface currents
- Optimization of antennas location
- Planar antennas, MIMO antennas

## **RESUME**

Ce travail a pour but d'étudier une méthode d'optimisation de structures (objets et antennes planaires) sous contraintes (champ diffracté, diagramme de rayonnement, ROS, ...).

La méthode utilisée est basée sur l'utilisation d'une technique de type gradient appliquée à une formulation intégrale mixte rigoureuse du champ électromagnétique (Combined Field Integral Equation ou CFIE) couplant les formulations du champ électrique et magnétique sur la surface (frontière extérieure) des objets étudiés. Le problème de diffraction ou de rayonnement est ramené à la résolution d'un système linéaire. Le problème d'optimisation sous contraintes conduit à la minimisation d'une fonctionnelle non linéaire (fonctionnelle coût) mesurant l'écart entre les données mesurées (champ diffracté, diagramme de rayonnement, ROS, ...) et les données issues de la formulation intégrale rigoureuse mise sous forme numérique.

Afin d'utiliser une technique d'optimisation basée sur un algorithme de descente du type gradient, il est nécessaire de calculer la dérivée de la fonctionnelle coût. Ce calcul est effectué analytiquement sur toutes les grandeurs (champ incident, champ diffracté, courants surfaciques, ...) intervenant dans la fonctionnelle coût. Ce qui confère à cette étude un caractère très général pour l'étude de systèmes antennaires quelconques.

Les applications étudiées concernent les systèmes antennaires planaires (systèmes multi-antennes) qu'ils soient illuminés par une ou plusieurs ondes incidentes ou excités sur une ou plusieurs voies dans le cadre d'optimisation de la localisation d'antennes au sein de réseaux multi-capteurs ou dans le cadre MIMO d'antennes multi-récepteurs.

### **Mots clés:**

- Méthode d'optimisation
- Formulation intégrale mixte rigoureuse
- Méthode des moments
- Dérivée analytique par rapport à la géométrie
- Dérivée des courants surfaciques
- Optimization de position d'antennes
- Antennes planaires, antennes MIMO

## **RIASSUNTO**

Il presente lavoro ha come obiettivo lo studio di un metodo di ottimizzazione di strutture (oggetti ed antenne planari) sottoposto a vincoli (campo diffratto, diagramma di radiazione, ROS, ...).

Il metodo utilizzato è basato sull'utilizzazione di una tecnica di tipo gradiente applicata a una formulazione integrale mista rigorosa del campo elettromagnetico (Combined Field Integral Equation CFIE) che accoppia le formulazioni del campo elettrico e del campo magnetico sulla superficie (frontiera esterna) degli oggetti studiati. Il problema della diffrazione o della radiazione è riportato alla risoluzione di un sistema lineare. Il problema dell'ottimizzazione sotto vincoli conduce alla minimizzazione di un funzionale non lineare (funzionale di costo) che misura lo scarto tra i dati misurati (campo scatterato, diagramma di radiazione, ROS, ...) e i dati ricavati dalla formulazione integrale rigorosa messa su forma numerica.

Al fine di utilizzare una tecnica d'ottimizzazione basata su un algoritmo di discesa a gradiente, è necessario il calcolo della derivata del funzionale di costo. Questo calcolo è eseguito in modo analitico su tutte le grandezze (campo incidente, campo diffratto, correnti superficiali,...) che intervengono nel funzionale di costo, ciò conferisce al presente studio un carattere molto generale per lo studio di sistemi di antenna qualsiasi.

Le applicazioni studiate riguardano i sistemi di antenne planari (sistemi multi-antenna) che sono illuminati da una o più onde incidenti o eccitati su una o più vie rispetto al quadro dell'ottimizzazione della localizzazione d'antenna in seno alle reti multi-captori o rispetto al quadro MIMO d'antenne multi-ricettori.

### **Parole chiave:**

- Metodo di ottimizzazione
- Formulazione integrale mista rigorosa
- Metodo dei momenti
- Derivata analitica rispetto alla geometria
- Derivata delle correnti superficiali
- Ottimizzazione della posizione d'antenna
- Antenne planari, antenne MIMO